Spatial and Temporal Development of Saltation in Air.

Arnold, Samantha Jane

Spatial and Temporal Development of Saltation in Air

Samantha Jane Arnold (B.Sc.)

A Thesis presented for the Degree of
Doctor of Philosophy

Department of Geography
Queen Mary and Westfield College
University of London

June 1998

DECLARATION

I hereby declare that this thesis has been composed by myself and has not been submitted previously for a high degree. The work has been my own except where indicated. All sources of information have been acknowledged.

DEDICATION

Without the help of many I would not have completed the work of this thesis. Without the continuous support and encouragement of my parents, however, this opportunity would never have existed. To my parents, with thanks:

Ozymandias

I met a traveller from an antique land
Who said: Two vast and trunkless legs of stone
Stand in the desert ... Near them, on the sand,
Half sunk, a shattered visage lies, whose frown,
And wrinkled lip, and sneer of cold command,
Tell that its sculptor well those passions read
Which yet survive, stamped on these lifeless things,
The hand that mocked them, and the heart that fed:
"My name is Ozymandias, king of kings:
Look on my works, ye Mighty, and despair!"
Nothing beside remains. Round and decay
Of that colossal wreck, boundless and bare
The lone and level sands stretch far away.

Percy Bysshe Shelley (1792-1822)

ACKNOWLEDGEMENTS

I would like to thank Graeme Butterfield for his initial confidence in my abilities and later his supervision and advice on the production of this thesis. The experience of Graeme Butterfield in both the field and the laboratory have made him an inspiration to work with.

My sincere thanks go to everybody at Queen Mary and Westfield College especially the Physical Geography Post Graduates with whom I have shared an office. I am extremely grateful for all of your assistance, discussions and friendship. It has been a pleasure to work here.

I am grateful to the Natural Environmental Research Council for funding this project. The financial support of the Social Sciences Research fund was also invaluable for the success of my field work. With respect to my field work on the Canary Island of Fuerteventura, my thanks are given to Professor Meco for his help in gaining permission for the experiments.

Finally, many thanks to my family and friends who have been so supportive and patient throughout my three years of research. Special thanks are given to Jarlath O'Brien. Both his practical help during my field work and his continuous emotional support and encouragement have been vital to the successful completion of this project.

ABSTRACT

A resurgence of interest in the concept of equilibrium in the aeolian saltation system has been witnessed in the 1990's. Throughout the aeolian field of research, i.e. wind tunnel, field and numerical models, many highly successful individual investigations have been conducted. Despite these data, however, the timing and location of the mass flux equilibrium have not been quantified.

This research investigates the simultaneous downwind spatial and temporal developments of the aeolian saltation system. Experiments were conducted in the laboratory and the field. By unification of the spatial and temporal dimensions in both environments one of the major limitations of contemporary aeolian science, the inability to relate data from different experimental environments, is addressed.

In the wind tunnel the development of the saltation system was measured over a streamwise length of 8m. Sediment transport was measured at 1m intervals by the downwind deployment of seven Aarhus sand traps. In the field the development of the saltation system was monitored over distances of 10m and 20m. Mass flux was measured by the downwind deployment of five 'total load' sand traps. In both environments temporal wind velocity and mass flux data were collected simultaneously at a single site. Spatial profile velocity data were later obtained by a streamwise traverse along the experimental area.

The downwind spatial development of the saltation system, from a point of initiation, in the laboratory and the field is manifest by an overshoot in mass flux and shear velocity. It is shown that in both environments mass flux increases with distance to a maximum at 4m downwind. This result is in remarkable agreement with existing data of a comparable scale. In the wind tunnel and the field experiments it

is found that shear velocity overshoots between 2-4m downwind of the overshoot in mass flux. The distance between the overshoot in mass flux and the overshoot in shear velocity is termed the 'separation distance'.

The existence of a 'separation distance' between the overshoots of mass flux and shear velocity questions the appropriateness of traditional mass flux formulae. It is found that conventional mass flux relationships with shear velocity, generated from data collected simultaneously at the same site, have the lowest predictive capability. The greatest confidence in the ability of shear velocity to predict the rate of mass flux is shown to occur when shear velocity data are collected downwind of mass flux data. The critical distance between the data collection points is demonstrated to be defined by the 'separation distance'.

The downwind spatial development of the saltation system without a point of initiation in the laboratory and the field is influenced by sand entering from upwind. The existence of high energy bombardment by saltation processes throughout the experimental area is shown to produce an accelerated development of the saltation system. It is found that the precise downwind development of mass flux and shear velocity are dependent on the exact rate of sand entering from upwind.

The temporal development of the saltation system is controlled essentially by the availability of transportable grains from the sand bed. In both the wind tunnel and the field experiments it is demonstrated that the saltation system develops through time from a transport-limited to a supply-limited system. The depletion of the sand bed through time limits the existence of the state of equilibrium. The equilibrium concept is thus shown to be inappropriate for the universal prediction of mass flux.

CONTENTS

CHAPTER 3 - SPATIAL AND TEMPORAL DEVELOPMENT OF THE SALTATION SYSTEM.

CHAPTER 5 - DEVELOPMENT OF THE SALTATION SYSTEM UNDER NATURAL ENVIRONMENTAL CONDITIONS.

CHAPTER 6 - SMALL SCALE SPATIAL AND TEMPORAL DEVELOPMENT OF THE SALTATION SYSTEM.

FIGURES

TABLES

SYMBOLS

α	Density of sand ($g.cm^{-3}$).
δ	Boundary layer depth (cm).
δ_*	Displacement thickness (cm).
λ	Constant = 1.1.
η	Turbulent eddy viscosity ($cm^2.sec^{-1}$).
μ	Laminar eddy viscosity ($cm^2.sec^{-1}$).
π	3.1416.
Π	Coles boundary layer profile parameter.
ρ	Fluid density ($g.cm^{-3}$).
τ	Surface shear stress ($N.cm^{-2}$).
υ	Kinematic viscosity ($cm^2.sec^{-1}$).
b	Exponent of the mass flux gradient.
d	Grain diameter (cm).
d_o	Displacement height (cm).
g	Acceleration due to gravity ($cm.sec^{-2}$, approximate value $981 cm.sec^{-2}$).
h	Height of the internal boundary layer (cm).
h'	Height of adapted boundary layer (cm).
k	Von Kármáns constant (0.418).
l	Dimensions of the body e.g. length, height, (cm).
l_m	Mixing length (cm).
m	Roughness change parameter. (calculated from the natural logarithm of the ratio $Z_{0-}:Z_{o+}$).
u	Velocity of flow ($cm.sec^{-1}$).
$u_{(z)}$	Velocity at height z ($cm.sec^{-1}$).
$w\left(\frac{y}{\delta}\right)$	Wake function.
y	Distance from the boundary (cm).
z	Height of measurement (cm).
+	Downstream data.
-	Upstream data.

A Coefficient, between 0.08-0.17, dependent on grain-size.

B Expression of erodability of the soil surface.

C integration constant equivalent to surface roughness.

C_D Drag coefficient.

Cl Climate parameter.

C_o Constant.

E Soil erosion measure.

F Wake function of White and Mounla (1991).

F' Wake function of Owen and Gillette (1984).

Fr Froude number.

H Height of wind tunnel (cm).

I Soil erodability measure.

K Surface roughness measure (cm).

L Unsheltered fetch length upstream (cm).

Q Total mass flux ($g.cm^{-1}.sec^{-1}$).

Qmx Maximum mass transportable by a particular wind ($g.cm^{-1}.sec^{-1}$).

Re Reynolds number.

U_* Velocity gradient du/dz, shear velocity or friction velocity ($cm.sec^{-1}$).

U_*' Velocity gradient during saltation ($cm.sec^{-1}$).

U_{*_i} Instantaneous shear velocity ($cm.sec^{-1}$).

U_{*_t} Fluid threshold velocity ($cm.sec^{-1}$).

U_t Sediment threshold velocity at Z_o' ($cm.sec^{-1}$).

U_∞ Free-stream velocity ($cm.sec^{-1}$).

U_+ Non-dimensional vertical axis.

V Measure of vegetation cover.

X Distance downwind (cm).

Y_+ Non-dimensional horizontal axis.

Z_o Roughness length (cm).

Z_o' Apparent roughness length during saltation.

CHAPTER 1

INTRODUCTION TO AEOLIAN SCIENCE

Aeolian processes 'result from the interaction of the atmosphere, lithosphere, and wind-blown particles' (Greeley, 1986, p.195). 'A unified study of these processes... requires a multidisciplinary approach. The approach commonly employed (however) is not only multidisciplinary but (also) combines field studies with laboratory simulations and theory' (Greeley & Iversen, 1985, p.3.).

(1.1.) A BRIEF HISTORY OF AEOLIAN SCIENCE.

Aeolian (or eolian) is associated with Aeolus, the Greek God of the winds (Clark, 1985). Geographically, the term 'aeolian' relates to all the components of wind action, i.e. wind-borne and wind-deposited sediments, as well as wind eroded landforms. In predominantly loose sediment environments aeolian processes dominate the geomorphology. However, aeolian processes also have a much wider relevance, for example, hazard management (Watson, 1985; Pearce, 1992), palaeoenvironmental reconstruction (Madole, 1995; Begin *et al.,* 1995), archaeology (Steers, 1937, 1959), extra terrestrial studies (Greeley & Blumberg, 1995; Greeley *et al.*, 1980, 1993) and industry (Barker & Grimson, 1990; Glennie, 1998).

The amazingly regular bedforms that form in sand (Bagnold, 1935) and the intriguing, yet uncomfortable, experience of a sand storm, both manifestations of the processes responsible for sand transport, have long caught the imagination of travellers and scientists alike. R.A. Bagnold (1941) was the founder of quantitative aeolian studies. Combining general experiences from the Libyan desert with later wind tunnel and field experiments, Bagnold (1941) detailed almost all of the basic principles of sand transport by wind.

Investigation of aeolian sand transport over the past 50 years has led to the modification and development of the ideas of Bagnold (1941). Advances in technology have facilitated many studies that would not previously have been possible. For example: high speed photography has permitted Willetts and Rice (1985a, 1985b, 1989) and Rice *et al.* (1996) to detail individual grain-bed collisions and the flight trajectories of sand grains in transport; armoured hot-wire probes have made it possible to record near-bed velocities in both the field and wind tunnel at high resolution even during sand transport (Butterfield, 1991, 1993, in press); and continuously recording sand traps have allowed the collection of sand in transport and velocity data over averaging periods of only seconds (Butterfield, 1991; Jackson, 1996a, 1996b; Bauer & Namikas, in press).

Complementary to the ability to collect data more rapidly has been the development in computing power. Modern computing has provided the means to analyse vast quantities of information. From the results of these detailed analyses, numerical model simulations of the sand transport system have been developed (McEwan & Willetts, 1991, 1993a, 1993b; Spies, 1996, Spies & McEwan, in press a and b). Indeed, to date, numerical model predictions of the behaviour of the sand transport system have advanced further than the available physical data required for their verification.

Despite advances in our understanding of the aeolian transport system, it is still not yet possible to predict reliably the rate of transport of sand at any but the most closely monitored sites (Anderson & Haff, 1991). Originally, discrepancies between the predicted and recorded rates of transport of sand were attributed to inefficient equipment, both for the initial collection of data from which the sand transport formulae were generated, and for the collection of data for its verification. Other explanations involved the problems of heterogeneous sand beds (Li & Martz, 1995) and the influence of environmental parameters such as salt (Nickling, 1984) and moisture contents (Bisal & Hsieh, 1966; Namikas & Sherman, 1995).

Continual effort has been expended in addressing the problem of predicting the rate of transport of sediment. One recent development has been the re-appraisal of the assumptions incorporated within the sand transport formulae. In particular, the appropriateness of the assumption of an equilibrium transport rate has been questioned (Sørensen, 1991; McEwan & Willetts, 1993a, 1993b, 1994).

(1.2.) EQUILIBRIUM MASS FLUX.

The rate of transport of sand by wind, or mass flux, 'is defined as the mass of sand passing a line transverse to the transport direction through unit width, in unit time' (McEwan & Willetts, 1994, p.1243). Existing sand transport formulae relate mass flux to some measure of the wind velocity. The derivation of most sand transport formulae includes the assumption of a time and space independent rate of mass flux, i.e. a state of mass flux equilibrium.

In geomorphology, the most applicable interpretation of the term 'equilibrium' is usually that of dynamic equilibrium. A system in dynamic equilibrium is one in which, despite continual internal motions, the external balance between the inputs and the outputs is maintained. With respect to the aeolian transport system, when mass flux is in equilibrium for a unit of time, the rate of sand entering a designated area from upwind is equal to the rate of sand exiting the designated area downwind. Within the designated area there is an exchange of sand grains between the wind and the bed.

In previous derivations (and verifications) of sand transport formulae, it is assumed that sand transport is occurring over a homogenous surface at equilibrium mass flux. In such conditions the rate of transport of sediment is mainly velocity dependent. Data that were time and place specific are thus theoretically, assumed to be universally applicable. The application of these sediment transport formulae is limited, however, to conditions approximating

to equilibrium. To refine and apply existing mass flux relations it is vital that the location and timing of the mass flux equilibrium can be determined.

Bagnold (1936) was the first to allude to the concept of an equilibrium mass flux. In wind tunnel experiments over a test bed of length 9m, Bagnold (1936, 1941) noted that mass flux developed through space. With distance downwind the rate of transport of sediment increased. By the end of the wind tunnel a stable rate of mass flux had apparently been achieved. Since the original experiments of Bagnold (1936, 1941), numerous workers have investigated the spatial development of the sand transport system. For example, in an experiment similar to those of Bagnold (1936, 1941), Shao and Raupach (1992) observed the development of mass flux along the 15m length of a wind tunnel.

In the field, Fryrear *et al.* (1991), Stout and Zobeck (1996), Stetler and Saxton (1996) and Gillette *et al.* (1996) have considered the development of mass flux over distances greater than 200m, whilst Jackson (1996a) and Greeley *et al.* (1996) have considered the development of mass flux over distances less than 200m. The numerical models of Chepil (1965), Stout (1990) and Sterk and Stein (1997), although incorporating a spatial parameter, do not simulate the development of mass flux with distance. At present, the only model to simulate the spatial development of mass flux is that of Spies (1996; Spies & McEwan, in press b) covering a distance of 50m.

The temporal development of the sand transport system was first highlighted by the numerical models of McEwan and Willetts (1991, 1993a, 1993b) and Anderson and Haff (1991). With the ability to simulate the temporal development of mass flux at one second intervals, previously unrecorded variations were witnessed. Butterfield (1991) later confirmed some of the model results in both field and laboratory investigations.

The longer term, periods of an hour or greater, temporal development of the sand transport system has not yet been simulated by the numerical models.

Practically, it is these longer term developments of mass flux that are of more relevance in comparison with field data. In the laboratory, the development of mass flux through time has been monitored over periods of an hour by Rasmussen and Mikkelsen (1991, in press). However, existing studies have yet to consider whether the depletion of the sand bed through time and space is as significant in the field as it is in the laboratory.

Despite existing data on both the spatial and the temporal development of the sand transport system, very little can be stated about the timing and location of the mass flux equilibrium. The problem does not so much stem from contradictory results, but from the varied scales of study which make relationships between available data sets unclear. It is unclear, in any physical environment (field or wind tunnel), when and where equilibrium mass flux is attained, either spatially or temporally. Indeed, it has not conclusively been proven that equilibrium transport is ever achieved in air.

The existence (or attainment) of equilibrium mass flux is essential only for the operation of current sediment transport formulae. Of greater overall importance are the 'three dimensional aspects of transport rate variability' (Butterfield, 1991, p.115). Through the continued study of the spatial and temporal development of the saltation system it may be possible to describe a consistent pattern of mutual development of mass flux and wind velocity.

Information on the three-dimensional development of the saltation system may be used to: explain the current discrepancies between the predicted and recorded mass flux results of sand transport formulae; clarify the location and timing of equilibrium mass flux conditions, if indeed they exist; and, aid the development of new mass transport equations that incorporate the development of the sand transport system through time and space.

In the field, the intermittency of sand transport by the wind, in addition to its three-dimensional nature, make the aeolian transport phenomenon extremely

difficult to measure. The use of wind tunnel environments overcome some of these problems and potentially yields valuable data. However, efforts must be made to relate the results from artificial environments to those of the natural environment; there is little advantage in the production of data that can not be related to the real world (McEwan & Willetts, 1991). This is especially relevant to the concept of equilibrium.

Controlled environments such as wind tunnels permit the reproducibility of experimental conditions. The location and timing of the attainment of equilibrium mass flux is thus constant for identical experimental conditions. In the field, each experiment is conducted under unique environmental conditions. The location for the attainment of equilibrium mass flux, if indeed it is ever achieved in natural environments is, therefore, also unique.

The uncertainty of the attainment of equilibrium in the field environment does not limit the compatibility of field and laboratory studies. Regardless of the attainment of equilibrium, the spatial and temporal developments of the saltation system prior to equilibrium are potentially similar in both environments. Possibilities such as these require further investigation because they present the opportunity to relate the Eulerian and Lagrangian reference frames.

In general, meteorological measurements are made from fixed points in space, i.e. the Eulerian reference system. Most of the fundamental theories of fluid mechanics, however, are based on the Lagrangian reference system, following the behaviour of a fluid element as it moves through the atmosphere. To relate theoretical and physically-collected data, and thus, gain a greater understanding of the aeolian transport system, it is essential that the two reference planes are not mutually exclusive.

In order to analyse the spatial and temporal developments of the saltation system in the research presented here, field and laboratory investigations

were conducted on comparable scales. Practically, the horizontal spatial replication of the experimental conditions required the field experiments to be conducted on the scale of the available wind tunnel facilities. By unifying the horizontal spatial dimension in the two environments one of the major variables limiting the existing data can be overcome. Furthermore, compatibility between data generated in different physical environments can be maximised.

(1.3.) STUDY AIMS.

The aims of this study are to:

- identify how sand transport by air flow is regulated, in space and through time, by the mutual interactions between the evolving states of the sand cloud, the boundary layer air flow and the state of the sand bed. This will be achieved by exploration of the spatial and temporal developments, and interactions between, mass flux, wind velocity and bed shear. (In the wind tunnel an additional consideration will be the influence of upwind artificial sand-feeding).
- conduct field and laboratory measurements (see Fig. 1.1.) on comparable spatial and temporal scales (and, where possible, scales appropriate to numerical models). By generating data on comparable scales from field and laboratory experimental procedures it may be possible to:

  (a) identify the relevant spatial and temporal scales in operation in the different experimental environments;

  (b) begin to address the incompatibilities between data from various experimental procedures, one of the main limitations of contemporary aeolian science;

  (c) decouple the effects of wind tunnel constraints (e.g. compressed boundary layers) from the physical processes controlling the sand transport rate;

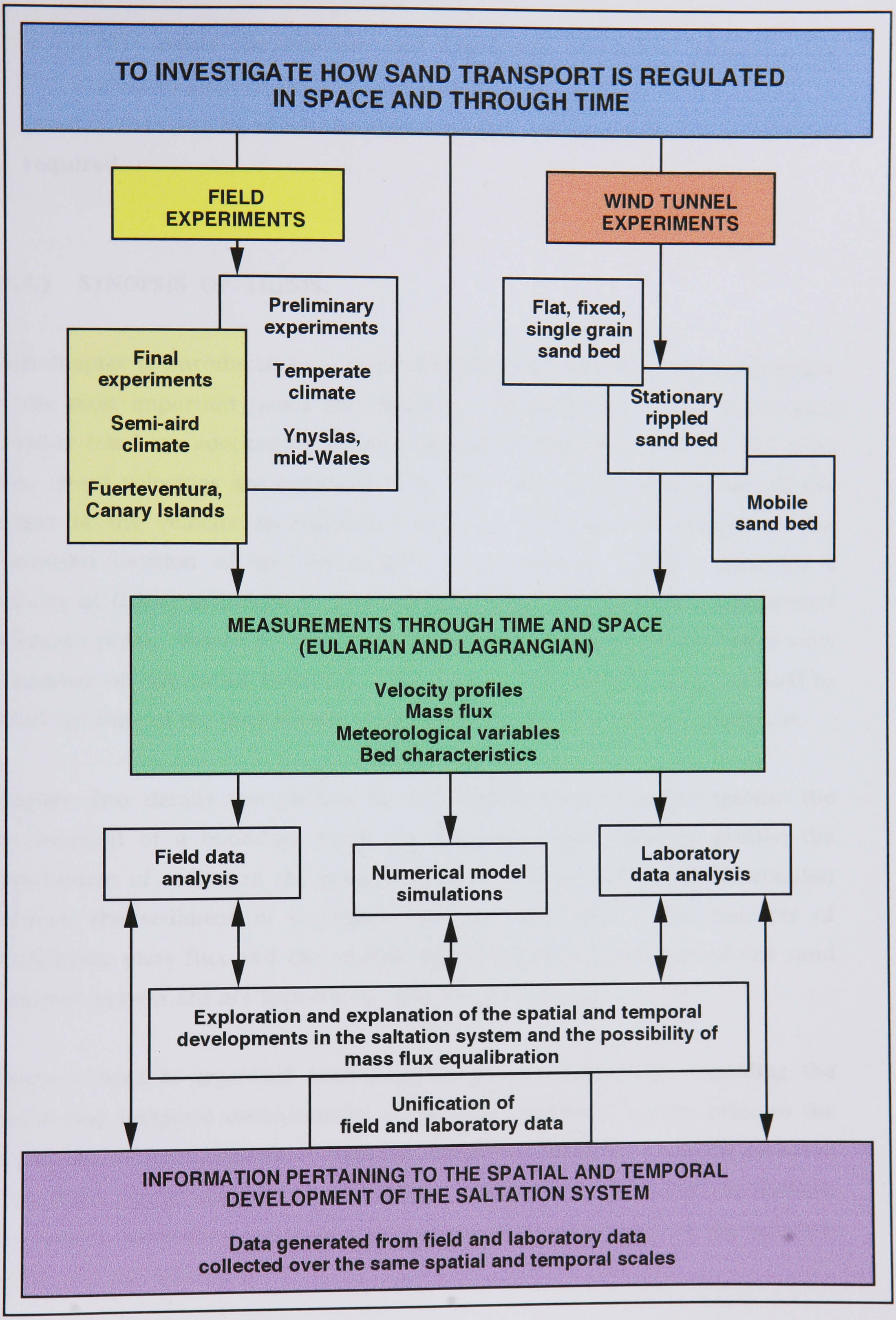

Fig. 1.1. Flow diagram of project data collection and rationale.

(d) relate the Eulerian and Lagrangian reference frames in the measurement of the saltation system.

- produce data sets by which theoretical models can be tested and modified as required.

(1.4.) SYNOPSIS OF THESIS.

Each chapter is introduced by a brief abstract and concluded with a summary of the most important issues and findings. Throughout the text a standard notation has been adopted to identify the spatial aspects of velocity and mass flux. Point velocities are represented by U_x^y. The super-script (y) details the height of the velocity measurement and the sub-script (x) designates the downwind location of the anemometer. For example, $U_{2.00m}^{0.80m}$ identifies a velocity at 0.80m in height at a downwind location of 2m from some defined reference point. Where no sub-script is included, the data are associated with a number of downwind locations. Temporally, the notation $T_{x\min s}$ is used to detail the time of the data sample with respect to the start of the experiment.

Chapter Two details the physics of the aeolian sand transport system: the development of a boundary layer; the boundary layer velocity profile; the entrainment of sediment; the grain-bed collisions; and the mutual interaction between the sediment in transport and the fluid flow. The concepts of equilibrium mass flux and the spatial and temporal development of the sand transport system are not introduced until Chapter Three.

Chapter Three is organised such that the present knowledge regarding the spatial and temporal developments of the sand transport system prior to the attainment of any equilibrium state are detailed separately. Data are included from wind tunnel and field experiments, and numerical model simulations. The factors controlling the spatial and temporal developments of the saltation system are also discussed.

Chapters Four and Five report, respectively, the results of the laboratory and field experiments conducted in this research. Each chapter begins with a detailed description of the experimental procedure and the equipment used. The spatial and temporal results of the development of the sand transport system are discussed initially separately. The mutual interactions of wind velocity and mass flux are reserved for the final section of each chapter.

Laboratory wind tunnel investigations explored the development of the sand transport system over an 8m length. Seven sand traps were located at 1m intervals downwind along the working section of a wind tunnel. Fieldwork was conducted over distances of 10m and 20m. Five sand traps were deployed downwind, spaced in combinations of 2m and/or 4m intervals, to record the mass of sand in transport.

Both field and laboratory data for mass flux are reported as five minute averages. In both environments spatial mass flux data were measured simultaneously at all sites throughout each experimental period. In addition, simultaneous measurements were made of velocity and mass flux at a single site. Following each experiment, spatial velocity data were measured adjacent to all the mass flux sampling sites.

Chapter Six investigates the compatibility of the laboratory and field data collected in this research. In experiments conducted with and without a point of initiation for the saltation system, the importance of the collection of data simultaneously in time and space is highlighted. Throughout the chapter the experimental results obtained in this study are compared to existing theory. Explanations are offered for any discrepancies between the results of various researchers. To conclude, the major findings of this work are reviewed with respect to the original aims of the study. Where appropriate, suggestions are also made for potential future research.

CHAPTER 2

PHYSICS OF THE SALTATION SYSTEM

Aeolian transport studies are but part of the wider study of the transport of solid particles by fluid. Investigation of 'geomorphic systems dominated by fluid flows and erodable surfaces requires an understanding of the mechanics that govern the entrainment, transport and deposition of sediment' (Bauer *et al.*, 1992, p.453). The numerical model of McEwan and Willetts (1991) has identified (and reproduced) the four dominant sub-processes of the saltation system and their mutual interactions (see Fig. 2.1.).

Beginning with the passage of clean air across the boundary surface the model of McEwan and Willetts (1991) simulates the initiation and development of the sand transport system. 'Bed grains are entrained initially aerodynamically, then increasingly by the impact of saltating grains until their numbers are limited through a decelerating wind profile and the system reaches equilibrium' (McEwan & Willetts, 1993a, p.102). Using a flow diagram (see Fig. 2.1.) as a basic structure, the physics of the saltation system are reviewed.

(2.1.) THE BOUNDARY LAYER VELOCITY PROFILE.

(i) Boundary layers.

Boundary layers form due to the adhesion of real fluids to a surface (Munn, 1966). With time and distance, the boundary effects are propagated throughout the entire air column. Due to the boundary retardation of the near wall motion velocity increases with height. Eventually, with increasing height, velocity asymptotically approaches the constant free-stream velocity. At the free-stream height the influence of the boundary surface is negligible.

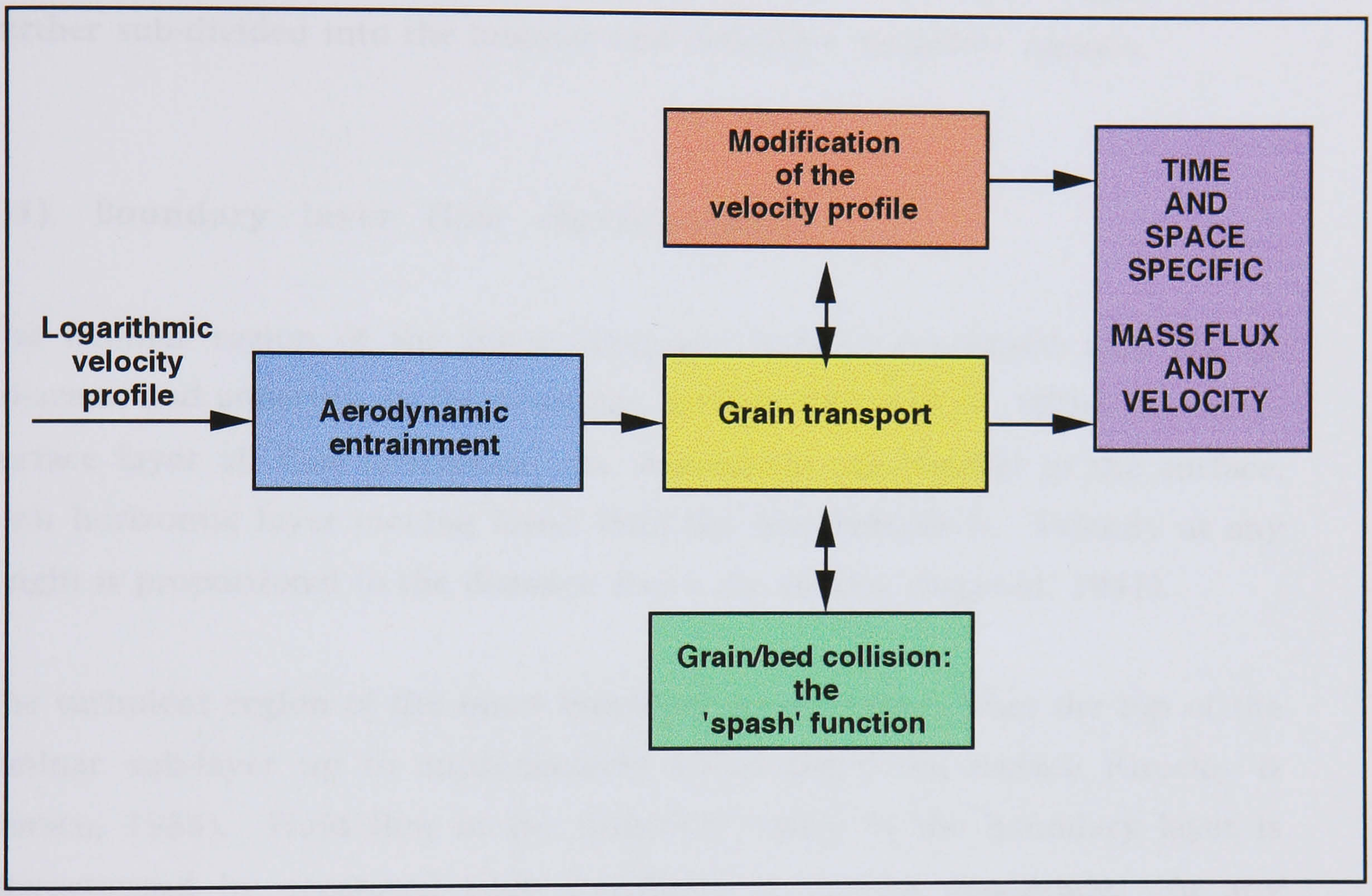

Fig. 2.1. A schematic diagram of the linking of the four main sub-processes of the saltation system. (modified from McEwan & Willetts, p.102, 1993a).

The depth of the boundary layer is generally defined by the height where velocity reaches 99% of the free-stream constant value (Munn, 1966). In the atmosphere the boundary layer is typically of the order of 1km in depth (Oke, 1978). Two regions within the atmospheric boundary layer can be identified: the inner region where frictional drag is influential; and the outer region where friction drag is negligible (Schlichting, 1968, see Fig. 2.2.). Only the inner region is of importance in aeolian studies. This inner region can be further sub-divided into the laminar and turbulent boundary regions.

(ii) Boundary layer flow characteristics.

The laminar region of the inner boundary layer is concerned with the air adjacent, and adhering, to the boundary surface (Oke, 1978). Within the near-surface layer all flow is laminar; the streamlines are parallel to the surface, each horizontal layer moving faster than the one beneath it. Velocity at any height is proportional to the distance above the surface (Bagnold, 1941).

The turbulent region of the inner boundary layer extends from the top of the laminar sub-layer up to approximately 100m above the surface (Greeley & Iversen, 1985). Fluid flow in the turbulent region of the boundary layer is characterised by organised eddy structures of varying magnitude. At any point velocity is instantaneously variable; description is possible only as an averaged condition.

Laminar and turbulent flows are characterised by viscous and inertial forces, respectively (Young, 1989). Above a critical velocity flow undergoes a transition from laminar to turbulent (Tennekes & Lumley, 1972). This transition was first noted by Reynolds who introduced the Reynold's number (Re), representing the ratio of viscous to inertial forces, to define the stability of a fluid. (Laminar and turbulent flows being characterised by small and large Reynold's numbers, respectively).

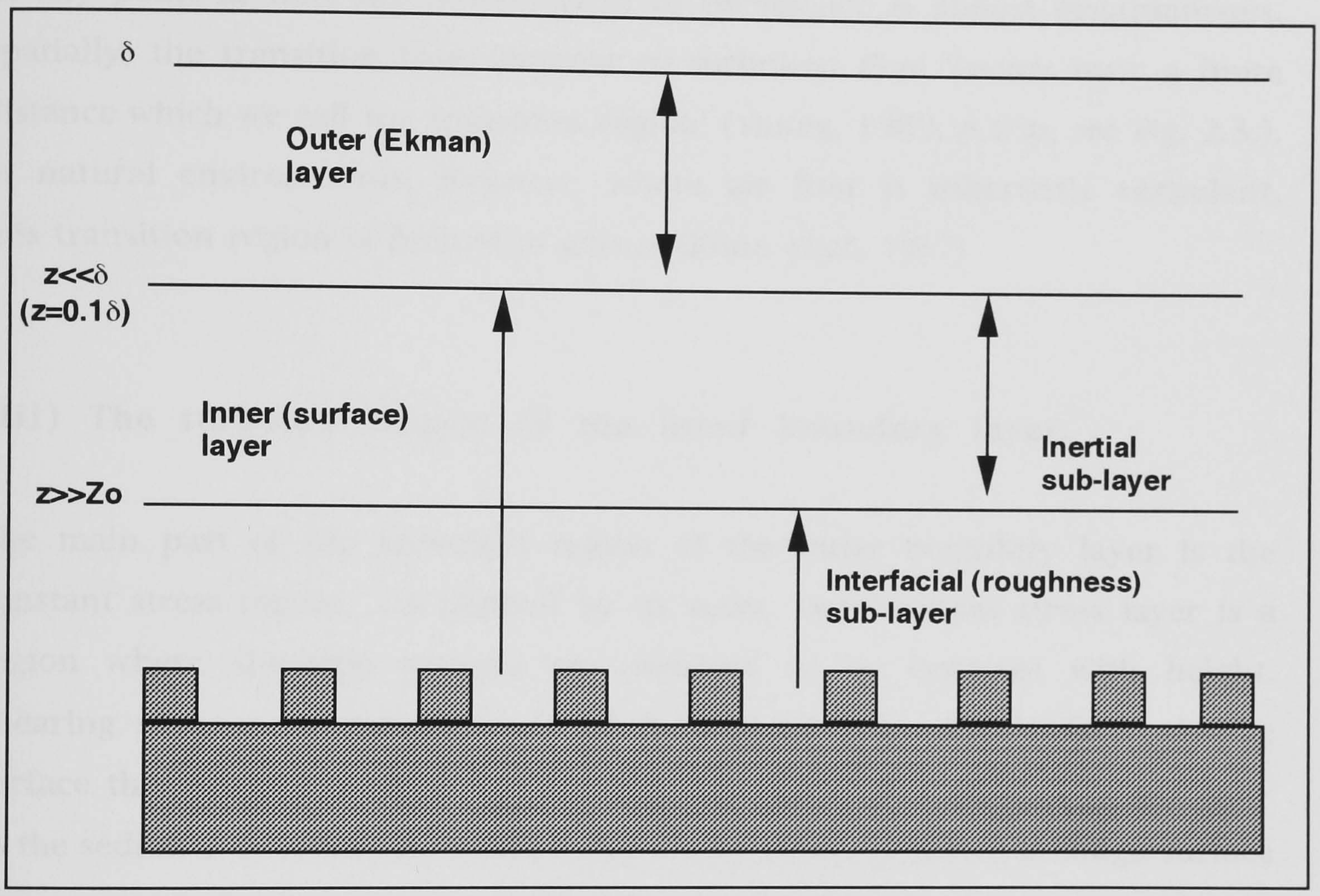

Fig. 2.2. Schematic representation of the atmospheric boundary layer, where δ is the boundary layer depth, z is the height of measurement, and Zo is the aerodynamic roughness (see Ch. 2.3.(iii)). (modified from Garratt, 1992, p.2).

$$Re = \frac{\rho u l}{\nu} \qquad \text{Eq. 2.1.}$$

where ρ = fluid density ($g.cm^{-3}$);

u = velocity of flow ($cm.sec^{-1}$);

l = dimensions of the body e.g. length, height (cm); and

υ = kinematic viscosity ($cm^2.sec^{-1}$).

At any point in time the development of turbulence is almost instantaneous. Spatially, the transition from laminar to turbulent flow 'occurs over a finite distance which we call the transition region' (Young, 1989, p.106, see Fig. 2.3.). In natural environments, however, where air flow is inherently turbulent, this transition region is limited in extent (Kline *et al.,* 1967).

(iii) The turbulent region of the inner boundary layer.

The main part of the turbulent region of the inner boundary layer is the constant stress region. As implied by its name, the constant stress layer is a region where shearing stresses are assumed to be constant with height. Shearing stresses are generated as air is dragged across the surface. At the surface the measure of the force per unit horizontal area applied tangentially to the sediment is called the *surface shear stress* (Oke, 1978). Although surface shear stress is fundamental to studies of sediment erosion, attempts to measure it directly have proved problematic (Zingg, 1953; Hayashi, 1984).

In general, surface shear stress is estimated indirectly from the shearing stresses propagated by the surface throughout the atmosphere. This is manifest by a change in wind velocity with height (Munn, 1966). Only within a boundary layer developed over clean air, neutral adiabatic atmospheric conditions over a homogeneous surface, however, does the constant distribution of shearing stresses and the resulting logarithmic velocity profile exist (Tritton, 1988).

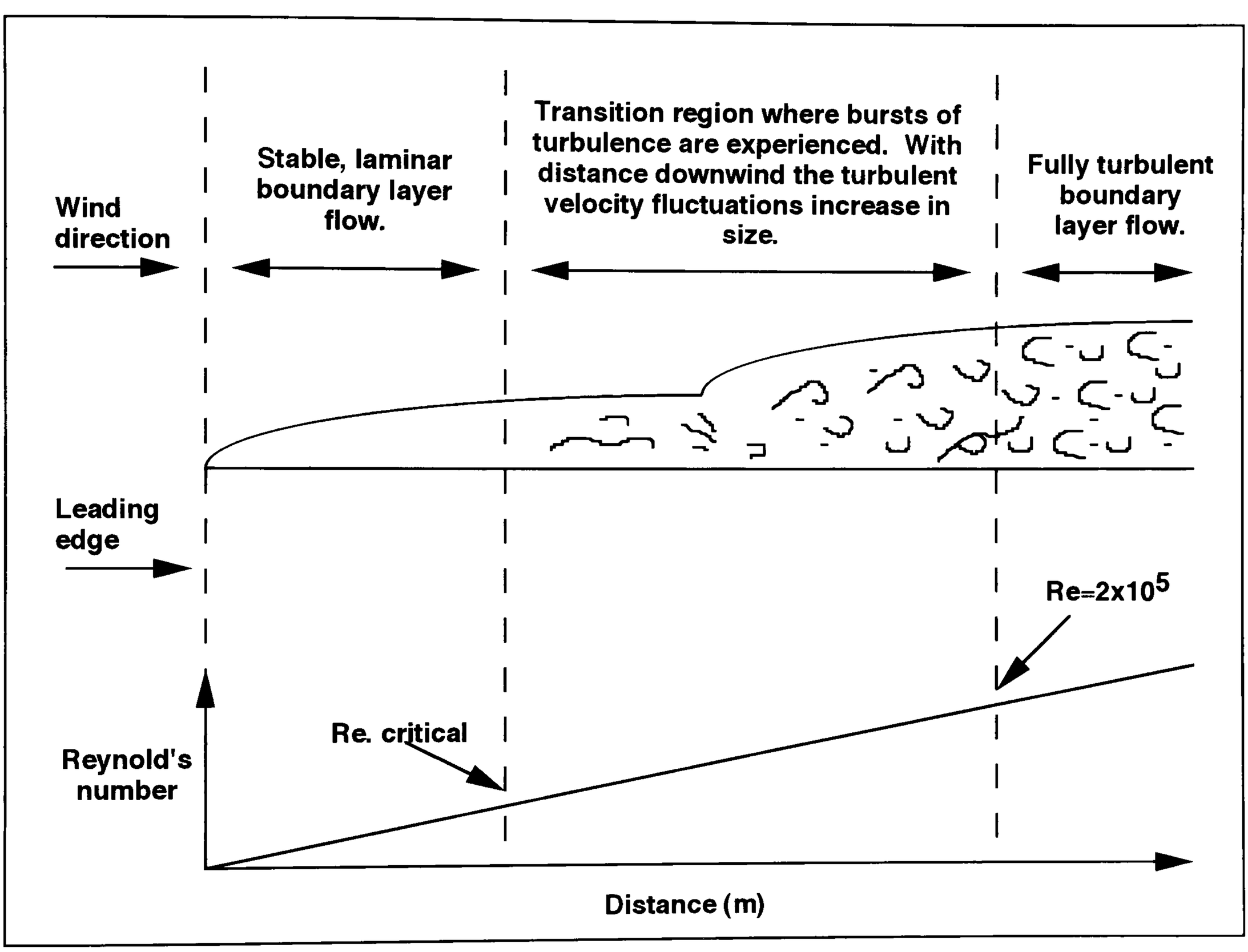

Fig. 2.3. Boundary layer flow transition from laminar to turbulent flow (over a flat plate) in the wind tunnel. (modified from Williams, 1986, p.144).

The full equations of motion of a viscous fluid are described in the Navier Stokes equations. These equations are too complex for general use and accepted boundary layer theory is founded on the work of Prandtl. Prandtl observed that the relative thickness of the boundary layer at large Reynolds numbers allowed simplifications to the Navier Stokes equations (Schlichting, 1968; Young, 1989). Prandtl showed that fluid flows could be described mathematically if the frictional effects connected with the viscosity of the fluid were considered only when essential.

By introduction of a mixing length (l_m) concept, Prandtl measured the distances travelled by an eddy before it became totally mixed within the fluid, i.e. the exchange of fluid momentum between a parcel of air and the surrounding atmosphere:

$$l_m = kz \qquad \text{Eq. 2.2.}$$

where k is von Kármán's constant.

The distribution of velocity with height within the constant stress region can be described by the Prandtl-von Kármán equations, collectively known as the 'Law of the Wall'.

$$u_{(z)} = \left(\frac{U_*}{k}\right) \ln\left(\frac{z - d_o}{Z_o}\right) \qquad \text{Eq. 2.3.}$$

where $u_{(z)}$ is velocity at height z ($cm.sec^{-1}$);

U_* is shear velocity ($cm.sec^{-1}$); and

d_o is the displacement height (cm).

However, d_o is insignificant compared to Z_o and so is generally neglected (Jackson, 1981).

According to the 'Law of the Wall' velocity is a logarithmic function of the relative distance from the bed, thus plotting as a straight line on semi-logarithmic paper (Young, 1989). Shear velocity is proportional to the slope of the velocity profile in the constant stress region. Bagnold (1941, p.51)

demonstrates the factor of proportionality to be 5.75. Shear velocity is related to the horizontal surface shear stress (τ) by the expression:

$$\tau = (\mu + \eta)\frac{du}{dz} \qquad \text{Eq. 2.4.}$$

where μ is the laminar eddy viscosity ($cm^2.sec^{-1}$);

η is the turbulent eddy viscosity ($cm^2.sec^{-1}$); and

$\frac{du}{dz}$ is the velocity gradient.

or

$$\tau = \rho U_*^2 \qquad \text{Eq. 2.5.}$$

Turbulent eddy viscosity can be expressed as:

$$\eta = \rho(l_m)^2 \frac{du}{dz} \qquad \text{Eq. 2.6.}$$

Ignoring the negligible effects of laminar viscosity within the turbulent boundary layer and substituting Eq. 2.6. into Eq. 2.4.:

$$\frac{du}{dz} = \frac{\tau}{\rho(l_m)^2 \frac{du}{dz}} \qquad \text{Eq. 2.7.}$$

Substituting Eq. 2.2. into Eq. 2.7. and additionally incorporating Eq. 2.5.:

$$\left(\frac{du}{dz}\right)^2 = \frac{\tau}{\rho(kz)^2}$$

$$\equiv \qquad \text{Eq. 2.8.}$$

$$\frac{du}{dz} = \left(\frac{\tau}{\rho}\right)^{\frac{1}{2}} \cdot \frac{1}{kz} \equiv \frac{U_*}{kz}$$

Integrating the above equation yields the logarithmic wind velocity profile of Eq. 2.3.

(iv) The wake region of the boundary layer.

Above the constant stress region there exists, in all boundary layers, a wake region. In natural environments the constant stress region of the boundary layer is of sufficient vertical extent for the wake region to be inconsequential to the collection of velocity data for particulate transport studies (McKenna Neuman & Maljaars, 1997). Even during saltation there is a large region of grain free air where the 'Law of the Wall' can be applied.

Originally, wind tunnel studies followed the same ideology as field studies for the calculation of shear velocity, i.e. the application of the 'Law of the Wall' to the whole of the constant stress region of the velocity profile during clean air conditions, and the grain free region of the velocity profile during conditions of sediment transport. This methodology, however, failed to acknowledge the complexities of constrained flows.

Under certain experimental conditions in a wind tunnel the boundary layer may be composed of both the constant stress and the wake regions (see Fig. 2.4.). In such conditions, the wind tunnel velocity profile, even in clean air, is non-logarithmic. The deviation from the logarithmic profile at height is due to the higher velocities associated with the wake region (Janin & Cermak, 1988; Spies *et al.,* 1995).

The existence of a wake region does not preclude the calculation of shear velocity from the constant stress region of a boundary layer. In small wind tunnels, however, the existence of a wake departure limits the vertical extent of the constant stress region and thus the data available. During saltation, furthermore, the constant stress region may be entirely engulfed by the saltation layer.

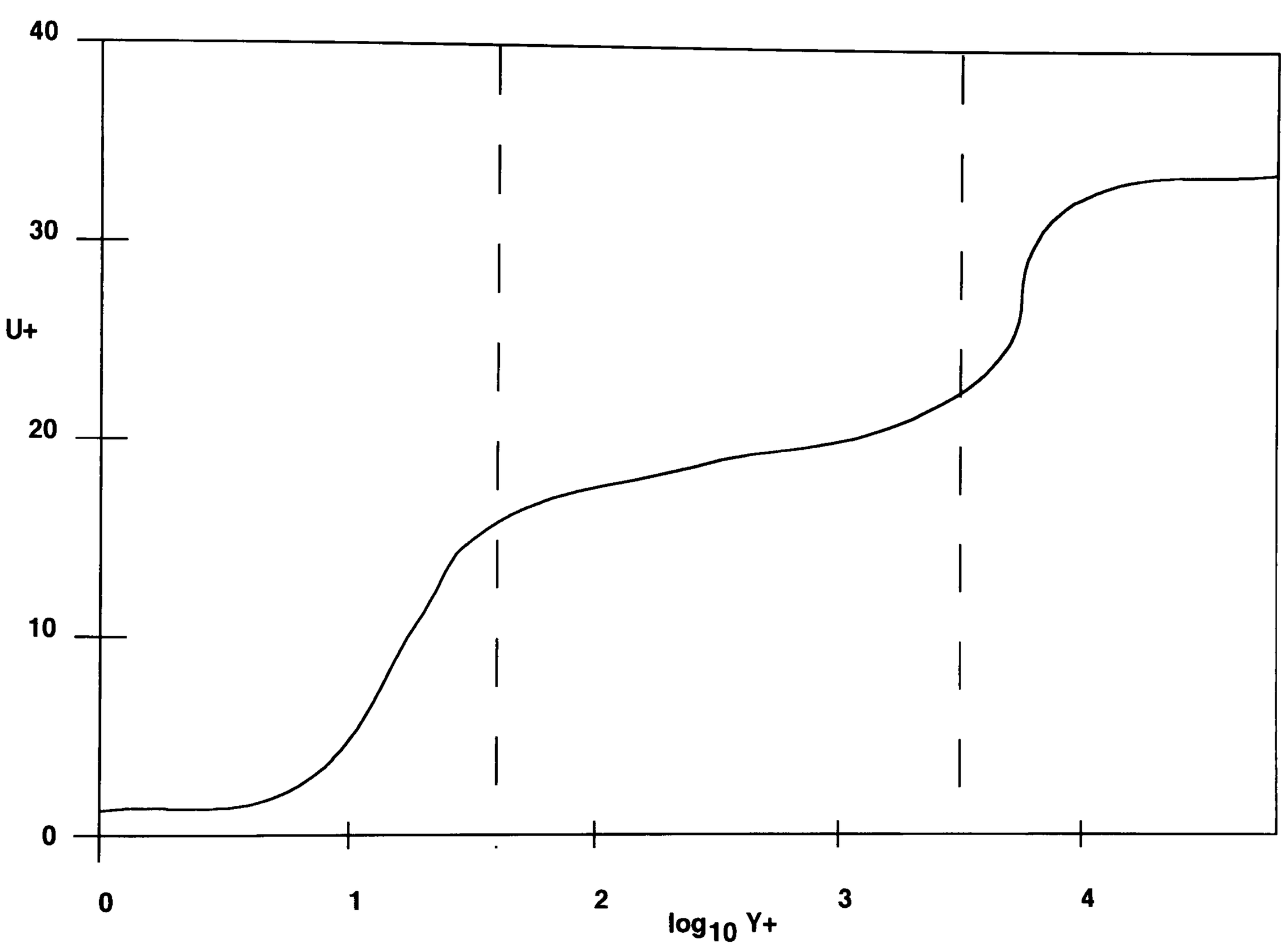

Fig. 2.4. Major divisions in a compressed turbulent boundary layer (plotted on non-dimensional axes where $Y+ = zU_*/\upsilon$ and $U+= u/U_*$). Three regions are distinguishable: the viscous sub-layer, $1<Y+<30$; the constant stress region, $30<Y+<3000$; and the outer region with the wake departure, $Y+>3000$. (modified from Spies *et al.*, 1995, p.516).

To permit the calculation of shear velocity from velocity data collected within the entire depth of the wind tunnel velocity profile (including data from the wake region) Spies *et al.* (1995) contend that Coles (1956) 'Law of the Wake' must be employed. The 'Law of the Wake' provides a full description of a non-logarithmic velocity profile:

$$\left(\frac{u_{(z)}}{U_*}\right) = \frac{1}{k}\ln\left(\frac{yU_*}{\upsilon}\right) + C + \frac{\Pi}{k}w\left(\frac{y}{\delta}\right) \qquad \text{Eq. 2.9.}$$

where y is distance from the boundary (cm);

C is an integration constant equivalent to the surface roughness;

Π is Cole's boundary layer profile parameter, $\Pi = k\left(\frac{\delta_* U_\infty}{\delta U_*}\right) - 1$;

δ^* is the displacement thickness (cm);

U_∞ is the free-stream velocity (cm.sec^{-1}); and

$w\left(\frac{y}{\delta}\right)$ is the wake function equal to $2\sin^2\left[\left(\frac{\Pi}{2}\right)\left(\frac{y}{\delta}\right)\right]$.

The dependency of the boundary layer parameter, Π, on shear velocity, the parameter ultimately required, complicates the use of the 'Law of the Wake'. However, attempts to calculate the value of the boundary layer parameter have been made from extrapolations of the non-dimensional velocity profile to its intersection with the ordinate axis (Coleman, 1981; Spies *et al.,* 1995). Using this method and measurements made by Klebanoff (1954, in Spies *et al.*, 1995), Coles estimates Π to be 0.55 for clean air profiles with a zero pressure gradient. (A value later confirmed by White and Mounla, 1991).

The existence of a wake deviation in wind tunnel velocity profiles is not detected by all aeolian researchers. McKenna Neuman and Maljaars (1997) do not record a deviation in their clean air velocity profiles. This result is essentially due to the greater vertical extent of their wind tunnel, as compared to the Queen Mary and Westfield wind tunnel employed by Spies *et al.* (1995). Secondary influences also include the use of a suction wind tunnel (Coles,

1956) and a marginal range of experimental velocities (Y+<4000, McKenna Neuman & Maljaars, 1997, see Fig. 2.4.).

The existence of a wake departure in a compressed boundary layer is obviously dependent on the design specifications of both the wind tunnel and the experiments. In the Queen Mary and Westfield wind tunnel, the clear deviation from the logarithmic velocity profile during clean air conditions supports the existence of a wake region. As a result, the 'Law of the Wake' is considered arguably the most correct method for the determination of shear velocity from velocity profiles generated within that environment.

(2.2.) SEDIMENT TRANSPORT.

(i) Aerodynamic entrainment.

'Fundamental to sediment transport is the turbulent transfer of momentum from the fluid to the bed' (Bauer *et al.*, 1992, p.453). The force of the wind on a particle at rest results in lift and drag forces. Vertical lift is generated by the acceleration of flow over a grain (Sarre, 1987). The lower pressures accompanying higher velocities (Bernoulli's equation) produce an upward suction or lift (Bagnold, 1956, 1973).

Drag acts horizontally in the direction of the wind and is the main process in operation downwind of a leading edge (Willetts *et al.*, 1991). Drag includes two components. Surface drag is the skin friction between the particles and the air and form drag is produced by the difference in pressure between the windward and the leeward sides of the particles. Once the forces of lift and drag exceed the collective gravitational weight and cohesive forces of the particle, entrainment results.

Bagnold (1941) describes the threshold movement of particles due to the direct pressure of the wind, for the whole bed, by:

$$U_{*t} = A\left[\left(\frac{\alpha - \rho}{\rho}\right) dg\right]^{\frac{1}{2}} \qquad \text{Eq. 2.10.}$$

where U_{*t} is the fluid threshold for motion ($cm.sec^{-1}$);

A is a coefficient dependent on grain characteristics, a value between 0.1 (Bagnold, 1941) and 0.17 (Lyles & Krauss, 1971);

α is the density of the sand ($g.cm^{-3}$);

d is grain diameter (cm); and

g is acceleration due to gravity ($cm.sec^{-2}$).

The minimum threshold velocity for entrainment occurs at a grain-size of approximately 0.08mm (see Fig. 2.5.) For grain-sizes <0.08mm, the coefficient A is inversely proportional to grain-size due to the higher resistance of finer material (Bagnold, 1954). The relationship between the coefficient A and grain-size for fine material is well described by the Shields entrainment function (Miller *et al.*, 1977; Shaw, 1988).

Numerous equations describe the entrainment threshold for specific grain-sizes. However, aerodynamic entrainment of particles only occurs when the turbulent intensity of the boundary layer produces instantaneous shear velocities (U_{*i}) greater than the fluid threshold for the particles (U_{*t}) (see Fig. 2.6.). Both these factors are variable in time and space.

The entrainment threshold of unimodal particles was evaluated by Williams *et al.* (1990a, 1994) in a wind tunnel (downwind on a flat plate) using a single grain depth strip of bed. Through time, at any location, the sand bed erodes according to an inverse exponential function proceeding upwind from the downwind edge (Williams *et al.*, 1990b). Spatially, the threshold for particle entrainment (U_{*t}) decreases downwind (Williams *et al.*, 1990b, 1994). However, the time for total erosion of the bed strips increases downwind due to the increased turbulence reducing the proportion of time when $U_{*i} > U_{*t}$.

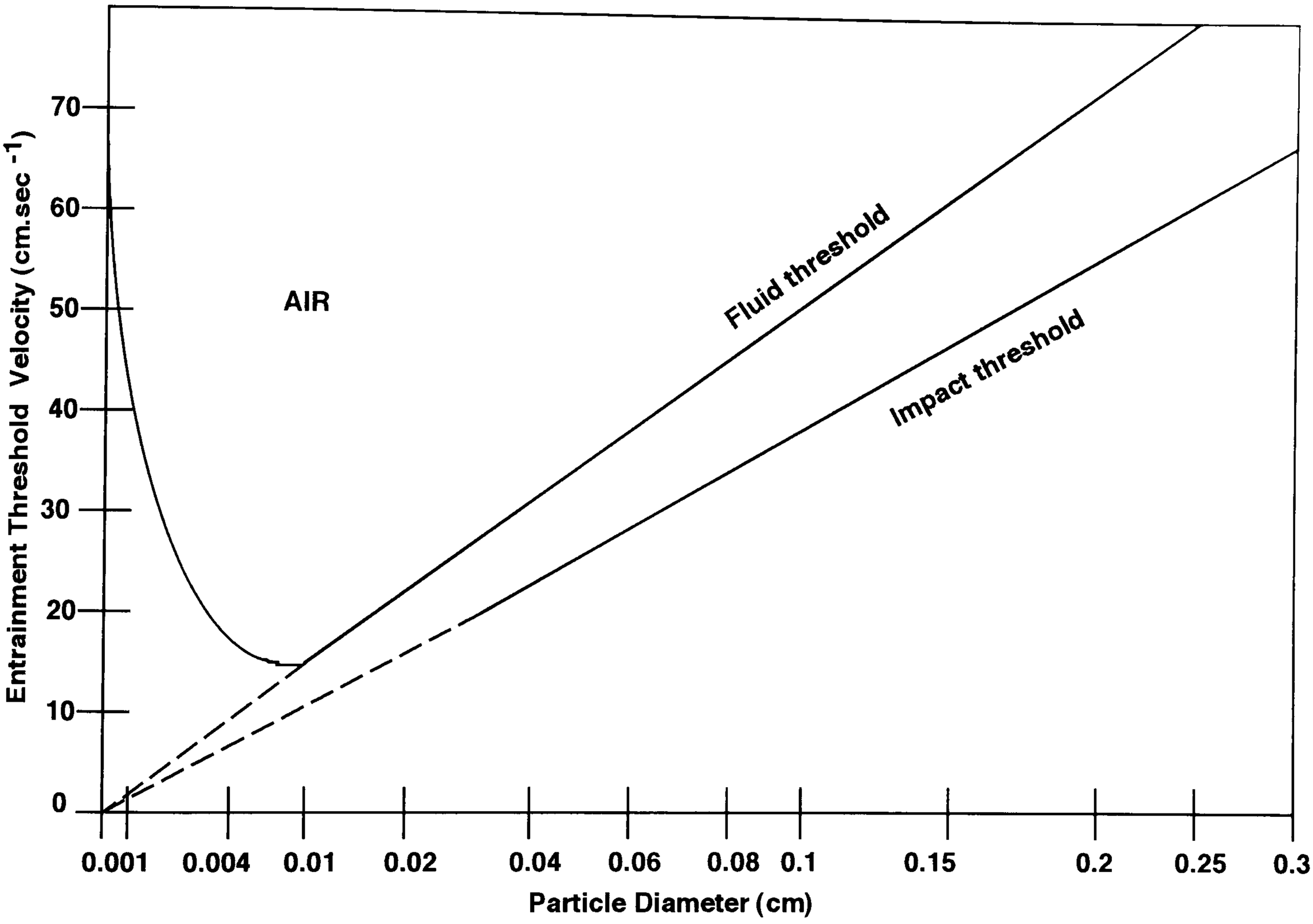

Fig. 2.5. Particle entrainment thresholds. (modified from Bagnold, 1941, p.58).

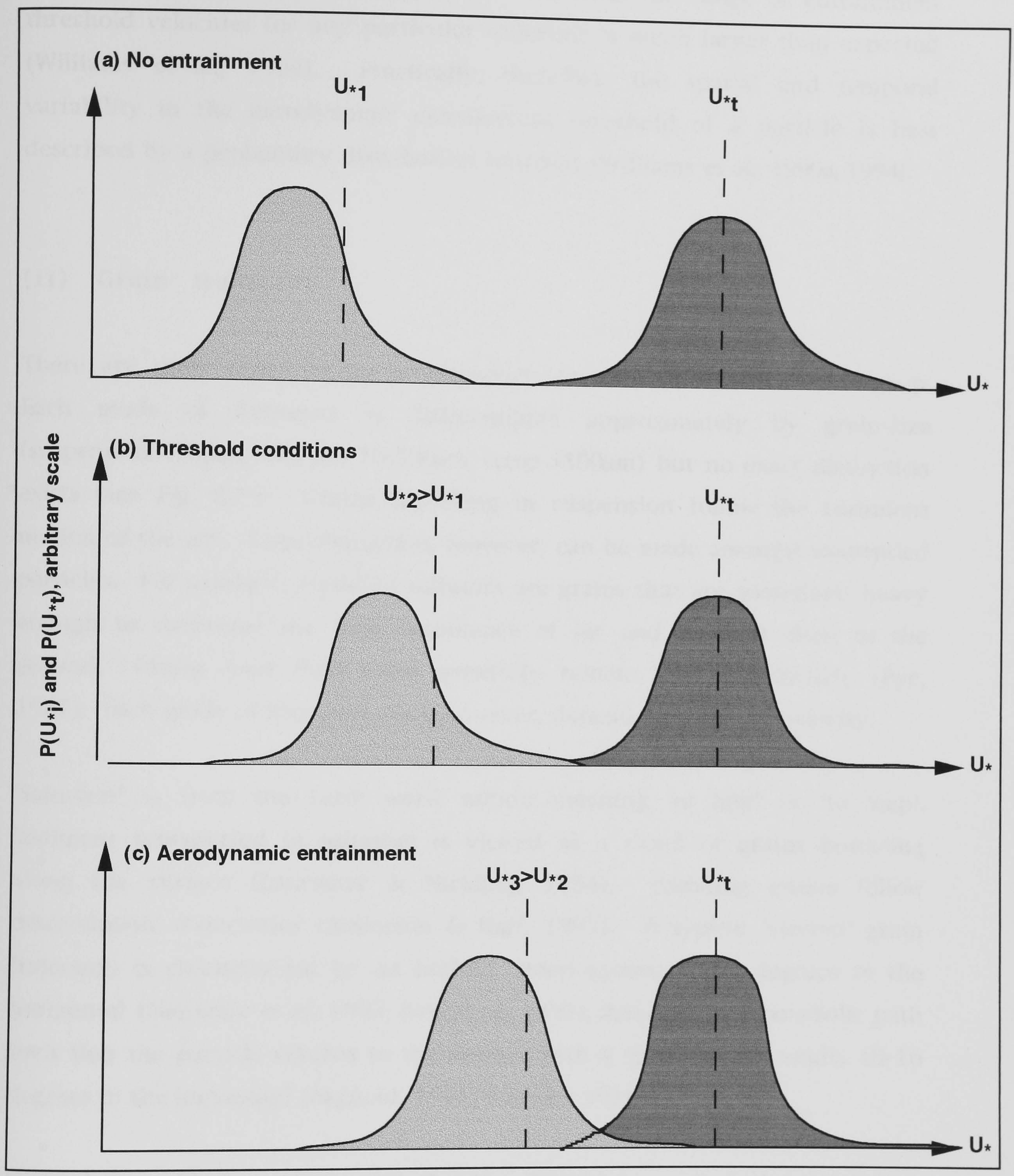

Fig. 2.6. Probability distribution of the fluid threshold and transport conditions. (modified from Williams *et al.*, 1994, p.321).

For any particular particle a unique fluid threshold can be defined according to its location and time (Grass, 1970). However, the range of entrainment threshold velocities for any particular sediment is much larger than expected (Williams *et al.*, 1994). Practically, therefore, the spatial and temporal variability in the aerodynamic entrainment threshold of a particle is best described by a probability distribution function (Williams *et al.*, 1990a, 1994).

(ii) Grain transport.

There are three main modes of transport: suspension, saltation and creep. Each mode of transport is differentiated approximately by grain-size (suspension <70μm, saltation 70-500μm, creep >500μm) but no exact distinction exists (see Fig. 2.7.). Grains travelling in suspension follow the turbulent motion of the air. Some distinction, however, can be made amongst suspended particles. For example, modified saltators are grains that are sometimes heavy enough to overcome the high turbulence of air and descend close to the ground. Grains finer than 20μm generally remain aloft indefinitely (Pye, 1987). Each mode of transport does, however, depend on the wind velocity.

'Saltation' is from the Latin word *saltare* meaning 'to hop' or 'to leap'. Sediment transported in saltation is viewed as a cloud of grains bouncing along the surface (Lancaster & Nickling, 1994). Saltating grains follow deterministic trajectories (Anderson & Haff, 1991). A typical 'ejected' grain trajectory is characterised by an initially steep ascent, 40-60 degrees to the horizontal (Nalpanis *et al.*, 1993; Rice *et al.*, 1995), followed by a parabolic path such that the particle returns to the surface with a small impact angle, 10-16 degrees to the horizontal (Bagnold, 1941; Rumpel, 1985).

Within the saltation layer the density distribution of grains decreases exponentially with height (Bagnold, 1941; Williams, 1964). Although a saltating grain in desert environments may reach 1.50-2m (Bagnold (1941)

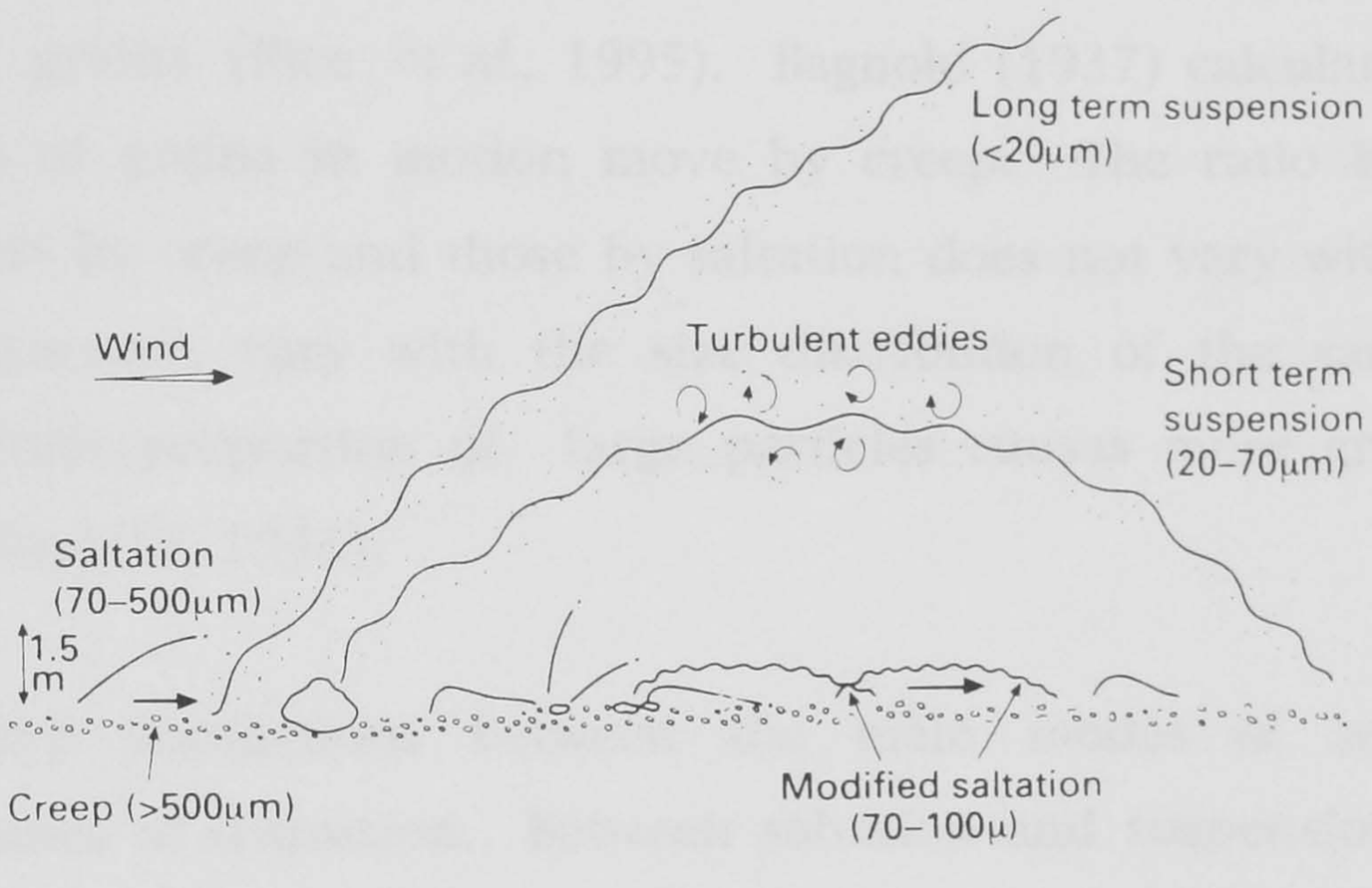

Fig. 2.7. Modes of particle transport by the wind. (Nickling, in Pye, 1994, p.309).

most grains travel within 1-2cm of the surface (Sharp, 1963). Vertically the grains are segregated by size (Belly, 1962, in Sarre, 1987; Stout & Zobeck, 1996; Stetler & Saxton, 1996), smaller particles tending to travel at higher levels (Greeley *et al*, 1983). At any height the sediment size in transport increases with increasing shear velocity (Williams, 1964; Gerety, 1985; Leys & McTainsh, 1996).

Creep is the movement of large particles (up to six times the size of the saltating grains) on the surface in response to impacting 'nudges' from incoming saltating grains (Rice *et al.,* 1995). Bagnold (1937) calculated that approximately 25% of grains in motion move by creep. The ratio between particles in transport by creep and those by saltation does not vary with wind speed. It does, however, vary with the size distribution of the sand bed population, i.e. a high proportion of large particles causes more grains to move in saltation (Bagnold, 1941).

There are no sharp distinctions between the main modes of sediment transport, rather zones of transition. Between saltation and suspension there are some particles, termed 'modified saltators', that display characteristics common to both regions, i.e. semi-random particle trajectories. In the transition between creep and saltation a population of low energy reptating grains exist. Reptating grains, unlike saltating grains, do not have the energy to continuously rebound (Ungar & Haff, 1987; Haff & Anderson, 1993). Both populations of grains, however, are generated via the impact of an existing saltating grain with the bed.

(iii) Grain/bed collisions: the 'splash' function.

Transport processes are initiated by direct aerodynamic entrainment (Willetts *et al.,* 1991). Once the sediment has been set in motion the impact of saltating grains with the surface act as 'seeding agents' for further dislodgements. The

change from an aerodynamically controlled, to an impact-dominated transport system was recorded by Bagnold (1941) in the reduction of the threshold velocity from the fluid to the impact value (see Fig. 2.5.).

The impact threshold velocity is approximately 80% of the fluid threshold velocity. The impact threshold can still, therefore, be described by Eq. 2.10. but with modification of the coefficient A from 0.10 to 0.08. The decrease in the threshold velocity with the development of the saltation system represents a hysteresis, less energy being required to maintain than initiate motion.

An impact of a saltating grain with the surface rarely occurs at a single site. More commonly, the impacting grain 'ploughs through the surface grains, hitting several on its way' (Rice *et al.,* 1996, p.21). The distance a grain covers as it hits the ground is known as the average bed contact length (Rice *et al.*, 1996).

On impact with a cohesionless bed of sand sized particles a saltating grain has over a 94% chance of rebounding or being replaced by another single ejecta (Mitha *et al.,* 1986). When a saltating grain ricochets from the bed it retains 50-60% of its original velocity; the remaining 40% is lost in the ejection of a number of other grains and the dissipation of energy to the surface (Rice *et al.*, 1996).

Grains ejected from the bed, in general, travel at one tenth the speed of the impacting grain (Rice *et al.,* 1996). Although ejecta can emerge at any angle between 0-180 degrees, most travel between 40-60 degrees, faster ejecta moving at lower angles. The number of grains ejected from a saltator impact with the bed is termed the 'mean replacement capacity'. Fewer grains are ejected as the average bed contact length increases (Rice *et al.,* 1996).

In the early stages of development of the saltation system the mean replacement capacity is large. The 'exponential growth in mass flux is only

curtailed when the extraction of momentum from the wind is sufficient to alter significantly the wind velocity profile, which in turn alters the impact velocity of the grains' (Anderson & Haff, 1988, p.822). With time and distance, the number of ejecta from each grain bed collision declines.

At a mean replacement capacity of unity, the wind is imparting only sufficient energy to the grains in transport to maintain, following the grain bed collisions, that original rate of transport of sediment. For any additionally entrained grain, therefore, another grain must be deposited. At this state the saltation system is technically in *equilibrium.*

Mathematically the grain bed collision has been described in a statistical 'splash function' (Ungar & Haff, 1987; Werner & Haff, 1988; Anderson & Haff, 1991). Incorporation of the 'splash function' into numerical models has permitted the more physically correct generation of an artificial saltation system. The only remaining limitation of the 'splash function' is the lack of cross-width spatial variability. An additional related factor may also be the need to continue to incorporate direct aerodynamic entrainment during impact processes, especially for grains of low sphericity Rice (1991).

(2.3.) SALTATION MODIFIED WIND VELOCITY PROFILES.

(i) Extraction of momentum by the grains in transport.

The 'Law of the Wall' describes the velocity profile within the constant stress region of the boundary layer only during clean air, neutral adiabatic atmospheric conditions, over a homogenous surface (see Ch. 2.1.(iii)). The application of the logarithmic equation to a velocity profile measured during saltation is not appropriate without modification.

Bagnold (1941) was the first to document the influence of the saltation cloud on the wind. He realised that the grains were not only accelerated by the

wind, but the wind itself was decelerated by the sand (Bagnold, 1935). In time this reactive mechanism should lead to the attainment of equilibrium transport conditions (see Ch. 2.2.(iii)).

Within the saltation cloud wind velocities at a given height above the bed are less than their clean air equivalent (Gerety, 1985, see Fig. 2.8.). The deviation in the near-bed velocities during saltation, compared to those extrapolated from the clean air velocities above the saltation cloud, produces a non-logarithmic, 'kinked' velocity profile (McEwan, 1993).

Bagnold (1937, 1941) interpreted the 'kink' in the velocity profile as the height of maximum sand transport (i.e. within 1-2cm of the bed (Sharp, 1963, Ch. 2.2.(ii))). Using the assumption of a characteristic saltation trajectory all the grains attain the bulk of their momentum from the wind at the top of their trajectory. It is at this height also that the grains impose the maximum drag on the air.

The velocity dependency of the height of the 'kink' in the velocity profile supports the hypothesis of Bagnold (1941). However, Anderson and Haff (1991) have shown the characteristic grain trajectory proposed by Bagnold (1941) to be an oversimplification of the saltation system. The 'kink' in the velocity profile has, therefore, been re-addressed by McEwan (1993) from first principles.

In all fluid flows total shear stress is constant with height. In clean air total shear stress is simply fluid shear stress. During sand transport total shear stress within the saltation layer is composed of two complementary components: grain borne shear stress (Owen, 1964); and fluid shear stress (McEwan & Willetts, 1993a, 1993b).

If it is assumed that fluid shear stresses are constant with height, i.e. as in clean air, then the 'Law of the Wall' describes the velocity profile (see Ch.

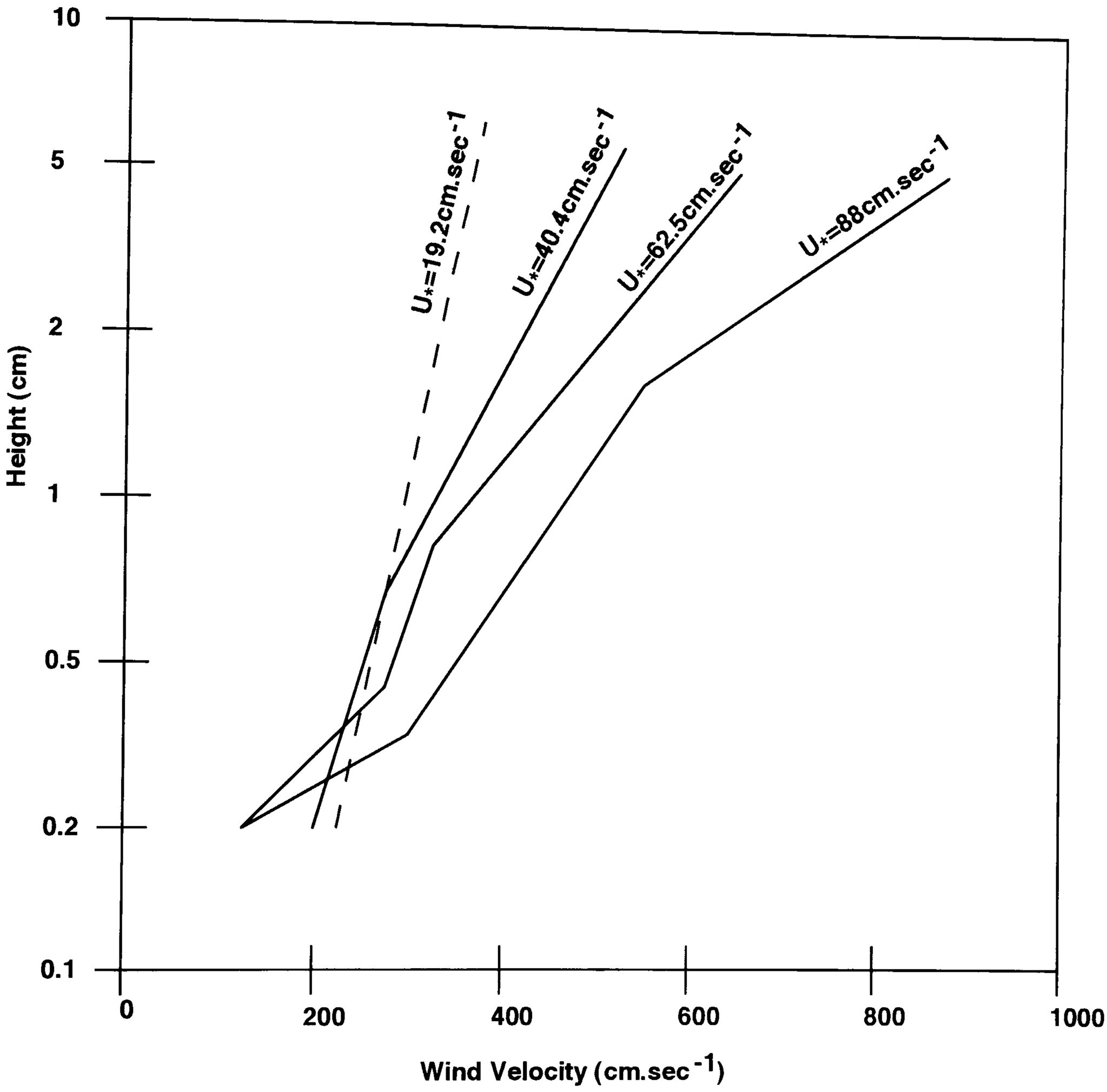

Fig. 2.8. Mean velocity profiles recorded in the wind tunnel. Solid plots indicate data collected during saltation. Dashed plot represents clean air data. (modified from Bagnold, 1941, p.58).

2.1.(iii)). By deduction, therefore, if the 'Law of the Wall' does not describe the velocity profile then it is reasonable to assume that this is because fluid shearing stresses are no longer constant with height (McEwan, 1993).

During saltation the vertical distribution of grains within the saltation layer is used as a surrogate for grain borne shear stress. Grain borne shear stress thus decreases exponentially as height increases. To maintain an overall constant total shear stress within the saltation layer, fluid shear stress is at a minimum at the surface rising to a maximum at the top of the grain layer.

McEwan (1993) uses a hyperbolic tangent to describe the fluid shear stress distribution (see Fig. 2.9.). Unlike the triangular fluid shear stress distribution, similar to Raupach's (1991) distribution within vegetation, the hyperbolic tangent distribution has no discontinuity at the top of the saltation layer. Instead, there is a 'kink' at z=10mm on the logarithmic vertical scale and z=5.77mm on the linear vertical scale.

Both of the velocity profiles generated from the triangular and hyperbolic tangent fluid shear stress distribution exhibit a curvature which is convex upwards (McEwan, 1993, p.151, Fig. 6). Mathematically a 'kink' represents the maximum rate of change in the velocity profile from the lower gradient segment to the higher. Only the velocity profile based on the hyperbolic tangent fluid shear stress distribution produces a mathematically definable 'kink'. The inflection point on the hyperbolic tangent fluid shear stress distribution may, therefore, help to explain the 'kink' in the velocity profiles.

Overall, McEwan (1993) partly confirms the original hypothesis of Bagnold (1941) that the extraction of momentum by the grains in motion are responsible for the 'kink' in the velocity profile. However, he additionally acknowledges and incorporates the suggestion by Anderson and Haff (1991), that the 'kink' is not due to the characteristic mean trajectory height of the particles but rather a manifestation of all grain trajectories.

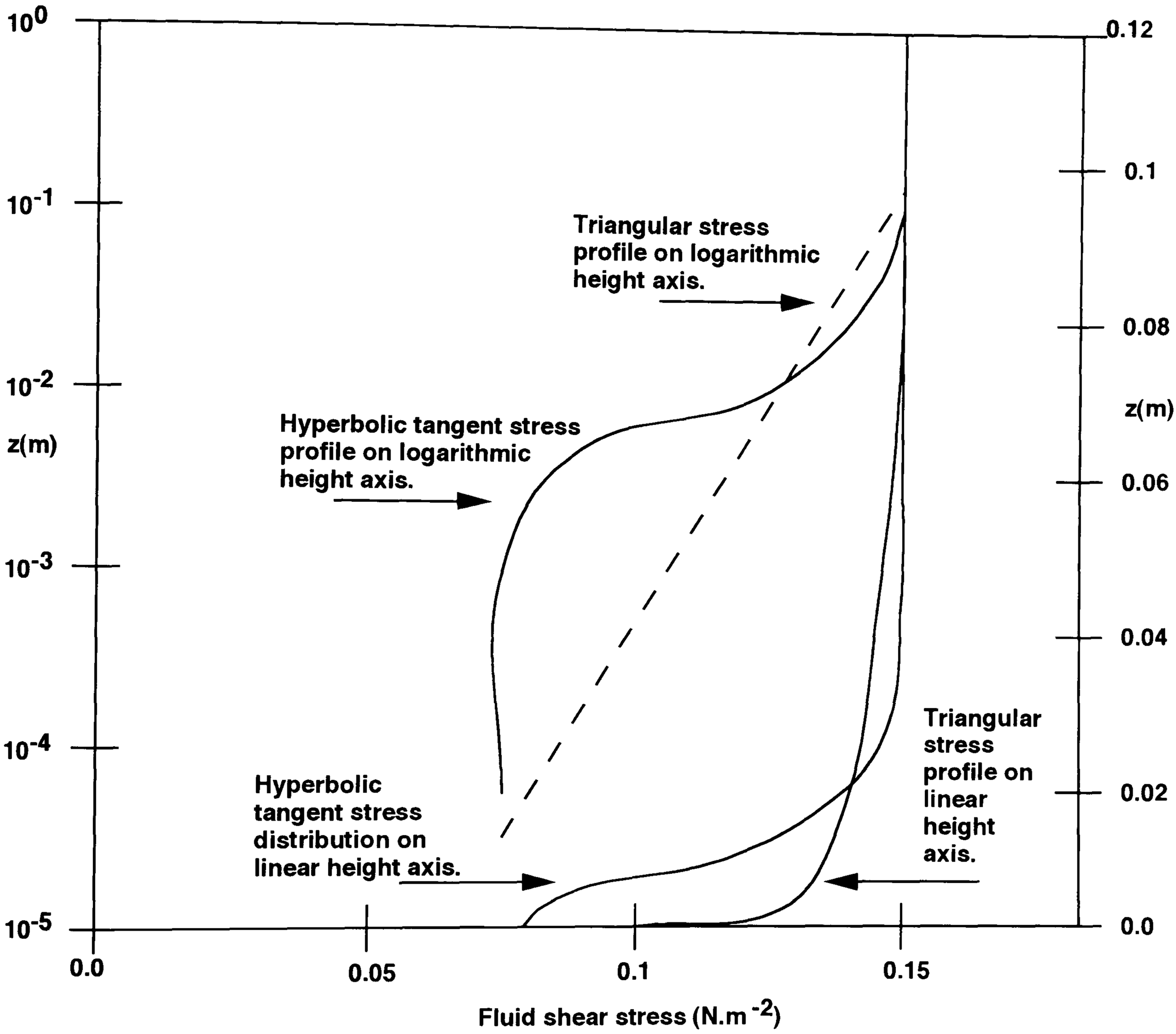

Fig. 2.9. Fluid shear stress distributions (triangular and hyperbolic tangent), represented on both linear and logarithmic height axes. (modified from McEwan, 1993, p.150).

(ii) Wake departure.

In wind tunnel experimental conditions where the wake departure does not exist (Ch. 2.1.(iv), McKenna Neuman & Maljaars, 1997) the change from a purely logarithmic velocity profile in clean air conditions to a 'kinked' velocity profile during saltation can be explained entirely by the presence of grains in transport (see Ch. 2.3.(i)). In the Queen Mary and Westfield wind tunnel the existence of a wake departure in clean air velocity profiles (see Fig. 4.13.) means that it is unknown whether the 'kink' apparent during saltation is due to the transport of grains, the wake phenomenon, or indeed the coincidental results of both processes (Spies *et al.*, 1995).

Despite uncertainties as to the exact cause of the velocity profile deviation in the Queen Mary and Westfield wind tunnel, the consistent use of the 'Law of the Wake', in both clean air and saltation, remains the most obvious method for the determination of shear velocity. During saltation, however, the dependency of the boundary layer parameter, Π (see Ch. 2.1.(iv)), on the sediment concentration of the flow introduces an additional complexity in the application of the 'Law of the Wake'.

Estimates of the boundary layer parameter during saltation in air have been made by Janin and Cermak (1988). Using a large wind tunnel (2m x 2m x 30m) Janin and Cermak (1988) were able to calculate shear velocity during saltation from a grain free portion of the logarithmic profile. By adjusting the value of the boundary layer parameter, Π, until the best approximation to their results was achieved, Π was found to increase from 0.60 until it becomes asymptotic to 1.80 for large shear velocities.

Accepting the variability of the boundary layer parameter, Spies *et al.* (1995) address the additional complication of the variability of the wake roughness parameter, C. During non-transport conditions, C, is equivalent to the bed

roughness. During saltation the apparent roughness is indicative of the height of the saltation cloud, itself dependent on the shear velocity of the flow.

The dependency of both the boundary layer parameter, Π, and the wake roughness parameter, C, on shear velocity, has led Spies *et al.* (1995) to state that, ideally, experiments during saltation require a velocity profile with a constant stress region sufficient in extent to contain a grain free region. In such a case, the 'Law of the Wake' need not be considered. With the upper 90% of compressed boundary layer velocity profiles best described by the 'Law of the Wake', however, these requirements are not easily met (Janin & Cermak, 1988).

(iii) Roughness length.

In wind tunnel experiments over a fixed bed Bagnold (1941) noted that the projection of the semi-logarithmic velocity profiles to the ordinate axis identified a point of convergence. Regardless of the velocity, the focal height over a particular surface remained constant, i.e. the focal height is purely a function of the surface roughness.

The aerodynamic roughness length (Z_o) is 'regarded as the basic measure of the degree of surface roughness' (Jackson, 1981, p.15). At the aerodynamic roughness length the wind velocity is theoretically zero; the height at which air movement first begins (Bagnold, 1941). The gradient of the velocity profile is determined, therefore, by the outer free-stream velocity and the roughness length. For the same ambient wind speed, shear velocity is greater over a rough surface than over a smooth surface.

Flows of air over water obey the 'Law of the Wall' for conditions of neutral buoyancy. It was recognised early that the aerodynamic roughness of the sea surface is not constant. As the wind speed increases there is a progressive

roughening of the surface as it adjusts to increased shearing stresses (Sherman, 1992). For fully turbulent flow Charnock's (1955) equation, based purely on dimensional considerations, describes this variable surface roughness:

$$Z_o' = C_o\left(\frac{U_*^2}{2g}\right) \equiv 5.75U_* \log\left(\frac{z}{Z_o}\right) + U_{*_t} \qquad \text{Eq. 2.11.}$$

where Z_o' is the roughness length during saltation (cm); and

C_o is a dimensionless constant with a value of 0.013 for water,
(or 0.016, according to Hicks (1972)).

Chamberlain (1983) drew attention to the similarities between sand, snow (see, Radok, 1968; Kind, 1976; Maeno *et al.*, 1979, in McEwan, 1991; McEwan & Willetts, 1993a, 1993b) and sea (Charnock, 1955). A general equation for all mobile surfaces is possible due to the uniform response of the surfaces, regardless of the composition of the medium, to shearing stresses. In all cases, the surface 'adapts itself to the flow by changing roughness; thus a dynamic equilibrium between the roughness length and the flow can be inferred' (McEwan & Willetts, 1993a, p.100).

Although Bagnold (1937, 1941) did record a 'kink' in the saltation laden velocity profiles (Ch. 2.3.(i)), by disregarding deviations and adopting a new focal point during transport, he was able to place a best fit line through all the velocity data points. Forcing the velocity profiles through a new visually determined focus, Bagnold (1941) showed that at a height of about 3mm velocity remains constant. Just as the aerodynamic roughness length, Z_o, was the convergence of the velocity profiles with the ordinate axis during non-transport conditions, so the apparent roughness length, Z_o', was the convergence of the velocity profiles during sand transport.

During saltation the apparent roughness length is described by both a certain height and a velocity. Appealingly, this new focus is greater than that during non-transport conditions implying that surface roughness is greater during

sand transport (Bagnold, 1941). By defining a new focus for the velocity profiles during saltation Bagnold (1941) was able, for a particular grain-size, to redefine shear velocity with only minor modifications to the original equation (see Eq. 2.3.):

$$u_{(z)} = 5.75U_*' \ln\left(\frac{z}{Z_o'}\right) + U_t \qquad \text{Eq. 2.12.}$$

where U_*' is shear velocity during saltation; and

U_t is the sediment threshold velocity at the height of Z_o'.

Gerety (1985) cast doubt on Bagnold's (1941) notion of a focal point during saltation, and this was later supported by Rasmussen and Mikkelsen (1991). After re-plotting and re-analysing on a comparable scale the velocity profiles reported by numerous researchers, Gerety noted that in none of these data sets was the focus of Bagnold (1941) obvious. At best only a focal zone existed. Picking a single focus height is, therefore, arbitrary (Gerety, 1985).

In 1964, Owen had suggested that the apparent roughness length during saltation was proportional to the thickness of the saltation layer as 'the grain layer behaves, so far as the flow outside it is concerned, as increased aerodynamic roughness' (Owen, 1964, p.226). The dependency of the apparent roughness length on shear velocity makes the relationship of Owen (1964), $Z_o' = C_o\left(U_*'^2/2g\right)$ where $C_o \cong 0.02$, more physically sound than that of Bagnold (1941). However, '$U_*^2/2g$ is not a good indicator of saltation layer thickness' (Lancaster & Nickling, 1994, p.450) and C_o, is 'not well constrained from wind tunnel or field data' (Butterfield, 1993, p.328). Neither the relationship of Bagnold (1941) nor Owen (1964), therefore, is fully correct.

(2.4.) SUMMARY.

- Surface shear stress (τ) is the measure of the force per unit horizontal area applied tangentially to the sediment. Surface shear stress is estimated from the shearing stresses propagated by the surface throughout the atmospheric boundary layer (Ch. 2.1.(i) and (iii)).
- For clean air moving over a homogenous surface under neutral adiabatic atmospheric conditions the turbulent region of the inner boundary layer experiences a constant distribution of shearing stresses. These shearing stresses are manifest by a logarithmic distribution of wind velocity with height (Ch. 2.1.(iii)).
- The logarithmic wind velocity profile in the constant stress region of the boundary layer is described by the 'Law of the Wall' (Eq. 2.3.). Shear velocity is proportional to the gradient of the logarithmic wind velocity profile and is related to the horizontal surface shear stress by Eq. 2.5.
- In the constrained boundary layer of some small wind tunnels, velocity measurements may be made from the whole of the velocity profile, not just the constant stress region. For a full description of the boundary layer in the Queen Mary and Westfield wind tunnel the 'Law of the Wake' must be employed (Ch. 2.1.(iv)).
- Following the aerodynamic entrainment of particles, surface impacts by saltating grains dislodge other particles. The initial exponential growth in mass flux is curtailed by the deceleration of the wind. When the mean replacement capacity reaches unity, the saltation system is technically in equilibrium (Ch. 2.2.(iii)).
- The transport of grains by the wind produces a deviation from the logarithmic profile. The 'kink' is due to an inflection in the fluid shear stress distribution produced by the grains in motion (Ch. 2.3.(i)).
- In clean air conditions, the intersection of the velocity profile with the height ordinate axis denotes the roughness length, Z_o. During saltation, a similar projection of the velocity profiles produces a focal zone indicative of the apparent roughness length Z_o' of the saltation cloud (Ch. 2.3.(iii)).

CHAPTER 3

SPATIAL AND TEMPORAL DEVELOPMENT OF THE SALTATION SYSTEM

The development of the saltation system has been investigated in both the spatial and temporal dimensions in the field (e.g. Jackson, 1996a, 1996b), wind tunnel (e.g. Butterfield, 1991, 1993, pers comm.), and by numerical models (e.g. Spies, 1996). Spatially, mass flux is shown to overshoot prior to declining towards equilibrium. Shear velocity meanwhile merely declines without overshoot. Temporally, both mass flux and shear velocity overshoot prior to a decline towards equilibrium.

Despite an understanding of the trends in development of the saltation system, very little is known about the distance and time required for the attainment of equilibrium. Essentially, this is due to the numerous scales of investigation. At the extremes, spatially equilibrium is reported between 9m (Bagnold, 1936) and >1000m (Jensen, 1978), and temporally between 30 seconds (McEwan & Willetts, 1991, 1993a, 1993b) and two hours (Rasmussen & Mikkelsen, 1991, in press).

(3.1.) SPATIAL DEVELOPMENT OF THE SALTATION SYSTEM.

(i) Spatial development of shear velocity following a step change in surface roughness.

The saltation system involves the mutual development of the near-surface atmospheric boundary layer and the mobile surface sediment. At its most basic the atmosphere is responding to a change in surface roughness (Owen, 1964). By accepting this hypothesis of Owen (1964) the development of the atmosphere following the initiation of saltation can be considered

approximately analogous to that following a step increase in surface roughness.

The passage of air across a surface discontinuity generates a region of modified air, an internal boundary layer (Oke, 1978). The internal boundary layer is manifest in the wind velocity profile as a 'kink' deviation from the logarithmic form. With distance downwind the depth of the internal boundary layer increases as the surface effects are diffused upwards (Garratt, 1990, see Fig. 3.1.). Correspondingly, shear velocity declines with distance downwind. However, prior to the decline, shear velocity overshoots to a value twice that of its equilibrium (Bradley, 1968, see Fig. 3.2.).

At large distances downwind of a step change in surface roughness the developing internal and remains of the original boundary layer merge and form a new atmospheric boundary layer. The shear stresses of the new atmospheric boundary layer, like those of the original atmospheric boundary layer, are in full adjustment to the new flow conditions (Bradley, 1968; Antonia & Luxton, 1971; Jensen, 1978; Garratt, 1990). However, the exact distance required for the reattainment of equilibrium is unclear (see Fig. 3.2., note the inclusion of the scale of Panofsky-Townsend (1964)).

Mathematically, Bradley (1968) represents equilibrium flow over a rough uniform surface by a drag coefficient, C_D:

$$C_D = \left(\frac{U_*}{u}\right)^2 = \frac{\tau}{\rho u^2} \qquad \text{Eq. 3.1.}$$

where velocity is measured at the height to which C_D is referred. Expressing the shear stress ratio as:

$$\frac{\tau_{rough}}{\tau_{smooth}} = \frac{1}{C_D \rho} \cdot \frac{\tau_{rough}}{\left(u_{ref}\right)^2} \qquad \text{Eq. 3.2.}$$

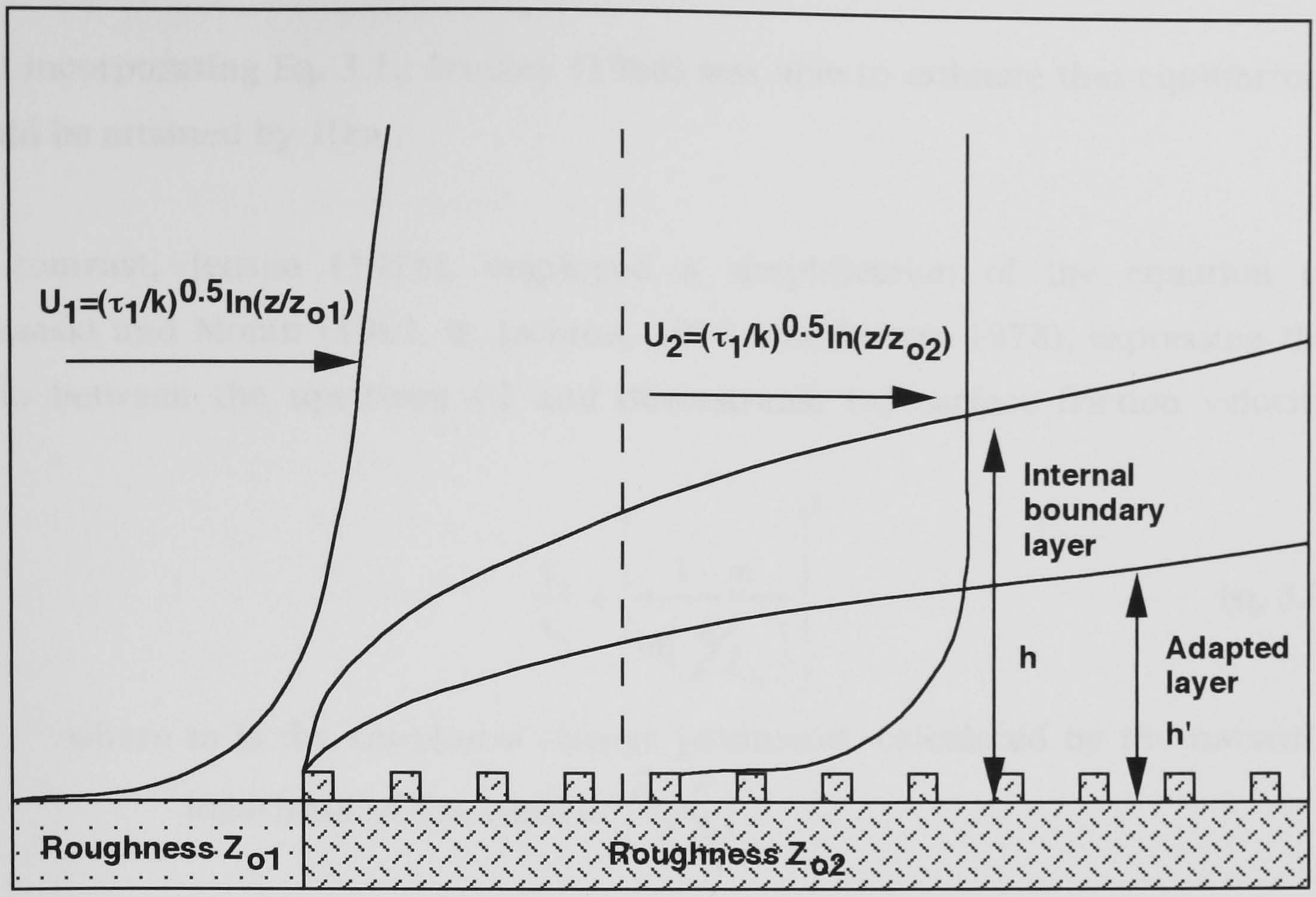

Fig. 3.1. Schematic representation of the development of an internal boundary layer downwind of step increase in surface roughness (where h is the height of the internal boundary layer (cm) and h' is the height of the adapted boundary layer (cm)). (modified from Blom & Wartena, 1969, p.256).

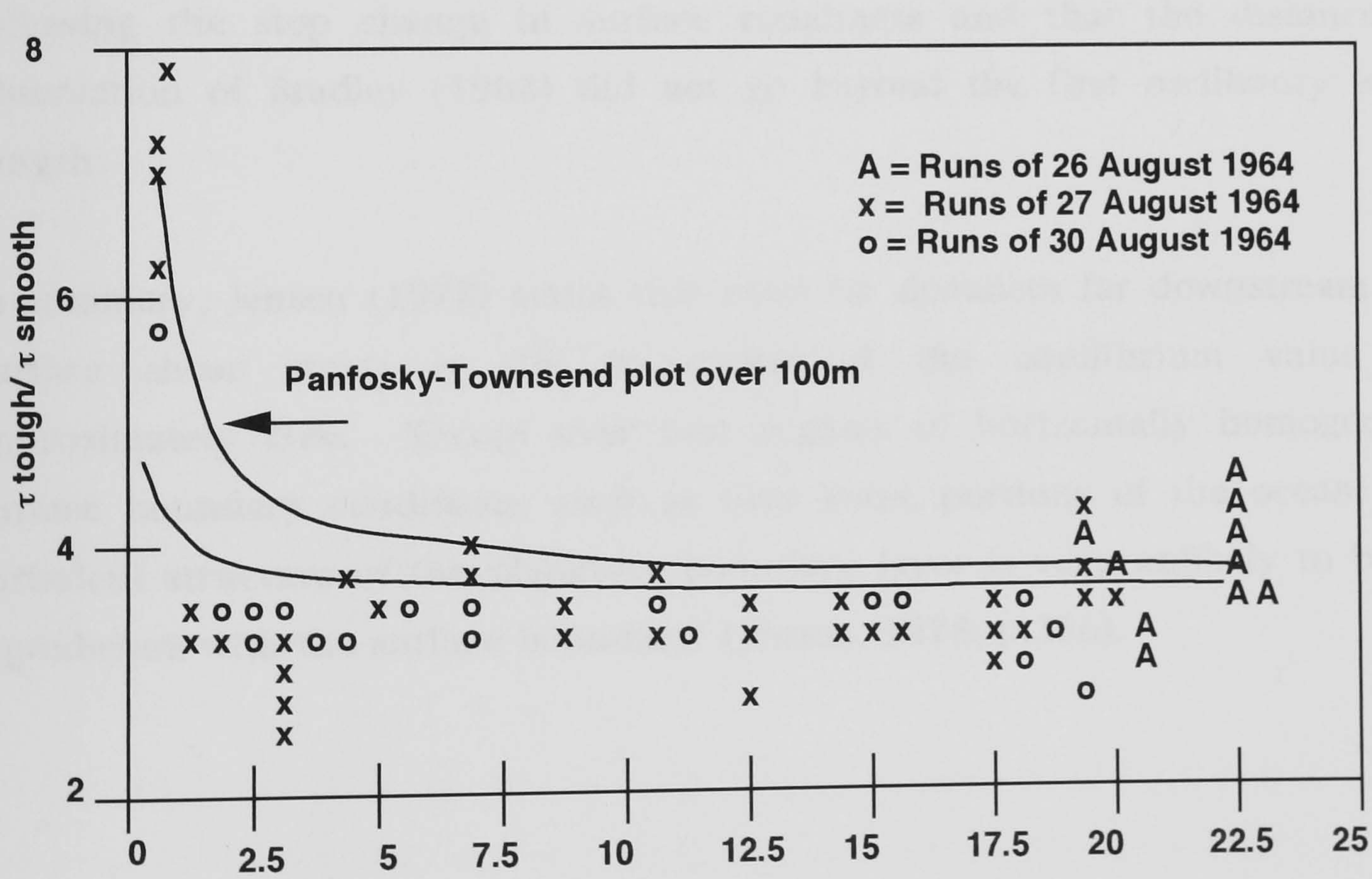

Fig. 3.2. Variation in surface shear stress downwind of a step increase in surface roughness. (modified from Bradley, 1968, p.368).

and incorporating Eq. 3.1., Bradley (1968) was able to estimate that equilibrium could be attained by 10m.

In contrast, Jensen (1978), employed a simplification of the equation of Kazanski and Monin (1961, in Jackson, 1976 and Jensen, 1978), expressing the ratio between the upstream (-) and downstream (+) surface friction velocity as:

$$\frac{\tau_+}{\tau_-} = \left[\frac{1-m}{\ln\left(h/Z_{0_+}\right)} \right]^2 \qquad \text{Eq. 3.3.}$$

where m is the roughness change parameter, calculated by the natural logarithm of the ratio of Z_{o_-}/Z_{o_+}.

For equilibrium to be attained by 10m as suggested by Bradley (1968) the terms in the equation of Jensen (1978) would have to include unrealistic values. As a result Jensen (1978) suggests that the surface shear stress may oscillate following the step change in surface roughness and that the distance of observation of Bradley (1968) did not go beyond the first oscillatory wave length.

In summary, Jensen (1978) states that even for distances far downstream the surface shear stress is still in excess of the equilibrium value by approximately 20%. 'Except over vast regions of horizontally homogenous surface boundary conditions, such as over some portions of the ocean, the turbulent structure of the planetary boundary layer is very unlikely to be in equilibrium with the surface boundary' (Jensen, 1978, p.356).

(ii) Spatial development of shear velocity following the initiation of saltation.

(a) Data from wind tunnels.

In a wind tunnel with a developing boundary layer, shear velocity declines asymptotically towards a constant value with distance downwind (see Fig. 3.3.). Unlike the case of a step change in surface roughness no overshoot in shear velocity is recorded prior to equilibrium. The lack of a shear velocity overshoot in the wind tunnel, as compared to the step change in surface roughness, may be due to the constraining dimensions of the wind tunnel. Indeed, Rasmussen and Mikkelsen (1991, p.136) suggest that 'a true equilibrium between the free-stream and the surface friction speed is rarely, if ever, reached in any aeolian tunnel'.

In an attempt to determine whether the size of a wind tunnel is of sufficient extent for its constraining influences on the saltation system to be ignored Owen and Gillette (1985) employ the Froude number (Fr):

$$Fr = \frac{u^2}{(gH)} \qquad \text{Eq. 3.4.}$$

where H is the wind tunnel height (cm).

In general, a Froude number <20 is required for the acceptability of wind tunnel results (Owen & Gillette, 1985). The influence of the value of the Froude number on the development of shear velocity, however, is still witnessed by the fact that smaller Froude numbers produce a more rapid consistency of shear velocity (White & Mounla, 1991).

(b) Data from field work.

In the field the lack of precise boundaries between upwind non-erodible elements and downwind erodible surfaces has limited the investigation of the downwind spatial development of shear velocity during a developing saltation system (Stout & Zobeck, 1996). Even in fieldwork where an upwind boundary

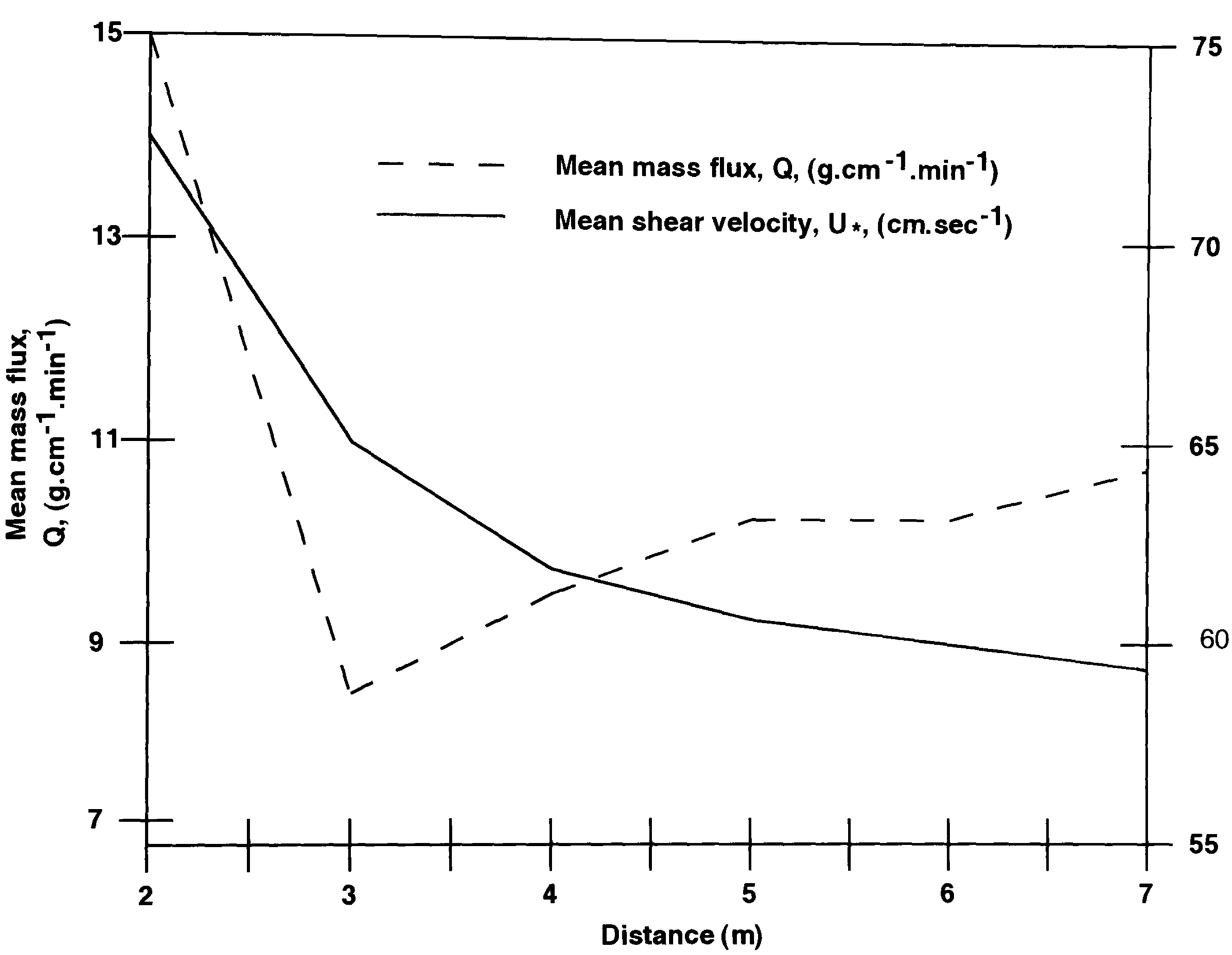

Fig. 3.3. Variation in mass flux and shear velocity in a developing boundary layer. Data collected in a wind tunnel of dimensions 9m x 0.30m x 0.30m. Experiment inclusive of upwind artificial sand-feed. (modified from Butterfield, pers comm.).

is defined, rarely do researchers actually begin monitoring from these boundaries (Gillette *et al.*, 1996; Greeley *et al.*, 1996; Jackson, 1996a). Instead, the boundaries are merely used to provide a means of estimating the fetch upwind of the experimental area.

Despite an initial fetch upwind of their experimental areas, both Greeley *et al.*, (1996) and Jackson (1996a) record a decrease in shear velocity and apparent surface roughness with distance downwind (see Fig. 3.4.). In contrast, Gillette *et al.* (1996) record no significant downwind development of shear velocity and an increase in apparent surface roughness with downwind distances >1000m. All these experiments, however, use limited instrumentation to make measurements over large distances, i.e. Greeley *et al.* (1996) use four anemometer arrays to detect the downwind variations in velocity over approximately 100m, whilst Jackson (1996a) uses two anemometers to cover 200m.

(c) Data from numerical models.

To date only the saltation model of Spies (1996) incorporates a spatial element. From an initial upwind logarithmic wind velocity profile, the velocity profile is then remodelled every 10m over a distance of 50m during saltation. With distance downwind, the modelled velocity profile becomes progressively 'kinked' due to the development of the sand cloud and the subsequent extraction of momentum by the grains in motion. Shear velocity declines asymptotically towards a constant value. The state of equilibrium is considered to have been achieved by 20m.

Despite the limited number of papers incorporating the downwind development of the velocity profile, the results from wind tunnel, field and numerical model studies show encouragingly similar trends, both for a step change in roughness and the initiation of saltation. All data confirm that with increasing distance downwind (i) the wind velocity profile develops a 'kink',

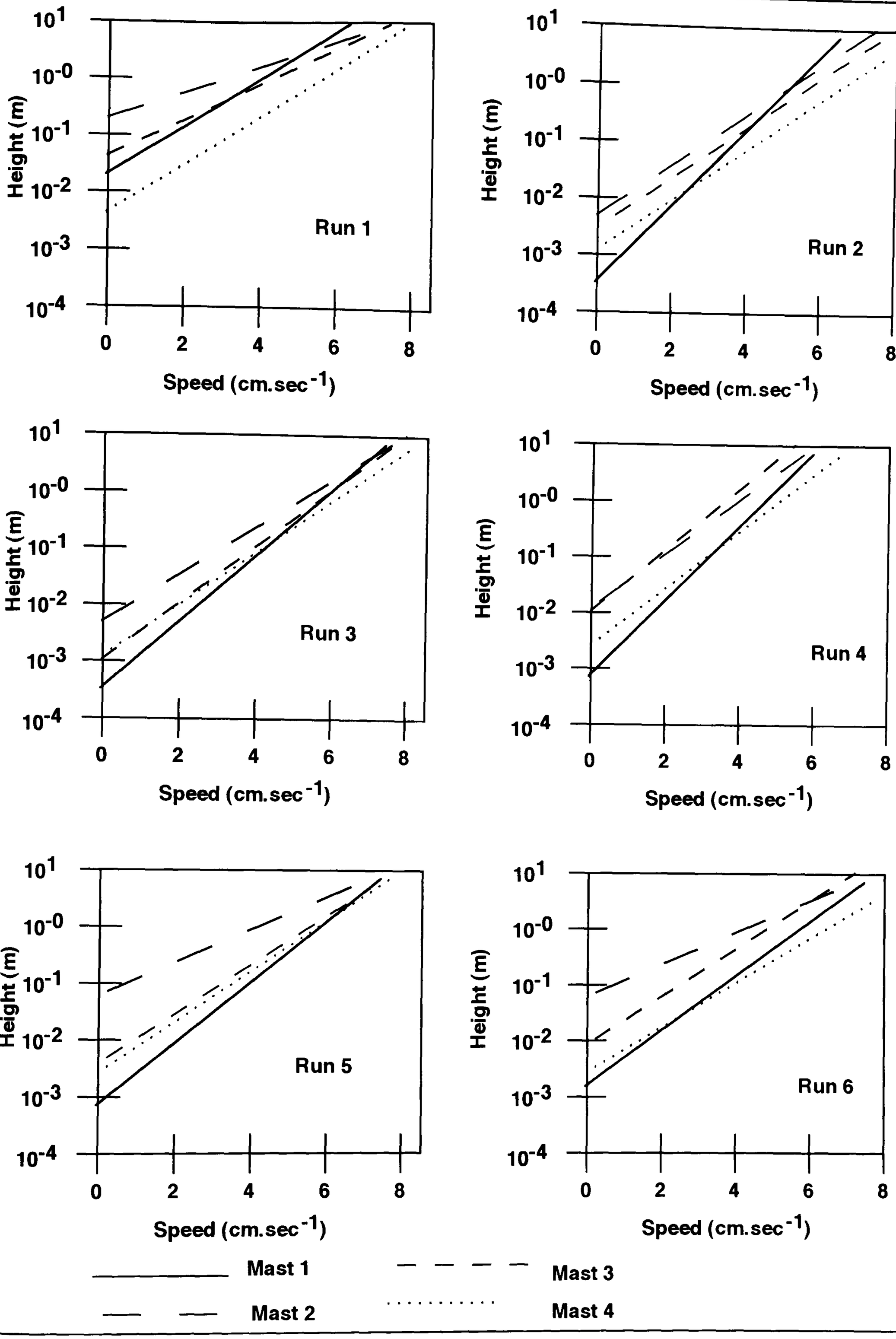

Fig. 3.4. Development of the velocity profile with distance downwind in the field. The two central anemometer masts, numbers 3 and 4, are offset laterally by 10m and located 25m downwind from mast number 2 and 25m upwind from mast number 1. Anemometer mast number 2 is located at the beginning of the experimental plot approximately 275m downwind from the high tide berm. (modified from Greeley *et al.*, 1996, p.45).

the height of which increases as the depth of the internal boundary layer increases and (ii) there is an asymptotic decline in shear velocity towards a constant value. The only significant uncertainties remaining are why during saltation there is no recorded overshoot in shear velocity and what is the distance required for equilibrium to be achieved in the saltation system?

(iii) Spatial development of mass flux.

(a) Data from wind tunnels without artificial sand-feeding. Two significant works have investigated the spatial development of mass flux in wind tunnels. Bagnold (1936, see Fig. 3.5.) conducted experiments, with and without upwind artificial sand-feed, in a wind tunnel 0.30m high and 9m long. Shao and Raupach (1992, see Fig. 3.6.) conducted experiments, without upwind artificial sand-feed, in a wind tunnel 0.90m high and 15m long.

Bagnold (1936) considers the spatial development of mass flux, without upwind artificial sand-feeding at two velocities (see Fig. 3.5.(b and c)). At the lower velocity (U_*=36cm.sec^{-1}, see Fig. 3.5.(b(iii))) mass flux increases gradually with distance. By 6m the final equilibrium rate has been achieved. For the higher velocity (U_*=92cm.sec^{-1}, see Fig. 3.5.(c)) mass flux clearly overshoots at 3-4m prior to declining towards an equilibrium rate.

In all their experiments Shao and Raupach (1992, see Fig. 3.6.) record an overshoot in mass flux prior to equilibrium. The timing and extent of the overshoot is velocity dependent, larger velocities producing a greater and more rapid overshoot. For all the velocities the overshoot in mass flux is almost twice the final equilibrium rate.

The lack of mass flux overshoot in the lower velocity experiment of Bagnold (1936, see Fig. 3.5.(b(iii)), U_*=36cm.sec^{-1}) as compared to the similar velocity experiment of Shao and Raupach (1992, see Fig. 3.6.(a), U_*=34cm.sec^{-1}) and the lesser degree of the overshoot in the higher velocity experiment of Bagnold

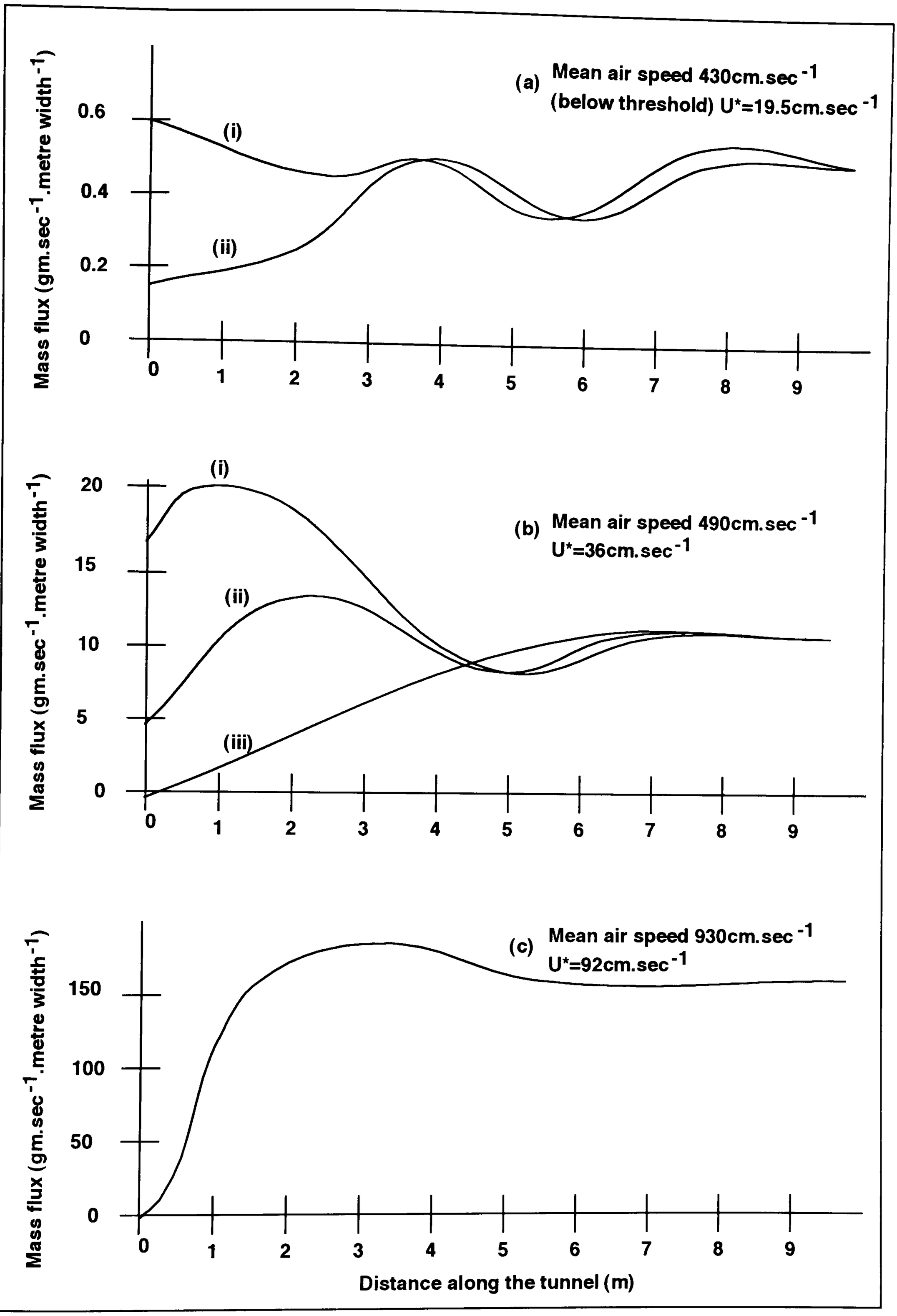

Fig. 3.5. Development of mass flux with distance downwind in a wind tunnel, with and without upwind artificial sand-feed. The wind tunnel dimensions are 9m x 0.30m x 0.30m. Mass flux is monitored by means of sprung balances below various sections of the wind tunnel, i.e. the mass flux data is spatially averaged. (modified from Bagnold, 1936, p.598).

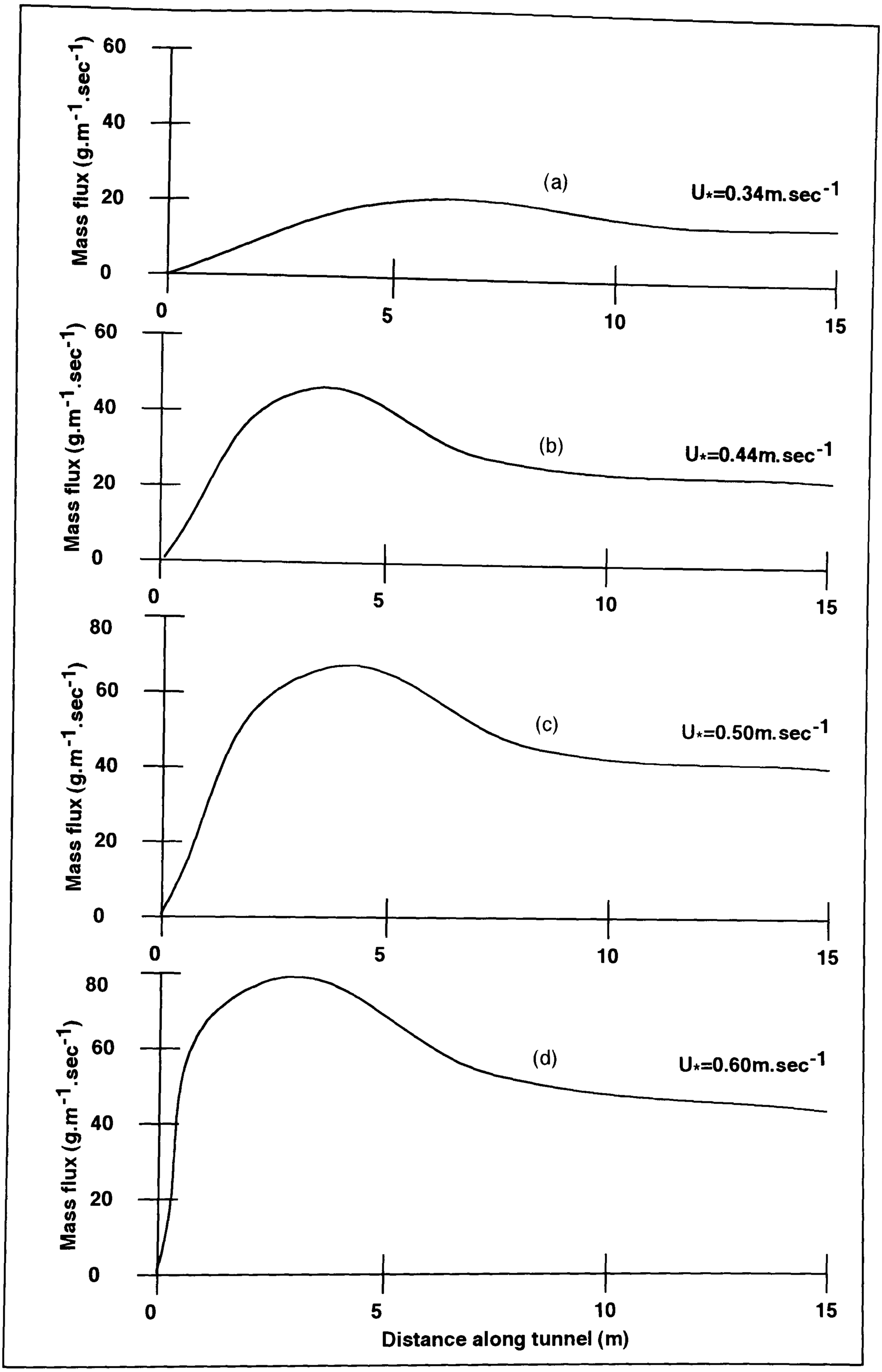

Fig. 3.6. Development of mass flux with distance downwind in a wind tunnel without upwind artificial sand-feed. Wind tunnel dimensions are 15m x 1.15m x 0.90m. Mass flux is monitored using 'Leach' traps, i.e. point data. (modified from Shao & Raupach, 1992, p.20362).

(1936, see Fig. 3.5.(c)) as compared to all of the experiments of Shao and Raupach (1992, see Fig. 3.6.), are not so much an artefact of the saltation system but the influence of wind tunnel dimensions. The model of Spies (1996) has considered the behavioural differences in the saltation system due to wind tunnel dimensions (see Fig. 3.7.).

The simulation of specific wind tunnel dimensions by the model of Spies (1996) has shown that the 'overshooting of the transport rate is not predicted for tunnel heights less than 60cm' (Spies, 1996, p.19, see Fig. 3.7.). The lack of mass flux overshoot in wind tunnels of smaller height is due to the fact that the whole depth of the air flow is rapidly affected by the momentum exchange between the air and the grains (Spies, 1996). With such a rapid feed-back the development of the peak in shear stress, and thus the mass flux overshoot, is limited.

For all aeolian experiments, the final rate, and timing, of equilibrium mass flux is velocity dependent (Bagnold, 1936, 1941; Shao & Raupach, 1992; Al-Sudairawi, 1992). The degree of influence of velocity on the distance required to achieve equilibrium, however, is unclear. The data of Bagnold (1936) suggests only a minimal velocity dependence, a doubling of the free-stream velocity from 490cm.sec^{-1} to 930cm.sec^{-1} reducing the distance for the attainment of equilibrium by only 1m (a decline from 7m to 6m). Shao and Raupach (1992), Al-Sudairawi (1992) and Al-Awadhi and Willetts (1998) meanwhile assume that the velocity dependence of the timing of the mass flux overshoot is similarly transferred to the distance required for the final equilibrium transport rate to be achieved.

To some extent, the discrepancies between the results of various wind tunnel experiments can be explained by: the influence of wind tunnel dimensions (see Ch. 3.1.(ii(a)) and Ch. 3.1.(iii(a))); the problems associated with the calculation of shear velocity in compressed boundary layers (see Ch. 2.1.(iv) and 2.3.(ii)); the initial preparation of the sand bed, i.e. working from a planar

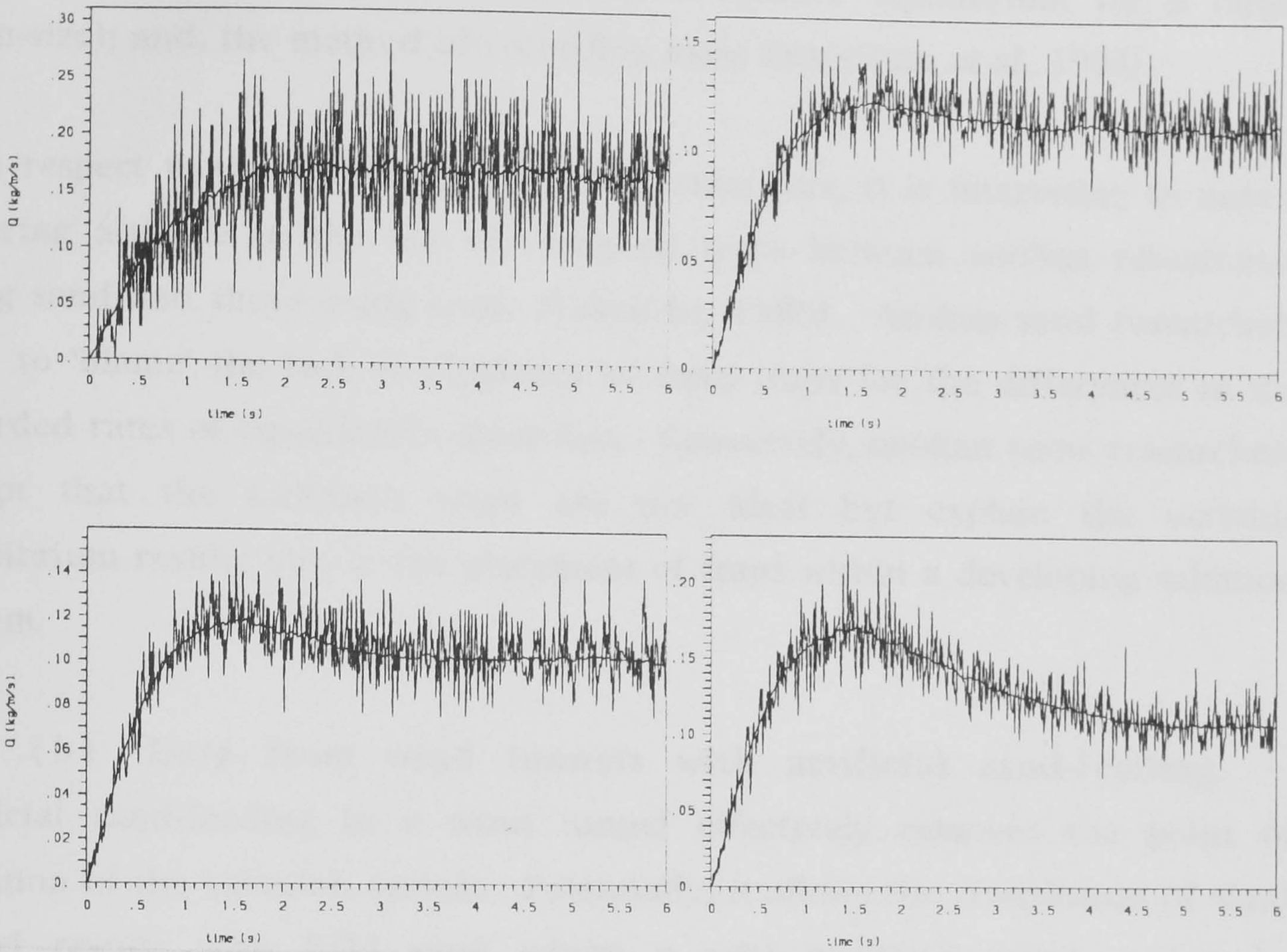

Fig. 3.7. The development of mass flux (Q) with time for different wind tunnel heights. Results from the self-regulatory numerical model of Spies (1996). Top left: tunnel height 0.30m. Top right: tunnel height 0.40m. Bottom left: tunnel height 0.60m. Bottom right: tunnel height 2m. The same initial shear velocity of 37cm.sec^{-1} was used in all cases. (Spies & McEwan, in press(a), p.16).

non wind-worked surface (Shao & Raupach, 1992) or allowing the prior development of a wind-worked surface before data collection (Al-Sudairawi, 1992); the grain-size distribution of the sand bed (e.g. Bagnold (1941) noted that greater distances were required to achieve equilibrium for a larger grain-size); and, the method of recording mass flux (Shao *et al.*, 1993).

With respect to the method of recording mass flux, it is interesting to note a differing attitude to the use of sediment traps between aeolian researchers using sand and those using snow (Takeuchi, 1980). Aeolian sand researchers tend to 'blame' the lack of efficiency of sand traps for the differences in the recorded rates of equilibrium mass flux. Conversely, aeolian snow researchers accept that the sediment traps are not ideal but explain the variable equilibrium results due to the placement of traps within a developing saltation system.

(b) Data from wind tunnels with artificial sand-feeding.

Artificial sand-feeding in a wind tunnel effectively removes the point of initiation of the saltation system. Potentially, it allows the comparison of wind tunnel results with field work where a zero transport point cannot be identified but the rate of transport of sand blowing into the defined experimental area can be quantified.

Bagnold (1936, 1937, 1941) considers the spatial development of mass flux augmented by various rates of upwind artificial sand-feed (see Fig. 3.5.(a(i) and a(ii)) and (b(i) and b(ii))). For the above-threshold wind velocity (see Fig. 3.5.(b(i) and b(ii))) sand-feed above and below the ultimate transport rate are introduced. The inclusion of sand-feed produces an oscillation in mass flux prior to the attainment of equilibrium. The results of Butterfield (pers comm., see Fig. 3.3.) support this development.

The final rate of, and distance for, the attainment of equilibrium appears to be independent of the inclusion of sand-feeding (Bagnold, 1936, 1937, 1941). Only

the development of mass flux prior to equilibrium is influenced by the inclusion of sand-feed. The influence of sand-feed is particularly influential for low velocities (Rasmussen & Mikkelsen, 1991).

The resilience of the condition of equilibrium in the aeolian saltation system to perturbations of the inflow of sand is reassuring for wind tunnel investigations where artificial sand-feeding is to be included. By including sand-feeding in wind tunnel experiments the point of initiation of the saltation system is effectively removed. Due to the limited number of field locations where a designated point of initiation for the saltation system can be identified (see Ch. 3.1.(ii)), the inclusion of upwind sand-feed in the wind tunnel potentially generates a compatibility between the wind tunnel environment and the most common field condition.

(c) Data from field work.

The downwind spatial development of mass flux has been investigated over sandy beaches by Jackson (1996a, see Fig. 3.8.) and Greeley *et al.* (1996). Both researchers employ a sand trap spacing of 10m. Jackson (1996a) uses the high water mark as the upwind boundary for the inception of saltation and monitors mass flux over 200m.

With distance downwind, Jackson (1996a) records an increase in mass flux to a maximum at 60m. Over the next 40m mass flux rapidly declines, then levels to a plateau. At 210m another drop in mass flux is witnessed and a final lower constant rate attained. The data of Greeley *et al.* (1996) is less clear due to a fetch of 265m upwind of the experimental site. Over the 100m experimental area, however, the data reveal a general decline in mass flux with distance downwind.

The experiments of Stout and Zobeck (1996, see Fig. 3.9.) at Wolfforth, Texas, and of Stetler and Saxton (1996) on the Columbia Plateau, are both based on agricultural fields with clear upwind boundaries. Both sets of researchers

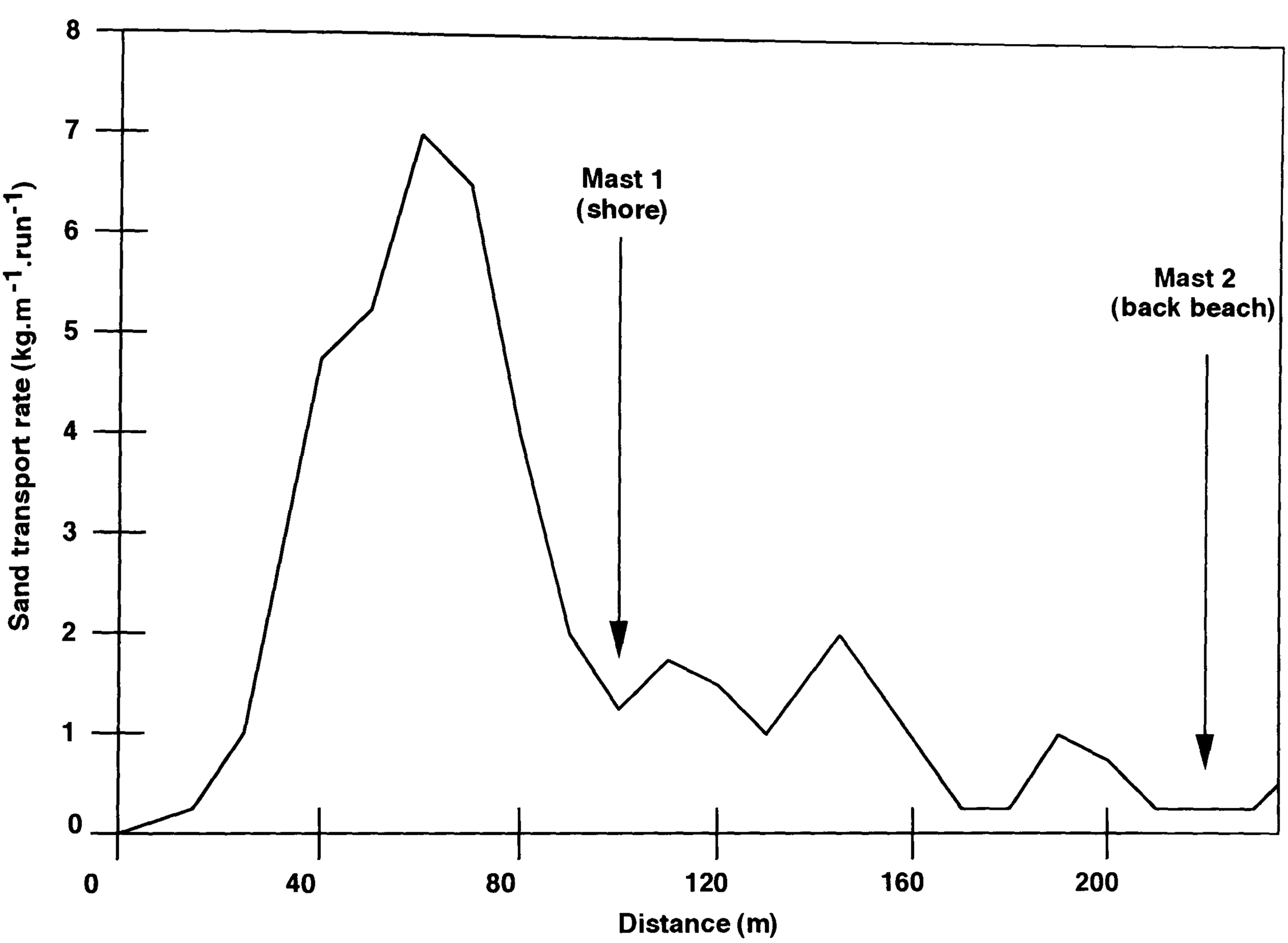

Fig. 3.8. Horizontal variations in sand transport along a beach. Mass flux is recorded every 10m downwind of the high water mark. (modified from Jackson, 1996a, p.198).

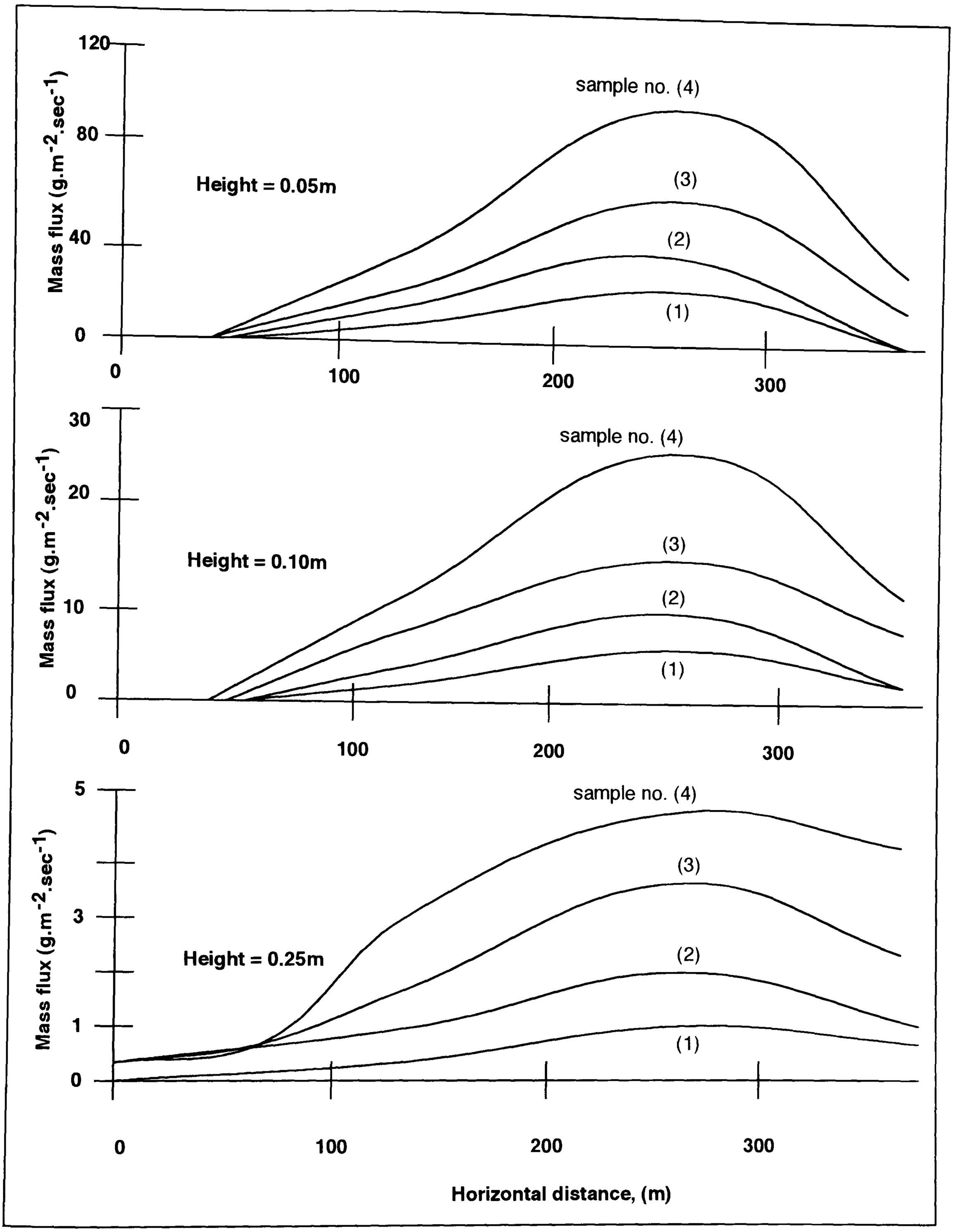

Fig. 3.9. Horizontal variation in sediment flux across an agricultural field at Wolfforth, Texas. Mass flux is monitored at three heights downwind of a clear upwind boundary. (modified from Stout & Zobeck, 1996, p.624).

collected data over distances of 400m using six BSNE (Big Spring Number Eight) traps sampling at five heights between 0.05m and 1.65m. The spatial development of mass flux revealed by the two data sets is very similar.

For heights below 0.50m an increase in mass flux is recorded as reaching a maximum at approximately 250m downwind (Stout & Zobeck, 1996; Stetler and Saxton, 1996). Over the final 150m of the experiment, Stout and Zobeck (1996) and Stetler and Saxton (1996) infer a decline in mass flux based on less sediment recorded at the final trap site. (Similar behaviour for snow flux is recorded by Takeuchi (1980) although over a fetch >1000m).

At heights above 0.50m, definable boundaries to transport are limited, i.e. suspended particles travel kilometres from their point of origin rising and falling with the air currents. Without a definable boundary condition there is 'virtually no gradient of sand transport with linear distance' (Cahill *et al.*, 1996, p.630; Stout & Zobeck, 1996; Stetler and Saxton, 1996). Similarly, the behaviour of sediment in transport over distances >1000m is inconsistent (Gillette *et al.*, 1996; Fryrear *et al.*, 1991) due to too few sampling locations (Gares *et al.*, 1996).

(d) Data from numerical models.

The earliest incorporation of a spatial parameter into the calculation of mass flux was by Chepil (1965). Chepil (1965) expressed soil erosion (E) from an agricultural field as a function of soil erodibility (I), climate (Cl), surface roughness (K), vegetation cover (V) and unsheltered field length in the upstream direction (L):

$$E = f(I, Cl, K, V, L) \qquad \text{Eq. 3.5.}$$

The limitations of this approach were soon realised but despite mounting evidence for over-and under-estimations of erosion no alternatives existed and so usage continued.

Decades of investigation into the aeolian transport system have come to fruition in the 1990's. Stout (1990) formulated the first new empirically-derived equation, since the soil loss equations of Chepil (1965), to include a distance parameter. Furthermore, the only physically based model of the saltation system to consider the spatial dimension has been developed (Spies, 1996; Spies & McEwan, in press a, in press b).

The empirically derived equation of Stout (1990, in Fryrear *et al.*, 1991):

$$Q = Qmx\left(1 - e^{-X/B}\right) \qquad \text{Eq. 3.6.}$$

where Q is the total mass at x metres (g.cm-width^{-1});

Qmx is the maximum mass transportable by this wind over this field surface (g.cm-width^{-1});

X is distance downwind; and

B is an expression of erodibility of the soil surface (cm).

(and a similar relationship by Sterk and Stein (1997)), predicts the exponential increase in mass flux with distance downwind. With distance downwind, mass flux eventually, asymptotically approaches an equilibrium value without overshoot.

Despite differing calculation methodologies, good agreement exists between the spatial development of mass flux predicted by the formulae of Stout (1990) and Sterk and Stein (1997). In brief, the equation of Stout (1990) is generated from the conservation of mass in both the horizontal and vertical, whilst Sterk and Stein (1997) use geostatistical theory and the concept of spatial correlation. (Spatial correlation considers if the observation of a regional variable at any two points close to each other are more similar than observations at any two points a larger distance away).

The physically based model of Spies (1996) for transport of sand predicts an increase in mass flux with distance, overshooting prior to a more gradual decline to equilibrium. The overshoot in mass flux is in agreement with the physically collected data where a clear upwind boundary for the inception of the saltation system has been defined (see Ch. 3.1.(ii(c))). Conversely, the lack of an overshoot in mass flux in the empirically-derived equations, (and in The Prairie Blowing Snow Model (PBSM) of Pomeroy *et al.* (1993) which covers a distance of 4000m, (see also Dery & Taylor, 1996)), is probably due to the lack of definable upwind boundaries.

The aeolian transport phenomenon has been investigated by three different methodologies, i.e. wind tunnel, field and numerical models, and at numerous scales of the study. Despite the multitude of individual studies there is good general agreement between the available data. The development of mass flux (below 0.5m in height) and from an identifiable upwind boundary, increases rapidly, peaks and then declines towards a sustainable equilibrium transport rate. The remaining uncertainties are the length-scale required for the attainment of equilibrium and the absolute value of mass flux at equilibrium.

(iv) Theories of spatial development of the saltation system.

The lack of data for the simultaneous spatial development of mass flux and wind velocity has hindered theories of spatial development. Four theories for the spatial development of mass flux exist: the 'lag hypothesis' of Bagnold (1941); the 'avalanching mechanism' of Chepil (1957); the 'aerodynamic feed-back mechanism' of Owen (1964); and the erosion susceptibility theory of Chepil (1946).

The 'lag hypothesis' of Bagnold (1941) suggests that there is an independent development of shear velocity (see Ch. 3.1.(ii)) and mass flux (see Ch. 3.1.(iii)

prior to equilibrium. From the separate downwind development of mass flux and shear velocity it has been seen that, in the initial stages of development of the saltation system, mass flux overshoots prior to declining towards an equilibrium value. Shear velocity meanwhile merely declines asymptotically with distance, i.e. there is no recorded overshoot (Spies, 1996).

According to Bagnold (1941, p.181) the 'lag, at any given point, between the sand flow there and the full effect of its drag upon the wind velocity' culminates in a situation where once mass flux has reached its sustainable maximum rate the air is still moving faster than the corresponding steady velocity. As a result, mass flux continues to increase, overshooting and saturating the saltation system.

The self-balancing mechanism of Owen (1964) can be invoked to explain the eventual attainment of equilibrium in the hypothesis of Bagnold (1941). At a rate of mass flux lower than the equilibrium rate, shearing stresses reaching the surface are 'above the value required merely to secure mobility' (Owen, 1964, p.223). More particles are thus entrained. Too large a volume of particles in transport and the grains carry all the vertical momentum of the wind and shearing stresses cannot maintain the sediment in transport. Numerous diminishing fluctuations about the equilibrium transport rate, therefore, eventually lead to the mutual stabilisation of both variables.

The 'avalanching mechanism' of Chepil (1957) is a concept termed the 'saltation cascade' by Nickling (1988). On initiation of saltation individual particles moving downwind dislodge additional grains upon impact with the surface. This generates an exponential increase in mass flux with distance (see Ch. 2.2.(iii)). Eventually, saturation of the wind by the grains reduces the near-bed velocities to below the threshold required to initiate any additional motion. The exponential growth of mass flux is thus curtailed and a constant transport rate is maintained.

Owen (1964) suggested a positive aerodynamic feed-back mechanism to explain the spatial development of both mass flux and shear velocity. Following the initiation of the saltation system an increase in the effective aerodynamic roughness height is experienced and an internal boundary layer develops (Ch. 3.1.(ii)). Within the internal boundary layer high shearing stresses produce a high momentum flux towards the surface. The result of these shearing stresses is the entrainment of more grains and a further increase in the roughness height (Raupach, 1991). A positive feed-back downwind, between aerodynamic surface roughness, shear velocity and mass flux, generates a rapidly increasing transport rate. The final equilibrium rate is attained either with or without an overshoot by the respective incorporation of the hypotheses of Bagnold (1941) or Chepil (1957).

The spatial development of soil erosion across agricultural fields has been explained by the variability in the susceptibility of the soil to erosion. Chepil (1946) noted that there is a tendency for the accumulation of easily eroded material at the leeward side of wind-eroded fields. With the accumulation of easily transportable soils increasing in the direction parallel to the wind this appears to be responsible for the increase in the quantity of soil in transport. The disintegration of aggregates by sand blasting (Chepil, 1946) could similarly induce a change of material from a non-erodible to an erodible state with distance downwind.

The theories of spatial development have been discussed independently but obviously they may operate simultaneously. Gillette *et al.* (1996) conclude that the fetch effect, i.e. the spatial development of mass flux, is in response to a combination of factors. In general, avalanching is dominant over the small scale <50-100m. At larger distances, over an aerodynamically smooth surface, the aerodynamic feed-back mechanism may dominate. Over soils, variations in resistance may be the most significant influence on transport. The extent and timing of the overshoot of mass flux, in all environments is controlled by the lag theory of Bagnold (1941).

(3.2.) TEMPORAL DEVELOPMENT OF THE SALTATION SYSTEM.

The two-stage temporal development of the saltation system was first highlighted by the numerical model simulations of McEwan and Willetts (1991, 1993a, 1993b), Anderson and Haff (1991) and Sørensen (1991). Under conditions of steady flow, any change in wind velocity is met by an initially rapid response from the saltation system (see Figs. 3.10. and 3.11). Only over longer periods does the saltation system progressively develop towards equilibrium.

(i) Response time of the saltation system.

The primary response of the saltation system to an acceleration in velocity is recorded in a rapid overshoot in mass flux, shear velocity and apparent roughness (see Figs. 3.10. and 3.11.). The primary response time of the saltation system is confirmed by all methods of aeolian investigation, i.e. numerical models (Werner, 1990; McEwan & Willetts, 1991, 1993a, 1993b; Anderson & Haff, 1991; Sørensen, 1991; and Spies, 1996), wind tunnels (Butterfield, 1991, 1993) and field work (Jackson & McCloskey, 1997), as 1-2 seconds (or even less in small wind tunnels (Butterfield, in press)). The exact response time of the saltation system is a weak function of shear velocity (McEwan & Willetts, 1993a, 1993b; Anderson & Haff, 1991; see Fig. 3.11.); for smaller increments of shear velocity longer times are required for the overshoot to be achieved.

'Sudden flow deceleration s are characterised by lagged rapid reductions in mass flux and progressive reductions in shear velocity and roughness' (Butterfield, 1993, p.305) over ten seconds or more. Recently, Jackson (1996a) and Jackson and McCloskey (1997), have recorded similar inertial effects in the field. The delayed reaction of the sediment transport system is due to the forward momentum of grains, regardless of subsequent changes in velocity. Whilst shear velocity may decline quite rapidly, therefore, the corresponding

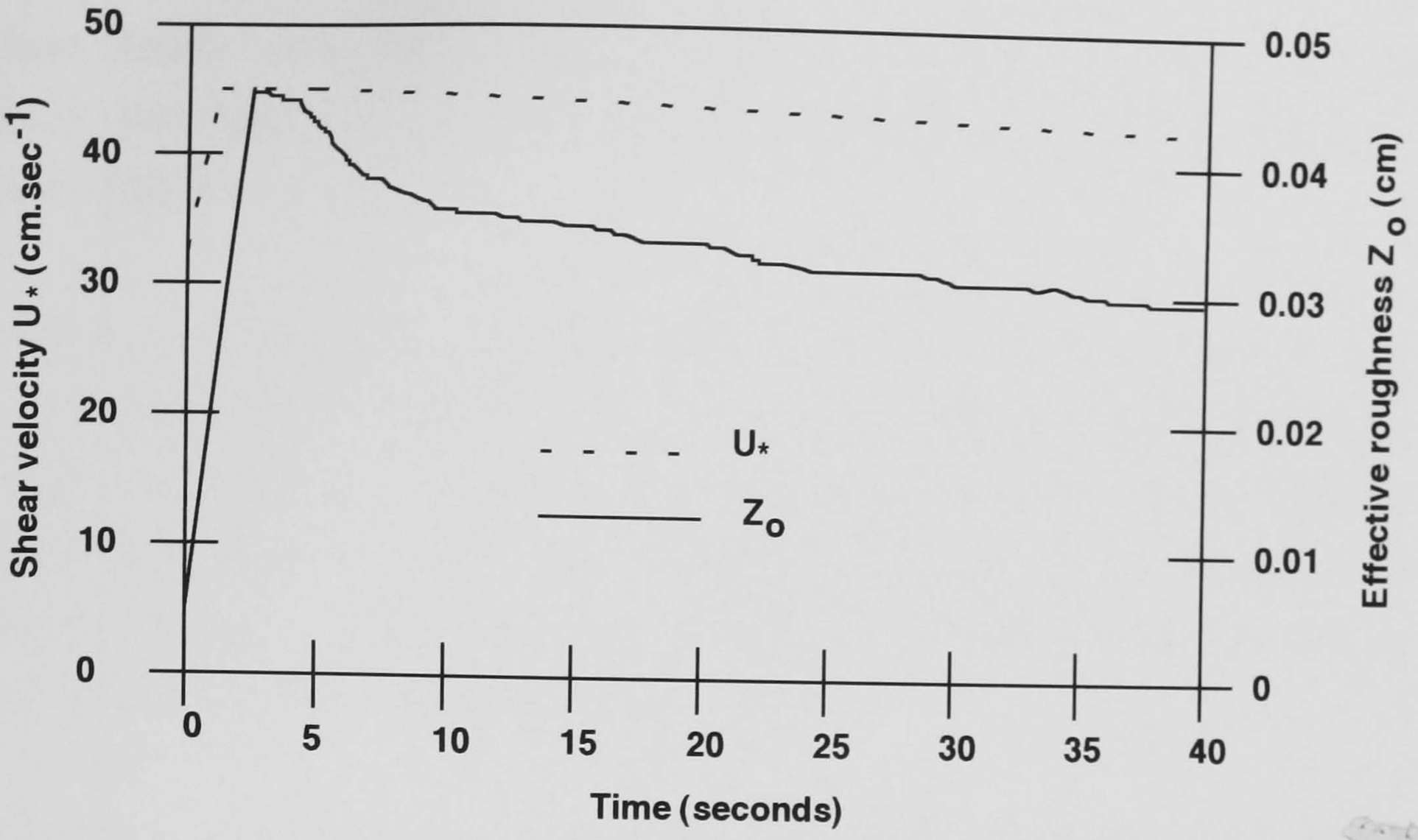

Fig. 3.10. Temporal development of shear velocity and surface roughness, calculated by the self-regulatory numerical model of McEwan & Willetts. (modified from McEwan & Willetts, 1991, in Butterfield, 1993, p.313).

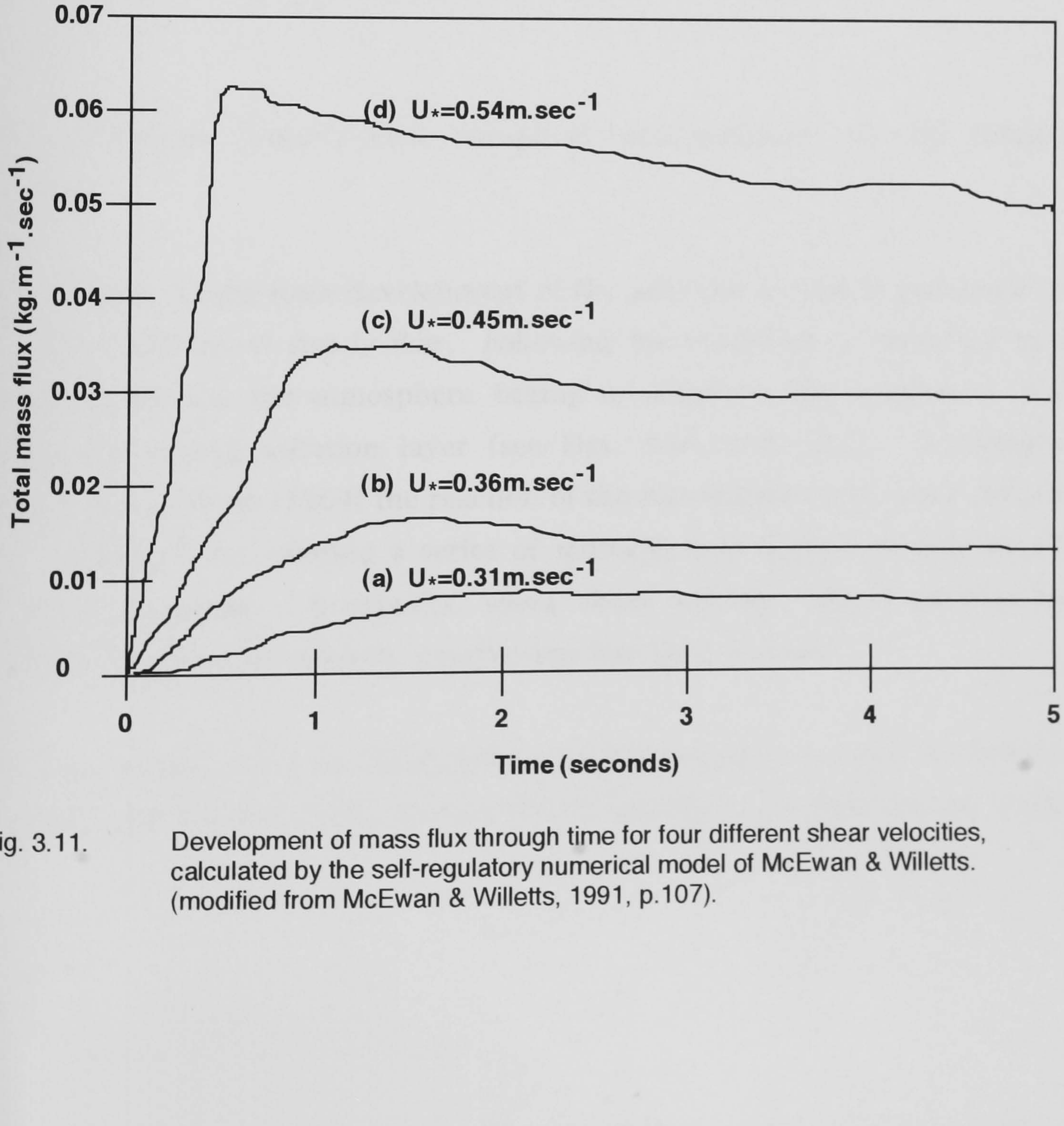

Fig. 3.11. Development of mass flux through time for four different shear velocities, calculated by the self-regulatory numerical model of McEwan & Willetts. (modified from McEwan & Willetts, 1991, p.107).

roughness levels and mass flux decline more slowly (Jackson, 1996a). Potentially this leads to an underestimation of mass flux by current sand transport formulae.

An important implication of all the response times of the saltation system, both the acceleration and deceleration scenarios, is that there is a high probability that 'sand transport rate measurements under field conditions do not indicate an equilibrium transport rate but rather an average of a sequence of temporally adjusting flows' (McEwan & Willetts, 1993b, p.14). A similar conclusion is reached by Butterfield (1991, 1993).

With extremely high frequency (>0.50Hz) fluctuations in velocity, mass flux is less sensitive (Spies, 1996). Conditions of equilibrium are, therefore, possible in unsteady velocity regimes. However, for gust sequences with periodicities <20 seconds the rate of mass flux is greater than that of a steady wind of the same mean wind speed (Butterfield, in press).

(ii) Idealised longer-term temporal development of the saltation system.

The second, longer-term development of the saltation system is witnessed only under conditions of steady flow. Following the overshoot of mass flux in the saltation system, the atmosphere begins to adjust to the roughness of the newly developing saltation layer (see Figs. 3.10. and 3.11.). Invoking the hypothesis of Owen (1964) the reaction of the atmosphere to the sand cloud can be considered as initiating a series of mutually interdependent modifications by both variables. Eventually, when shear velocity and mass flux have achieved time independence, equilibrium has been reached.

For the second stage of development of the saltation system the model of McEwan and Willetts (1991, 1993a, 1993b) predicts a gradual decline of shear

velocity, effective roughness and mass flux towards equilibrium (see Figs. 3.10. and 3.11.). In contrast to the numerical model, the wind tunnel results of Butterfield (1993) show the decrease in mass flux accompanied by a gradual increase in both shear velocity and effective roughness. Assuming effective roughness reflects the developing sand cloud these data appear incompatible.

The increase in effective roughness, as experienced in the wind tunnel (Butterfield, 1993), can be explained by consideration of the developing bedforms as well as the sand cloud. More problematic is the behaviour of shear velocity through time. To explain the increase in shear velocity with time it may be suggested that the constraints of the wind tunnel roof limit the propagation of surface shear stresses upwards (Spies, 1996). If this explanation is accepted, however, then data from wind tunnels are limited in their applicability.

A discrepancy in the time required for the saltation system to achieve equilibrium is highlighted by the comparison of temporal mass flux data of various researchers. The numerical model of McEwan and Willetts (1991, 1993a, 1993b) predicts a period of 30-40 seconds for the attainment of equilibrium mass flux. The wind tunnel experiments of Butterfield (1993), Al-Awadhi and Willetts (1998) and Rasmussen and Mikkelsen (1991, in press) suggest a longer period.

In the wind tunnel experiments of Butterfield (1993) a period of 100-200 seconds is required for the attainment of equilibrium mass flux. The wind tunnel experiments of Al-Awadhi and Willetts (1998), however, identify a period of 2-4 minutes in experiments without upwind artificial sand-feed and 8-9 minutes in experiments with upwind artificial sand-feed. Rasmussen and Mikkelsen (1991, in press) monitoring the rate of mass flux, from a wind-worked surface over a two hour period, furthermore, note that despite a relatively constant transport rate during the first thirty minutes of the experiment, the rate of mass flux subsequently declines.

Overall, the numerical model results of McEwan and Willetts (1991, 1993a, 1993b) and Anderson and Haff (1991), supported by the wind tunnel work of Butterfield (1991, 1993), highlight the temporal two-stage development of the saltation system towards equilibrium. The first component of the steady state can be considered as the wind and the saltation cloud reaching an equilibrium. The second component of the steady state is the boundary layer above the saltation layer reaching equilibrium with the new surface roughness of the saltation cloud. The first reaction is rapid in comparison with the time taken for the boundary layer adjustments. However, the saltation system can only be considered in equilibrium once the second stage of its development has been completed.

Despite agreement as to the trends of temporal development of the saltation system, the time required for the attainment of equilibrium is unclear. At the extremes equilibrium is attained between 30 seconds and two hours. Compared to the five to ten hour period required to establish equilibrium in a water flume (Bennett & Bridge, 1995), however, the reactions of the aeolian saltation system in air are relatively rapid.

(iii) Temporal control mechanisms of the saltation system.

The most widely accepted control mechanism limiting the rate of mass flux in the saltation system is the negative feedback between the grains in transport and the wind. Self-regulation of aeolian transport is achieved due to the retardation of the wind by the presence of the sand grains it is carrying (see Ch. 2.2.(iii)). Gradually, a mutual balance between wind velocity and sand mass in transport is achieved.

Although the retardation of the air flow by the grains was the first, and remains the primarily accepted self-limiting mechanism for the attainment of equilibrium mass flux (Ungar & Haff, 1987; Anderson & Haff, 1988; Werner &

Haff, 1988; Werner, 1990; McEwan & Willetts, 1991, 1993a, 1993b; Sørensen, 1991; Spies, 1996), further investigation has led to the acknowledgement of other influencing factors.

Sørensen and McEwan (1996) investigated the probability of mid-air collisions of saltating grains, a hypothesis they term 'soft bed', although they note that it 'is closely related to the 'choking' of the transport process observed at high wind speeds by Williams (1987)' (Sørensen & McEwan, 1996, p.65). The high concentration of low energy grains near the sand bed during saltation results in a high probability of a descending saltating grain colliding with another grain in mid-air. The loss of energy experienced as a result of a mid-air collision reduces the intensity of the grain-bed collision. With fewer particles in transport the probability of mid-air collisions declines. A controlling mechanism on the volume of sediment in transport can thus be envisaged.

A further mechanism in the attainment of equilibrium mass flux is the sand bed (Rice *et al.*, 1995). Numerical models of aeolian sand transport consider, at present, a homogenous, single grain-size bed. The influence of the bed is incorporated only by a stationary 'splash function' (Ungar & Haff, 1987), thus excluding the spatial and temporal developments of both the sand bed and the atmospheric boundary layer (Williams *et al.*, 1990a, 1990b, 1994, see Ch. 2.2.(i)).

Through time there is an exponential decline in the dislodgement rate of particles from the bed as the sand bed changes from a non wind-worked, open-packed surface to a wind-worked surface (Rice *et al.*, 1995). The change in the sediment size distribution of the bed during the development from a 'transport-limited' to a 'supply-limited' system (Nickling & McKenna Neuman, 1995) is not well understood. Through time Rice *et al.* (1995) record little change in the mean grain-size of the sand bed whilst Martz and Li (1997) note a reduction in the mean grain-size.

Spatially variations in the dislodgement rate of the grains from the bed show a decline in grain availability for all sites. The severity of the reduction rate diminishes with distance. The data of Li and Martz (1995) suggest that equilibrium of the dislodgement rate is achieved by ten minutes. Although the same trends are evident for all grain-sizes, the convergence to a constant rate takes longer for larger grain-sizes (Bagnold, 1941; Willetts & Rice, 1985b).

Information relating to the interaction of multiple grain-size beds with the wind, and the spatial and temporal development of these surfaces is vital to the future modelling of the sand cloud evolution and attainment and maintenance of mass flux equilibrium. At present, the overriding self-limiting control included in the numerical models is the retardation of the air flow by the grains in motion. Yet to be included, but now recognised as being significant, are the effects of mid-air collisions and the evolution of the sand bed. Until all of these processes are included in the numerical models, equilibrium of the saltation system cannot be accurately predicted or explained.

(3.3.) SUMMARY.

At present, only the numerical model of Spies (1996) considers the simultaneous spatial and temporal development of the saltation system (see Fig. 3.12.). The numerical model simulation shows a rapid growth in the transport rate over the first 10m. For downwind distances <15m stationarity of the transport rate is achieved after approximately two seconds. Further downwind (>15m) stationarity of the transport rate is not reached until three seconds.

Good agreement exists between the trends of development of mass flux and shear velocity shown by the individual studies and by the numerical model. However, until the three-dimensional development of the saltation system has been verified at all scales, by all methods of aeolian investigation, caution is required in the acceptance of results from any particular methodology.

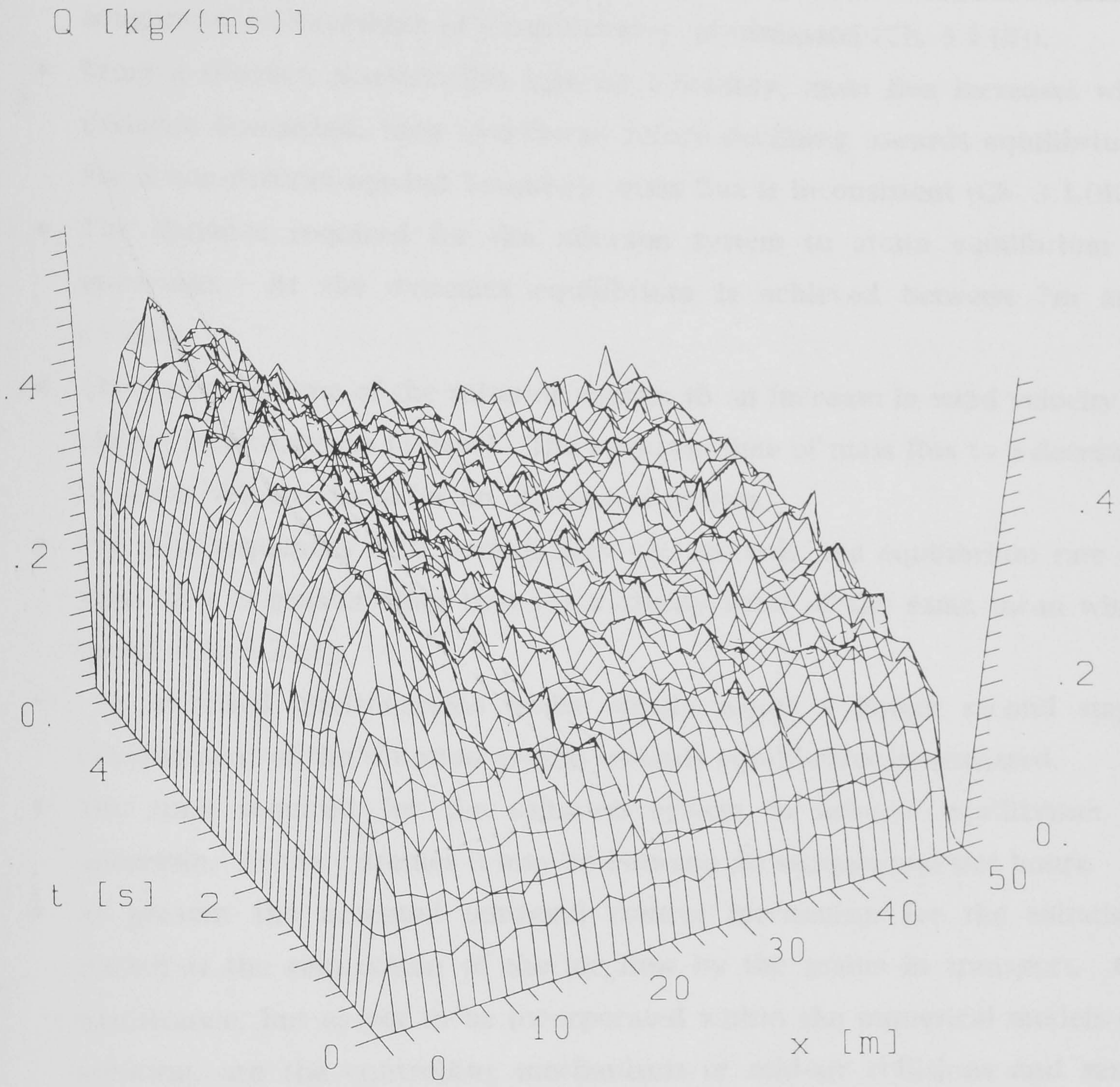

Fig. 3.12. Development of mass flux (Q) through time (t seconds) and space (x metres) calculated by the self-regulatory numerical model of Spies (1996). Initial shear velocity is 0.60m.sec^{-1}. (Spies & McEwan, in press b, p.7).

Review of existing literature pertaining to the spatial and temporal development of the saltation system allows the following statements to be made:-

- With distance downwind, shear velocity during saltation declines asymptotically towards equilibrium. Unlike a step change in surface roughness, no overshoot of shear velocity is witnessed (Ch. 3.1.(ii)).
- From a distinct, non-erodible upwind boundary, mass flux increases with distance downwind, then overshoots before declining towards equilibrium. For a non-distinct upwind boundary, mass flux is inconsistent (Ch. 3.1.(iii)).
- The distance required for the saltation system to attain equilibrium is uncertain. At the extremes equilibrium is achieved between 7m and >1000m.
- The response time of the saltation system to an increase in wind velocity is almost instantaneous (1-2sec). The response time of mass flux to a decrease in shear velocity includes an element of inertia.
- For gust sequences with periodicities <20 seconds, the equilibrium rate of mass flux is greater than that for a steady wind of the same mean wind speed. (Ch. 3.2.(i)).
- In idealised environments under steady winds a longer second stage development of the saltation system towards equilibrium is witnessed.
- The time required for the saltation system to achieve equilibrium is uncertain. At the extremes it may be between 30 seconds and two hours.
- At present the accepted temporal control mechanism for the saltation system is the retardation of the air flow by the grains in transport. Of significance, but as yet to be incorporated within the numerical models of saltation, are the controlling mechanisms of mid-air collisions and sand bed developments.
- At present only the numerical model of Spies (1996) considers the simultaneous spatial and temporal development of the saltation system. The trends in development of mass flux and shear velocity shown by individual laboratory and field studies are in good agreement with those of the numerical model.

CHAPTER 4

DEVELOPMENT OF THE SALTATION SYSTEM UNDER CONTROLLED ENVIRONMENTAL CONDITIONS

In the present study, wind tunnel experiments were designed to investigate the downwind spatial and temporal development of the saltation system under controlled environmental conditions. The development of the saltation system was monitored over a streamwise length of 8m. Sediment transport was measured at 1m intervals by the downwind deployment of seven Aarhus sand traps. Temporal wind velocity and mass flux data were collected alternately at approximately 7m downwind. Velocity data were later collected at all the mass flux monitoring sites; under steady velocities all of the data from the same experimental conditions can be amalgamated.

(4.1.) EXPERIMENTAL ARRANGEMENTS AND PROCEDURES.

(i) Experiments.

Wind tunnel experiments were designed to monitor both the downwind spatial and temporal development of the saltation system (see Fig. 4.1.). Mass flux was monitored, at approximately 1m intervals, by the downwind deployment of seven Aarhus sand traps. Mass flux was recorded at all sites simultaneously. The sand trap sampling stations were alternately offset laterally, 5cm either side of the wind tunnel center, to avoid interference between consecutive sampling stations. Mass flux was thus monitored 10cm from the left-hand tunnel wall at sampling stations X = 2.10, 4.10, 6.10 and 8m downwind, and 20cm from the front wall at sampling stations X = 3.05, 5.05 and 7m downwind.

Velocity data were collected during the experiments at the center of the wind tunnel, at $X_{7.20m}$. Velocity data could not be collected simultaneously with the corresponding mass flux data at $X_{7.00m}$ due to the close proximity of the hot-

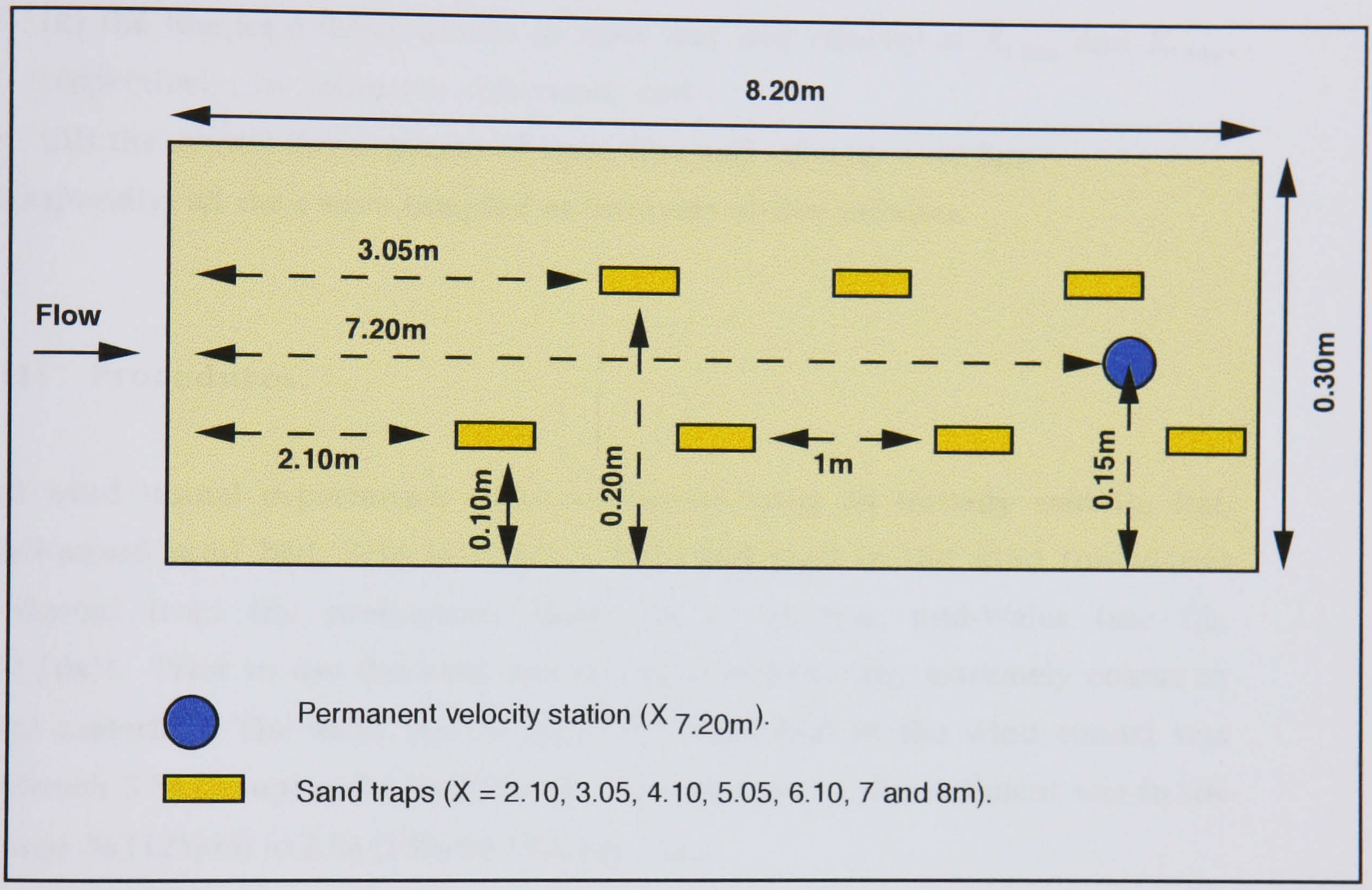

Fig. 4.1. Schematic diagram of the Queen Mary and Westfield wind tunnel experimental arrangement. Mass flux has monitored at approximately 1m intervals. The sand trap sampling stations were alternatively offset laterally, 5cm either side of the center, to avoid interference between consecutive sampling stations. Velocity data were collected during the experiments at the center of the wind tunnel at 7.20m. After each experiment velocity data were collected at all mass flux monitoring sites.

wire probes and the sand trap. As a result, velocity data were obtained for the periods immediately prior to the collection of mass flux data. After each experiment, spatial velocity data were collected at X = 1.20, 2.20, 3.10, 4.10, 5.15, 6.15 and 7.20m downwind.

For each experiment data were obtained for:

- (i) the spatial and temporal development of sand in transport;
- (ii) the temporal development of mass flux and velocity at $X_{7.00m}$ and $X_{7.20m}$, respectively, by alternate collection; and
- (iii) the spatial development of mass flux and velocity over 8m.

Temporally, all data were sampled at intervals of five minutes.

(ii) Procedures.

All wind tunnel experiments were conducted using an initially smooth, flat, well-mixed sand bed, 3cm in depth. The sand used in the wind tunnel was collected from the preliminary field site at Ynyslas, mid-Wales (see Ch. 5.1.(iia)). Prior to use the sand was sieved to remove any extremely coarse or fine material. The sand laid to form the sand bed of the wind tunnel was between 3.5ϕ (90μm) and 1.5ϕ (355μm). Sixty percent of the sediment was in the range 3ϕ (125μm) to 2.5ϕ (180μm) (see Fig. 4.2.).

Prior to each experiment a detailed velocity profile of 24 points (0.20-1cm in 0.20cm intervals and 1-10cm in 0.50cm intervals) was measured. The sand bed was then thoroughly re-mixed and smoothed prior to the collection of mass flux data. The seven sand traps were attatched onto their support rods and inserted in the wind tunnel (see Ch. 4.1.(iv(b))). The sand traps were held elevated at the wind tunnel roof. Once the wind tunnel had been sealed the tunnel was started ($T_{0\,secs}$) and run for 15 seconds. This period, prior to data collection, allows the stabilisation of both the wind velocity and the sand bed.

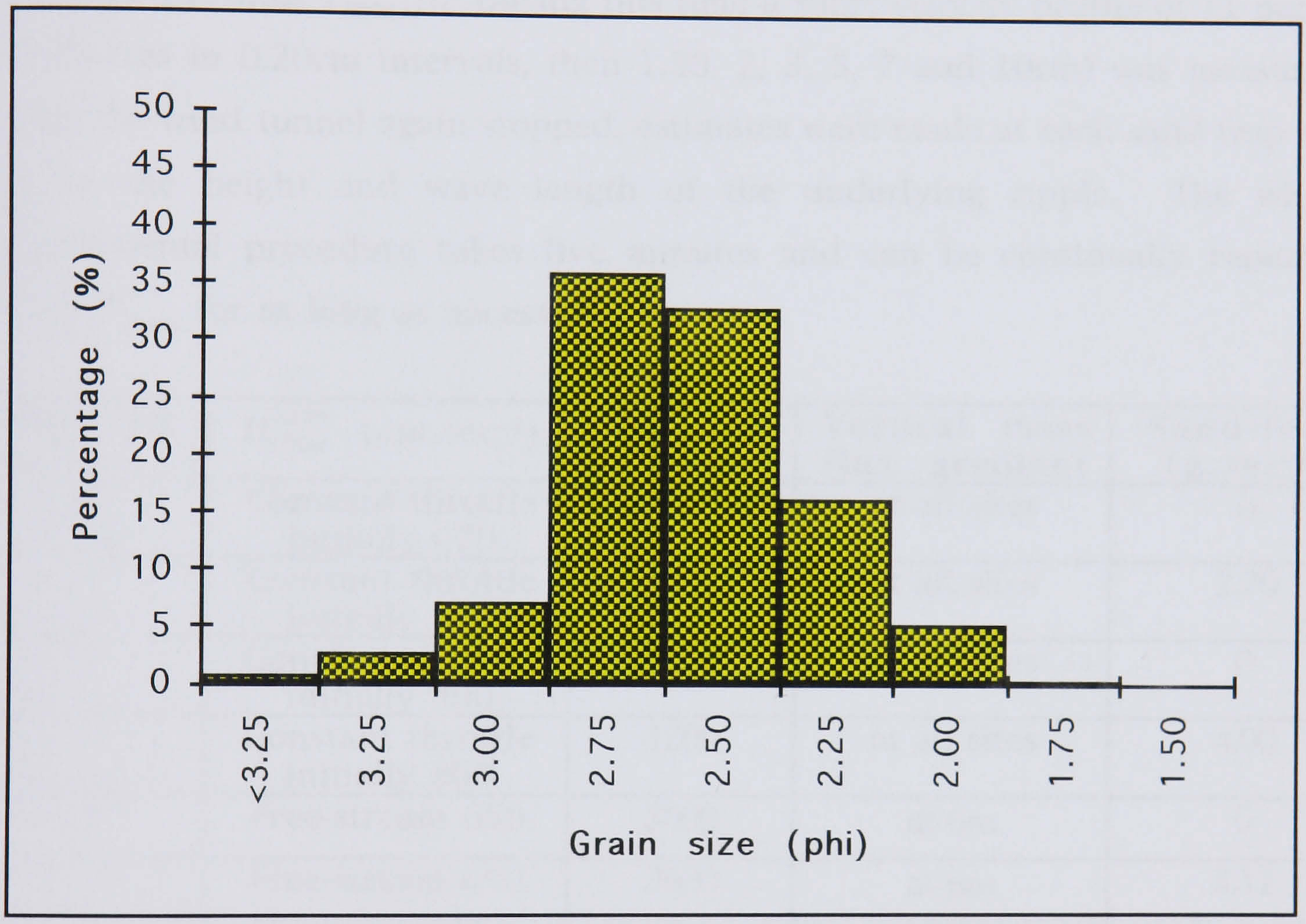

Fig. 4.2. Grain-size distribution of sand used in the experiments in the Queen Mary and Westfield wind tunnel. The sand used was collected from the preliminary field site at Ynyslas, mid-Wales.

The sand traps were lowered to the bed, in order from 8-2m, at T_{15secs}. After 90 seconds of mass flux collection, at $T_{105secs}$, the sand traps were raised to the wind tunnel roof in the same order as they were dropped. The wind tunnel was then stopped. With the wind tunnel stopped, all the sand traps were removed from the wind tunnel and replaced. The empty sand traps were again positioned at the wind tunnel roof.

Prior to the second collection of mass flux the wind tunnel was run for 195 seconds (i.e. until $T_{300secs}$). During this time a short velocity profile of 11 points (0.20-1cm in 0.20cm intervals, then 1.50, 2, 3, 5, 7 and 10cm) was measured. With the wind tunnel again stopped, estimates were made at each sand trap site as to the height and wave length of the underlying ripple. The whole experimental procedure takes five minutes and can be continually repeated from T_{0secs} for as long as necessary.

Data Set	$U_{7.20m}^{0.15m}$ (cm.sec^{-1})	Duration (secs)	Vertical mass flux gradient	Sand-feed (g.sec^{-1})
1	Constant throttle initially 670	1200	at all sites	0
	Constant throttle initially 670	1200	at all sites	2.70
	Constant throttle initially 800	1200	at all sites	0
	Constant throttle initially 800	1200	at all sites	4.00
2	Free-stream 650	3600	at 6m	0
	Free-stream 650	3600	at 6m	3.11
	Free-stream 700	3600	at 6m	0
	Free-stream 700	3600	at 6m	3.34
	Free-stream 750	3600	at 6m	0
	Free-stream 750	3600	at 6m	3.50
	Free-stream 800	3600	at 6m	0
	Free-stream 800	3600	at 6m	4.00

Table 4.1. Summary of wind tunnel experiments.

Table 4.1. details the <u>two</u> sets of mass flux experiments conducted:

(i) 'Data Set 1' is composed of experiments conducted at two constant wind tunnel throttle settings. Each experiment is 1200 seconds long and consists of four $T_{300secs}$ sampling periods. The vertical distribution of mass flux is monitored at all sites. At each throttle setting experiments are conducted with and without sand-feed.

(ii) 'Data Set 2' is composed of experiments conducted at four constant free-stream velocities. Each experiment is 3600 seconds in duration and consists of 12 sampling periods, each of $T_{300secs}$. The vertical distribution of mass flux is monitored at $X_{6.00m}$. At each velocity experiments are conducted with and without sand-feed.

(iii) Controlled environment.

(a) Wind tunnel.

The wind tunnel at Queen Mary and Westfield College has a working section 8.20m long (see Figs. 4.3. and 4.4.). Flow is generated by a 1.1Kw motor unit powering a variable pitch axial flow fan (0.45m in diameter). The rate of flow can be controlled electronically by either pre-programming flow sequences or manually adjusting the rate of flow as required.

Prior to the flow entering the working section of the wind tunnel it passes through: a 1m long flow straightening section which consists of a honeycomb, three gauzes and an air bleed throttle control; a contraction section 1.40m long and of a ratio 2:1; and a 0.80m long section of artificially roughened floor (Butterfield, 1993). The artificially roughened floor is used to trip and enhance the wind tunnel boundary layer development.

The working section of the wind tunnel comprises eight units each approximately 1m long and 0.30m square in cross-section. The beginning of the working section of the wind tunnel is located at the end of the artifically

Fig. 4.3. Queen Mary and Westfield College wind tunnel - external view.

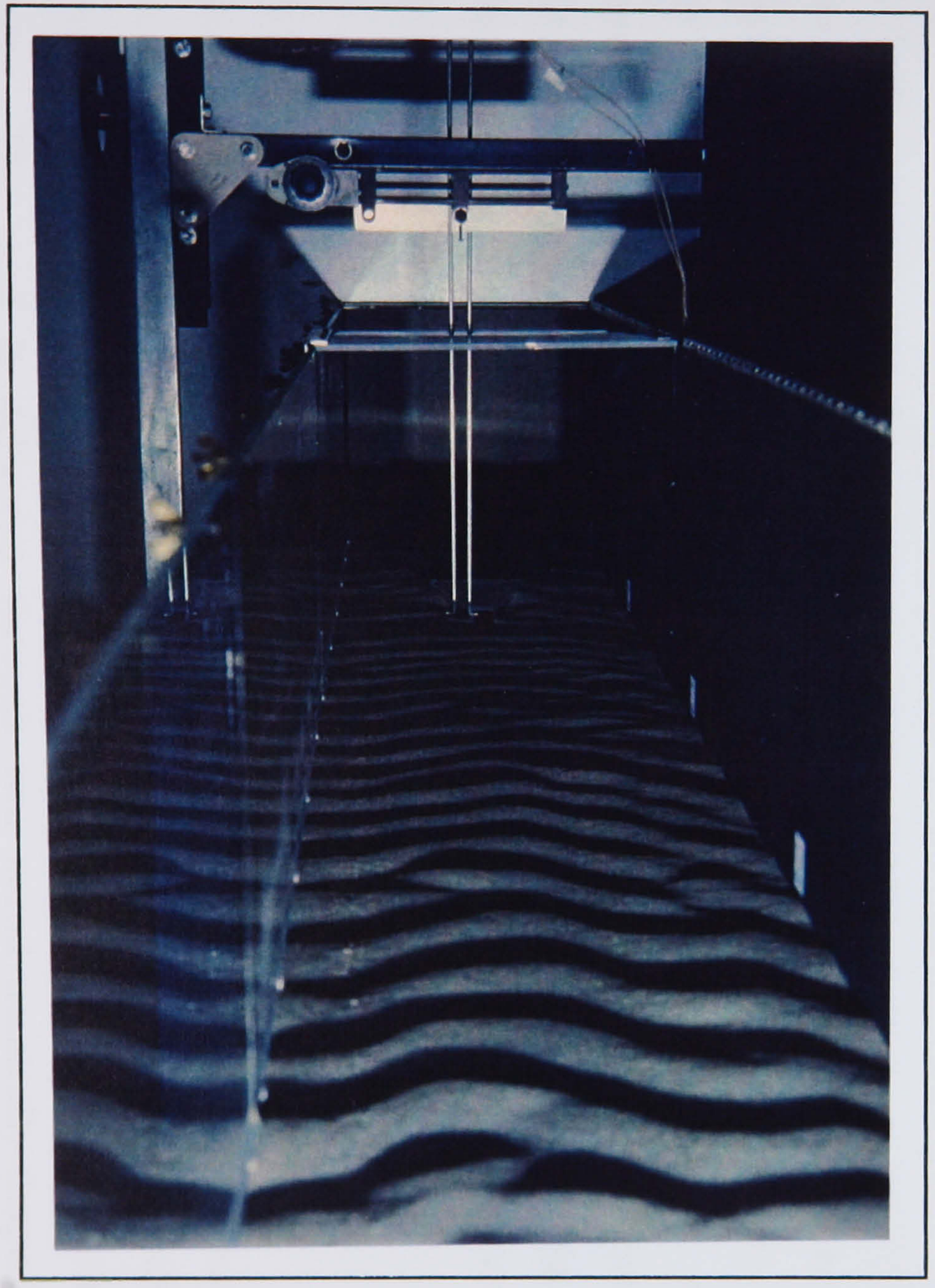

Fig. 4.4. Queen Mary and Westfield College wind tunnel - internal view.

roughened floor, upwind of the sand bed. The right-and left-hand walls of the wind tunnel are made of aluminium and Plexiglass, respectively. (Henceforth, all following lateral measurements use 0cm located at the left-hand wall facing downstream).

The floor of the working section consists of boards fixed with a single grain layer of sand. When empty of loose sand the wind tunnel flow can be calibrated over a representative sand roughness. By adjusting the vertical height of the floor boards a loose bed of test sand of various depths can be employed. Access to the inside of the working section of the wind tunnel is gained through hinged sections of the roof.

At the exit of the working section of the wind tunnel there is a settling chamber (2.40 x 1.20 x 1m) ventilated by gauze. Within the settling chamber a funnelling system may be installed to direct sediment onto an electronic balance. The weight of sediment transported through the wind tunnel is used for the determination of an appropriate rate of sand-feed (see Ch. 4.1.(iii(b))).

Butterfield (in press) has shown that for the dimensions of the Queen Mary and Westfield wind tunnel the Froude numbers (see Ch. 3.1.(ii(a))) are <20 only for free-stream velocities $\leq$770cm.sec^{-1}. Although the highest velocity experiments of this study (see Table 4.1.) exceed the acceptable free-stream velocity, no adverse effects were recorded within the results (see Fig. 4.20.). The majority of the results are, however, derived from experiments with free-stream velocities $\leq$770cm.sec^{-1}.

(b) Upwind artificial sand-feed.

When required, a sand hopper is used to introduce artificially-fed sand into the saltation system. Sand is fed into the near-bed region of the wind tunnel (the exact height is adjustable) at the beginning of the artificially roughened floor. The sand is delivered through two aerodynamically-shaped tubes, 7.50cm either side of the wind tunnel centre, i.e. 7.50cm and 22.50cm from the

left-hand wall. At the base of the sand-feed tubes dispersion plates aid the distribution of sand across the entire width of the wind tunnel.

The rate of artificial sand-feeding is controlled manually using valves which adjust the size of the funnelling apertures. Sand can be fed into the saltation system at any rate between $0.10 g.sec^{-1}$ and $4 g.sec^{-1}$. A slight imbalance does exist between the two sand-feed tubes, the tube at 22.50cm delivering marginally less sand than the tube at 7.50cm. However, for rates of sand-feed used by the experiments, $>2.50 g.sec^{-1}$, the difference in the volume of sand delivered by the two tubes is <1%.

For experiments with sand-feed an attempt was made to find an equilibrium rate, i.e. input ≈ output, over a designated time period (Al-Awadhi & Willetts, 1998). For the experiments using a constant throttle setting (Data Set 1, see Table 4.1.), the time taken for a known quantity of sand to be fed into the airflow was noted. The wind tunnel was then stopped and the quantity of sand collected in the settling chamber weighed. This procedure was repeated, varying the rate of fed sand, until an appropriate balance was achieved between the input and the output of sand.

For the experiments using a constant free-stream velocity (Data Set 2, see Table 4.1.), the rate of sand-feeding was based on the mass flux results at $X_{8.00m}$. Rates of transport of sand were adjusted to the wind tunnel cross-sectional area and time of collection. The corresponding rate of sand-feed was then applied. With the introduction of sand-feed the mass flux at $X_{8.00m}$ was again recorded. The rate of sand-feed was then adjusted until an approximate balance was achieved with $Q_{8.00m}$.

(iv) Instrumentation

(a) Wind velocity.

Wind velocity profiles were conducted using a vertical traverse by a single steel-clad Dantec hot-wire probe (see Fig. 4.5.). The probe is 1mm in diameter and 'specially configured to minimise flow disturbance' (Butterfield, 1993, p.314). Initial probe elevations relative to the sand bed surface were determined to within ± 0.05cm using a vernier racking system. Flow velocities were averaged over 10 seconds by standard Dantec Flow Master temperature-compensated thermal anemometers.

(b) Mass flux.

In all environments, but especially those of confined space, sand traps intrude into and disturb the conditions to be monitored (Sarre, 1988). Equipment does exist for the non-obtrusive collection of mass flux but it is costly. The use of optical mass flux sensors (Butterfield, in press) at numerous sites is not practical. Despite the low efficiencies of some designs (Horikawa & Shen, 1960) sand traps remain the most common method for gaining short-term mass flux data (Butterfield, 1991).

In this investigation, vertically segmented Aarhus traps were constructed from polycarbonate, twin-wall sheet, of wall thickness 0.50mm (see Fig. 4.6.). Each trap is 14.80cm long, 10.80cm high and 0.80cm wide, and consists of ten horizontal chambers each 0.80 x 0.90cm in cross-section. Each chamber is ventilated with 150μm gauze at the back and sides (each side with a gauze region 5 x 0.60cm in size). Considerable ventilation was included in the design to alleviate air stagnation within the sand trap (Jones & Willetts, 1979).

The sand traps at each sampling station are manoeuvred within the wind tunnel by means of metal suspension rods passing through the wind tunnel roof (see Fig. 4.6.). Spring clips located on the wind tunnel roof allow the metal rods (and thus the sand traps), to be raised, lowered and held at any distance between the wind tunnel roof and the sand bed. The use of adjustable

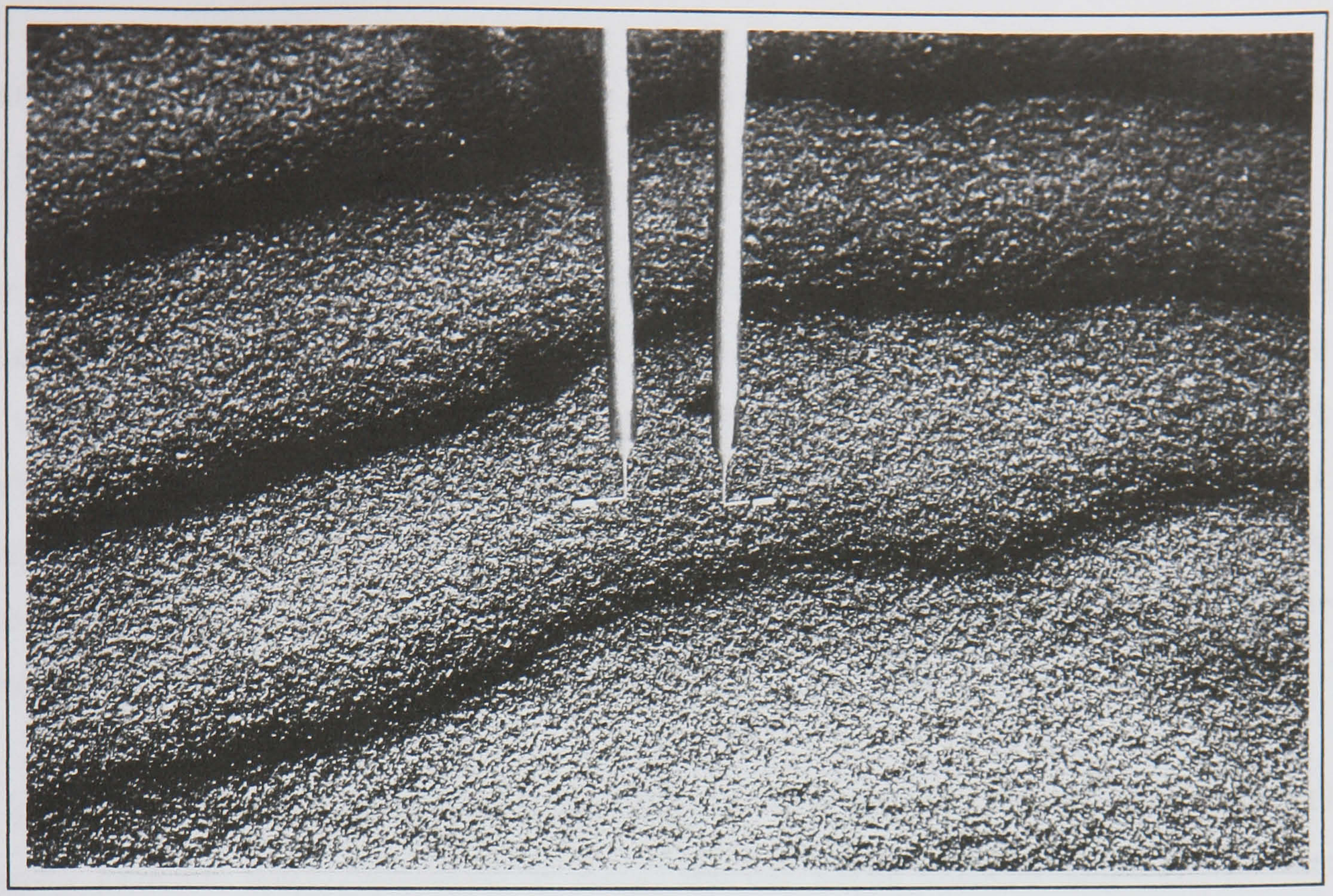

Fig. 4.5. Dantec armoured hot-wire probes 'in situ' in the wind tunnel at the 7.20m velocity monitoring station.

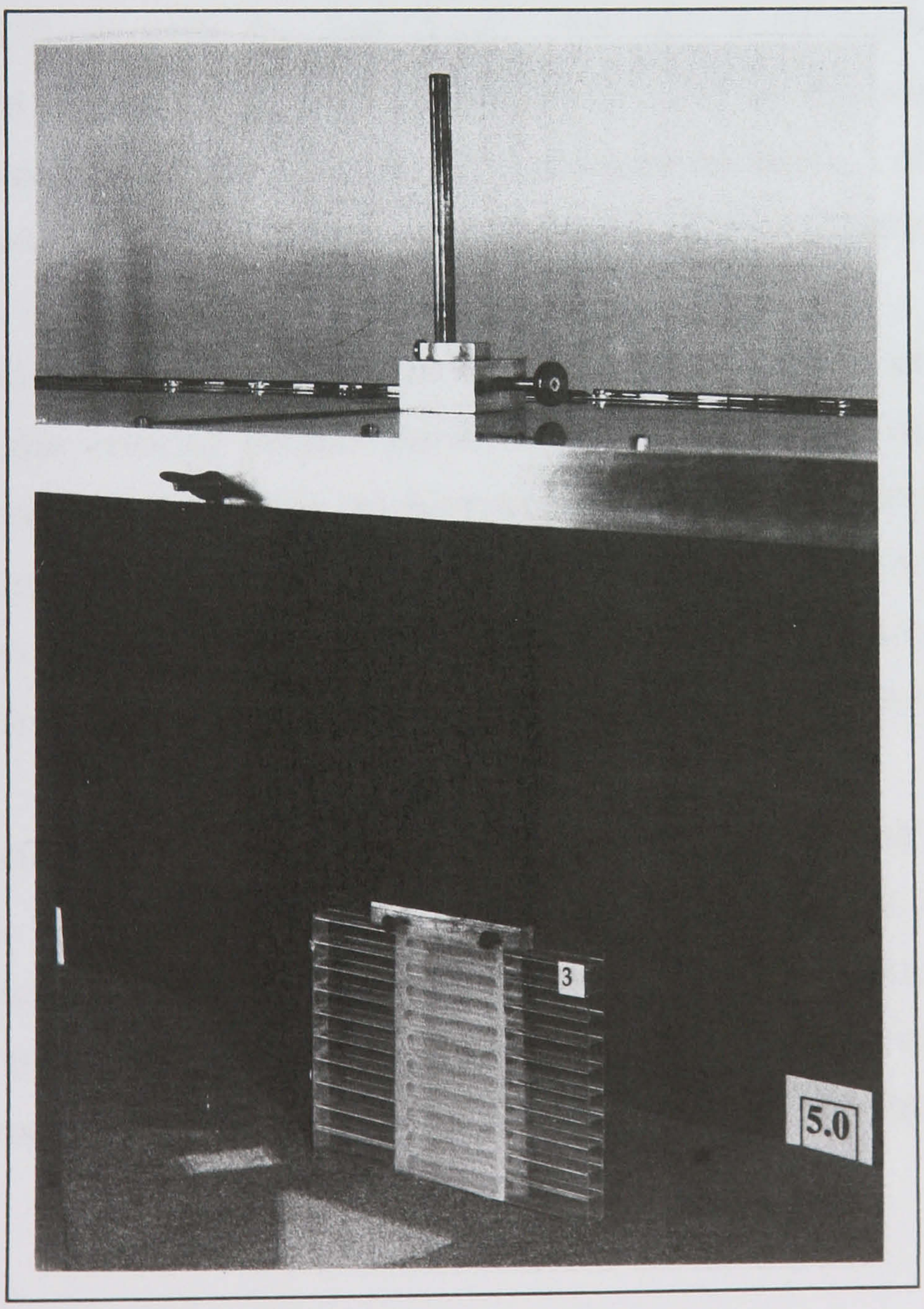

Fig. 4.6.
Aarhus sand trap 'in situ' in the wind tunnel. The traps are manoeuvred within the wind tunnel by means of metal suspension rods. The sand traps can be raised, lowered and held at any distance between the wind tunnel roof and the sand bed.

collars on the metal suspension rods allow the sand traps to be dropped rapidly to a pre-determined elevation or flush with the sand bed.

Over a flat sand bed without saltation the sand trap can be lowered flush to the surface. During saltation, as the bed ripples, the sand trap position relative to the surface varies. Ripples were observed to pass within the lower chambers of the sand trap with little modification. At high velocities, however, the lower chambers of the sand traps became approximately half full, sufficient to reduce the ventilation significantly, in 90 seconds. During this period scour around the sand trap remained minimal.

To investigate the effect of the sand traps on the air-flow in the wind tunnel velocity profiles were measured at $X_{7.20m}$ during three experimental situations: (i) no sand traps in the wind tunnel; (ii) all seven sand traps in the wind tunnel and held at the roof; and (iii) all seven sand traps in the wind tunnel and flush with the sand bed. (For the third experimental arrangement the sand trap at $X_{7.00m}$ was continuously held at the wind tunnel roof due to its proximity to the velocity measurement station). All three experiments were considered both during clean air conditions and with saltation.

In clean air conditions the introduction of sand traps has no significant effect on the velocity profile above 6cm (see Fig. 4.7.). Below 6cm, the introduction of sand traps causes an increase in velocity, the greatest increase experienced being when the sand traps are flush with the sand bed. It is suggested that the velocity increase in the lower region of the boundary layer is due to the increased pressure gradients generated as air is forced around the sand traps.

During saltation the sand traps are an insignificant influence on the flow (see Fig. 4.7.). The lack of effect of the sand traps on the velocity profile during saltation is due to the greater mixing associated with the transport of sediment. In situations where mass flux will be sampled, therefore, the sand traps can be considered an inconsequential influence on the system being monitored.

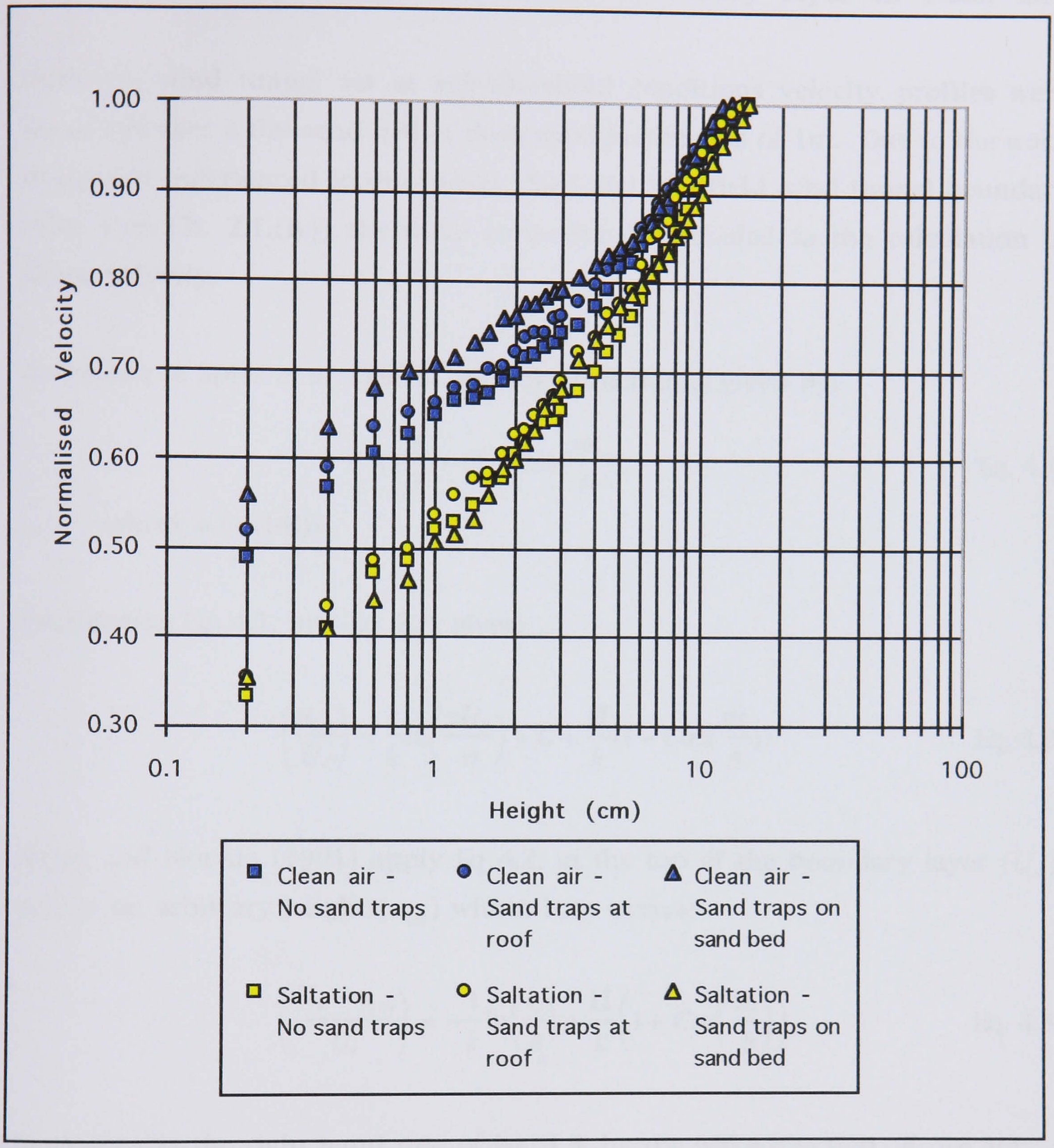

Fig. 4.7. Effect of the introduction of sand traps in the Queen Mary and Westfield wind tunnel. Velocity profiles were measured at 7.20m during three experimental situations: (i) no sand traps in the wind tunnel (square symbols); (ii) sand traps held at the wind tunnel roof (circular symbols); (iii) sand traps flush with the wind tunnel sand bed (triangular symbols). All three experiments were considered both during clean air conditions (blue symbols) and saltation (yellow symbols).

(4.2.) WIND TUNNEL CALIBRATION.

(i) Streamwise developments of the boundary layer in clean air.

With the wind tunnel set at sub-threshold conditions velocity profiles were measured over a flat sand bed at downwind increments of 1m. Due to the wake departure experienced in the Queen Mary and Westfield wind tunnel boundary layer (see Ch. 2.1.(iv)) the wake correction is included in the calculation of shear velocity.

According to Spies *et al* (1995) the wake function is given by:

$$w(\frac{y}{\delta}) = (1 - Cos(\frac{\pi z}{\delta})) \qquad \text{Eq. 4.1.}$$

where $\pi = 3.1416$.

Substituting Eq. 4.1. into Eq. 2.9. gives:

$$\left(\frac{u_{(z)}}{U_*}\right) = \frac{1}{k}\ln\left(\frac{yU_*}{\upsilon}\right) + C + \frac{\Pi}{k}(1 - Cos(\frac{\pi z}{\delta})) \qquad \text{Eq. 4.2.}$$

White and Mounla (1991) apply Eq 4.2. at the top of the boundary layer (U_∞) and at an arbitrary height ($u_{(z)}$) within it to derive:

$$\left(\frac{U_\infty - u_{(z)}}{U_*}\right) = -\frac{1}{k}\ln\left(\frac{z}{\delta}\right) + \frac{\Pi}{k}\left(1 + Cos\left(\frac{\pi z}{\delta}\right)\right) \qquad \text{Eq. 4.3.}$$

Representing the right hand side of Eq. 4.3. by the wake function, F, we get:

$$U_\infty - u_{(z)} = U_* F \qquad \text{Eq. 4.4.}$$

Hence, U_* is the gradient of the plot of F (on the x-axis) against $U_\infty - u_{(z)}$ (on the y-axis).

Alternatively, the similar method of Owen and Gillette (1985) can be used:

$$u_{(z)} = U_* F' \qquad \text{Eq. 4.5.}$$

where $F' = \frac{1}{k}\ln\left(\frac{z}{\delta}\right) + (0.5\lambda)(1 - Cos(\frac{\pi z}{\delta})$; and

$\lambda = 1.1.$

Shear velocity in this case is the gradient of the plot of F' against $u_{(z)}$ (see Fig. 4.8.). (Note, use of the term 0.5λ in Eq. 4.5. is equal to using a clean air value of $\Pi = 0.55$ in Eq. 4.3. (White & Mounla, 1991, see Ch. 2.1.(iv) and Ch. 2.3.(iii)).

With distance downwind shear velocity decreases due to the propagation of surface shear stress upward through a boundary layer of increasing depth (see Fig. 4.9.). Shear velocity in both the laboratory and the field results is represented as a normalised value. In the field the amalgamation of data from different sites and times requires the information to be normalised (due to fluctuations in wind velocity). In the laboratory the constant velocity flow negates the need for this procedure. By normalising <u>all</u> velocity profiles to their individual free-stream value, i.e. all sites have a free-stream value of unity, the differences due to the differing spatial development of the boundary layer in the different environments are minimised.

(ii) Cross-stream development of velocity in clean air.

In a wind tunnel, boundary layers develop on all four constraining walls. Only the central section of the flow is workable. All the aforementioned information pertaining to the wind tunnel calibration has been obtained from centrally-based measurements. The lateral distribution of flow within a wind tunnel, however, is rarely perfectly symmetrical (Philips, 1980, in Abdullah, 1996). The decision to sample mass flux 5cm either side of the centre of the wind tunnel made it imperative that the flow cross-profile was quantified.

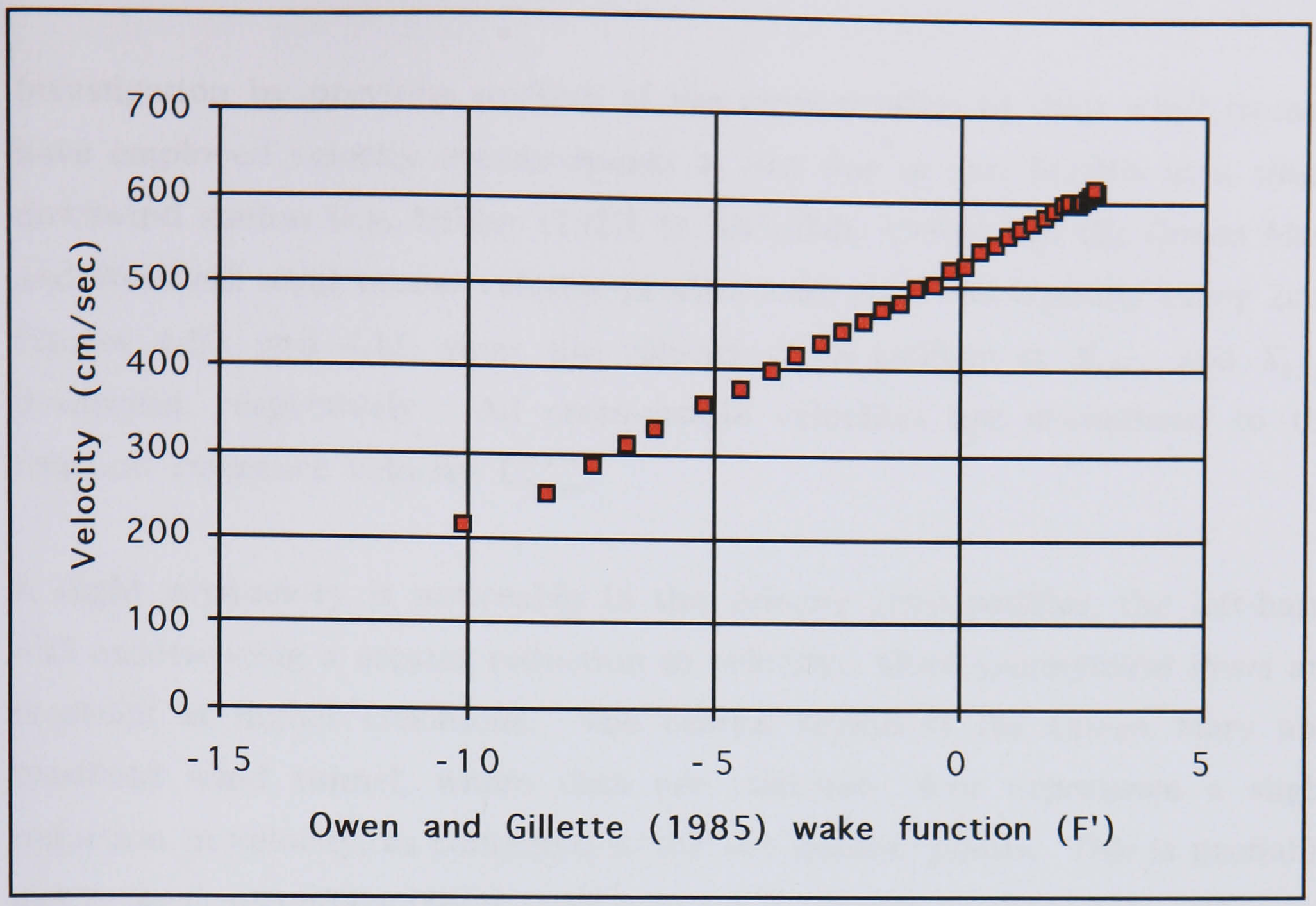

Fig. 4.8. Calculation of shear velocity using the wake correction method plotting the wake function (F') against velocity (u_z).

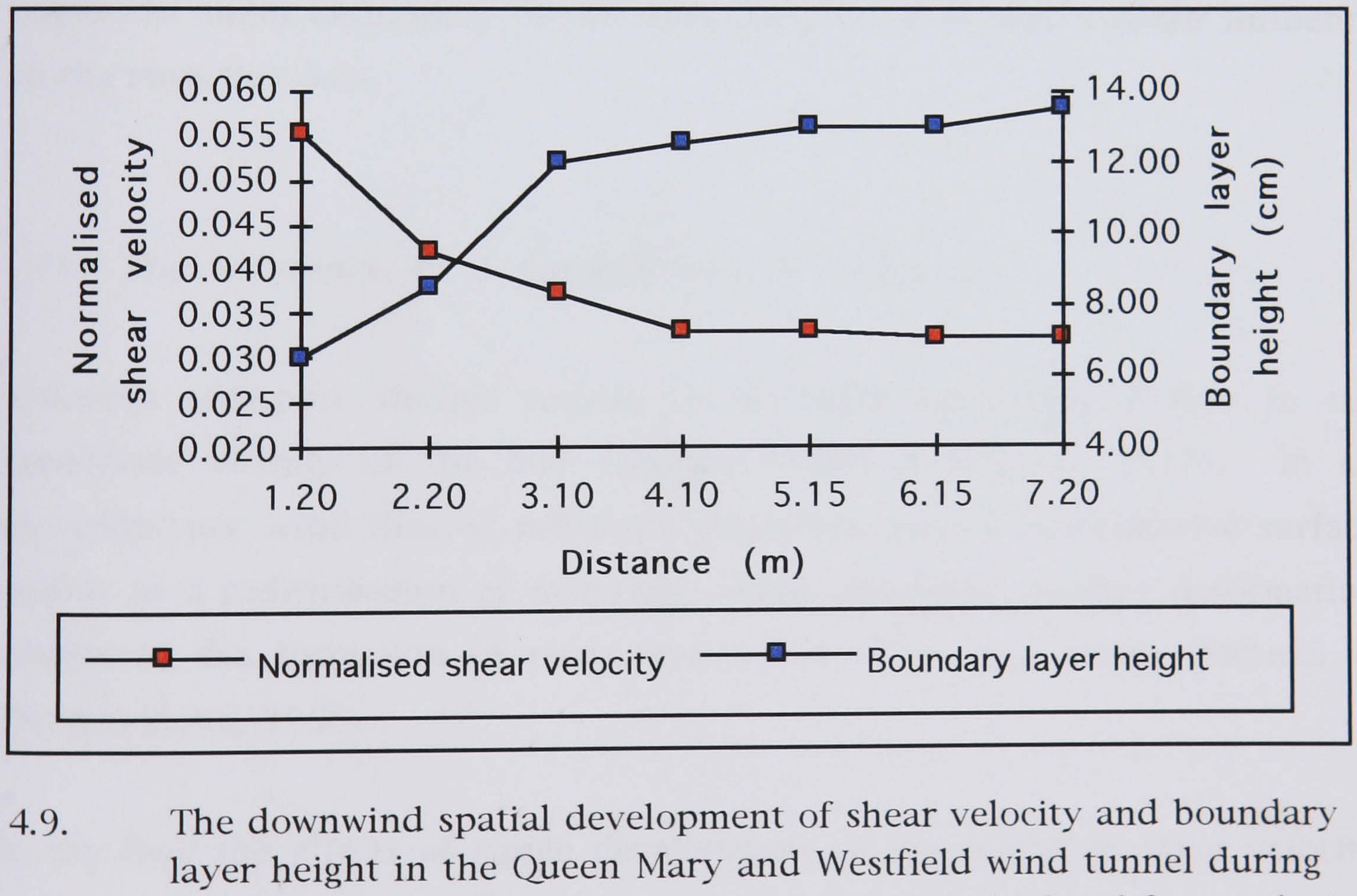

Fig. 4.9. The downwind spatial development of shear velocity and boundary layer height in the Queen Mary and Westfield wind tunnel during conditions of clean air. Shear velocities are calculated from velocity profiles normalised to their free-stream value. The boundary layer height is characteristic of the $U_{7.20m}^{0.15m} = 600\text{cm.sec}^{-1}$ experiment.

Investigation by previous workers of the cross-profiles in their wind tunnels have employed velocity measurements at just one or two heights at a single downwind station (e.g. Philips (1980, in Abdullah, 1996)). In the Queen Mary and Westfield wind tunnel velocity profiles were recorded laterally every 2cm. Figures 4.10. and 4.11. show the velocity cross profiles at $X_{3.10m}$ and $X_{6.15m}$ downwind, respectively. All cross-profile velocities are normalised to the constant reference velocity $U_{8.00m}^{0.15m}$.

A slight asymmetry is noticeable in the velocity cross-profiles, the left-hand wall experiencing a greater reduction in velocity. More symmetrical flows are recorded at higher elevations. The central region of the Queen Mary and Westfield wind tunnel, where data are collected, does experience a slight reduction in velocity, as compared to the two quarter points. This is probably due to weak secondary circulations induced by blower wind tunnels. However, from Figure 4.12. it can be seen that all the sand traps sample between the faster moving flow at the quarter points and the central region of reduced flow. The slight asymmetry of the wind tunnel flow is thus a minor influence on the mass flux data.

(iii) The influence of a rippled bed in clean air.

Sediment transport studies require an accurate knowledge of flow in the immediate vicinity of the bed (Dungan Smith & McLean, 1977). In all environments, wind flow of sufficient magnitude over a non-cohesive surface results in a redistribution of materials. Most commonly, surface deformation results in the formation of transverse waves of varying scales (McLean & Dungan Smith, 1986).

In the field the effects of ripple development on the boundary layer velocity profile and sediment transport can generally be ignored. The deviation of the bed by 2-3cm in vertical extent is a minor influence on averaged velocities

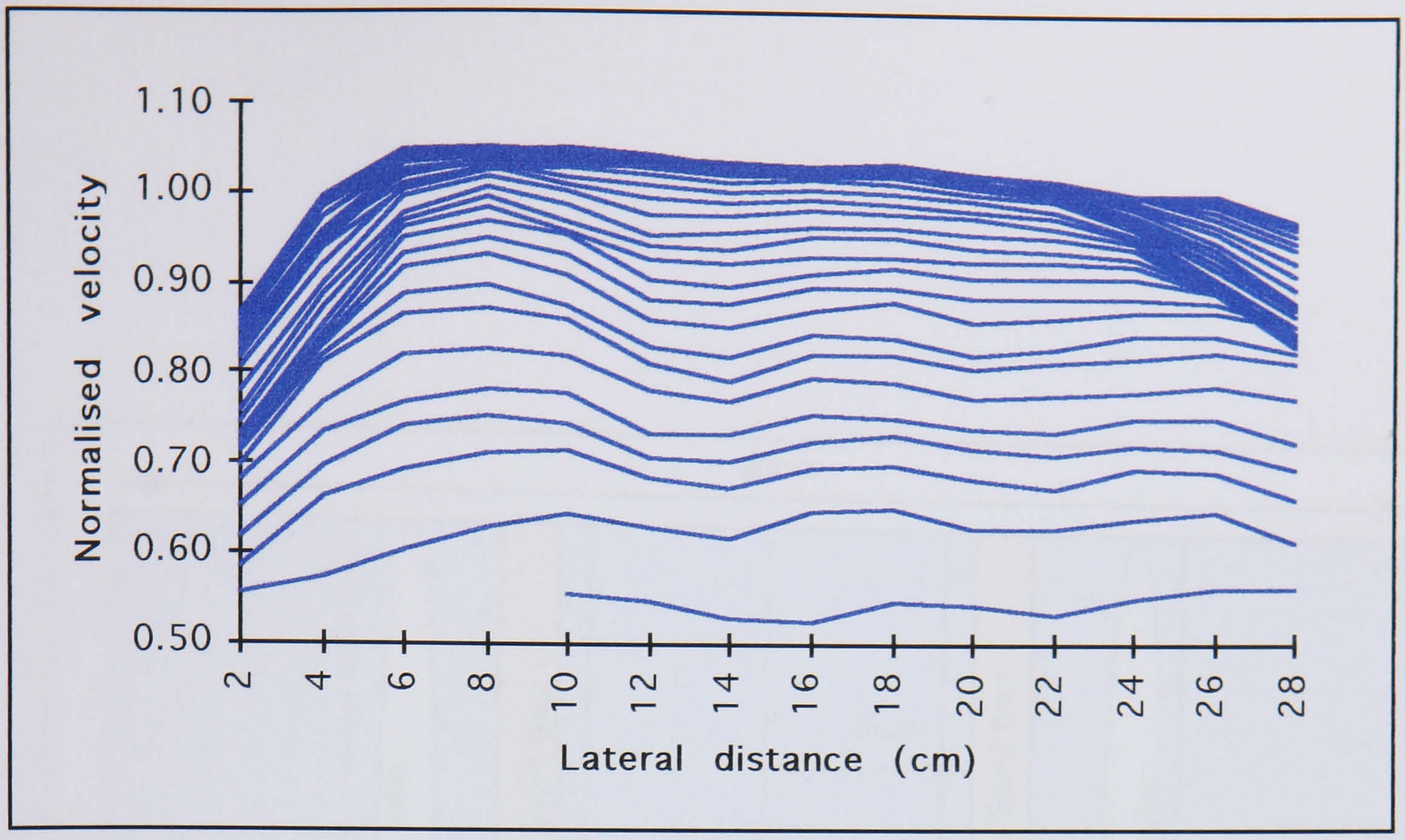

Fig. 4.10. Lateral distribution of velocity at 3.10m downwind in the Queen Mary and Westfield wind tunnel, in clean air (see caption below for details).

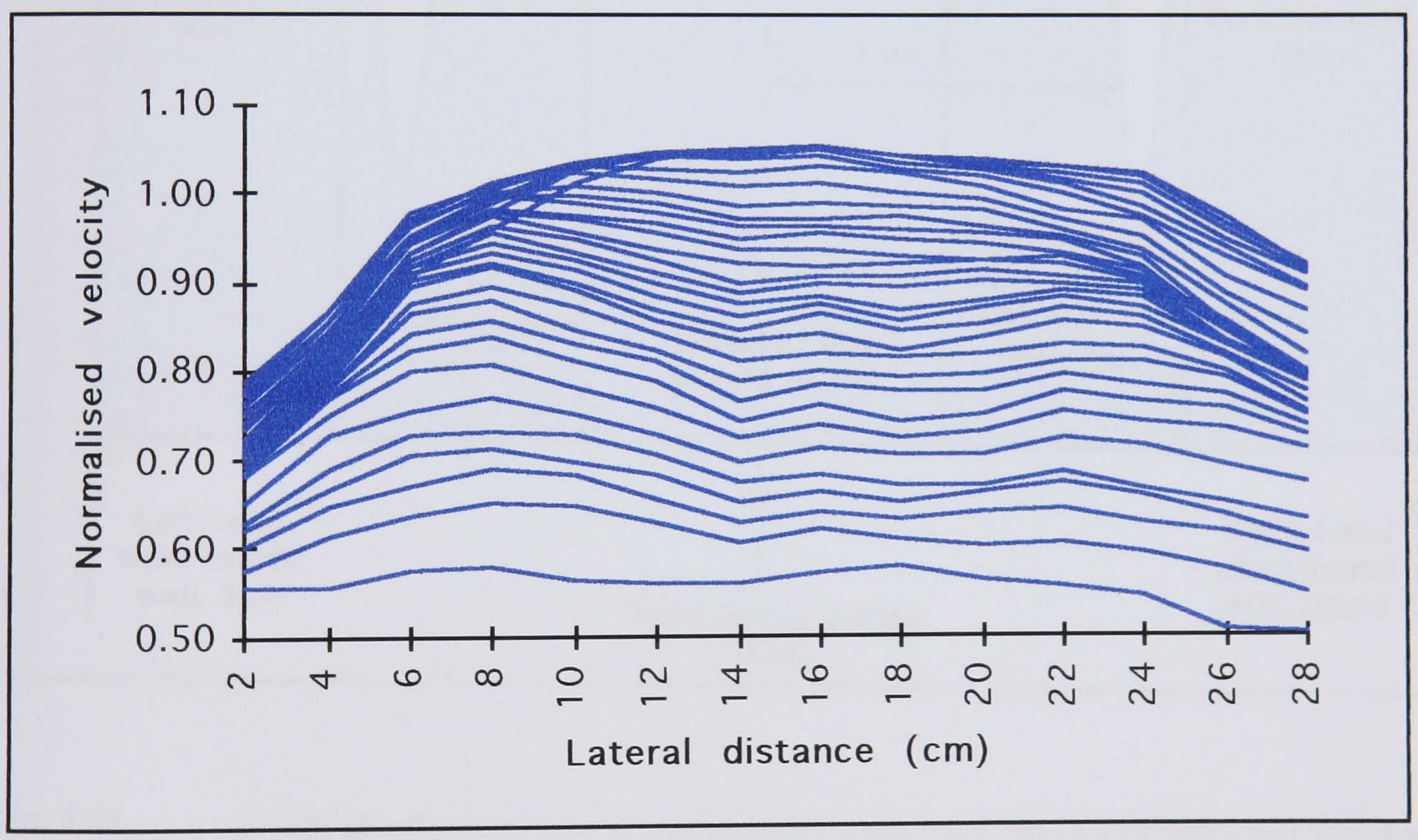

Fig. 4.11. Lateral distribution of velocity at 6.15m downwind in the Queen Mary and Westfield wind tunnel, in clean air. Velocity profiles were recorded every 2cm laterally across the wind tunnel. Throughout the experiments data are normalised to the constant free-stream velocity $U_{8.00m}^{0.15m}$ in the center of the wind tunnel. Note the greater concentrations of isovels at the top of Fig. 4.10. as compared to Fig. 4.11. highlighting the downwind development of the boundary layer height.

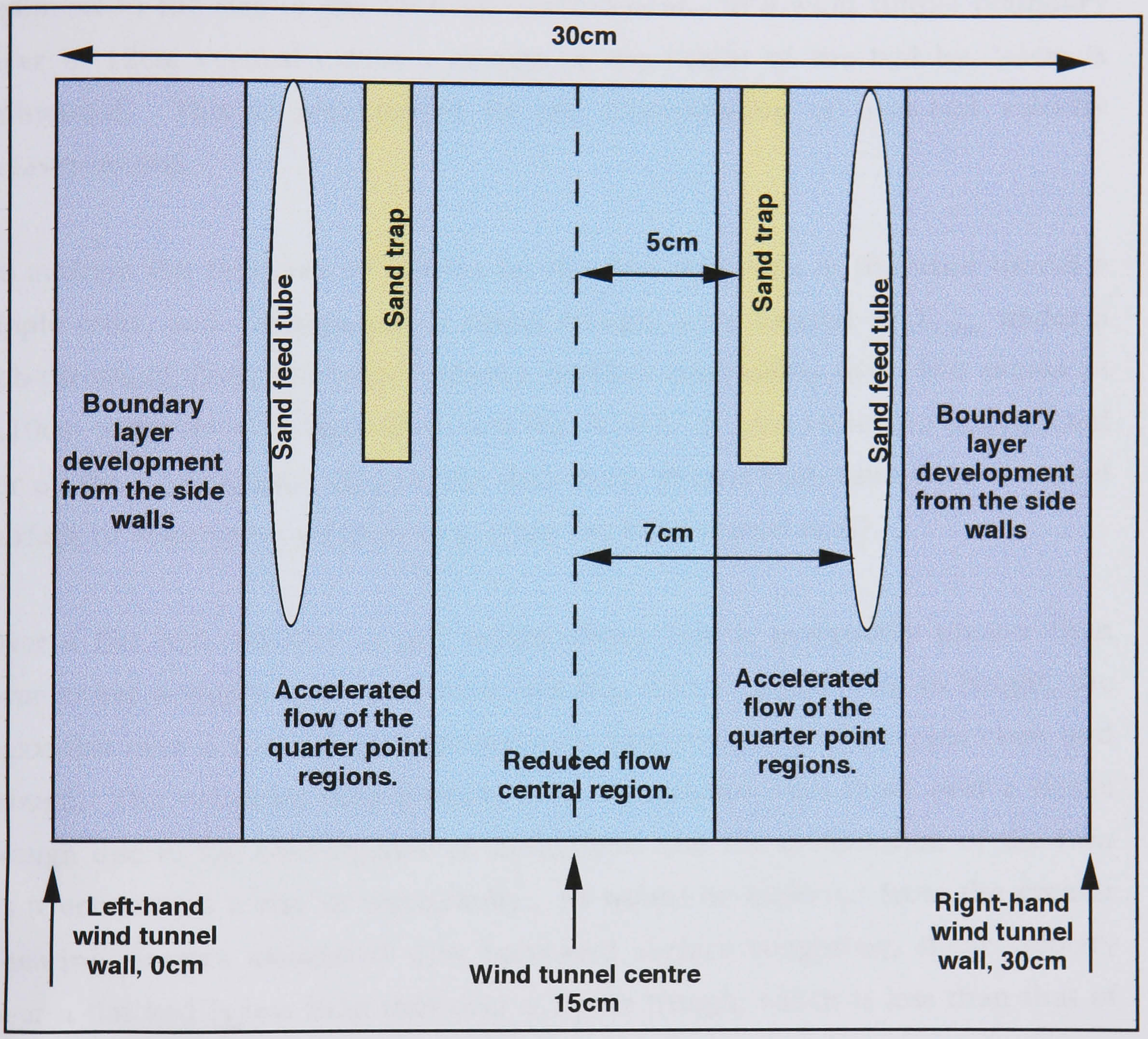

Fig. 4.12. Schematic diagram showing the different regions of the Queen Mary and Westfield wind tunnel flow and the relative locations of the equipment. It is noted that the wind tunnel sand hopper tubes coincide with the location of the faster regions of flow at the quarter points. All the sand traps, however, sample between the faster moving flow at the quarter points and the central region of reduced flow.

measured 0.10m (and greater) above the surface. Moreover, the scale of the bed forms is insignificant in comparison to the vertical extent of the total boundary layer and surrounding topography.

In the wind tunnel, ripples are 'larger than life' due to the inability to scale sediment to the size of the artificial environment. In a wind tunnel boundary layer of 12cm vertical extent a change in the height of the bed by 2-3cm is influential. This is accentuated by the close-spacing of near-bed velocity measurements.

To address the influence of ripples on the flow structure in the wind tunnel a ripple crest, and subsequently a ripple trough, were located at $X_{7.20m}$ under a sub-threshold flow. Detailed velocity profiles comprising over 100 points at 0.10cm intervals were measured (see Fig. 4.13.). A zero reference plane, fixed for all the experiments, allowed the data to be plotted both relative to the sand surface or relative to a datum (e.g. from the wind tunnel roof).

Over a flat bed, velocity at any height above 1cm is marginally greater than over either a ripple crest or trough (see Fig. 4.13.). Below 1cm in height, the velocities over a flat bed lie appropriately between those of a ripple crest and trough. The velocities over a ripple crest are greater than those over a ripple trough due to the convergence of streamlines and the acceleration of the flow as it encounters a rise in topography. As would be expected from the greater shearing stresses associated with increased surface roughness, shear velocity over a flat bed is less than that over a ripple trough, which is less than that of a ripple crest.

During the experiments it was hoped that observations of the relative position of ripples beneath the sand traps would explain some of the recorded variations in mass flux. Despite evidence for greater shearing stresses over a ripple crest, however, no correlation could be found between the measured rate of mass flux and the surface feature below the sand trap.

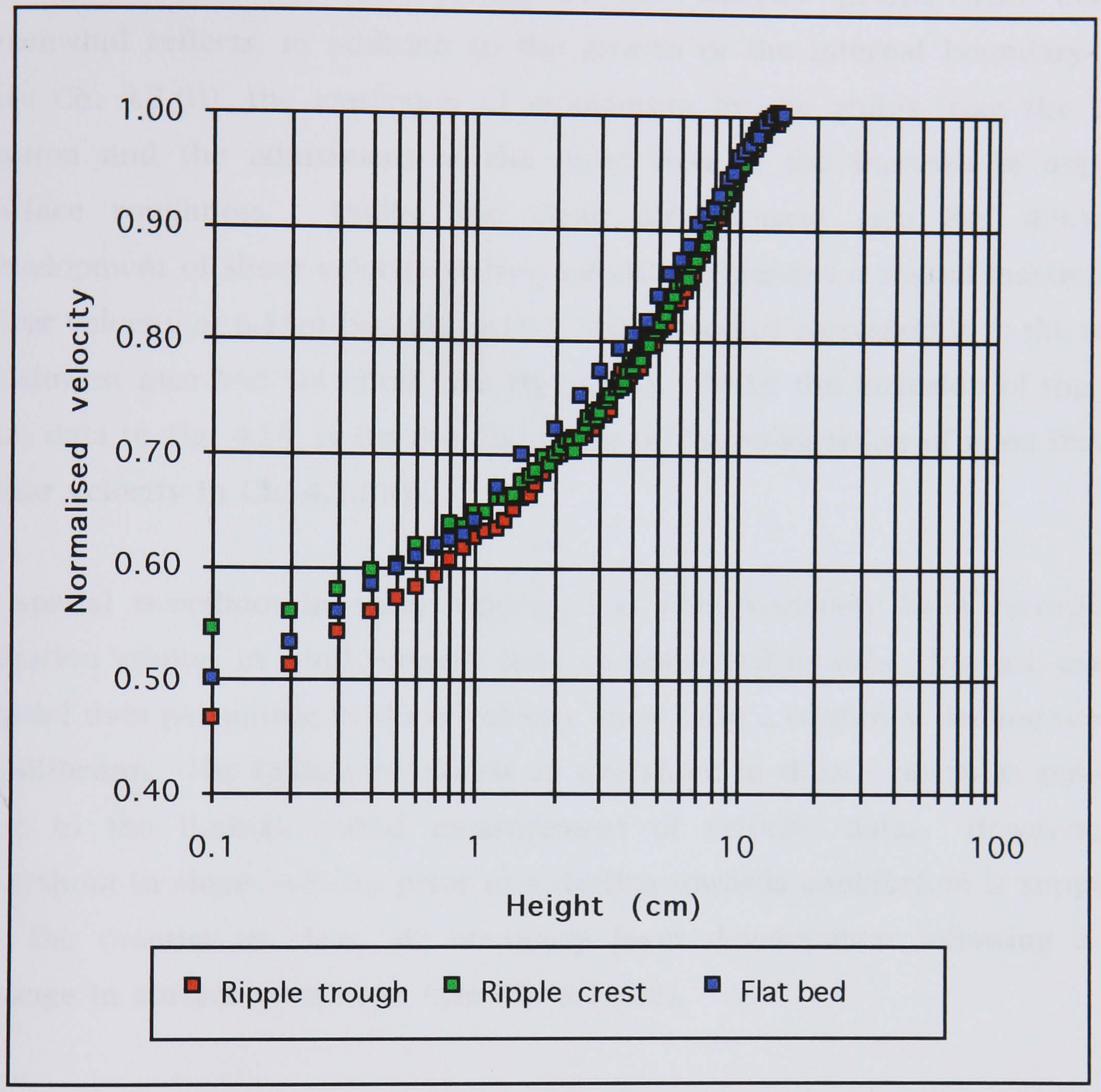

Fig. 4.13. Queen Mary and Westfield wind tunnel velocity profiles over various surface features. Data were collected in clean air at 7.20m downwind. All data are normalised to the constant free-stream velocity $U_{7.20m}^{0.15m}$ and plotted relative to the elevation of the sand bed.

(4.3.) RESULTS: THE SPATIAL DEVELOPMENT OF THE SALTATION SYSTEM.

(i) Spatial development of velocity.

During saltation the development of the velocity profile with distance downwind reflects, in addition to the growth of the internal boundary layer (see Ch. 4.2.(i)), the extraction of momentum by the grains from the air in motion and the adjustment of the outer flow to the increase in apparent surface roughness. Unlike the clean air scenario (see Fig. 4.9.), the development of shear velocity during saltation generates a spatial maximum in shear velocity at 6.15m (see Fig. 4.15.). This distance corresponds to the region of slowest near-bed velocities (see Fig. 4.14.). (Note, the inclusion of the mass flux data in Fig. 4.15. is for the discussion of the co-variation of mass flux and shear velocity in Ch. 4.3.(iii)).

A spatial overshoot in shear velocity has not previously been recorded in saltation studies in wind tunnels, field or numerical models. Instead, existing spatial data pertaining to shear velocity show only a continual decline towards equilibrium. The failure to witness an overshoot in shear velocity is generally due to the limited spatial measurement of velocity data. However, the overshoot in shear velocity prior to a decline towards equilibrium is supported by the theories of clean air boundary layer development following a step change in surface roughness (see Ch. 3.1.(iv)).

The introduction of sand-feed significantly influences the development of shear velocity with distance downwind (see Fig. 4.16.). The injection of sand into the wind tunnel overcharges the saltation system and forces the first 4.10m into disequilibrium. The 'accelerated development' of the sand cloud is gradually encompassed by the saltation system, and the initially high levels of shearing stress decline with distance as both the boundary layer height and the extent of the saltation layer increase.

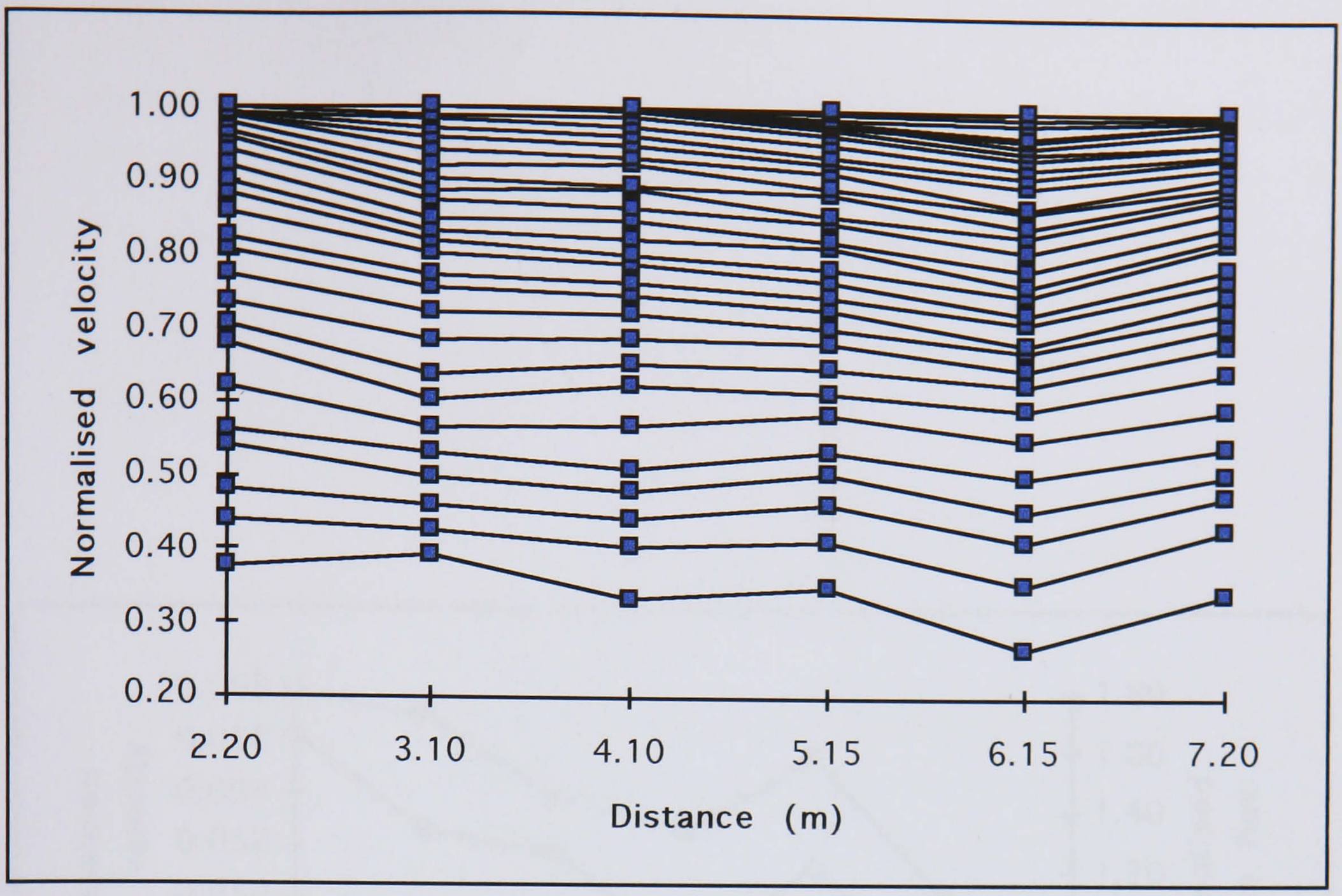

Fig. 4.14. Downwind spatial development of velocity in the Queen Mary and Westfield wind tunnel during saltation (without sand-feed). Velocity data were measured at heights 0.20-1cm in 0.20cm intervals, 1-17cm in 0.50cm intervals. All velocities are normalised to the free-stream $U^{0.15m}$ of each profile.

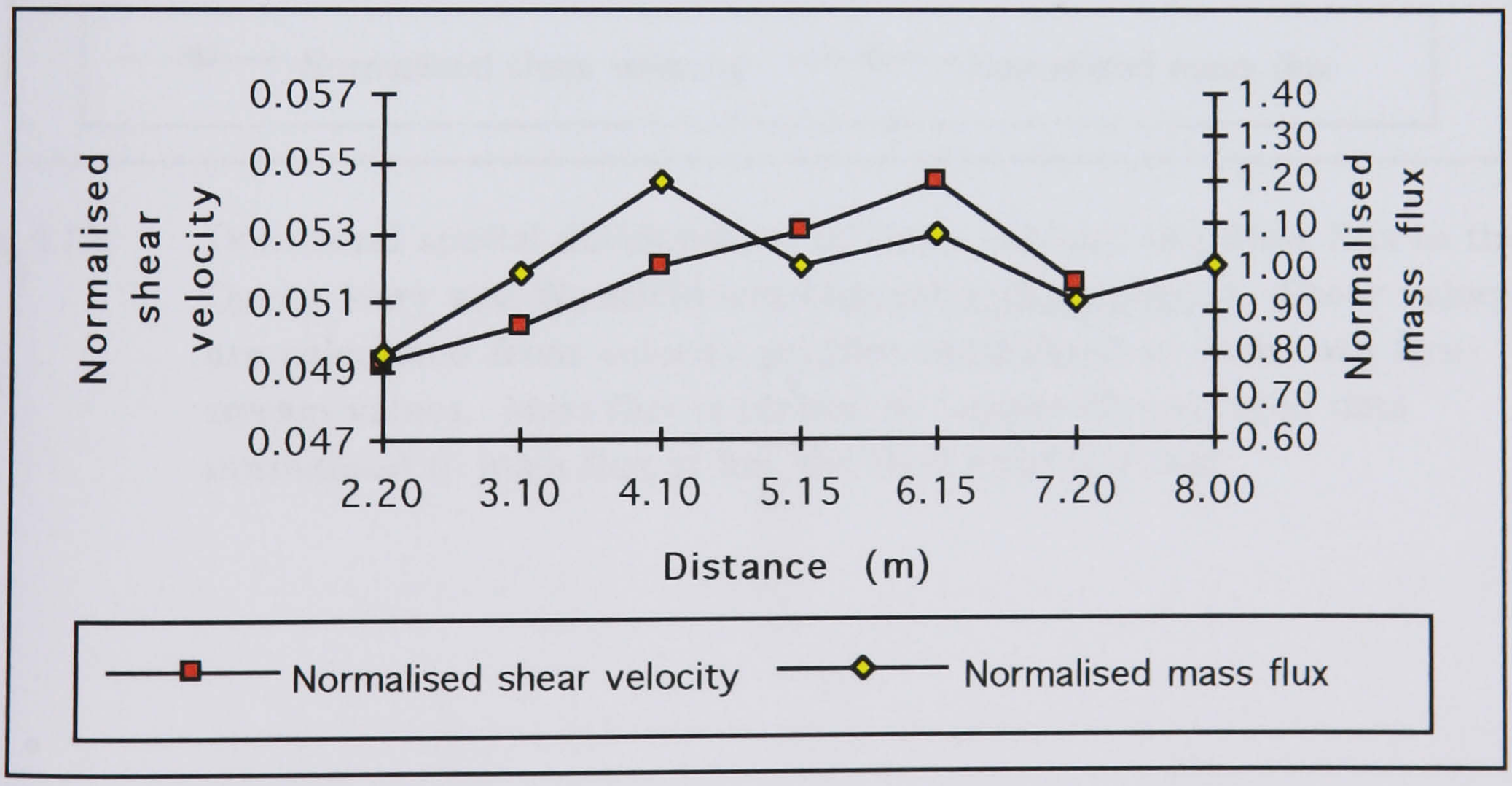

Fig. 4.15. Downwind spatial development of shear velocity and mass flux in the Queen Mary and Westfield wind tunnel (without sand-feed). Shear velocities are calculated from the velocity profiles normalised to their own free-stream values. Mass flux is plotted as temporally-averaged data normalised to the mass flux at 8m, the final sand trap site.

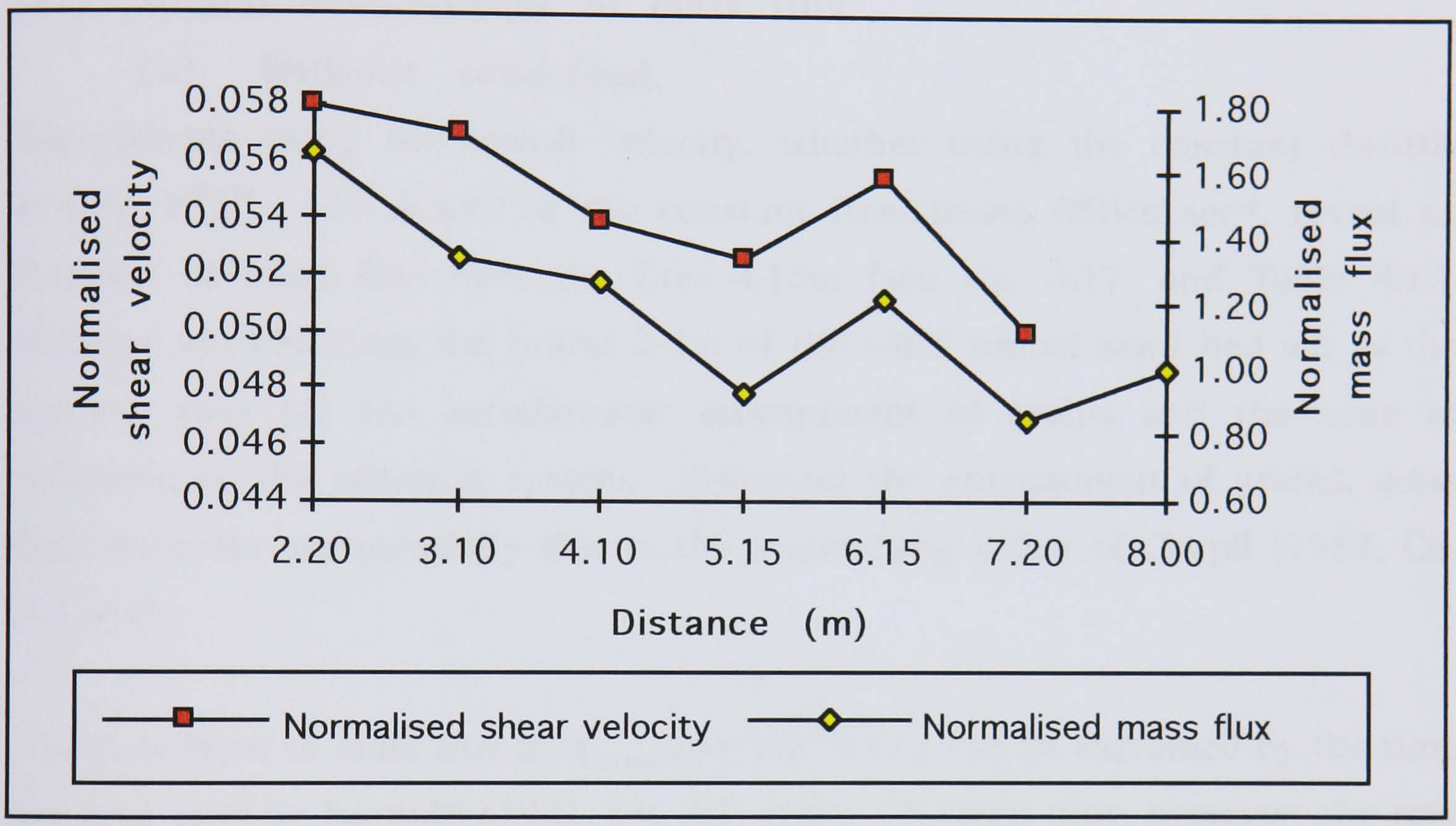

Fig. 4.16. Downwind spatial development of shear velocity and mass flux in the Queen Mary and Westfield wind tunnel with sand-feed. Shear velocities are calculated from velocity profiles normalised to their own free-stream values. Mass flux is plotted as temporally-averaged data normalised to mass flux at 8m, the final sand trap site.

At distances greater than 4.10m the saltation system is developing as 'normal' (see Fig. 4.16.). Shear velocity is independent of the inclusion of sand-feed and peaks at $X_{6.15m}$ (as in the experiments without upwind artificial sand-feed (see Fig. 4.15.)). As the overshoot in shear velocity occurs so near to the end of the wind tunnel the longer-term development of the boundary layer is not witnessed in experiments with or without sand-feed.

(ii) Spatial development of mass flux.

(a) Without sand-feed.

Experiments using the lowest velocity, whether using the constant throttle setting $U_{7.20m}^{0.15m}$ = 670cm.sec^{-1} or the constant free-stream 650cm.sec^{-1}, reveal an increase in mass flux over the first 4.10m (see Fig. 4.17. and Table 4.1.). Without sand-feeding, the initial 2-3m of the wind tunnel sand bed act as the source areas for the aerodynamic entrainment of grains and the zone of initiation of the saltation system. Following the entrainment of grains, mass flux increases exponentially due to the avalanching effect of Chepil (1957, Ch. 3.1.(iv)).

The overshoot in mass flux at $X_{4.10m}$ (see Fig. 4.17.) can be explained by the time lag proposed by Bagnold (1941, Ch. 3.1. (iv)). Through time, however, the rate of mass flux, over the first 4.10m, decreases due to the armouring of the sand bed (see Ch. 4.4.(i)). Consequently, through time larger fetches are required for the saltation system to reach saturation and there is a downwind movement of the mass flux overshoot from $X_{4.10m}$ to $X_{6.10m}$.

The greater energy of the higher velocity experiments (see Fig. 4.18.) initiates the saltation system upwind of the first sampling site at $X_{2.10m}$. Furthermore, at the higher velocities the armouring of the sand bed is less significant. There is, therefore, a time independence of the mass flux overshoot.

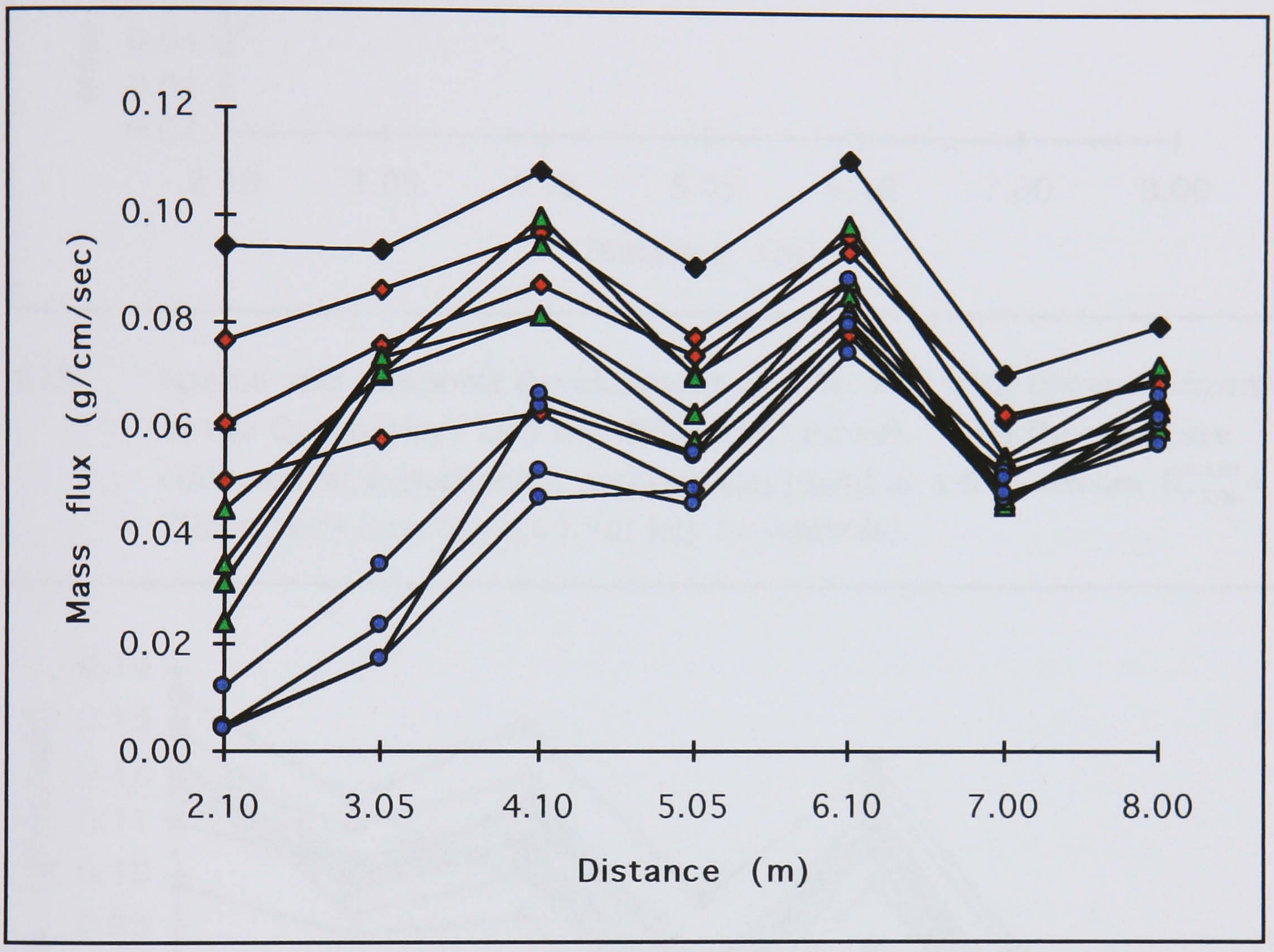

Fig. 4.17. Spatial and temporal development of mass flux with distance downwind in the Queen Mary and Westfield wind tunnel. Data are collected in experiments without sand-feed at a free-stream velocity $U_{7.20m}^{0.15m}$ = 650cm.sec^{-1}.
Key: the black diamond symbols represent sample 1 in the first 5 minutes; the red diamond symbols represent samples 2-4 between 10-20 minutes; the green triangular symbols represent samples 5-8 between 25-40 minutes; and the blue circular symbols represent samples 9-12 between 45-60 minutes.

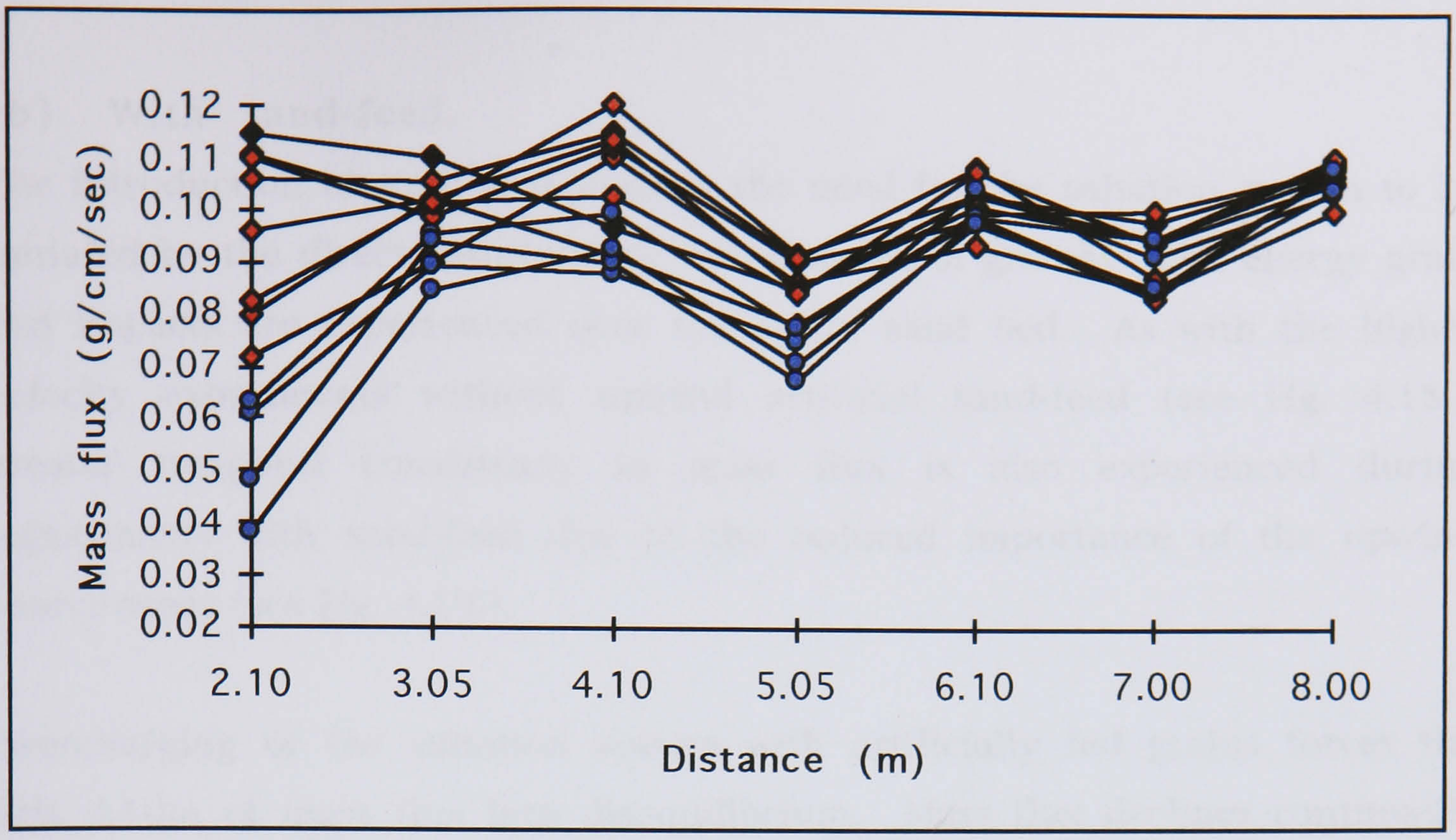

Fig. 4.18. Spatial and temporal development of mass flux with distance downwind in the Queen Mary and Westfield wind tunnel. Mass flux data are collected in experiments <u>without sand-feed</u> at a free-stream $U_{7.20m}^{0.15m}$ = 700cm.sec^{-1} (see Fig. 4.19. for key to symbols).

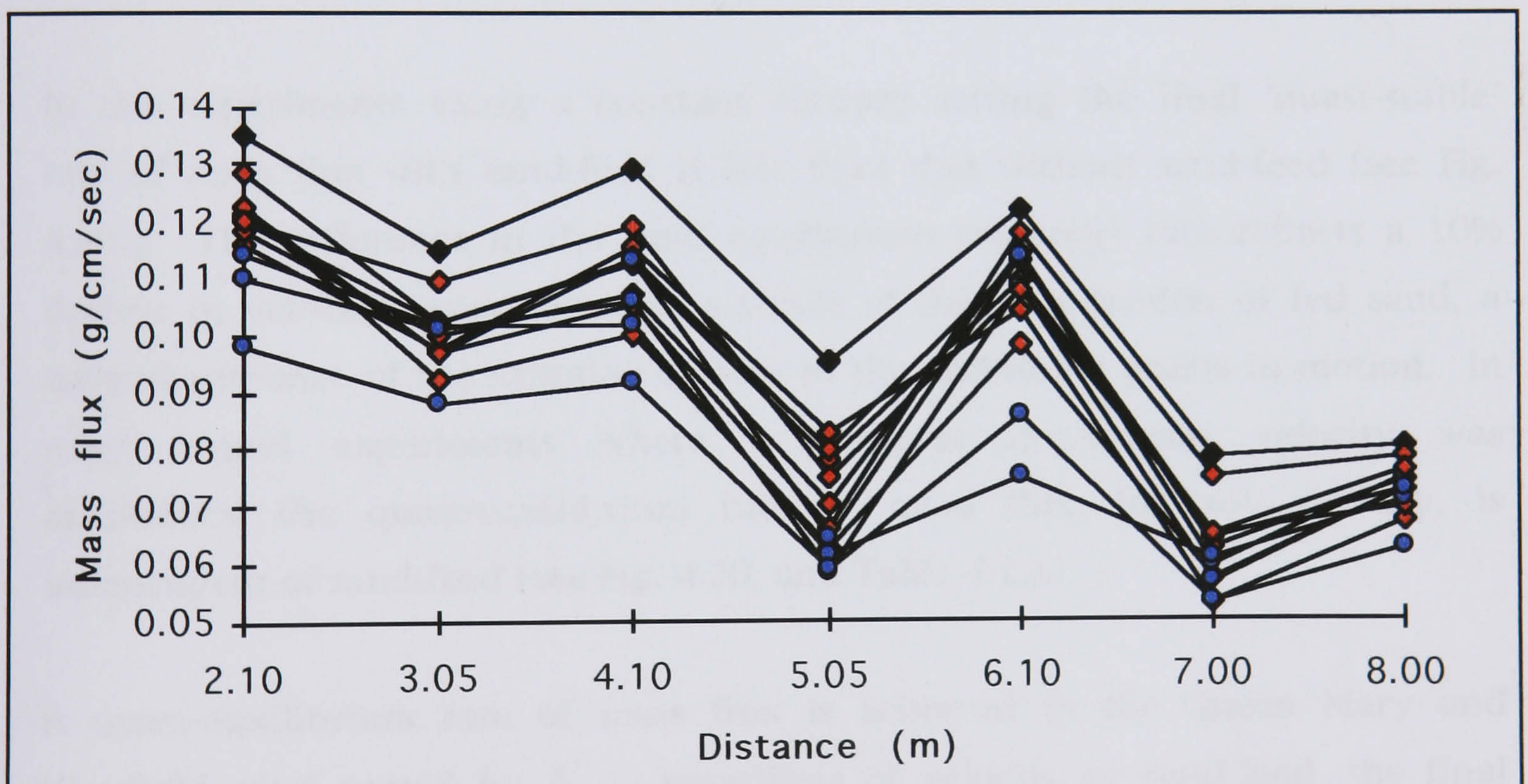

Fig. 4.19. Spatial and temporal development of mass flux with distance downwind in the Queen Mary and Westfield wind tunnel. Mass flux data are collected in experiments <u>with sand-feed</u> at a velocity $U_{7.20m}^{0.15m}$=650cm.sec^{-1}. Key: the black diamond symbols represent sample 1, the first 5 minutes; the red diamond symbols represent samples 2-7 between 10-40 minutes; and the blue circular symbols represent samples 8-12 between 45-60 minutes.

(b) With sand-feed.

The introduction of sand-feed negates the need for the saltation system to be initiated by the direct aerodynamic entrainment of grains. High energy grain bed impacts are experienced over the entire sand bed. As with the higher velocity experiments without upwind artificial sand-feed (see Fig. 4.18.), greater temporal consistency in mass flux is also experienced during experiments with sand-feed due to the reduced importance of the upwind source areas (see Fig. 4.19.).

Overcharging of the saltation system with artificially fed grains forces the first 4.10m of mass flux into disequilibrium. Mass flux declines continually with distance downwind in response to the increase in boundary layer height and the incorporation of the additional, artificially-introduced sand into the saltation cloud (see Fig. 4.19.). At downwind distances greater than 5.05m the saltation system is relatively unaffected by the inclusion of sand-feed.

In the experiments using a constant throttle setting the final 'quasi-stable' rate of mass flux with sand-feed is less than that without sand-feed (see Fig. 4.20.). The difference in the final equilibrium transport rate reflects a 10% decline in velocity experienced as a result of the introduction of fed sand, a natural response of the saltation system to the additional grains in motion. In wind tunnel experiments where a constant free-stream velocity was maintained the quasi-equilibrium rate of mass flux, for any velocity, is independent of sand-feed (see Fig. 4.20. and Table 4.1.).

A quasi-equilibrium rate of mass flux is achieved in the Queen Mary and Westfield wind tunnel by $X_{6.10m}$ regardless of velocity or sand-feed, the final rate of mass flux being dependent on velocity (see Figs. 4.17., 4.18., 4.19. and 4.20.). Beyond $X_{6.10m}$ fluctuations in mass flux most probably result from the differential locations of the sand traps on ripple crests or troughs (see Ch. 4.2.(iii)).

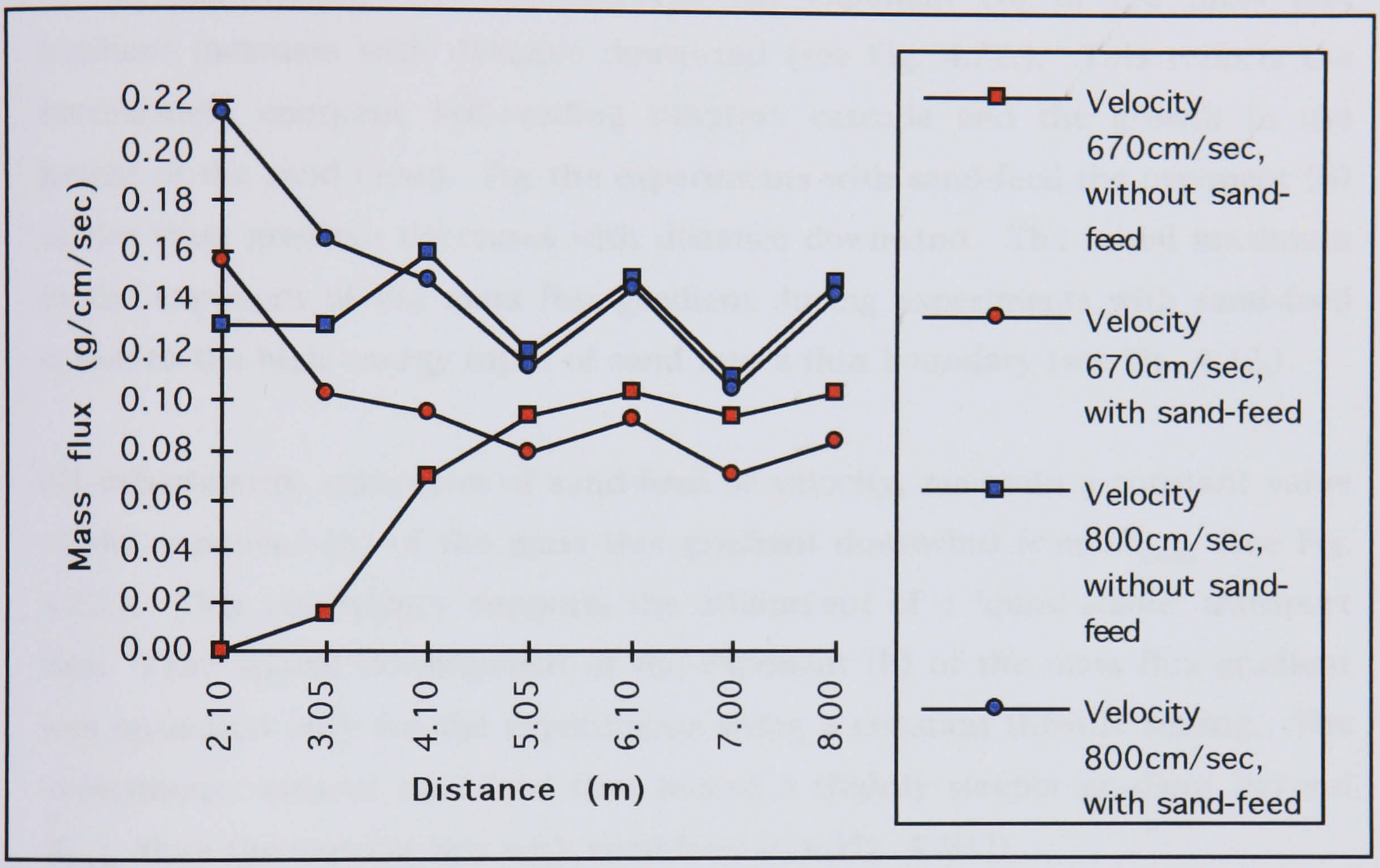

Fig. 4.20. Spatial development of temporally averaged mass flux in the Queen Mary and Westfield wind tunnel at two velocities, with (circular symbols) and without (square symbols) sand-feed.

(c) The exponent of the mass flux gradient.

The vertical distribution of mass flux (see Fig. 4.21.) is independent of velocity, downwind location and sand-feed. Regression of the logarithm of mass flux with height produces a negative regression exponent (b) representative of the vertical extent of the sand cloud.

In the experiments without sand-feed the exponent (b) of the mass flux gradient increases with distance downwind (see Fig. 4.22.). This reflects the increasingly energetic self-seeding saltation cascade and the growth in the height of the sand cloud. For the experiments with sand-feed the exponent (b) of the mass gradient decreases with distance downwind. The initial maximum in the exponent of the mass flux gradient during experiments with sand-feed is due to the high energy input of sand into a thin boundary (see Fig. 4.22.).

All experiments, regardless of sand-feed or velocity, maintain a constant value of the exponent (b) of the mass flux gradient downwind from $X_{5.05m}$ (see Fig. 4.22.). This consistency supports the attainment of a 'quasi-stable' transport rate. (The spatial development of the exponent (b) of the mass flux gradient was measured only for the experiments using a constant throttle setting. The experiments without sand-feed thus record a slightly steeper gradient beyond $X_{5.05m}$ than the experiments with sand-feed (see Fig. 4.20.)).

(iii) Spatial co-variation of mass flux and wind velocity.

Spatially, both mass flux and shear velocity overshoot prior to declining towards an equilibrium (see Fig. 4.15.). The overshoot in mass flux at $X_{4.10m}$ prior to the overshoot in shear velocity at $X_{6.15m}$ illustrates the lag hypothesis of Bagnold (1941, see Ch. 3.1.(iv)). By invoking the self-balancing mechanism of Owen (1964, see Ch. 3.1.(iv)) an eventual state of equilibrium can be envisaged.

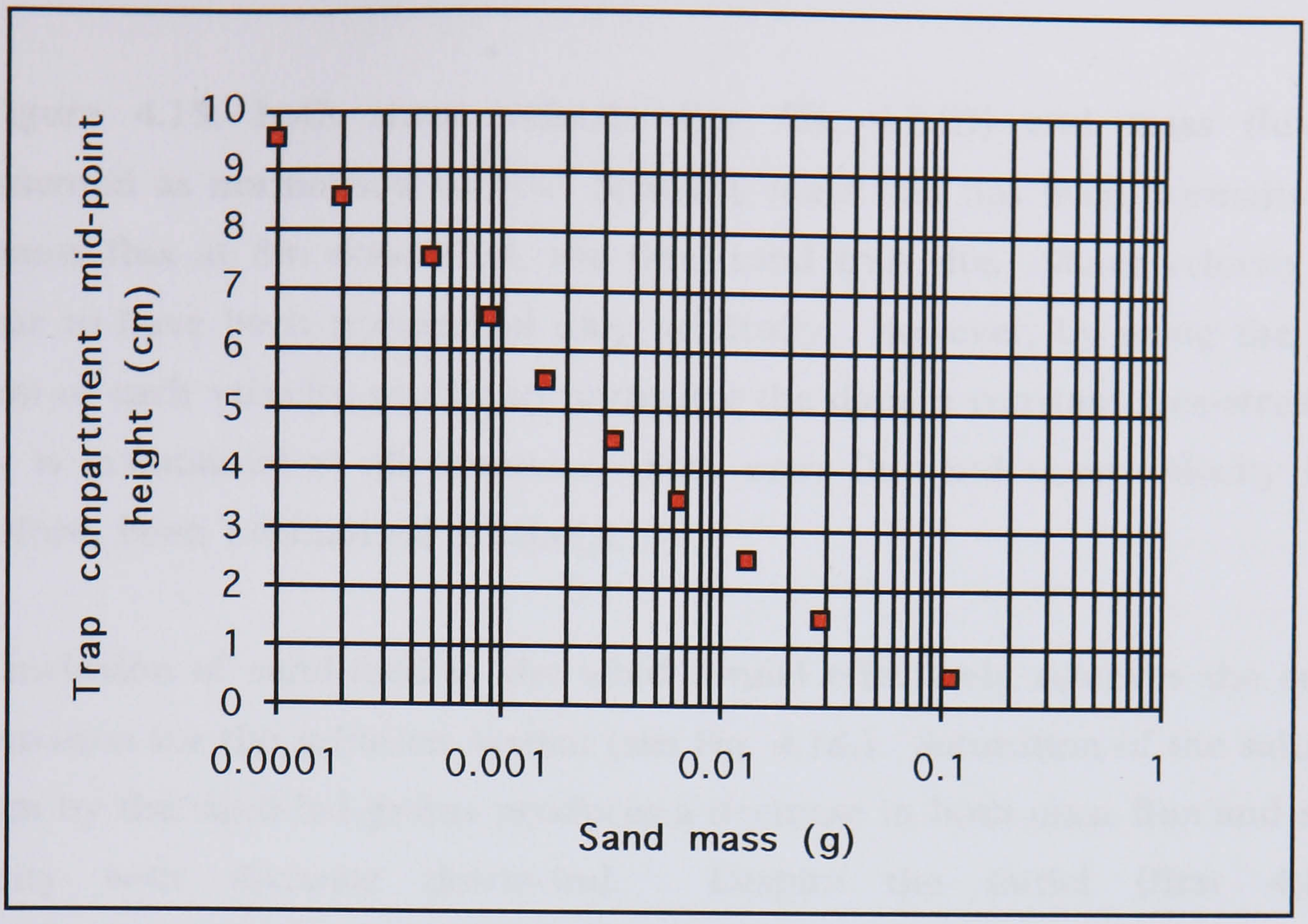

Fig. 4.21. The vertical distribution of mass flux in the Queen Mary and Westfield wind tunnel. Regression of mass flux with height produces the exponent (b) of the vertical mass flux gradient, representative of the vertical extent of the saltation cloud.
In this example, $y = -3.1118.\mathrm{Log}(x)+3.054$, $R^2 = 0.991$, thus $b = -3.1118$.

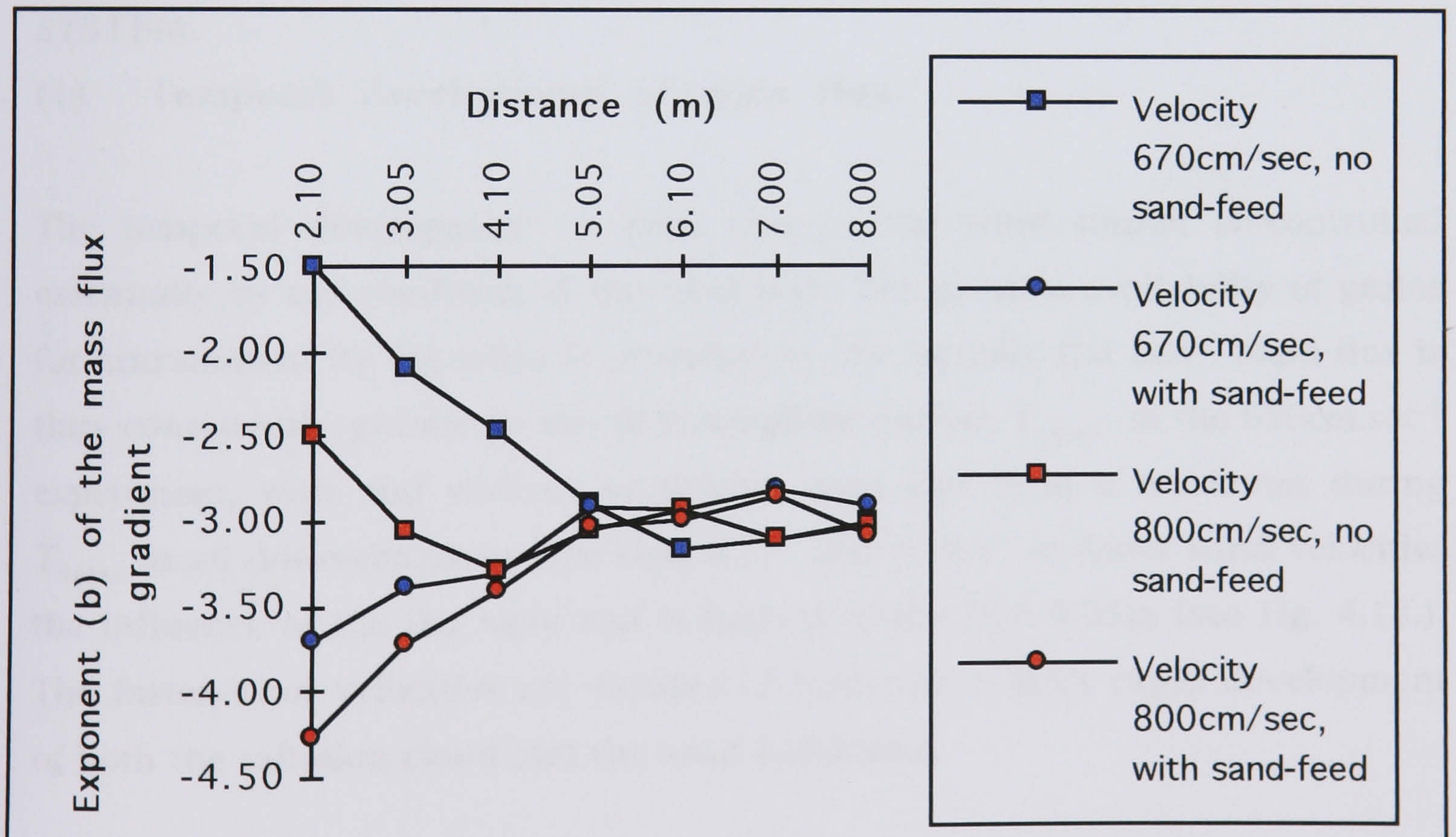

Fig. 4.22. Spatial development of the temporally averaged exponent (b) of the mass flux gradient in the Queen Mary and Westfield wind tunnel with (circular symbols) and without (square symbols) sand-feed. Both velocity experiments relate to constant throttle settings.

In Figure 4.15. both shear velocity (see Ch. 4.2.(i)) and mass flux are represented as normalised values. Spatially mass flux has been normalised to the mass flux at 8m downwind, the final sand trap site. Shear velocity may appear to have been normalised only vertically. However, by using the free-stream of each velocity profile to normalise the data, a constant free-stream of unity is maintained at all distances. Both mass flux and shear velocity have, therefore, been normalised spatially.

The inclusion of sand-feed in the wind tunnel effectively removes the region of initiation for the saltation system (see Fig. 4.16.). Saturation of the saltation system by the sand-fed grains produces a decrease in both mass flux and shear velocity with distance downwind. Despite the initial (first 4.10m) disequilibrium of the saltation system, however, at distances greater than 6.15m a quasi-equilibrium transport rate is attained.

(4.4.) RESULTS: THE TEMPORAL DEVELOPMENT OF THE SALTATION SYSTEM.

(i) Temporal development of mass flux.

The temporal development of mass flux in the wind tunnel is controlled essentially by the condition of the sand bed. The greatest availability of grains for entrainment by the wind is provided by the initially flat bed. Mass flux is thus consistently greater in the first sampling period, T_{5mins}. In the 650cm.sec^{-1} experiment, with and without sand-feed, mass flux is at a maximum during T_{5mins} at all downwind sites (see Figs. 4.17. and 4.19.). At faster wind velocities the influence of the flat sand bed is limited to the first 3.05m (see Fig. 4.18.). The faster wind velocities are capable of initiating a more rapid development of both the saltation cloud and the sand bed-forms.

Exposure of the flat sand bed to an 'above-threshold' wind leads to the redistribution of materials and the formation of ripples. The reduction in the

availability of grains for transport following the stabilisation of the sand bed is reflected in the decline in mass flux from T_{5mins} to T_{10mins} (see Figs. 4.17. and 4.19.). (The change from a flat to a rippled sand bed is also recorded in the decline in the exponent of the mass flux gradient). Subsequent temporal developments of mass flux are site-dependent.

In experiments without sand-feed, the first 2-3m of the wind tunnel sand bed act as the source areas for the aerodynamic entrainment of grains (see Figs. 4.17. and 4.18.). The gradual depletion of the sand bed through time at these sites produces an ever decreasing rate of mass flux. In the low velocity experiment, $U_{7.20m}^{0.15m}$ = 650cm.sec^{-1}, the armouring of the sand bed in the first 2-3m results in the majority of the grains in the latter time periods ($T_{40-55mins}$) having to be entrained from 4-5m. The longer fetch required for the entrainment of grains, and the subsequent saturation of the saltation system, leads to the downwind relocation of the mass flux overshoot through time.

At faster velocities the rate of decline in mass flux through time in the first 2-3m of the wind tunnel is less severe (see Fig. 4.18.). The ability of the wind to entrain the majority of the sediment most of the time reduces the significance of the sand bed depletion. As a result, the location of the mass flux overshoot remains constant at $X_{4.10m}$ throughout the 55 minute experimental period. Over longer sampling periods the depletion of the sand bed may eventually become influential and a downwind relocation of the mass flux overshoot be experienced.

Greater temporal consistency in mass flux is recorded at all sampling locations for both the higher velocity experiments without sand-feed (see Fig. 4.18.), and all the experiments with sand-feed (see Fig. 4.19.). A greater temporal consistency is experienced due to the more rapid spatial development of the saltation system. All the mass flux sampling stations thus record the transport of sand by ballistic processes rather than direct fluid action. Furthermore, and as a result, the armouring of the sand bed is less significant.

The only significant temporal development of mass flux in both the higher velocity experiments without sand-feed (see Fig. 4.18.) and all the experiments with sand-feed (see Fig. 4.19.) remains the decline in mass flux following the initial sampling period over a flat bed. The temporal development of the exponent of the mass flux gradient confirms the importance of the change from a flat to a rippled bed following the first sampling period, $T_{5\,mins}$.

The relative values of the exponent of the mass flux gradient also indicate the appropriateness of the rate of sand-feed. For experiments using the same velocity, with and without sand-feed the exponent identifies the degree of over-or under-feeding of the saltation system. For example: the values of the exponent from the $U_{7.20m}^{0.15m}$ = 650cm.sec^{-1} and 700cm.sec^{-1} experiments are greater with sand-feeding than without; the values of the exponent from the $U_{7.20m}^{0.15m}$ = 750cm.sec^{-1} experiments are independent of sand-feed; and the values of the exponent from the $U_{7.20m}^{0.15m}$ = 800cm.sec^{-1} experiments are greater without sand-feed. As velocity increases, therefore, the rate of sand-feed becomes less extreme as compared to the natural capabilities of the saltation system.

(ii) Temporal co-variation of mass flux and shear velocity.

Mass flux and shear velocity were recorded alternately through time in the fully developed boundary layer at $X_{7.00m}$ and $X_{7.20m}$, respectively. The only major temporal development in mass flux, at distances greater than 4.10m downwind, has been identified as the decline in the transport rate following the stabilisation of the sand bed (see Ch. 4.4.(i)). More detailed investigation of the saltation system, however, highlights the minor temporal variations in mass flux and the developing relationship between mass flux, shear velocity and the near-bed wind velocities.

Maintaining a constant free-stream velocity through time in the wind tunnel experiments emphasises the influence of the saltation cloud on the velocity profile. All reductions in the near-surface velocities in the temporal data are due to the extraction of momentum by the grains in transport. The deviations in the near-bed velocities are subsequently manifest in the value of shear velocity. Through time, therefore, mass flux would be expected to maintain an inverse relationship with the near-bed velocities and a direct relationship with shear velocity.

Initial inspection of data from the first five minutes of sand transport (see Figs. 4.23. and 4.24.) appears to contradict these expected relationships. Mass flux and near-surface velocities both decline through time, and shear velocity and mass flux have an inverse relationship. These results can be explained by consideration of the overriding influence of the flat bed.

The increase in shear velocity through the first ten minutes is a reflection of the reduction in near-surface wind velocities due to the extraction of momentum by the grains in transport (see Fig. 4.24.). The near-surface wind velocities decline, despite a reduction in mass flux during the same period, because of the high rate of transport of sand (see Fig. 4.23.). The relatively high rate of transport of sand is generated by the abundance of entrainable grains from the flat bed (see Fig. 4.24.).

Following the stabilisation of the sand bed (at time periods greater than $T_{5\,mins}$), mass flux and shear velocity develop simultaneously and with an inverse relationship to the near-surface wind velocities (see Fig. 4.24.). The maxima in mass flux and shear velocity values at T_{10mins}, T_{30mins} and T_{45mins} are reflected in low values of the near-surface velocities at the same time periods. Similarly, the minima of mass flux and shear velocity values at T_{25mins}, T_{35mins} and T_{50mins} are reflected in the high values of the near-surface velocities at the same time periods (see Fig. 4.23.).

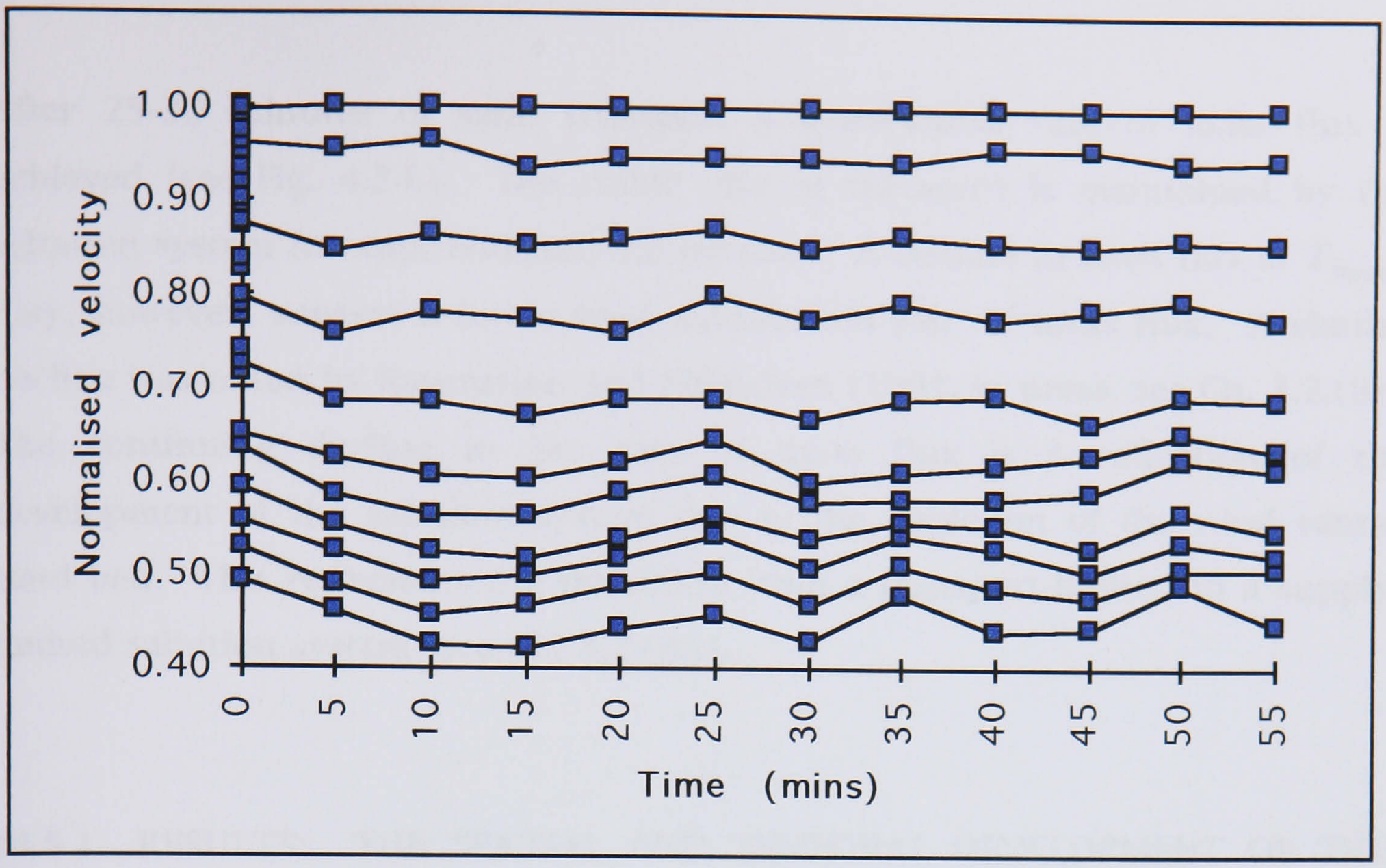

Fig. 4.23. Temporal development of velocity in the Queen Mary and Westfield wind tunnel during saltation without sand-feed. Velocity data were measured at heights 0.40-1cm in 0.20cm intervals then 1.50, 2, 3, 5, 7, 10 and 15cm. Velocities are normalised to the free-stream velocity of each profile.

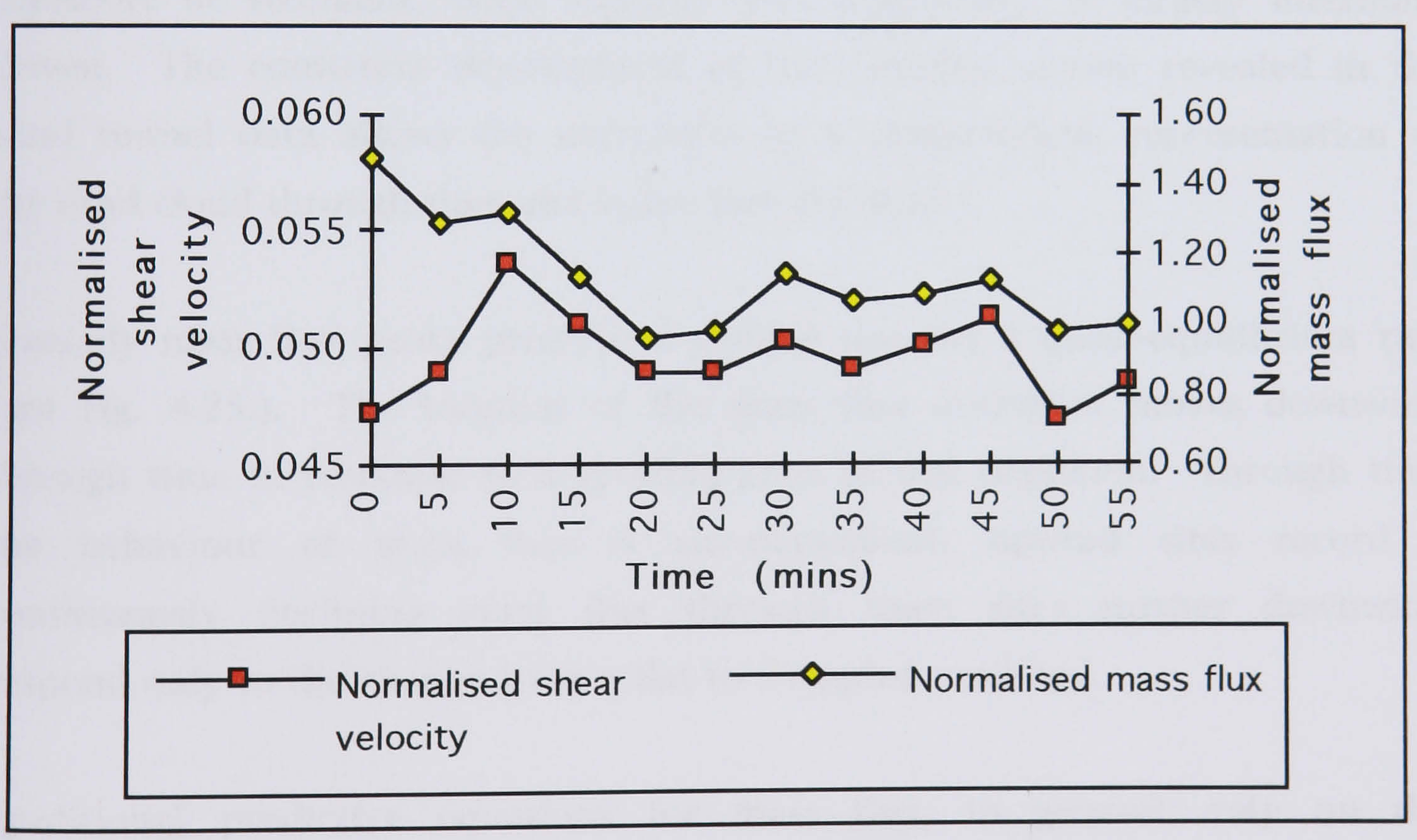

Fig. 4.24. Temporal development of shear velocity and mass flux in the Queen Mary and Westfield wind tunnel without sand-feed. Mass flux and shear velocity data were recorded at 7.20m and 7m, respectively. Shear velocities are calculated from the velocity profiles normalised to their own free-stream value. Mass flux is plotted as temporally averaged data normalised to mass flux at T_{55secs}.

After 25-30 minutes of sand transport a quasi-stable rate of mass flux is achieved (see Fig. 4.24.). The stable rate of transport is maintained by the saltation system for approximately 20 minutes. A decline in mass flux at $T_{50\min s}$ may, however, suggest a lower final equilibrium rate of mass flux. A similar decline was noted by Rasmussen and Mikkelsen (1991, in press, see Ch. 3.2.(ii)). The continuing decline in the rate of mass flux is a reflection of the development of the saltation system due to the depletion of the wind tunnel sand bed. This represents the transition from a transport-limited to a supply-limited saltation system (see Ch. 3.2.(iii)).

(4.5.) RESULTS: THE SPATIAL AND TEMPORAL DEVELOPMENT OF THE SALTATION SYSTEM.

The initiation of the saltation system requires an above-threshold wind. Following the development of the saltation system, however, the rate of transport of sediment, both spatially and temporally, is largely internally driven. The consistent development of the saltation system revealed in the wind tunnel data allows the derivation of a characteristic representation of the sand cloud through time and space (see Fig. 4.25.).

Spatially mass flux peaks prior to a decline towards a quasi-equilibrium rate (see Fig. 4.25.). The location of the mass flux overshoot moves downwind through time in response to a growing zone of bed depletion. Through time the behaviour of mass flux is site-dependent: upwind sites record a continuously declining mass flux through time; sites further downwind respond only to the change from a flat to a rippled sand bed.

Traditional predictive equations for mass flux, in general, rely on the existence of equilibrium. In the Queen Mary and Westfield wind tunnel the assumption of equilibrium may be considered to be satisfied, working from an initially flat sand bed, after a distance of 6m and following a period of ten

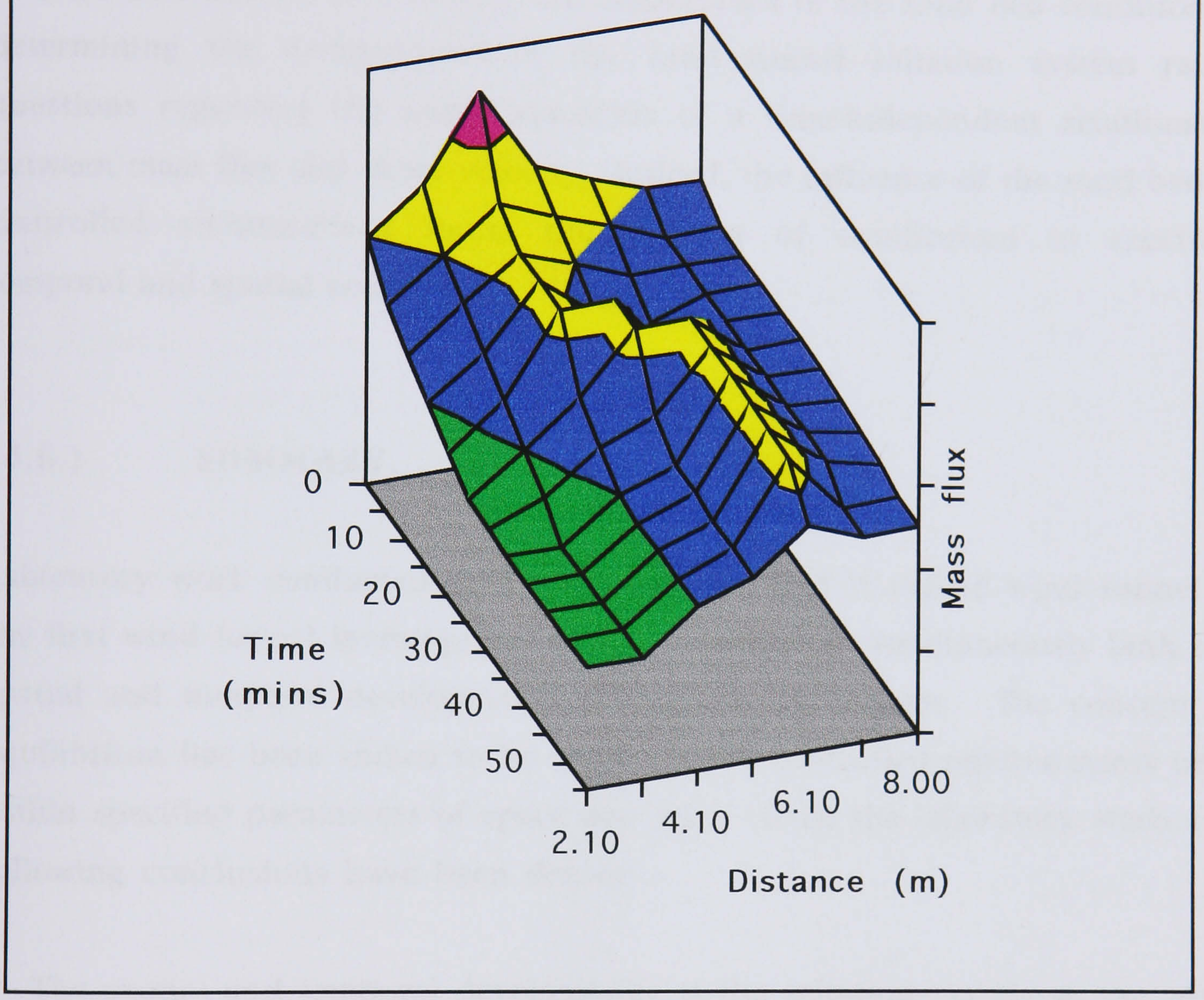

Fig. 4.25. Schematic representation of the idealised spatial and temporal development of the saltation cloud in the Queen Mary and Westfield wind tunnel without sand-feed.

minutes, i.e. within the fully developed boundary layer and following the stabilisation of the sand bed from planar to rippled (see Fig. 4.25.).

In the wind tunnel, the depletion of the sand bed through time, and the potential transition from a transport-limited to a supply-limited system, remains a significant influence on both the spatial and temporal development of mass flux and shear velocity. The importance of the sand bed condition in determining the development of the wind tunnel saltation system raises questions regarding the appropriateness of a time-independent relationship between mass flux and shear velocity. Indeed, the influence of the sand bed in controlled environments limits the concept of equilibrium to specified temporal and spatial scales.

(4.6.) SUMMARY.

Laboratory work conducted in the Queen Mary and Westfield wind tunnel is the first wind tunnel investigation to have considered simultaneously both the spatial and temporal development of the saltation system. The concept of equilibrium has been shown to be applicable in controlled environments only within specified parameters of space and time. From the laboratory study the following conclusions have been drawn:-

- The spatial and temporal development of the saltation system in the wind tunnel is controlled essentially by the condition of the sand bed.
- Spatially, equilibrium is attained in the Queen Mary and Westfield wind tunnel at some distance >6m, regardless of velocity or sand-feed (see Figs. 4.17., 4.18., 4.19., 4.20. and 4.22.).
- In experiments without sand-feed, mass flux overshoots between 4-6m prior to the decline towards equilibrium. The location of the mass flux overshoot progresses downwind through time in response to an increasing zone of bed depletion (see Figs. 4.17. and 4.18.).

- An overshoot in shear velocity prior to a decline towards equilibrium is recorded in the experiments without sand-feed (see Fig. 4.15.).
- Spatially, in experiments without sand-feed, there is a lag between the overshoot in mass flux at $X_{4.10m}$ and that of shear velocity at $X_{6.15m}$ (see Fig. 4.15.).
- The spatial development of the exponent of the mass flux gradient in experiments without sand-feed highlights the increase in the vertical extent of the sand cloud with distance downwind (see Fig. 4.22.).
- The introduction of sand-feed induces a disequilibrium in the saltation system in the range 0<X<4m. Mass flux, shear velocity and the exponent of the mass flux gradient all decline with distance downwind (see Fig. 4.19.).
- Temporally, the saltation system attains equilibrium at some time >10 minutes.
- The first sampling period ($T_{5\,mins}$) records an exaggerated mass flux due the high grain availability from a flat sand bed (see Fig. 4.17.).
- The temporal developments of mass flux are site-dependent. In the first 2-3m mass flux declines continuously through time due to the depletion of the sand bed. At distances greater than 4m mass flux is independent of time once the sand bed has stabilised.
- The introduction of sand-feed generates high levels of temporal consistency in mass flux at all downwind sites (see Fig. 4.19.).

CHAPTER 5

DEVELOPMENT OF THE SALTATION SYSTEM UNDER NATURAL ENVIRONMENTAL CONDITIONS

Field experiments were designed to investigate the downwind spatial and temporal development of the saltation system under natural environmental conditions. The development of the saltation system was monitored over distances of 10m and 20m. Sediment transport was measured by the downwind deployment of five sand traps. Temporal wind velocity data were collected simultaneously with mass flux measurements at a single site. Spatial profile velocity data were obtained by a streamwise traverse along the experimental area. All wind velocity data are normalised to their respective profile free-stream value.

(5.1.) EXPERIMENTAL ARRANGEMENTS AND PROCEDURES.

(i) Experiments.

Field experiments were designed to monitor both the downwind spatial and temporal development of the saltation system (see Fig. 5.1.). Generally, the natural environment conditions the parameterisation of the artificial simulations of that environment. Unusually, in this study, the field experiments are parameterised by the laboratory experiments, i.e. the field experiments are scaled to the length of the available wind tunnel facilitates. The data from the 8m long Queen Mary and Westfield wind tunnel is imitated by a 10m long field experiment, whilst data from longer wind tunnels (e.g. Shao and Raupach, 1992) are matched by a 20m long field experiment (see Table 5.1.).

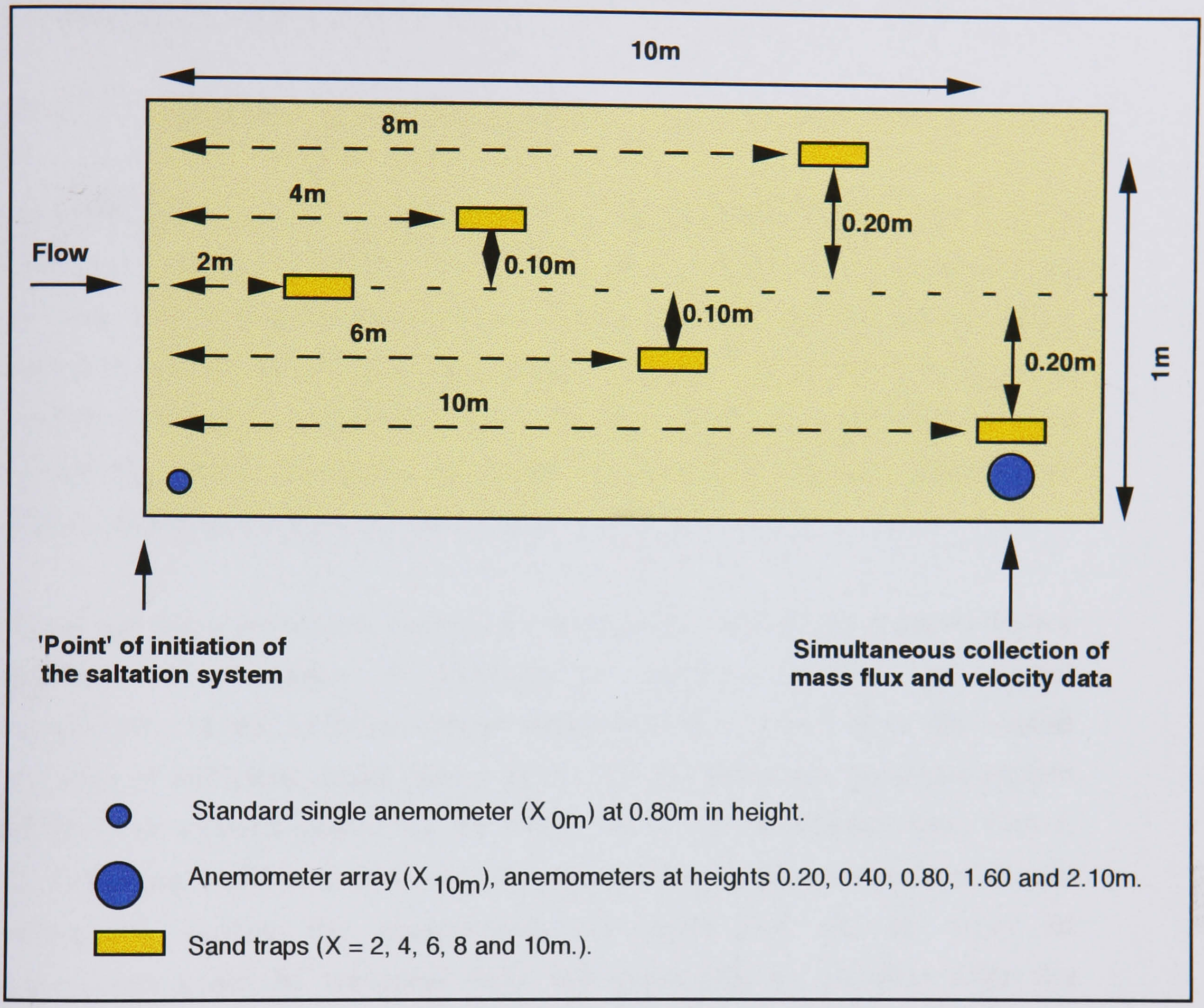

Fig. 5.1. Schematic diagram of the 10m field work experimental arrangement. Mass flux was monitored at approximately 2m intervals. The sand trap sampling stations were alternately offset to avoid interference between consecutive sampling stations. Velocity data were collected during the experiments at the point of initiation of the saltation system (0m) and at 10m downwind. After each experiment velocity data were collected at all the mass flux monitoring sites.

Experiment	Sand trap locations downwind (m)	Duration of mass flux data at each site (mins)	Velocity data collected downwind (m)
10m	2, 4, 6, 8, 10	60	0, 10
20m	4, 8, 12, 16, 20	75	0, 20

Table 5.1. Summary of field experiments.

In the field, mass flux was monitored downwind of a designated point (0m) of initiation of saltation (see Ch. 5.1.(ii(b))). Five continuously recording sand traps (see Ch. 5.1.(iii(b))) were spaced in intervals of 2m for the 10m long experiment and 4m for the 20m long experiment (see Table 5.1.). Mass flux was recorded at all sites simultaneously. The sand trap sampling stations were alternatively offset laterally to avoid interference between consecutive sampling stations (see Figs. 5.2. and 5.3.).

Throughout the experiments there is a compromise between the need to deploy equipment at a number of locations in order to observe the spatial characteristics of the saltation system and the need to have, from the overall area, data of sufficient detail (Bauer *et al.*, 1990). With only six anemometers available, two options existed for the collection of spatial velocity data. Either, each sand trap could be paired with an adjacent single anemometer and record continuously during the measurement of mass flux or, an array of anemometers could be traversed from one sand trap to the next after the measurement of mass flux.

Although the deployment of single anemometers allows the simultaneous spatial development of mass flux and velocity to be recorded at each sand trap site the calculation of shear velocity from a single point velocity incorporates the unrealistic assumption of constant surface roughness during saltation (Hsu, 1971a, 1971b). As a result, in this study, the use of a traversed array of anemometers was preferred.

Fig. 5.2. Deployment of equipment for the 10m experiment at the Corralejo field site. Each sand trap is laterally offset to avoid interference between consecutive sampling stations. The velocity profile is adjacent to the final sand trap site.

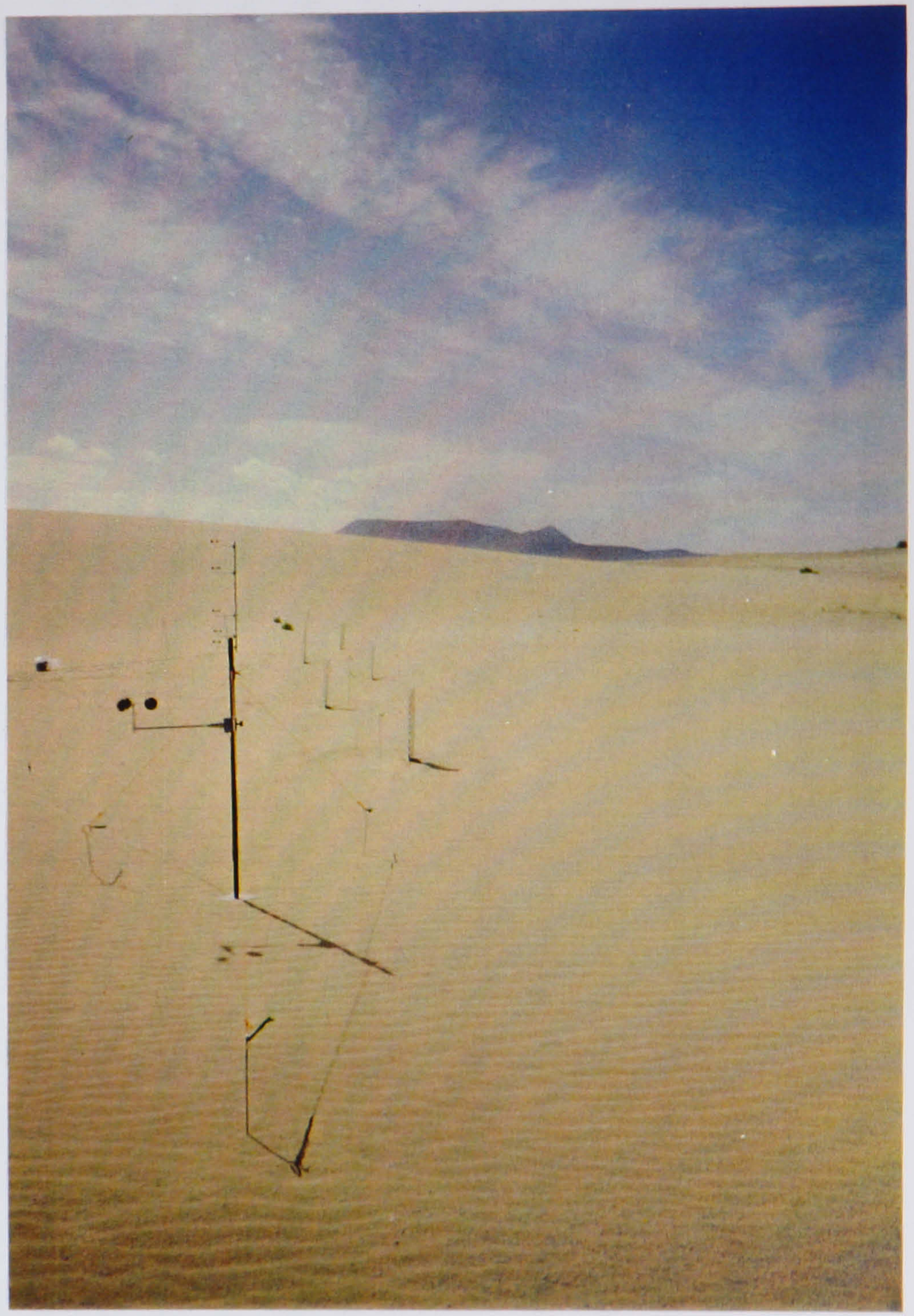

Fig. 5.3. Full experimental deployment of equipment for the 20m experiment at the Corralejo field site. The five sand traps are spaced at 4m intervals and laterally offset.

Using a single array of anemometers prohibits the collection of spatial velocity data during the period of mass flux collection. However, it does permit the direct calculation of shear velocity from the resulting velocity profile. Velocity profile data (see Ch. 5.1.(iii(a))) were collected simultaneously with mass flux measurements at 10m downwind for the 10m experiment and 20m downwind for the 20m experiment. For both experiments a single anemometer was located at the upwind end (0m) of the experimental area (see Fig. 5.1.).

After each experimental run, spatial velocity data were collected by traversing the anemometer array along the sand trap sites. Temporal variations in velocity experienced during the collection of data at various sites were overcome by the normalisation of the velocity data to the $U^{2.10m}$ values of the respective velocity profiles (Mulligan, 1988, p.528). By using the upper-most velocity for the normalisation procedure, a constant boundary condition analogous to the free-stream reference level of a wind tunnel is obtained.

For each experiment data were obtained for:

- (i) the spatial and temporal development of mass flux;
- (ii) the simultaneous temporal development of mass flux and wind velocity at 10m for the 10m experiments and 20m for the 20m experiments; and
- (iii) the spatial development of mass flux and wind velocity.

Temporally, all data are reported as five minute average values, the same as used in the laboratory results. (Note: the raw data were recorded in the field as 30 second average values).

(ii) Field site.

(a) Location.

Preliminary field work was conducted over the inter-tidal sands at Ynyslas, mid-Wales. Whilst this region was sufficiently windy for the testing of the equipment and methodology, the actual field experiments required idealistic environmental conditions, i.e. flat, loose, dry sand, above threshold

unidirectional winds and an identifiable point of initiation of saltation, to aid the compatibility with laboratory data. As a result, the final field work was undertaken at a drier location on the Canary Island of Fuerteventura (see Fig. 5.4.).

The Canary Island archipelago is situated between latitudes 27, 37'N and 29, 25'N and longitudes 13, 20'W and 18, 10'W (of Greenwich) in the North East Atlantic Ocean. The Eastern Canary Islands of Fuerteventura and Lanzarote are located merely 125km off of the Moroccan coast at Cape Juby. Fuerteventura is extremely arid, with rainfall less than 10cm per year (Rodriguez Rodriguez *et al.*, 1993, p.12), and is 'considered as the western outpost of the Saharan Zone' (Damnati *et al.*, 1996, p.37). This association is strengthen by the existence of aeolian deposits of Saharan origin and active aeolian processes maintained by the trade winds (Rodriguez Rodriguez *et al.*, 1993; Damnati *et al.*, 1996; Meco *et al.*, pre print).

Two main aeolian regions exist on the Island of Fuerteventura, Corralejo in the north - north west, and Jandia in the south east. Only Corralejo is easily accessible, without the need for off-road vehicles, and this area was used for the experiments. The general area of the field sites at Corralejo is to the west of road FV1 at Km20 (see Fig. 5.4.). The extent of the Corralejo sand deposit is illustrated in Figure 5.5. The mountain in the distance is within the range of the Montanas de la Blanca approximately 13Km away.

(b) Site description and meteorological conditions.

The field experiments were conducted in November 1996. During the experimental period, cool (17°C), calm mornings (wind speeds <65cm.sec^{-1}) enabled the equipment to be installed in conditions free from sand transport. As noon approached, the wind velocities increased initiating the saltation system. Although the wind direction was generally from the North East only on occasional days was the direction sufficiently constant to permit data collection.

Fig. 5.4. Map of Fuerteventura. The Playas de Corralejo are in the north east of the Island. The field site is located west of road FV1 at Km20.

Fig. 5.5. View North West over the Jable del Moro, at the Playas de Corralejo, Fuerteventura.

Fig. 5.6. On the 19th November 1996, access to the field site (west of the road) was blocked by sand deposited from intense aeolian activity during the previous 24 hours.

The wind erosion maximum at Corralejo, in general, occurred between 13:30 and 15:00 hours. During this time the transported sand grains saltated to a height of approximately 0.40m. Extreme transport conditions were also experienced in the region. Figure 5.6. highlights the result of a sand storm from 10:00 to 18:00 hours on the 19th November 1996. The following day similar conditions pertained and resulted in the inaccessibility of the area until bulldozers had cleared the sand.

The 10m experiment was conducted on Sunday 17th November 1996. The experimental area was an expanse of flat sand with a gradient of less than two degrees in the downwind direction. Upwind was a zone of increased roughness 15-20m in extent. In the rough zone the sand surface was protected by an armour of shell fragments and nodules of fused sand (longest axis 2-3cm in length). The change in roughness between the loose and armoured sand provided the location (0m) of the point of initiation of the saltation system. A similar boundary condition was used by Gillette *et al.,* (1996, p.646).

In clean air the change in surface roughness between the armoured and loose sand produces an adjustment of the atmospheric boundary layer to a decrease in surface roughness. During saltation the atmospheric boundary layer is adjusting from the roughness of the armoured sand to the apparent roughness, Z_o' (see Ch. 2.3.(iii)), of the saltation cloud. This increase in surface roughness is relatively minor with respect to the future downwind development of the sand cloud. As a result the boundary condition is considered an insignificant influence on the development of the saltation system.

The 20m experiment was conducted on Tuesday 19th November 1996. Unfortunately, an accessible, 20m expanse of flat sand downwind of a zone of increased roughness could not be located. The 20m experiment was, therefore, conducted on the top of a deposit of raised sand. The upwind side of the sand deposit comprised a steep slip-face approximately 1.50m high. The top of the

slip-face was used to locate (0m) the point of initiation of the saltation system, however, it can not be categorically stated that no sand was blown across the deposit from the lower areas upwind.

The mean sand size of the two experimental regions was 2.0ϕ - 1.5ϕ (250μm - 325μm) (see Fig. 5.7.), with 42% of the sediment within this range. Eighty five percent of the sediment lies in the range 2.5ϕ - 1.0ϕ (180μm - 500μm). The coarser tail of the sediment is composed entirely of shell fragments. Bedforms measured throughout the experimental period remained uniform, approximately 8-9cm in wavelength and 0.50-1cm in amplitude.

(iii) Instrumentation.

(a) Wind velocity.

Natural wind velocity profiles were measured using a Thornthwaite Wind Profiling System, Model 106. 'The profiling system, consists of six sensitive, matched cup anemometers (cup assembly weight 7g; distance constant 83.30cm) that may be mounted at variable heights on a single mast or singly on individual masts located up to 60m distant from a single control unit' (Butterfield, 1991, p.103). The anemometer array as configured for the present study comprised five anemometers located at 0.20, 0.40, 0.80, 1.60 and 2.10m above the ground. The single, standard anemometer was mounted at 0.80m (see Ch. 5.1.(i)).

(b) Mass flux.

The measurement of mass flux in the field required transportable, continuously-recording, total flux sand traps. For this investigation a 'total load' sand trap based on the Ames trap of Rasmussen and Mikkelsen (in press) and the near-isokinetic trap of Nickling and McKenna (1997) was developed. The successful Ames trap 1 : 10 (Rasmussen & Mikkelsen, in press) inlet-to-back vent ratio was included to maximise capture efficiency and minimised back-pressure (Jones & Willetts, 1979; Rasmussen & Mikkelsen, in press).

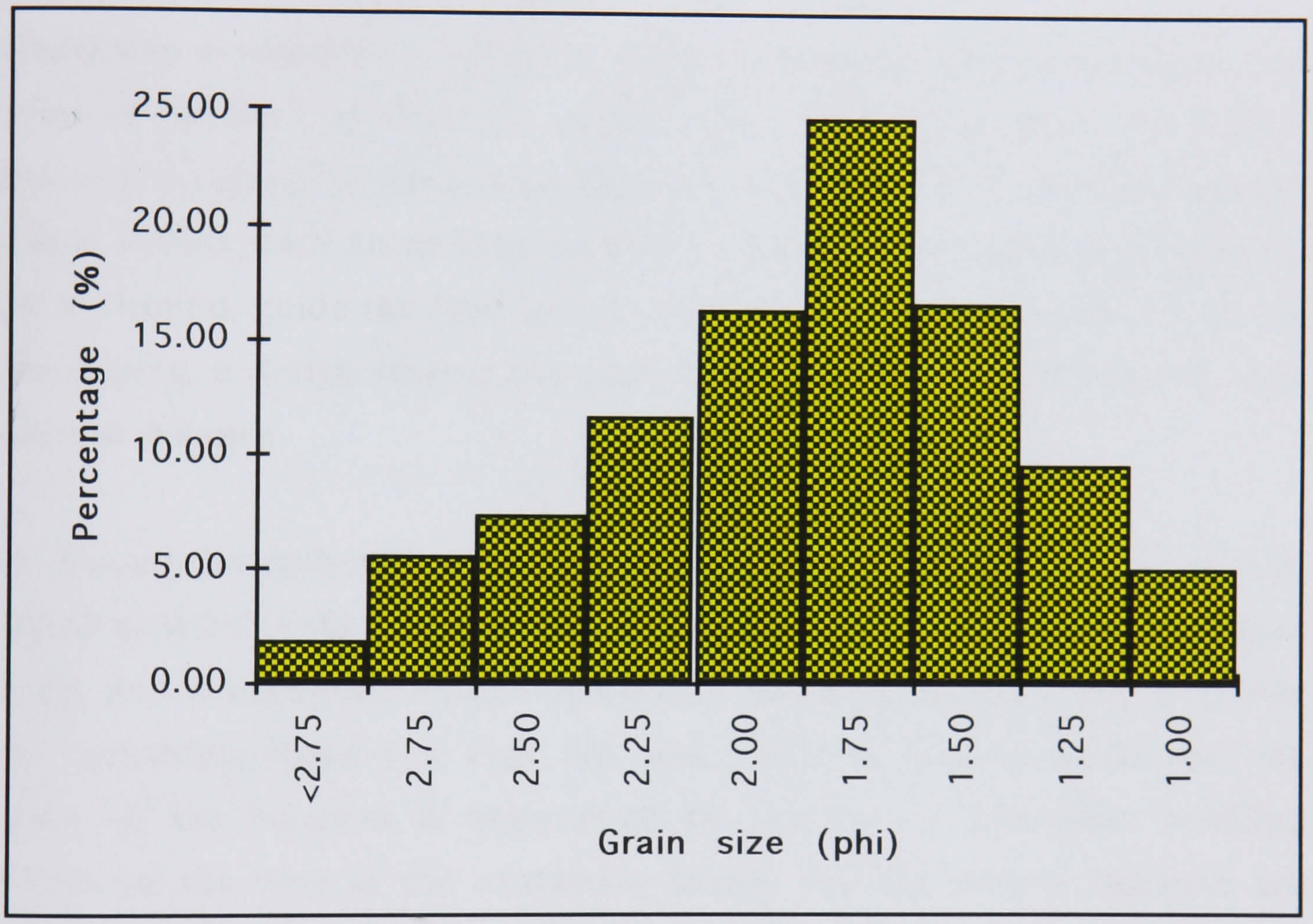

Fig. 5.7. Grain-size distribution of the Corralejo field site.

The 'total load' sand trap is wedge-shaped with an inlet of 0.5cm flaring to 5cm over 15cm (see Fig. 5.8.). The sand trap has an above ground height of 0.50m (see Figs. 5.8., 5.9. and 5.10.), sufficient to intercept most grains in saltation (Bagnold, 1941). To aid collection of the near-bed transport 4cm long horns, either side of the trap front, were included. Although the horns are only 2cm in height they are essential to the maximisation of near-bed transport and minimise scour. At ground level a ramp or lip further encourages the passage of near-bed grains into the sand trap.

The sand trap is constructed of light weight aluminium, 1mm in thickness, and the sides of the front aperture are shaped almost to a blade edge. The back is vented with 63μm nylon gauze (see Figs. 5.8., 5.9. and 5.10.). Within the sand trap nine baffles, each 10cm long, located 5cm apart and angled at 30 degrees to the horizontal, guide the sand grains downwards. The base of the sand trap is also sloping, a design feature incorporated to funnel sediment directly onto an electric balance.

Below ground, beneath each sand trap, is an electric balance (OHAUS Portable advanced model CT600, powered via mains or battery supply, with a resolution of 0.10g and a maximum weight of 600g). The balances are housed within plastic containing boxes (see Figs. 5.8. and 5.9.). In unlevel conditions, the accuracy of the balances is maintained by the use of adjustable levelling platforms on the base of the containing boxes. All the electric balances are connected to a single control panel that can be located approximately 20m away. The control panel not only shows the weight of sand on each balance but also allows the balances to be simultaneously tared.

The sand trap is connected to the containing box by means of an interconnecting tube fitted at its base (see Figs. 5.8. and 5.9.). The sand trap tube slides into a tube fixed within the lid of the containing box (and located directly over the load cell). With approximately 5cm of vertical movement

CROSS SECTIONS:

TOP

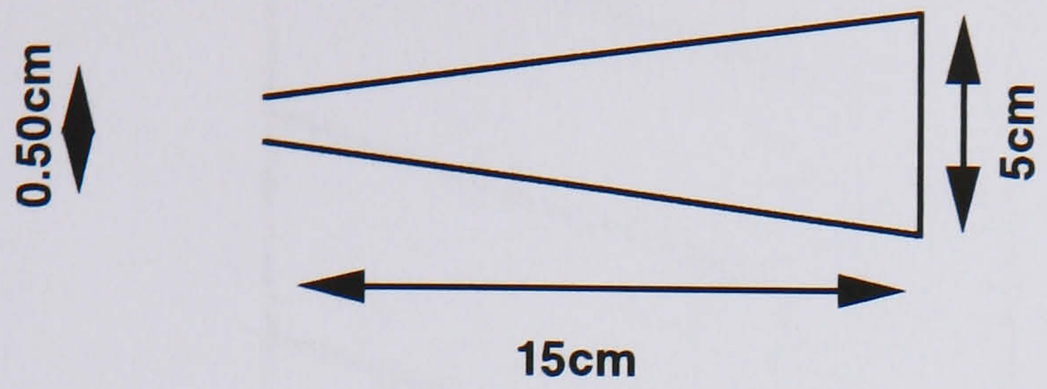

MIDDLE

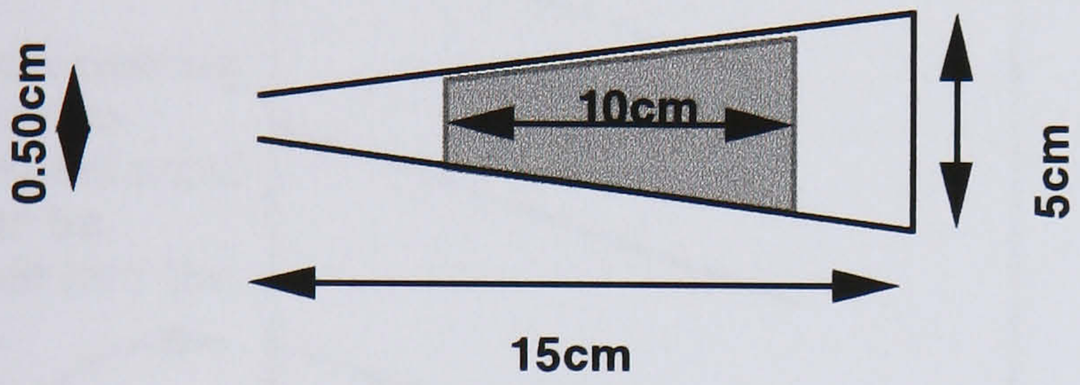

Baffles (30 degrees to the horizontal).

BASE

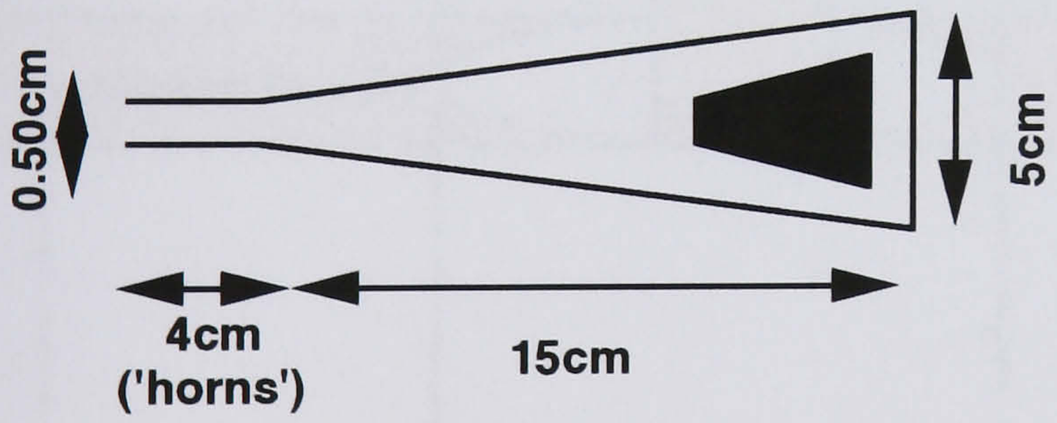

Outlet hole over the balance (balance housed in the containing box).

SIDE VIEW & INTERNAL:

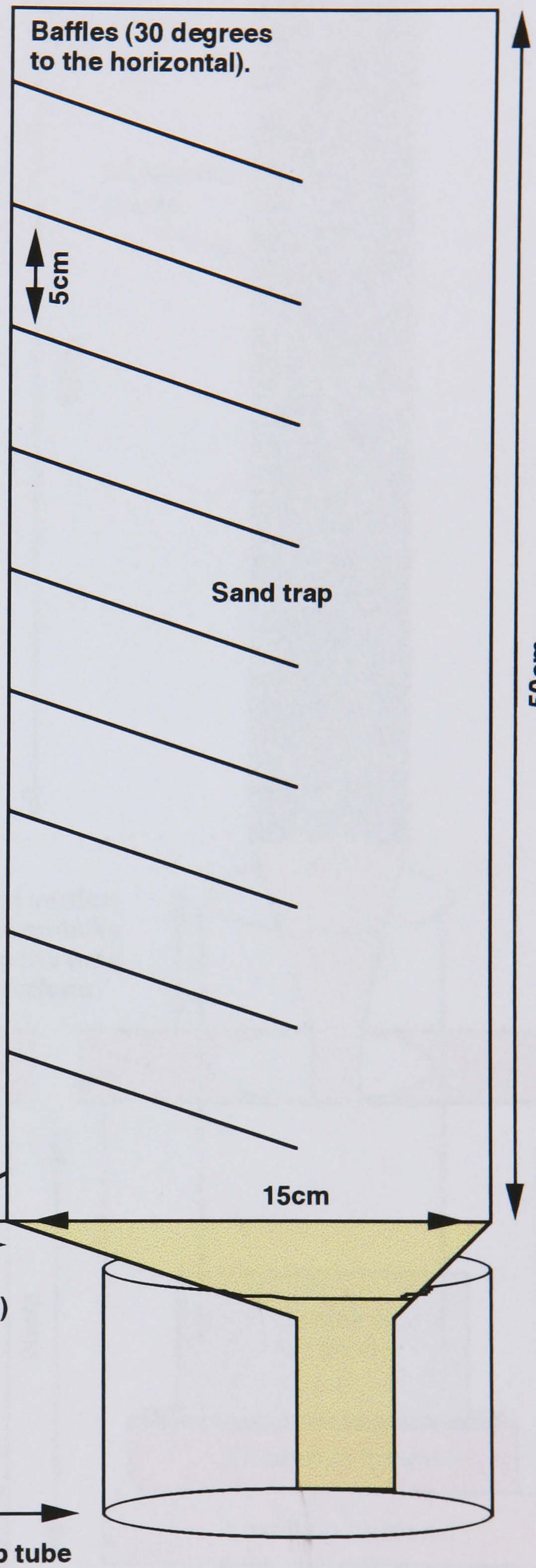

Sloping base of sand trap acts to funnel sand onto the balance. 'Funnel' section of the trap is housed within a tube, that interconnects with the tube in the lid of the containing box.

Fig. 5.8. 'Total load' sand trap design.

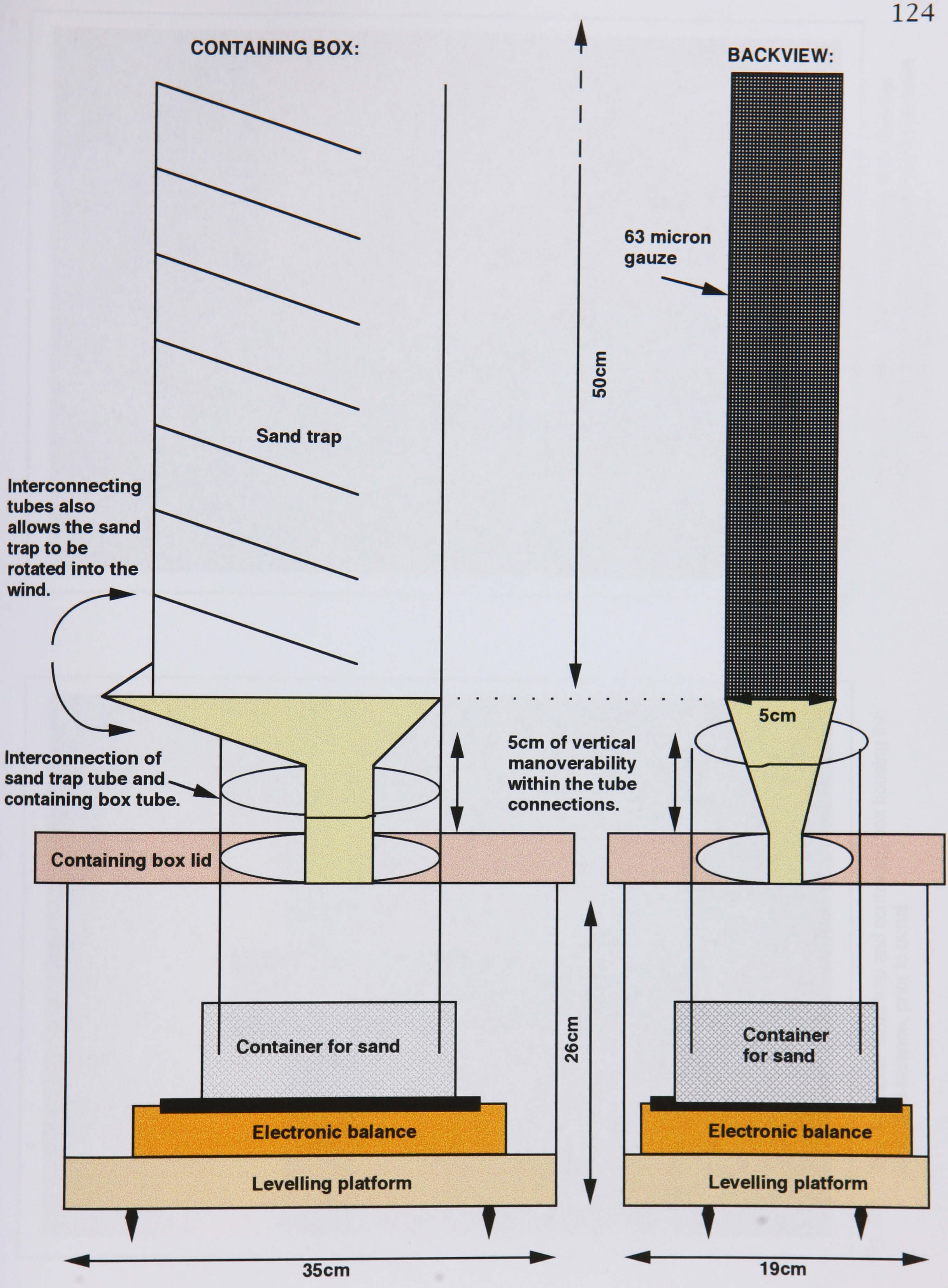

Fig. 5.8. cont. 'Total load' sand trap design.

Fig. 5.9. The 'total load' sand trap and containing box housing the electronic balance, prior to burial.

Fig. 5.10. Sand trap '*in-situ*'. The initial surface disturbances caused by the burial of the containing box have been recovered by the passage of ripples.

within the connection of the two tubes some adjustment to the level of the sand trap with the ground can be made following their installation.

The interconnecting tubes of the sand trap and the containing box do allow directional adjustments to be made to the sand trap. In this study, however, investigation of the spatial development of mass flux downwind of a designated point of origin required the relocation of the sand traps downwind of each other following any directional change in the wind.

(5.2.) RESULTS: THE SPATIAL DEVELOPMENT OF THE SALTATION SYSTEM.

All aeolian field experiments are, to some extent, unique. Even exact replications of field experiments will not yield the same results due to environmental parameters outside of human control. The appropriateness of field work lies, therefore, in the identification of recognisable traits and the physical explanation of results. Although the following discussion derives from the results of a specific combination of environmental conditions, emphasis is placed on the extraction of information that can be universally employed in the future study of aeolian processes.

(i) Spatial development of velocity.

During saltation the development of the wind velocity profile with distance downwind reflects the growth of the internal boundary layer, the extraction of momentum by the grains in motion and the adjustment of the outer flow to the increase in apparent roughness. For the 10m experiment (see Fig. 5.11.) the downwind reduction in velocity, due to the increasing height of influence of the saltation cloud, produces a minimum in the near-surface velocities at $X_{8.00m}$.

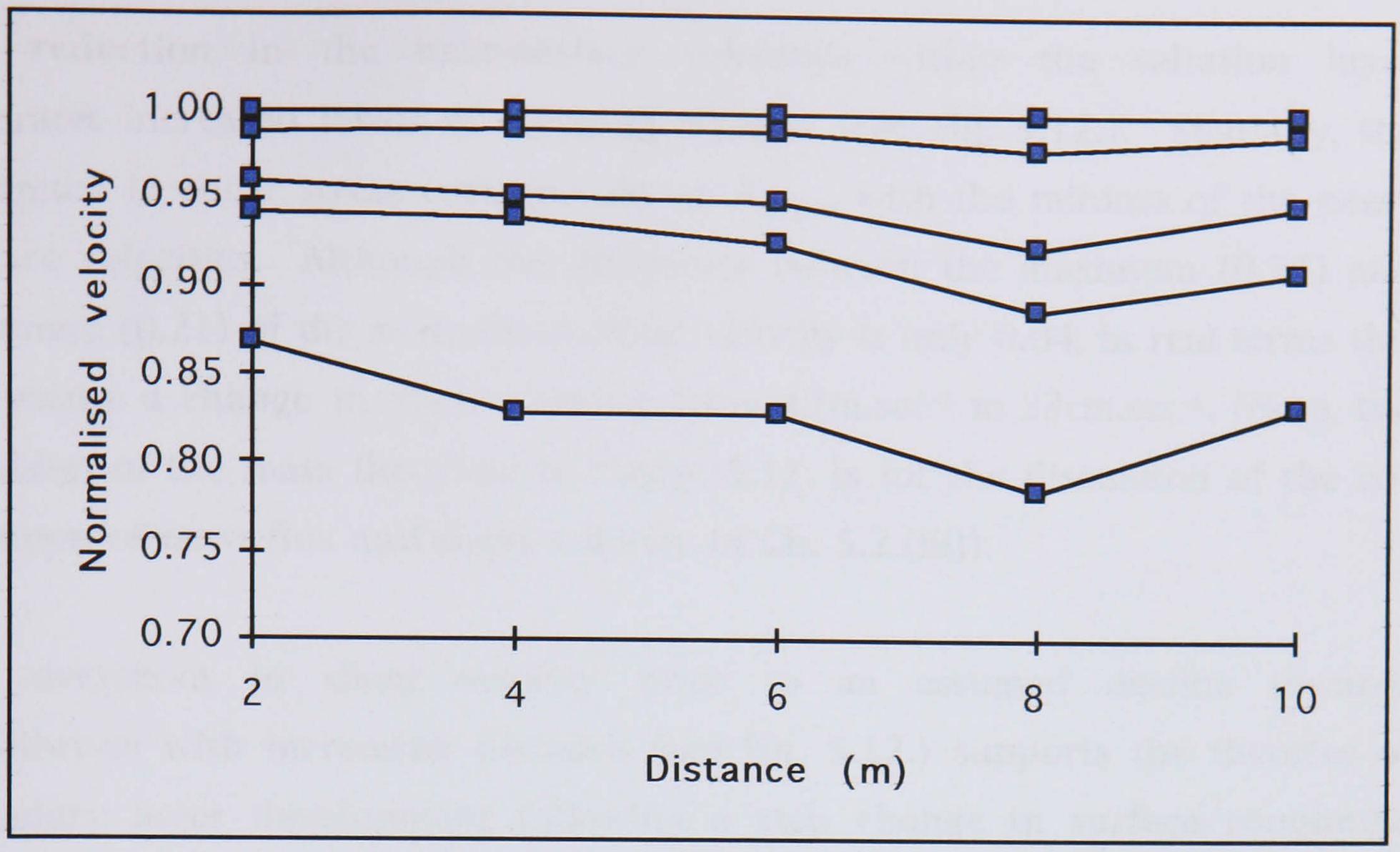

Fig. 5.11. Downwind spatial development of velocity for the 10m experiment at Corralejo during saltation. Velocity data were measured at heights 0.20, 0.40, 0.80, 1.60 and 2.10m. All velocities are normalised to the $U^{2.10m}$ value of each profile.

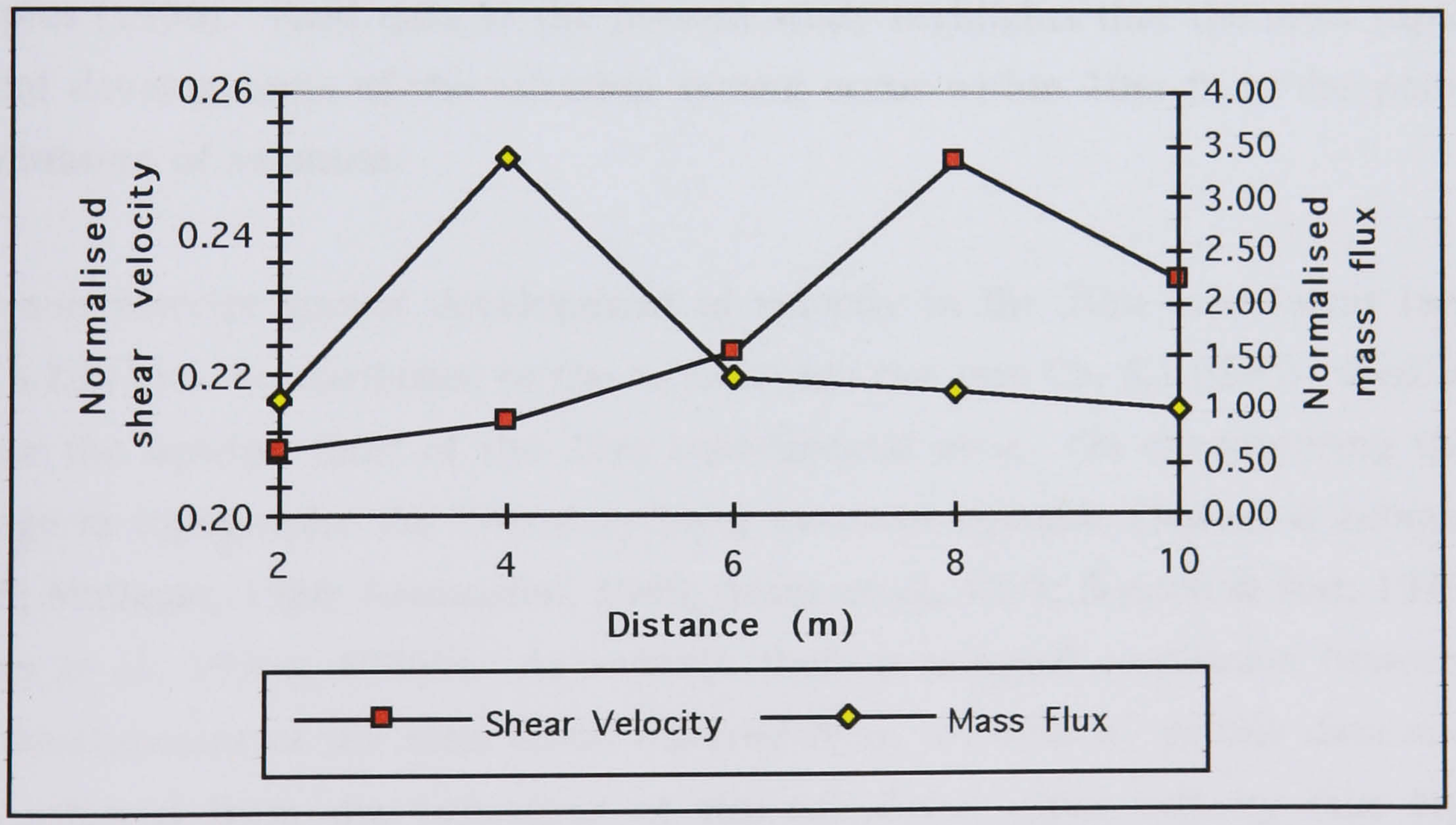

Fig. 5.12. Downwind spatial development of shear velocity and mass flux in the 10m Corralejo field experiment. Shear velocities are calculated from the velocity profiles normalised to the $U^{2.10m}$ value. Mass flux is plotted as hourly averages normalised to the mass flux value at 10m, the final sand trap site.

The reduction in the near-surface velocities within the saltation layer generates increased levels of shearing stresses (see Fig. 5.12.). Spatially, the maximum in shear stress corresponds, at $X_{8.00m}$, with the minima of the near-surface velocities. Although the difference between the maximum (0.25) and minimum (0.21) of the normalised shear velocity is only 0.04, in real terms this represents a change in shear velocity from 12m.sec^{-1} to 23cm.sec^{-1}. (Note, the inclusion of the mass flux data in Figure 5.12. is for the discussion of the co-variation of mass flux and shear velocity in Ch. 5.2.(iii)).

The overshoot in shear velocity prior to an assumed decline towards equilibrium with increasing distance (see Fig. 5.12.) supports the theories of boundary layer development following a step change in surface roughness (see Ch. 3.1.(i)). Previous saltation studies have not recorded a spatial overshoot in shear velocity, a result inherently due to the problem of scale (see Ch. 4.3.(i)). Previously, the smallest scale of investigation into the spatial development of the saltation system was the 50m used in the numerical model of Spies (1996). Field data in the present study highlights that the most rapid spatial developments of the saltation system occur within 10m from the point of initiation of saltation.

The non-descript spatial development of velocity in the 20m experiment (see Fig. 5.13.) may be attributed to the topographic rise (see Ch. 5.1.(ii(b))) used to define the upwind limit of the 20m experimental area. On encountering the change in topography the boundary layer becomes unstable (Jensen & Zeman, 1985; Mulligan, 1988; Rasmussen, 1989; Arens *et al.*, 1995; Bennett & Best, 1995; Wiggs *et al.*, 1996a, 1996b). As a result, there is minimal correlation between the development of the sand cloud inferred from the velocity profile data and that inferred from the behaviour of the calculated shear velocity (see Fig. 5.14.).

It should be noted that determination of which velocity data should be included in the calculation of shear velocity during saltation is controversial (Gerety,

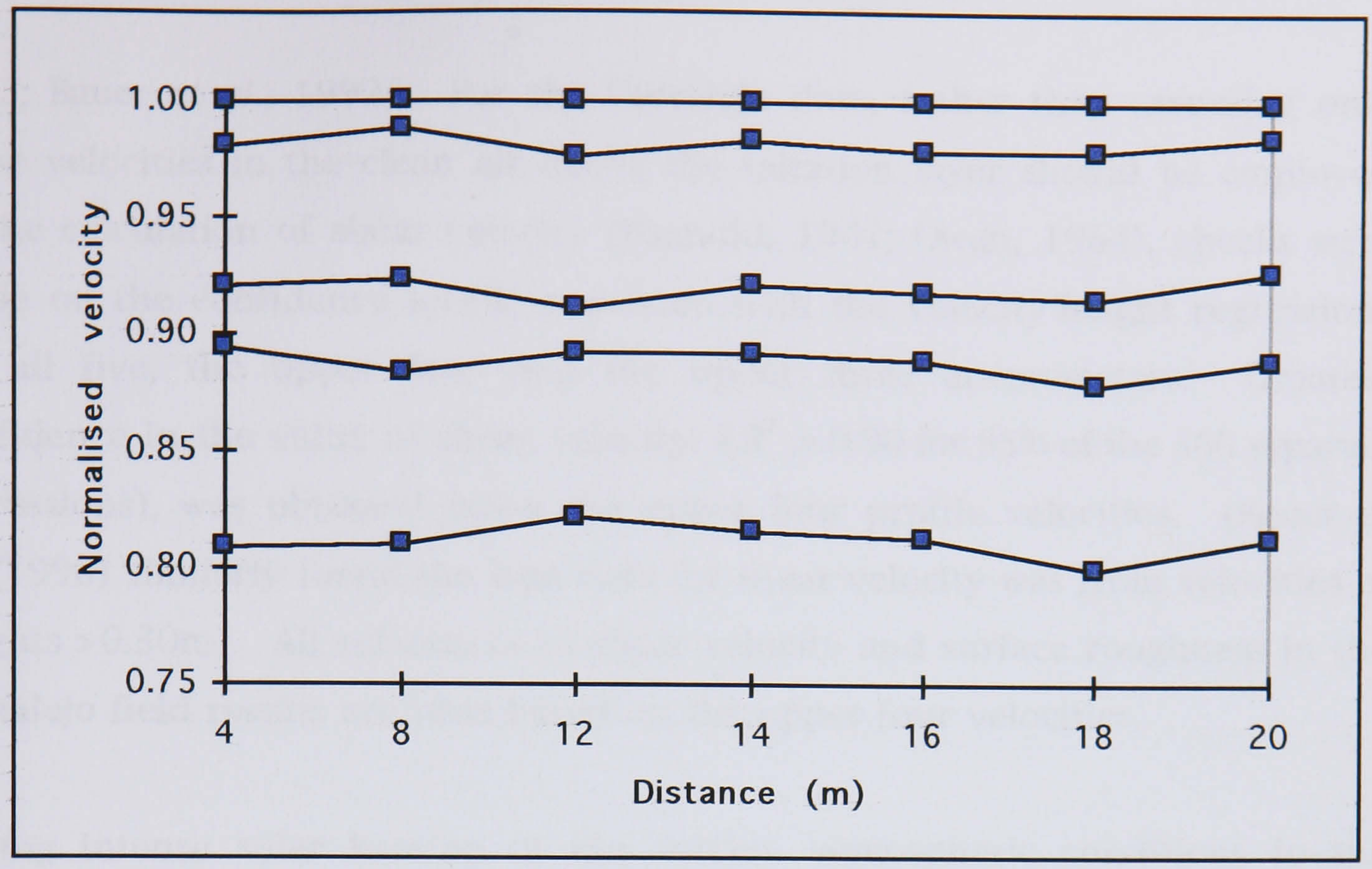

Fig. 5.13. Downwind spatial development of velocity for the 20m experiment at Corralejo during saltation. Velocity data were measured at heights 0.20, 0.40, 0.80, 1.60 and 2.10m. All velocities are normalised to the $U^{2.10m}$ value of each profile.

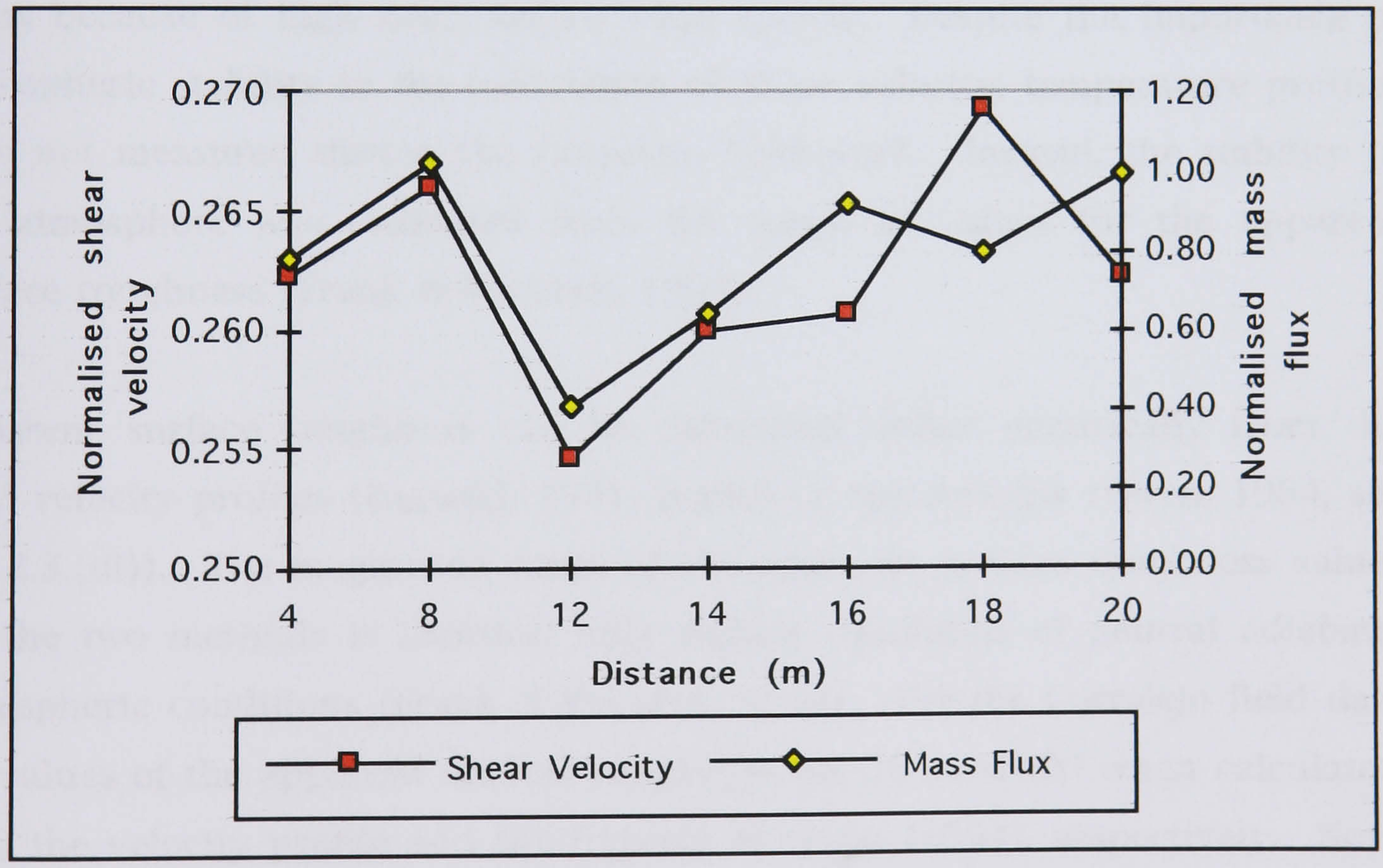

Fig. 5.14. Downwind spatial development of shear velocity and mass flux in the 20m Corralejo field experiment. Shear velocities are calculated from the velocity profiles normalised to the $U^{2.10m}$ value. Mass flux is plotted as hourly averages normalised to the mass flux value at 20m, the final sand trap site.

1985; Bauer *et al.,* 1992). For the Corralejo data, rather than assuming only those velocities in the clean air above the saltation layer should be employed in the calculation of shear velocity (Bagnold, 1941; Owen, 1964), checks were made on the confidence levels associated with the velocity:height regressions for all five, the upper four and the upper three anemometers. Greatest confidence in the value of shear velocity, ($R^2 > 0.90$ for 95% of the 360 separate regressions), was obtained using the upper four profile velocities. (Bauer *et al.* (1990) similarly found the best data for shear velocity was from velocities at heights >0.30m). All references to shear velocity and surface roughness in the Corralejo field results are thus based on the upper four velocities.

During intense solar heating of the surface 'atmospheric conditions in the lowest several metres become unstable, resulting in enhanced convection and vertical mixing so that the velocity gradient changes little with height' (Frank & Kocurek, 1994, p.735). Unstable atmospheric conditions produce a reduction in shear stresses due to intense vertical mixing, but increased surface shear stress because of high near-surface wind speeds. Despite the importance of atmospheric stability in the calculation of shear velocity, temperature profiles were not measured during the Corralejo field work. Instead, the stability of the atmosphere was estimated from the range of values for the apparent surface roughness (Frank & Kocurek, 1994).

Apparent surface roughness can be calculated either empirically from the wind velocity profiles (Bagnold, 1941, p.490) or theoretically (Owen, 1964, see Ch. 2.3.(iii)). The magnitude range of the apparent surface roughness values for the two methods is identical only during conditions of neutral adiabatic atmospheric conditions (Frank & Kocurek, 1994). For the Corralejo field data the values of the apparent surface roughness are 10^{-5} and 10^{-1} when calculated from the velocity profile and the formula of Owen (1964), respectively. Non-neutral atmospheric conditions must, therefore, have existed during data collection.

Despite the probable existence of unstable atmospheric conditions during the Corralejo field work, no corrections have been incorporated within the calculations of shear velocity. It has been suggested that for velocity profiles measured between 0.50m and 6m the errors in the calculated shear velocity values, based on data collected in stable and non-stable atmospheric conditions, are less than 2% (Arens *et al.*, 1995). Furthermore, Wiggs *et al.* (1996a, p.22) conclude that an upper anemometer at a height of approximately 2m is 'sufficiently close to the surface to negate the need to account for air flow instability induced by excessive surface heating'. At such near-surface heights the effect of buoyancy on the distribution of shear stresses is not significant (Rasmussen *et al.*, 1985).

Potential errors in the calculated values of shear velocity in the Corralejo field data are acknowledged. Indeed, caution is invoked in the use of the absolute values of shear velocity for either the calculation of mass flux or for the comparison with other data sets. These limitations are not specific to this field work but a problem universal to aeolian studies. Within the Corralejo data a consistent methodology in the calculation of shear velocity, however, does permit the examination of relative developments in the saltation system.

(ii) Spatial development of mass flux.

The observed downwind spatial development of mass flux over the 10m length (see Fig. 5.12.) is in full agreement with existing studies (see Ch. 3.1.(iii)). In the 10m experiment mass flux overshoots at $X_{4.00m}$ and then declines, presumably towards an equilibrium constant rate. The initial rapid increase and overshoot in mass flux can be explained by the avalanching effect proposed by Chepil (1957) and the time lag concept proposed by Bagnold (1941), respectively, (see Ch. 3.1. (iv)). The final equilibrium rate of transport of sand represents the mutual adjustment between the volume of sediment in transport and the wind velocity.

The 20m field experiment shows a more complex development of mass flux (see Fig. 5.14.). The slip face used to designate the point of initiation of the saltation system does not provide a precise boundary condition. Furthermore, the wind velocity profile is in a stage of transition following the rise in topography. The combination of these factors hinders the 'normal' development of the saltation system.

The passage of saltating grains over the slip face in the 20m experiment is analogous to the upwind artificial sand-feeding of the wind tunnel experiments (see Figs. 3.3. and 3.5.). Mass flux peaks where the sand grains are introduced, either by sand-feed or by breaching of the slip-face, and then declines rapidly as saturation occurs. Following the overload of the saltation system, mass flux recovers and the saltation system develops as 'normal'.

Assuming that the saltation system experiences no lasting adverse effects following the saturation of the flow from sand entering from upwind, the 10m and 20m field experiments are potentially comparable. In the 20m field experiment, X_{1200m} is designated the point of initiation for the 'normal' development of the saltation system (see Fig. 5.14.). From X_{1200m} onwards the development of mass flux mirrors that recorded by the 10m field experiment (see Fig. 5.12.).

From the designated point of initiation for the 'normal' development of the saltation system (i.e. X_{0m} in the 10m field experiment and X_{1200m} in the 20m field experiment), maxima are recorded in mass flux and shear velocity at 4m downwind and 8m downwind, respectively (see Figs. 5.12.). The 10m and 20m experiments, and wind tunnel experiments with and without sand-feed (see Ch. 4.3.(ii)), are therefore, seemingly comparable once the effects of influxes of sand from upwind have been taken into account.

(iii) Spatial co-variation of mass flux and wind velocity.

The lag hypothesis originally proposed by Bagnold (1941, Ch. 3.1.(iv)) is exemplified by the spatial results of the 10m experiment (see Fig. 5.12.). Spatially, both mass flux and shear velocity overshoot prior to declining towards an equilibrium. The overshoot in mass flux ($X_{4.00m}$) prior to the overshoot in shear velocity ($X_{8.00m}$) is most likely due to the lagged response of the wind to the grains in transport.

It is unclear from the 10m experiment whether equilibrium has been achieved within the 10m length (see Fig. 5.12.). It is suggested, therefore, that some distance in excess of 10m is required for mass flux and shear velocity to attain equilibrium. A more precise distance can not be determined as numerous oscillations about the constant transport rate may be witnessed before equilibrium is finally achieved (see Ch. 3.1.(i)).

The lagged response of mass flux and shear velocity is not evident within the data from the 20m experiment due to the lack of a definable point of initiation for the saltation system (see Fig. 5.14.), i.e. sand can breach the slip-face. However, with sand blowing into the 20m experimental area from a upwind fetch of hundreds of meters the data confirms the above suggestion, that at distances >10m downwind, mass flux and shear velocity do respond in phase.

(5.3.) RESULTS: THE TEMPORAL DEVELOPMENT OF THE SALTATION SYSTEM.

The temporal development of the saltation system in the field is controlled essentially by the variations in wind velocity. In the 10m experiment, mass flux and wind velocity were recorded simultaneously through time at 10m downwind (see Figs. 5.15. and 5.16.). Mass flux and shear velocity can be seen to follow a generally similar temporal development to the wind velocity; all the

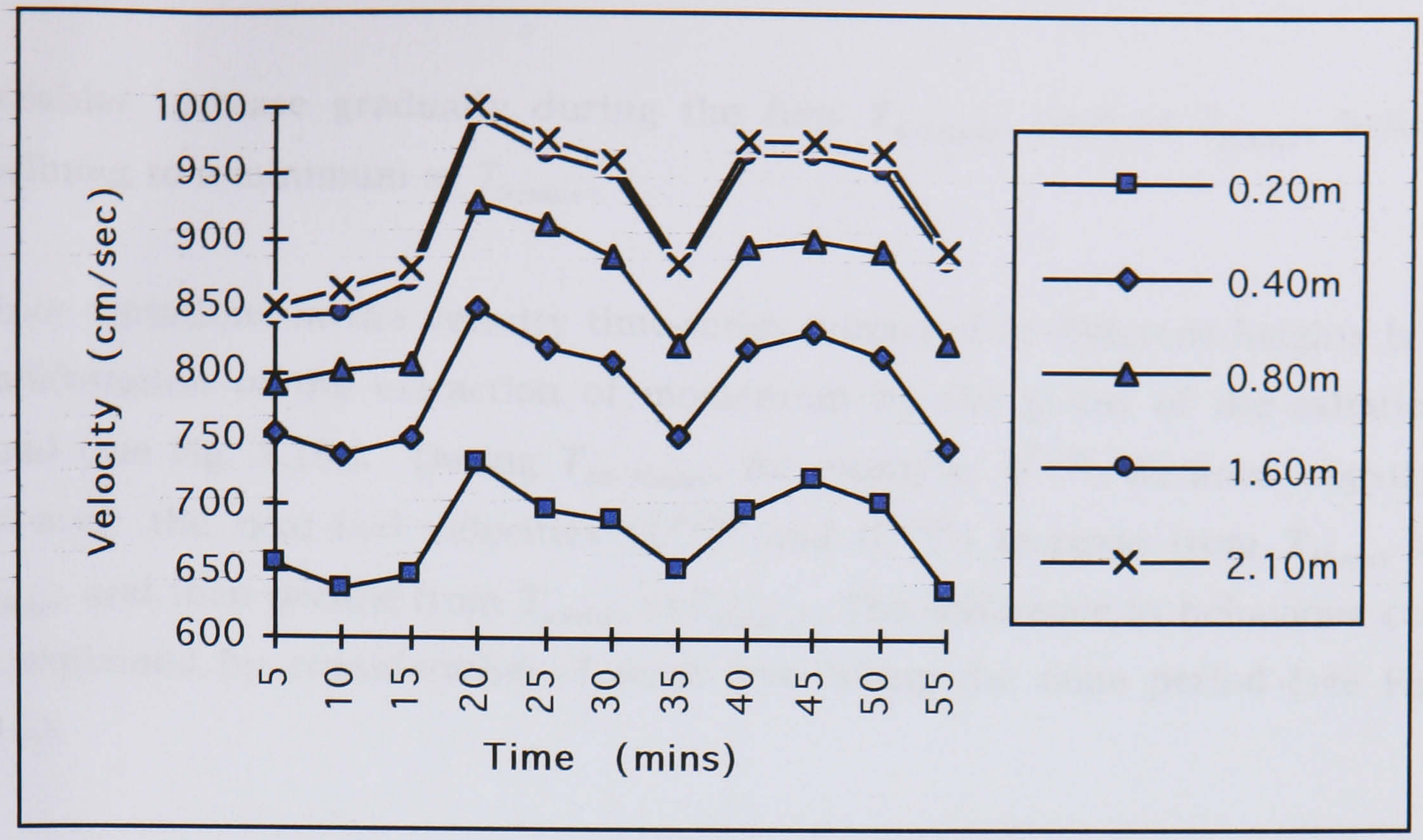

Fig. 5.15. Temporal development of velocity for the 10m experiment at Corralejo during saltation.

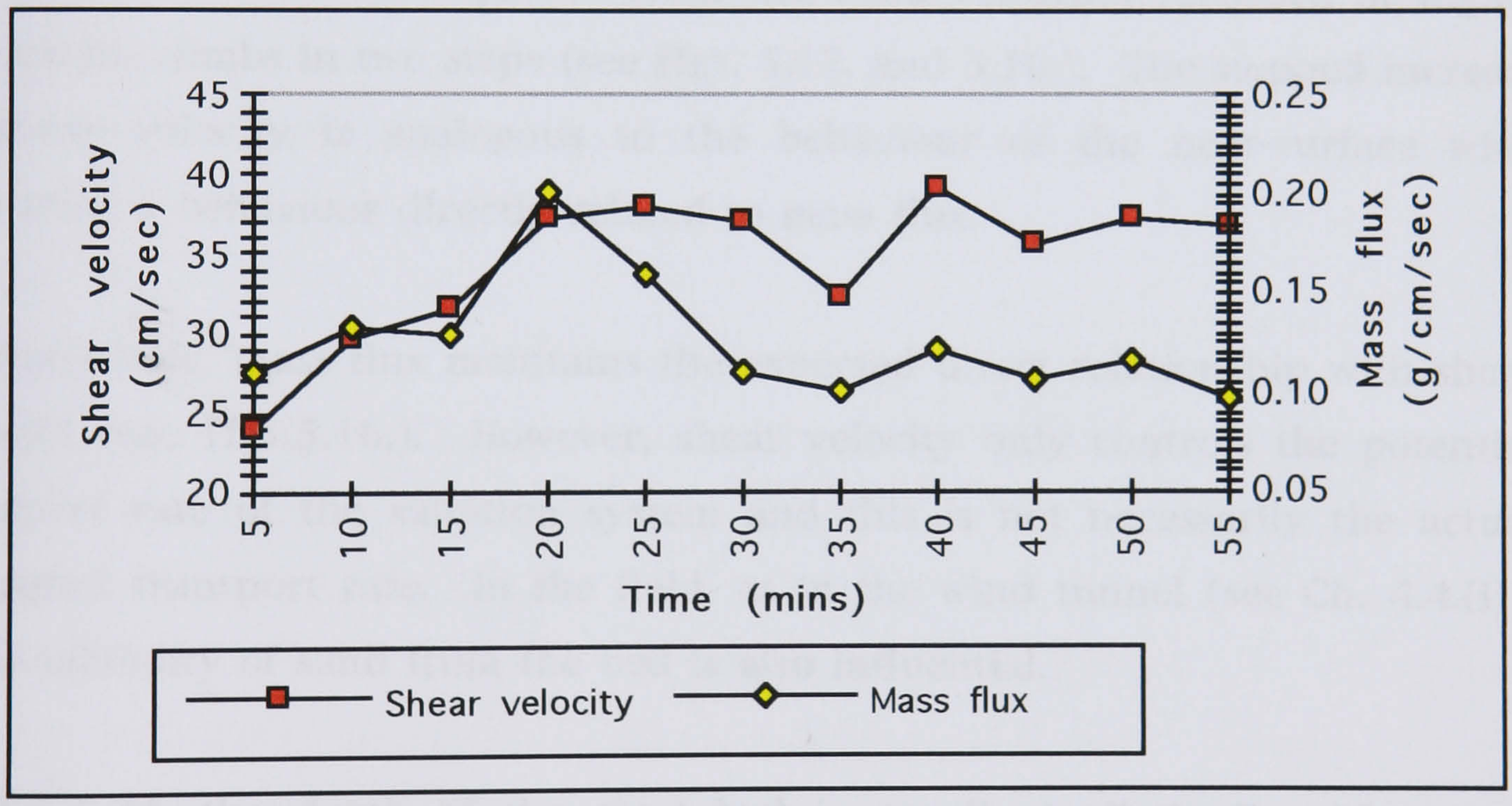

Fig. 5.16. Temporal development of shear velocity and mass flux for the 10m experiment at Corralejo. Mass flux and shear velocity data were recorded simultaneously at 10m downwind from the point of initiation of saltation.

ables increase gradually during the first $T_{5-15\min s}$, peak at $T_{20\min s}$, before ining to a minimum at $T_{35\min s}$.

ıor variations in the velocity time-series measured at different heights is a nifestation of the extraction of momentum by the grains of the saltation ud (see Fig. 5.15.). During $T_{40-50\min s}$, for example, $U^{2.10m}$ declines slightly, wever, the near-bed velocities ($U^{0.20m}$ and $U^{0.40m}$) increase from $T_{40\min s}$ to $_{5\min s}$ and then decline from $T_{45\min s}$ to $T_{50\min s}$. The difference in behaviour can explained by consideration of mass flux during the same period (see Fig. 16.).

ıe reduction in the near-surface velocities due to the extraction of ıomentum by the grains in motion is subsequently manifest in the value of ıear velocity. During $T_{5-15\min s}$ shear velocity, rather than increasing radually, as would be expected from the wind velocities recorded at higher levations, climbs in two steps (see Figs. 5.15. and 5.16.). The stepped increase n shear velocity is analogous to the behaviour of the near-surface wind elocities, a behaviour directly related to mass flux.

Through time, mass flux maintains the expected direct relationship with shear velocity (see Fig. 5.16.). However, shear velocity only controls the potential transport rate of the saltation system and this is not necessarily the actual measured transport rate. In the field, as in the wind tunnel (see Ch. 4.4.(i)), the availability of sand from the bed is also influential.

In the field, the depth of the sand bed is usually 'unlimited'. Of greater importance is the variability in the availability of entrainable particles through space and time. In the 10m experiments a change in the saltation system is witnessed from a 'transport-limited' to a 'supply-limited' system (see Fig. 5.16.). During the first $T_{5-20\min s}$ mass flux increases in direct proportion with shear velocity. From $T_{20\min s}$ onwards, however, despite a relatively

constant shear velocity value ($U_* = 37$cm.sec^{-1}), mass flux declines during $T_{20\text{-}30\,\text{mins}}$ to a new lower 'quasi-equilibrium' rate.

The different rates of mass flux associated with the 'single' value of shear velocity give an insight into the relative development of the sand bed through time (see Fig. 5.16.). During the initial $T_{5\text{-}20\text{mins}}$ the sand bed is relatively 'fresh' and there are a large range of sediment sizes and a supply of easily entrainable grains. At $T_{20\text{min}\,s}$, therefore, mass flux can fulfil the potential transport rate of the corresponding shear velocity.

After $T_{20\text{min}\,s}$ the majority of the most easily entrainable grains have been eroded from the sand bed (see Fig. 5.16.). Despite the wind maintaining the same potential transport rate, the actual transport rate declines due to the armouring of the sand bed. For a relatively constant wind velocity the actual 'quasi-stable' transport rate thus becomes controlled by the sediment availability from the sand bed. Through time the transport rate may again decline as the grain-size distribution of the surface changes; only the onset of higher velocity winds can destabilise the surface and lead to an increase in mass flux.

In the 20m field experiment grains breaching the slip-face from upwind initiate the saltation system (see Ch. 5.1.(ii(b))). The high energy bombardment of the surface by saltating particles reduces the influence of the sand bed development through time and space. Throughout the experimental period, therefore, mass flux, shear velocity and wind velocity develop simultaneously (see Figs. 5.17. and 5.18.).

Although in the 20m field experiment there is no change from a transport-limited to a supply-limited system the development of the sand bed is still influential. Through time, for any particular shear velocity, the rate of mass flux declines (see Fig. 5.18.). Over a relatively non wind-worked surface at $T_{25\text{mins}}$, for example, a shear velocity of approximately 38cm.sec^{-1} generates a

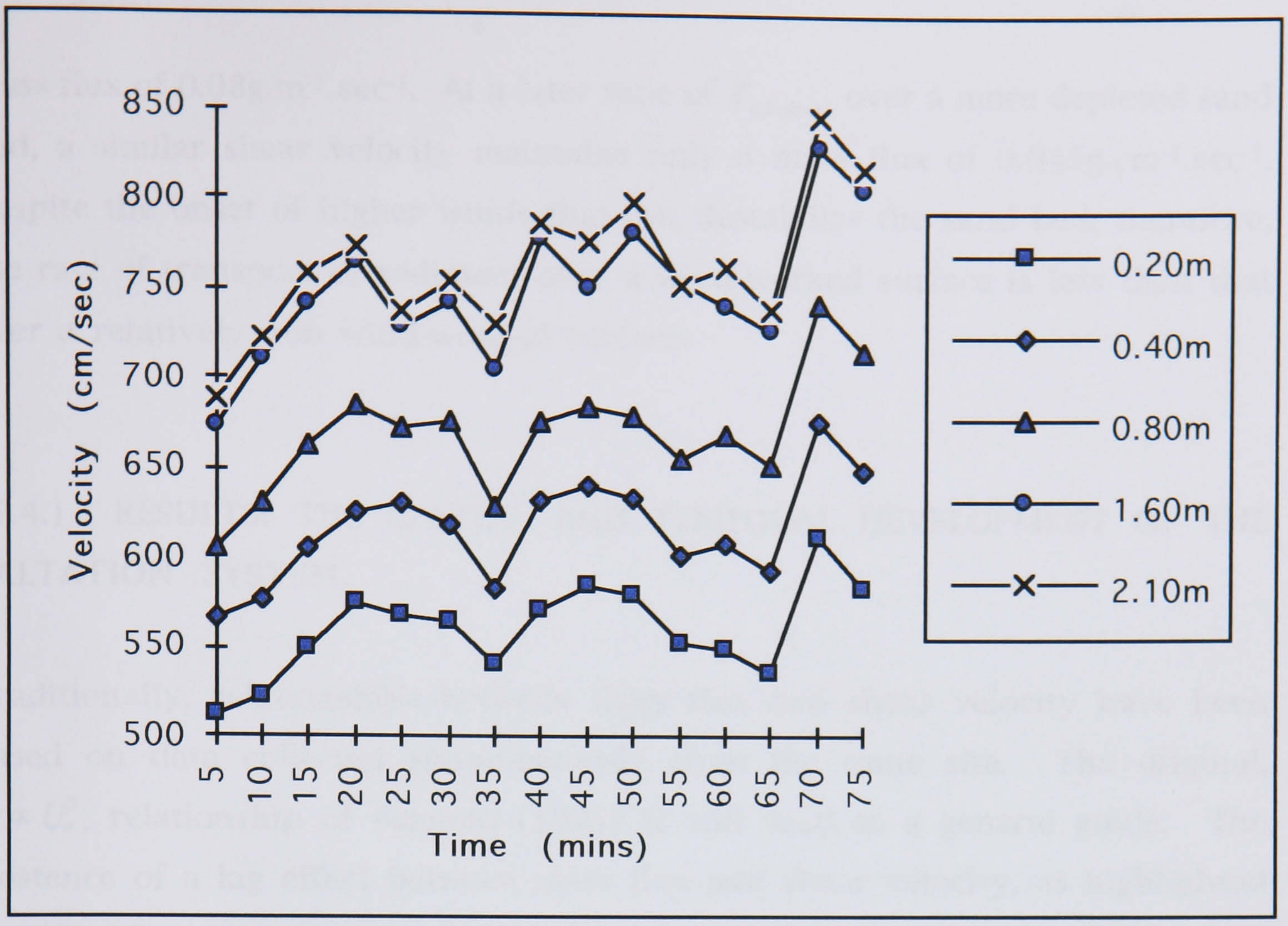

Fig. 5.17. Temporal development of velocity for the 20m experiment at Corralejo during saltation.

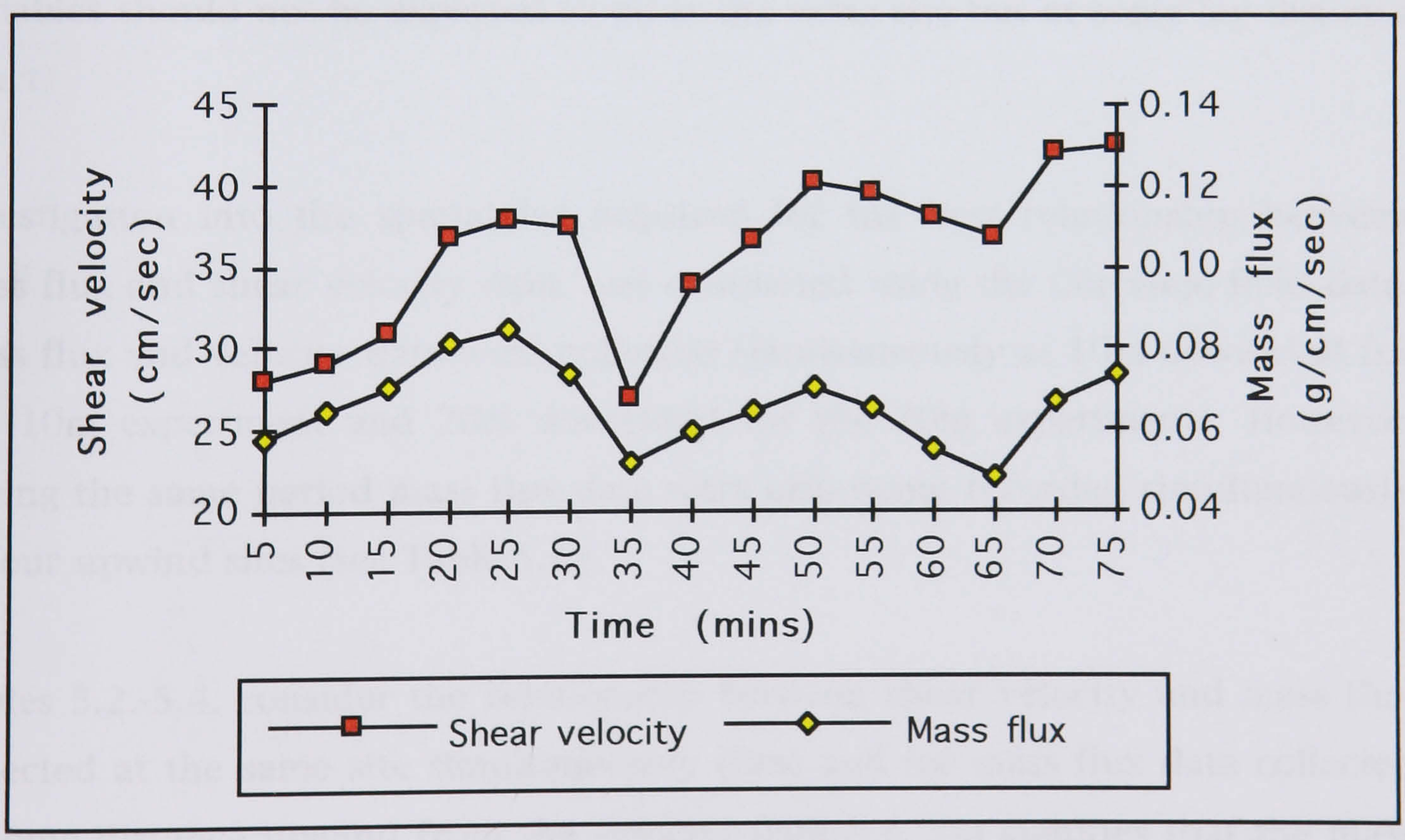

Fig. 5.18. Temporal development of shear velocity and mass flux for the 20m experiment at Corralejo. Mass flux and shear velocity data were recorded simultaneously at 20m downwind from the point of initiation of saltation.

mass flux of 0.08g.m^{-1}.sec^{-1}. At a later time of T_{65mins}, over a more depleted sand bed, a similar shear velocity maintains only a mass flux of 0.045g.cm^{-1}.sec^{-1}. Despite the onset of higher winds that can destabilise the sand bed, therefore, the rate of transport of sediment over a wind-worked surface is less than that over a relatively non wind-worked surface.

(5.4.) RESULTS: THE SPATIAL AND TEMPORAL DEVELOPMENT OF THE SALTATION SYSTEM.

Traditionally, relationships between mass flux and shear velocity have been based on data collected simultaneously from the same site. The original, $Q \propto U_*^3$, relationship of Bagnold (1941) is still used as a general guide. The existence of a lag effect between mass flux and shear velocity, as highlighted in the 10m experiment (see Fig. 5.12.), questions the appropriateness of relationships between mass flux and shear velocity collected simultaneously at the same site. Indeed, it is suggested that the best relationship between the two variables should not be expected to be at the same site but at some lag distance apart.

Investigation into the spatial lag required for the best relationship between mass flux and shear velocity data, was conducted using the Corralejo field data. Mass flux and velocity data were collected simultaneously at 10m downwind for the 10m experiment and 20m downwind for the 20m experiment. However, during the same period mass flux data were also being recorded simultaneously at four upwind sites (see Table 5.1.).

Tables 5.2.-5.4. consider the relationship between shear velocity and mass flux collected at the same site simultaneously (0m) and for mass flux data collected at some distance upwind from the velocity data (i.e. 2m signifies that the mass flux data were collected 2m upwind from the velocity data).

	Distance (m) mass flux data were measured up-wind of velocity.							Spatially Averaged
Experiment	0	2	4	6	8	12	16	
10m	-6*	46	84	62	38			57
20m	4	24	75	-10*	78	65	39	72

Table 5.2. Confidence (%) values from the regression of the natural logarithms of shear velocity and mass flux.

	Distance (m) mass flux data were measured up-wind of velocity.							Spatially Averaged
Experiment	0	2	4	6	8	12	16	
10m	1.35*	4.01	6.43	3.47	3.56			3.38
20m	1.59	4.88	12.60	66.69*	16.88	10.17	59.94	5.72

Table 5.3. Exponent values from the regression of the natural logarithms of shear velocity and mass flux.

		Distance (m) mass flux data were measured up-wind of velocity.							Spatially Averaged
Experiment	Velocity Heights (m)	0	2	4	6	8	12	16	
10m	0.20	15	64	65	83	24			85
	0.40	16	66	71	85	28			90
	0.80	16	63	79	86	61			92
	1.60	10	61	83	84	60			89
	2.10	12	61	83	85	60			91
20m	0.20	-8*	-18*	-0.5	-9	-0.1	4	0.5	3
	0.40	-8*	-11	6	0	6	13	7	11
	0.80	-8*	10	25	14	26	32	27	30
	1.60	-5*	50	50	29	52	53	49	53
	2.10	-5*	56	57	40	60	62	58	61

Table 5.4. Confidence (%) values from the regression of the natural logarithms of point velocity and mass flux.

Note: in all of the above Tables an asterisk (*) adjacent to any value indicates F<F critical for the regressional relationship between shear velocity and mass flux. As a result the quoted R^2 value is statistically insignificant.

Table 5.2. shows the relationship between mass flux and shear velocity, expressed as the confidence (%) of the regressional relationship (R^2) between the natural logarithm of shear velocity and the natural logarithm of mass flux. Mass flux and velocity data collected at the same site simultaneously (0m) generally produces the least good relationship. Often the figures quoted indicate a statistically insignificant regression.

As the separation distance between the sites for the collection of the mass flux and shear velocity data increases so does the confidence in the ability of shear velocity to predict the rate of mass flux (see Table 5.2.). For the 10m experiment the greatest confidence in the ability of shear velocity to predict the rate of mass flux occurs at a separation distance of 4m. This distance is consistent with the lag separation distance between the peak in mass flux at $X_{4.00m}$ and the peak in shear velocity at $X_{8.00m}$ (see Fig. 5.12.).

In the 20m experiment the greatest confidence in the prediction of mass flux from shear velocity occurs at a separation distance of 8m (see Table 5.2.). The greater separation distance for the 20m experiment, as compared to the 10m experiment, is explained by lower wind velocities and the abrupt change in topography at $X_{0.00m}$ (see Ch. 5.1.(ii(b))). The change in topography affects the relationship between shear velocity and mass flux; the unstable boundary layer effectively decoupled from the saltation system. The lower wind velocities lead to a longer transferral time between the generation of a saltation event and the arrival of the wind-borne sand grains at the velocity station.

Table 5.3. shows the regression exponent of the relationship between the natural logarithm of shear velocity and the natural logarithm of mass flux. No relationship between shear velocity and mass flux produces an exponent particularly close to the cubic relationship of Bagnold (1941). Indeed, the universal applicability of mass flux equations using the relationship between

shear velocity and mass flux is limited by the fact the exponents of the relationships change with environmental conditions.

It has long been recognised that velocity measurements at one elevation hold enough information to predict the rate of mass flux at that site (O'Brien & Rindlaub, 1936; Kawamura, 1951; Jackson & McCloskey, 1997). Table 5.4. reports the results of an attempt to test the predictive power of $u_{(z)}$ at various heights. For both the 10m and 20m experiments there is a general increase in the predictability of mass flux from a single point velocity with height. Above 0.80m, the original atmospheric forcing of the saltation system is recorded and this provides a good indicator of mass flux. The 'saltation-reduced' near-bed velocities are in general, more significant for the value of shear velocity than for the prediction of mass flux.

For the 10m experiment greatest confidence in the prediction of mass flux from a point velocity is achieved at a separation distance of 6m (see Table 5.4.). This distance relates to the location of the spatial overshoot in mass flux, i.e. the mass flux overshoot occurs at $X_{4.00m}$ downwind from the point of initiation of the saltation system (see Fig. 5.12.) or 6m upwind from the site of collection of the velocity data. Similarly, in the 20m experiment greatest confidence in the prediction of mass flux from a point velocity is achieved at a separation distance of 12m, corresponding with the overshoot in mass flux at $X_{8.00m}$ downwind (see Fig. 5.14.).

Included in Tables 5.2.-5.4. is a figure for the average of the spatial data, i.e. the average of mass flux from all five traps. The statistical significance of the relationships between shear velocity and mass flux is often greatest for these averaged data. Similarly, the regressional exponent (see Table 5.3.) of the averaged data also provide the closest approximation to the original cubic value of Bagnold (1941). These results confirm that the condition of equilibrium is a spatially and temporally average concept.

The development of the saltation system through time and space towards an approximate state of equilibrium is evident only in spatially and temporally averaged data (see Fig. 5.19.). Point data collected within the equilibrium region record non-equilibrium conditions due to short-term irregularities, such as lateral inhomogenities in the flow and localised surface heterogenities. Equilibrium conditions are evident only by the amalgamation of sufficiently substantial volumes of non-equilibrium point data.

(5.5.) SUMMARY.

The Corralejo field work is the first investigation to have operated on the scale of laboratory and numerical model studies. The results of the small-scale field work have verified some of the existing ideas pertaining to the spatial and temporal development of the saltation system, but also introduced new areas for investigation. Ironically, the direct study of equilibrium, rather than clarifying this state, has emphasised the uncertainty of its measurement. The following conclusions have been drawn from the Corralejo field data:-

- Equilibrium between shear velocity and mass flux is evident only in spatially and temporally averaged data. Over short time periods or distances, the relationship between shear velocity and mass flux indicate non-equilibrium conditions.
- Spatially, the saltation system attains equilibrium at some distance >10m.
- From a designated spatial point of initiation of the saltation system, mass flux overshoots at $X_{4.00m}$ prior to the decline towards equilibrium
- A previously unrecorded peak in shear velocity at $X_{8.00m}$, prior to a decline towards equilibrium is identified. The development of shear velocity during saltation is thus analogous with that during clean air conditions following a step change in roughness (see Ch. 3.1.(i)).
- There is a lag between the overshoot in mass flux and shear velocity in the initial stages of development of the saltation system.

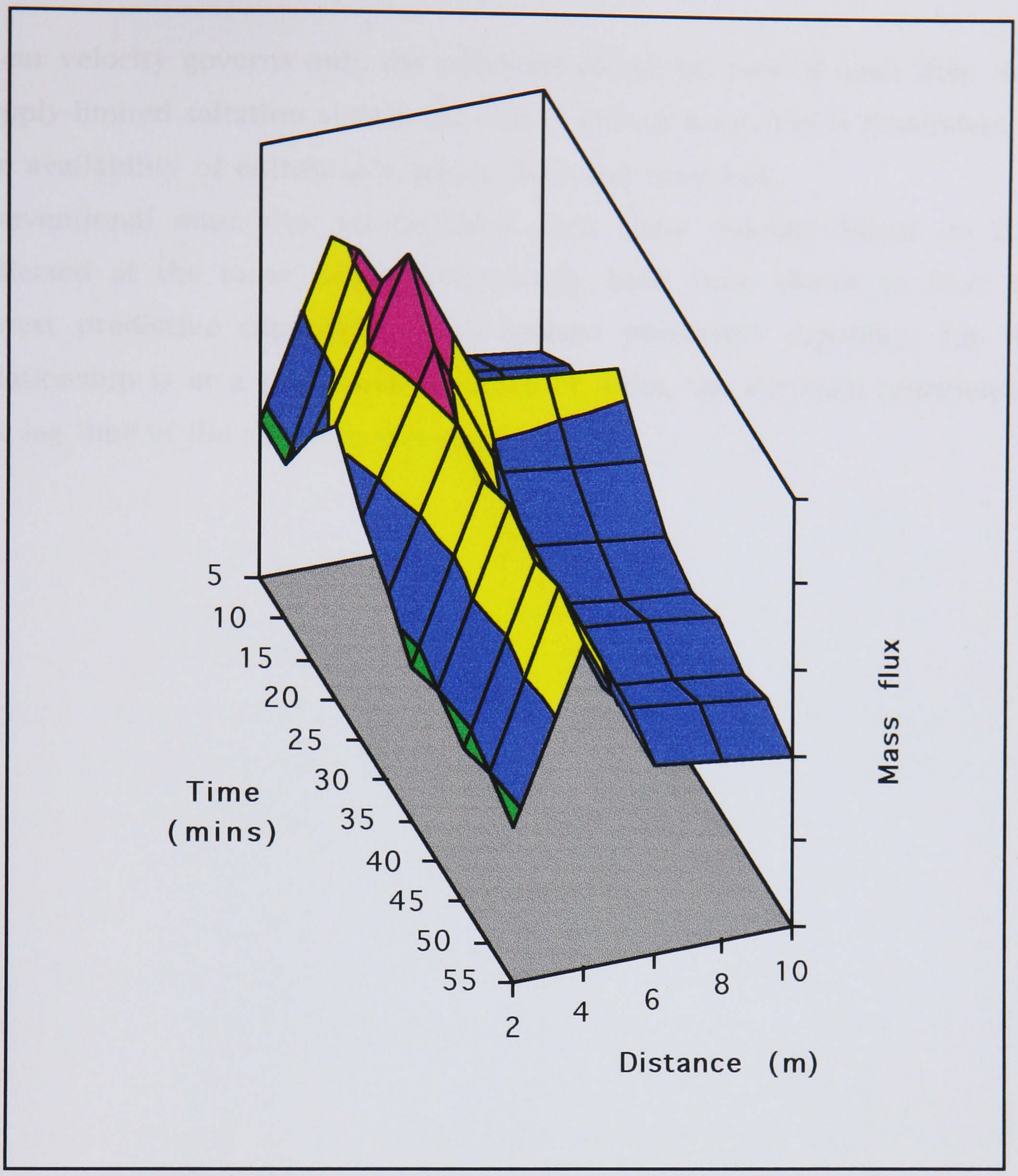

Fig. 5.19. Schematic representation of the idealised spatial and temporal development of the saltation cloud, from a point of initiation, for the 10m experiment at Corralejo.

- Shear velocity governs only the potential maximum rate of mass flux. In a supply-limited saltation system the actual rate of mass flux is dependent on the availability of entrainable grains from the sand bed.
- Conventional mass flux relationships with shear velocity based on data collected at the same site simultaneously have been shown to have the lowest predictive capability. The highest predictive capability for this relationship is at a separation distance of 4-6m, the distance representing the lag time of the saltation system.

CHAPTER 6

SMALL SCALE SPATIAL AND TEMPORAL DEVELOPMENTS OF THE SALTATION SYSTEM

Equilibrium is a function of velocity, time and space. Rather than focus on the unique state of equilibrium itself the three-dimensional spatial and temporal developments of the saltation system prior to equilibrium are considered. The following chapter considers the relationships between the laboratory and the field data. Attention is given to: whether visually similar results from the different environments are compatible; explaining discrepancies between the results of the laboratory and the field environments; the spatial and temporal co-variation of the saltation system; and relating the experimental results obtained in this study to existing work.

(6.1.) DOWNWIND SPATIAL AND TEMPORAL DEVELOPMENTS OF THE SALTATION SYSTEM FROM A DESIGNATED POINT OF INITIATION.

The downwind spatial and temporal development of the saltation system was considered, from a point of initiation, in both the wind tunnel (experiments without upwind sand-feed (see Fig. 4.25.)) and the field (10m experiment (see Fig. 5.19.)). Use of the same horizontal dimension (approximately 10m) potentially maximised the compatibility of the data generated in the different environments (see Ch. 1.3.). Temporally, data are reported over the period of one hour (see Tables. 4.1. and 5.1.).

(i) Spatial development of the saltation system.

The downwind spatial development of the saltation system is manifest in results from both the laboratory (see Fig. 4.15.) and the field (see Fig. 5.12.) by the overshoot in mass flux and shear velocity. An overshoot in shear velocity has not previously been identified in saltation studies. This has been due to the limited spatial deployment of velocity equipment or to the large length scales of study. An overshoot in shear velocity during saltation is consistent with the overshoot in surface shear stress experienced in the clean air boundary layer developments following a step change in surface roughness (Bradley, 1968, see Ch 3.1.(i)).

In both the wind tunnel (see Fig. 4.15.) and the field (see Fig. 5.12.) mass flux increases with distance downwind to a maximum at $X_{4.00m}$. (The overshoot in mass flux in the wind tunnel is reinforced by the behaviour of the exponent of the mass flux gradient (see Fig. 4.22.)). This is in remarkable agreement with exiting data of a comparable scale. For example, the results of Bagnold (1936, see Fig. 3.5.), Shao and Raupach (1992, see Fig. 3.6.) and Spies (1996, see Fig. 3.12.) all demonstrate an overshoot in mass flux between 3-6m downwind from the point of initiation of the saltation system.

In the wind tunnel (see Fig. 4.15.) and the field (see Fig. 5.12.) it is found that shear velocity overshoots between 2-4m downwind of the overshoot in mass flux, i.e. at $X_{6.15m}$ and $X_{8.00m}$, respectively. The overshoot in shear velocity downwind of the overshoot in mass flux is a spatial manifestation of the time lag of the saltation system. The time lag between the entrainment of grains and the deceleration of the wind by the grains in motion produces the overshoot in mass flux (Bagnold, 1941, see Ch. 3.1.(iv)). Similarly, the time lag between the maximum in sediment transport and the associated minima in near-surface velocities produces the overshoot in shear velocity downwind of the mass flux maxima.

The discrepancy in the location of the shear velocity overshoot between the results of the laboratory (see Fig. 4.15.) and the field (see Fig. 5.12.) experiments may be due to the marginally higher wind velocities experienced in the field $17<U_*<45 cm.sec^{-1}$ as compared to the wind tunnel $11<U_*<35 cm.sec^{-1}$. A further consideration, however, must be the environmental conditions of the wind tunnel.

(a) Developing wind tunnel boundary layer: fully developed atmospheric boundary layer.

In the field the saltation system and the internal boundary layer are initiated by, and developing within, a fully developed atmospheric boundary layer (see Ch. 2.1.). The unlimited vertical extent of the atmospheric boundary layer renders the development of the saltation cloud only a minor intrusion into the constant stress region of the boundary layer. Furthermore, at heights above the saltation cloud the development of the atmosphere with distance downwind merely reflects the merging of the internal and the original atmospheric boundary layer.

In the wind tunnel the saltation system and the internal boundary layer are initiated by, and developing within, a newly developing atmospheric boundary layer. The maximum depth of the atmospheric boundary layer (0.15m) is reached by 4m downwind (see Fig. 4.9.). Due to the inability to scale the saltation system to the simulated atmospheric environment sand is transported to a height of 0.10m (see Fig. 4.21.), throughout the constant stress region and intruding into the wake region of the atmospheric boundary layer (see Fig. 2.4.). The significant proportion of the boundary layer occupied by the saltation system means that the free-stream velocity has to be adjusted manually to maintain the original $U_{7.20m}^{0.15m}$ value.

The confined, newly-developing, wind tunnel boundary layer, saturated by the presence of the saltation system, is incompatible with a fully developed, naturally adjusting boundary layer, where the saltation system is only

influential in the lower regions. Both environments, however, are experiencing the effects of near-bed velocity deceleration due to the extraction of momentum by the grains in transport (see Ch. 3.2.(iii)). If the presence of saltation is of greater significance to the flow than the influence of the stage of development of the atmospheric boundary layer then the two boundary layers may be comparable.

In a wind tunnel the simultaneous development of a newly-developing boundary layer and a saltation system generates opposing developments of shear velocity. In a clean air boundary layer shearing stresses naturally decline with distance downwind as the height of the boundary layer increases (see Fig. 4.9.). During saltation shear velocity increases with distance downwind in response to mass flux (see Fig. 4.15.). In the wind tunnel experiments during saltation the mass flux overshoot occurs at $X_{4.00m}$, coincident with the maximum depth of the boundary layer. However, if the confined wind tunnel environment is forcing the behaviour of the saltation system then the overshoot in shear velocity would be expected to be before, or coincident with, the overshoot in mass flux.

The results from laboratory and field experiments in this research (see Figs. 4.15. and 5.12.) show that the overshoot in shear velocity occurs downwind of the overshoot in mass flux. It is suggested that in the early stages of development of the saltation system the internal momentum of the sand cloud dominates the external developments of the atmospheric boundary layer. The value of shear velocity is responding, therefore, predominantly to the development of the sand cloud. Even if the decrease in shear velocity associated with the increase in boundary layer depth does influence the development of mass flux with distance downwind, the result is merely a dampening of the mass flux overshoot.

In the simulations of the wind tunnel environment by the numerical model of Spies (1996) the saltation system is initiated by an above threshold,

logarithmic wind velocity profile, of the full vertical extent of the calculation space. With distance downwind the vertical distribution of velocity is recalculated from the momentum exchange between the grain cloud and the wind (Spies, 1996, p.34). In the simulation of the field environment it is appropriate for the model to calculate the initiation, and development, of the saltation system within a boundary layer of maximum vertical extent. In the wind tunnel, however, a developing boundary layer is experienced. The eventual maximum height of the boundary layer is controlled by the wind tunnel dimensions.

Despite the failure of the numerical model of Spies (1996) to include the development of the boundary layer height within the wind tunnel simulations, the spatial development of mass flux is unaffected. Both the actual physical wind tunnel experiments of Bagnold (1941, see Fig. 3.5.) and Shao and Raupach (1992, see Fig. 3.6.) and the numerical model simulations of these wind tunnel experiments produce similar results. The development of the boundary layer with distance downwind during sand transport thus appears to be a minor influence on the behaviour of the saltation system.

(b) Limited wind tunnel height: unlimited atmospheric boundary layer height.

The constraining influence of the wind tunnel height has been used to explain the behavioural differences in the development of the saltation system generated in different wind tunnels (Rasmussen & Mikkelsen, 1991; Shao & Raupach, 1992; Spies, 1996; Spies & McEwan, in press a). Simulation of various wind tunnel dimensions by the numerical model of Spies (1996; Spies & McEwan, in press a) has shown that in small wind tunnels, <0.60m, no overshoot in mass flux, in either time or space, is experienced (see Fig. 3.7.). The lack of overshoot in mass flux is due to the rapid momentum exchange between the atmosphere and the sediment in transport in confined environments (Spies, 1996).

Simulation by the numerical model of Spies (1996) of both the $U_* = 0.36\text{m.sec}^{-1}$ experiment of Bagnold (1936) in the 0.30m wind tunnel (see Fig. 3.5.(b(iii))) and the $U_* = 0.60\text{m.sec}^{-1}$ experiment of Shao and Raupach (1992) in the 0.90m wind tunnel (see Fig. 3.6.(d)) are used to illustrate the influence of wind tunnel height on the spatial development of the saltation system. In agreement with the original wind tunnel data of Bagnold (1936) and Shao and Raupach (1992), the numerical model simulations of Spies (1996) illustrates that the results from lower wind tunnels do not show an overshoot in mass flux. However, in contrast to the expectations of the numerical model of Spies (1996) the highest velocity experiment of Bagnold (1936, see Fig. 3.5.(c)) and the results of the wind tunnel experiments in this study do show an overshoot in mass flux.

Supported by existing data (Shao & Raupach, 1992, see Fig. 3.6.), it is suggested that wind tunnel height does not preclude the occurrence of an overshoot in mass flux, merely its location. In environments of large vertical extent the location and extent of the mass flux overshoot are velocity dependent. In environments of limited vertical extent, such as the Queen Mary and Westfield wind tunnel and the wind tunnel used by Bagnold (1936), the location of the mass flux overshoot is velocity independent (see Figs. 4.17. and 4.18.; and Bagnold, 1941, Ch. 3.1.(iii(a)) Fig. 3.5.).

In environments of limited vertical extent the location of the mass flux overshoot is potentially controlled, not by the internal momentum of the saltation system but, by the saturation of the constrained atmospheric boundary layer by the grains in motion. The dependence of the location of the mass flux overshoot on the vertical extent of the experimental environment limits the applicability of wind tunnel results without field validation. From the results of this study, the wind tunnel overshoot in mass flux at X_{400m} has been validated as a natural representation of the development of the saltation system by a similar recorded overshoot in mass flux in the field.

The mass flux overshoot in the Queen Mary and Westfield wind tunnel may be unaffected by the limited height of the experimental environment. The constrained atmospheric boundary layer may, however, explain the difference in the location of the shear velocity overshoot between the laboratory ($X_{6.15m}$) and the field ($X_{8.00m}$) data (see Figs. 4.15. and 5.12.). Employing the original argument of Spies (1996) for the non-occurrence of the mass flux overshoot in small wind tunnels a premature overshoot in shear velocity in the wind tunnel can be envisaged. This result may suggest that shear velocity is more sensitive to the vertical extent of the experimental environment than is mass flux.

(c) The attainment of equilibrium?

The overshoot of shear velocity, in both the wind tunnel (see Fig. 4.15.) and the field (see Fig. 5.12.) experiments occurs spatially too near the end of the experimental regions for a clear state of equilibrium to be identified. It can only be stated that following the overshoot of mass flux and shear velocity, both variables decline towards a presumed mutual equilibrium (Owen, 1964).

The failure to achieve equilibrium by 10m is not surprising. Jensen, in 1978, questioned the calculations of Bradley (1968, see Fig. 3.2.) and his proposed equilibrium by 10m. Indeed Jensen (1978) suggests that numerous oscillations of mass flux and shear velocity about the final equilibrium rate make the identification of the equilibrium state unlikely except over vast homogeneous surfaces. This suspicion is reinforced by the ambiguous trends of development of the field data collected over large horizontal distances (e.g. Gillette *et al.*, 1996, see Ch. 3.1.(iii(c))).

In this study, it is not possible to relate the laboratory and field results from experiments 10m in length (see Figs, 4.15. and 5.12.) to other data from significantly greater lengths. Over many scales of study an overshoot and decline in mass flux is recorded, e.g. Stout and Zobeck (1996, see Fig. 3.9.). The variability in the transport rate in the experiments of this study over only

10m, however, does highlight the caution required in interpretation of data extrapolated over large distances (Gares *et al.*, 1996).

(ii) Temporal development of the saltation system.

The power of the wind controls the potential maximum transport rate of the saltation system. Only during the existence of a transport-limited saltation system, however, is the potential transport rate of the wind achieved (Nickling & McKenna Neuman, 1995, see Ch. 3.2.(iii)). During conditions of a supply-limited system the actual transport rate is governed by the availability of transportable grains from the sand bed. In the experiments of this study, under both constant (wind tunnel experiments (see Figs. 4.23. and 4.24.)) and natural (field experiments (see Figs. 5.15. and 5.16.)) wind regimes the change from a transport-limited to a supply-limited system is evident.

(a) Flat: rippled bed.

In the field the experimental surface was already rippled (see Ch. 5.1.(ii(b))). In the wind tunnel all experiments were conducted from an initially flat sand bed (see Ch. 4.1.(ii)). The high availability of grains from a flat, non wind-worked surface (Rice *et al.*, 1995, see Ch. 3.2.(iii)) is evident in the wind tunnel results. The greatest mass flux is recorded in the first sampling period, $T_{5\,mins}$ (see Fig. 4.17.). The development of a wind-worked surface in the wind tunnel produces a decline in mass flux from $T_{5\,mins}$ to T_{10mins} (see Figs. 4.17., 4.18. and 4.24.). Following the development of ripples, both the laboratory and field sand beds are similar.

(b) Transport-limited: supply-limited systems.

The naturally fluctuating wind velocity of the field prohibits the direct comparison of temporal field (see Figs. 5.15. and 5.16.) and wind tunnel (Figs. 4.23. and 4.24.) velocity data. However, the development of mass flux between the wind tunnel and field can be compared as the saltation system changes

from a transport-limited to a supply-limited system (Nickling & McKenna Neuman, 1995, see Ch. 3.2.(iii)).

In the wind tunnel transport-limited conditions may be considered to be in existence during the first $T_{10\min s}$. In contrast to the field results, however, in the wind tunnel mass flux and shear velocity have an inverse relationship. This result may be explained by the extreme availability of grains from a flat sand bed (see Ch. 4.4.(ii)).

The depletion of the sand bed through time in both the wind tunnel and the field environments produces a supply-limited saltation system (see Fig. 4.24., $T_{10\min s}$-$T_{20\min s}$, and Fig. 5.16., $T_{20\min s}$-$T_{30\min s}$.). In a supply-limited system, for any particular shear velocity, the quasi-equilibrium mass flux declines as the grain-size distribution of the sand bed surface changes (see Fig. 4.24., $T_{50\min s}$). A similar result was recorded by Rasmussen and Mikkelsen (in press). Only the onset of higher velocity winds, able to destabilise the armoured surface, leads to a response in mass flux.

In the field a supply-limited system is identified by periods of relatively constant mass flux despite fluctuating values of shear velocity (see Fig. 5.16.). In the wind tunnel under constant wind velocities a supply-limited system is identified by the simultaneous development of mass flux and shear velocity. Any reductions in mass flux, due to the depletion of the sand bed, are reflected directly in the value of shear velocity. This is due to the rapid momentum exchange between the grains in motion and the atmospheric boundary layer (Spies, 1996; Spies & McEwan, in press a).

(c) Potential or actual equilibrium transport rate?

The numerical models of saltation simulate only transport-limited saltation systems. The inability to consider supply-limited saltation systems is due to their assumption of a single grain-size bed. Any wind capable of initiating sediment transport, therefore, is also above the ultimate threshold for the sand

bed. The potential transport rate of a wind is thus equivalent to the actual transport rate. In the laboratory and the field environments, despite multiple grain-sized sand beds, only a few researchers discriminate between transport-limited and supply-limited saltation systems (e.g. Nickling & McKenna Neuman, 1995; Rice *et al*, 1995; Martz & Li, 1997). Failure to recognise the importance of the development of the sand bed through time may explain some of the discrepancies that exist between predicted and actually measured rates of sediment transport.

Traditional mass transport equations are based on the data collected under conditions of equilibrium and in transport-limited situations. For the accurate prediction of mass flux in a supply-limited saltation system a relationship must be found between the spatially and temporally changing grain-size distribution of the sand bed and mass flux, under various wind velocities. With respect to the development of the sand bed it can be stated that through time the grain-size distribution of the bed changes as the most easily entrainable grains are removed. The precise change in the grain-size distribution of the sand bed (see Rice *et al.,* 1995; Martz & Li, 1997; Ch. 3.2.(iii)), and how this relates to mass flux, however, is unclear.

(6.2.) DOWNWIND SPATIAL AND TEMPORAL DEVELOPMENTS OF THE SALTATION SYSTEM WITHOUT A DESIGNATED POINT OF INITIATION.

The downwind spatial and temporal development of the saltation system was considered, without a point of initiation, in both the wind tunnel (experiments with upwind sand-feed (see Ch. 4.16.)) and the field (20m experiment (see Ch. 5.14.)). In the 20m field experiment (see Ch. 5.1(ii(b))) sand entering from upwind, over the slip-face, is analogous to the introduction of artificially fed sand into the beginning of the working section of the wind tunnel. Temporally, data are reported over periods of one hour (see Tables. 4.1. and 5.1.).

(i) Spatial development of the saltation system.

The introduction of sand from upwind in both the wind tunnel and field environments lessens the role of the direct aerodynamic initiation of the saltation system (see Ch. 2.2.(i)). The existence of high energy bombardment processes throughout the experimental area produces an accelerated development of the saltation system (see Ch. 2.2.(iii)). The downwind development of mass flux and shear velocity is dependent on the exact rate of sand entering from upwind.

(a) Extreme rates of sand entering from upwind.

In experiments where extreme rates of sand enter the developing saltation system from upwind the saturation capacity of the wind is rapidly exceeded. In the wind tunnel experiments of Butterfield (pers. comm., see Fig. 3.3.), and in the 20m field experiment (see Fig. 5.14.) reported here, the peak saturation of the saltation cloud is followed by the decline and eventual minimum in mass flux (see Fig. 3.3., $X_{3.00m}$; and Fig. 5.14., X_{1200m}). At greater distances downwind the saltation system recovers and mass flux develops as 'normal', i.e. as would be experienced from a saltation system without sand entering from upwind (see Ch. 5.2.(ii)).

In the wind tunnel the overloading of the saltation system by extreme rates of upwind sand-feed produces a continual decline in shear velocity with distance downwind (see Fig. 3.3.). The most rapid rate of decline in shear velocity is associated with the saturation of the saltation system. Following the recovery of the saltation system at downwind distances >3m the rate of decline in shear velocity lessens. By the end of the wind tunnel both mass flux and shear velocity may be assumed to be approaching a mutual equilibrium.

The greater experimental length of the field experiment (see Fig. 5.14.) permits the development of the saltation system, following its saturation by sand from upwind, to be more clearly witnessed. In the first 12m length of the

experiment shear velocity develops simultaneously with mass flux. Both variables experience a peak induced by saturation and then a decline. From X_{1200m} onwards the saltation system begins to develop as 'normal' (see Ch. 5.2.(ii)).

(b) Moderate rates of sand entering from upwind.

Moderate rates of sand entering from upwind, like the extreme rates of sand entering from upwind, still produce a saturation of the sand cloud (see Fig. 4.16.). With distance downwind, however, the additional upwind grains are gradually incorporated into the saltation cloud. Unlike the extreme rates of sand entering from upwind, therefore, no minimum in mass flux is experienced. Instead, mass flux and shear velocity decline continuously towards a sustained mutual equilibrium.

In the Queen Mary and Westfield wind tunnel experiments, although an attempt was made to introduce an approximately equilibrium rate of sand-feed, in reality the saltation system was overfed (see Ch. 4.1.(iii(b))). The introduction of moderate rates of sand-feed forces the first 4m of the saltation system into disequilibrium (see Figs. 4.16. and 4.19.). At downwind distances greater than $X_{5.15m}$ the saltation system is unaffected by the inclusion of upwind sand.

(c) Marginal rates of sand entering from upwind.

Rates of sand entering from upwind marginally above or below the final equilibrium transport rate of the saltation system produce an accelerated development of the sand cloud. In experiments by Bagnold (1936, see Fig. 3.5.(b)), the introduction of upwind sand generates an overshoot of mass flux prior to the attainment of equilibrium. The location of the mass flux overshoot is dependent on the rate of sand entering from upwind. Greater rates of sand entering from upwind produce a more rapid overshoot in mass flux.

(d) The attainment of equilibrium?

In the wind tunnel regardless of the rate of, or existence of, sand entering from upwind, the final rate of, and distance to, the equilibrium of the saltation system are unaffected (see Figs. 3.5.(b) and 4.16.). In the field fluctuating wind velocities and the different site locations for experiments with and without sand entering from upwind do not permit the effects of upwind sand on the final equilibrium transport rate to be determined. Following the saturation of the sand cloud in the field by sand entering from upwind, however, the saltation system recovers and begins to develop as 'normal' (see Fig. 5.14.). It may be expected, therefore, that the transport rate is again determined by the conditions of the wind and the state of the sand bed and not the addition of upwind sand.

(ii) Temporal development of the saltation system.

The temporal development of the saltation system without a point of initiation, in both the wind tunnel and the field (see Figs. 4.19. and 5.18.), displays greater temporal consistency than the development of the saltation system with a point of initiation (see Figs. 4.17. and 5.16.). Greater temporal consistency in experiments without a point of initiation is a reflection of the higher energy bombardment processes experienced throughout the experimental area.

In the wind tunnel experiments with upwind sand-feed, mass flux declines at all sites through time (see Fig. 4.19.). The rate of decline in mass flux is less severe and more consistent at all downwind sites, than in experiments without upwind sand-feed (see Fig. 4.17.). In the 20m field experiment, despite the persistence of a transport-limited saltation system throughout the experimental period, i.e. the simultaneous development of mass flux, shear velocity and wind velocity, the evolution of the sand bed is still evident (see Fig. 5.18.). For any particular wind velocity the sustainable rate of sediment transport declines through time.

In both the wind tunnel and the field environments an input of sand from upwind reduces the influence of the sand bed armouring and thus the rate of decline in mass flux. Although the higher energy of the particles entering from upwind delays the development of the saltation system from a transport-limited to a supply-limited system, eventually the armouring of the sand bed becomes influential. Only winds consistently above the ultimate threshold of the whole of the bed sediment are able to maintain, indefinitely, a transport-limited system.

(6.3.) CO-VARIATION OF THE SPATIAL AND TEMPORAL DEVELOPMENTS OF THE SALTATION SYSTEM.

In both the wind tunnel and the field the downwind spatial and temporal development of the saltation system is similar (see Figs. 4.25. and 5.19.). In both environments, in space and through time, mass flux and shear velocity increase to a peak prior to declining towards an assumed quasi-equilibrium transport rate (see Figs. 4.15. and 5.13.). Temporally the overshoots in mass flux and shear velocity are caused by the time lag between the entrainment of grains and the deceleration of the wind (Bagnold, 1941, see Ch. 3.1.(iv)); the spatial lag between the overshoot in mass flux and shear velocity is also attributed to this cause.

In the constant velocity environment of the wind tunnel, the depletion of the sand bed is reflected, not only in the final equilibrium transport rate, but also in the spatial development of mass flux. For the lower velocity wind tunnel experiments, the depletion of the sand bed through time in the initial 2-3m produces a temporal decrease in mass flux and a spatial relocation of the mass flux overshoot (see Fig. 4.17.). The development of mass flux, therefore, is temporally site-dependent and spatially time-dependent.

For the wind tunnel experiments conducted at higher velocities (see Fig. 4.18.) and for the fluctuating winds of the field experiment (see Fig. 5.12.), the ability of the wind to entrain a larger population of grain-sizes reduces the significance of the armouring of the sand bed. As a result there is no downwind relocation in the mass flux overshoot during the experimental period.

The influence of the development of the sand bed through time and space, in both the wind tunnel and field environments, during transport-limited and supply-limited conditions, reinforces the need for future numerical model simulations of the saltation system to incorporate a non-stationary 'splash function' (Ungar & Haff, 1987, see Ch. 2.2.(iii)). Simulating the natural environment rather than generating unrealistic experimental environments must be the main objective of all future investigations. Only by adopting such ideals in the field, laboratory and numerical model investigations will a complete understanding of the saltation system be obtained. Furthermore, by applying the same data collection requirements to all environments the compatibility of data will be maximised.

(6.4.) SUMMARY.

A summary of the main conclusions from the laboratory and field experiments are considered with reference to the original aims of the study (see Ch. 1.3.). In addition, the main practical importance of this work is emphasised.

(i) Regulation of the sand transport system.

Investigation of how the sand transport system by air flow is regulated, in space and through time, has highlighted the need to distinguish between transport-limited and supply-limited saltation systems. In all sediment

transport systems, mass flux is regulated by the mutual interactions between the evolving states of the sand cloud, the boundary layer air flow and the state of the sand bed (see Ch. 2.2.(iii)). The relative importance of these factors, however, varies.

- Mass flux in a transport-limited saltation system is regulated by the interaction of the developing sand cloud and boundary layer air flow (see Ch. 2.2.(iii)). The development of the sand bed through time and space is only a secondary influence on the transport rate, the potential transport rate of the wind being fulfilled by the availability of entrainable grains from the sand bed (see Ch. 3.1.(iv)).

- In a supply-limited saltation system the actual mass flux is less than the potential sediment transport rate of the wind (see Ch. 3.2.(iii)). The actual mass flux is determined by the changing availability of grains from the sand bed. Although the air flow is still decelerated by the sediment in transport this interaction no longer regulates the saltation system.

(ii) Compatible spatial and temporal scales of study.

By conducting field and laboratory work on compatible spatial and temporal scales it has been possible to directly compare laboratory and field data (see Ch. 1.3.). The development of the saltation system under different environmental conditions has identified both the success of the wind tunnel in permitting the reproduction of the saltation system under controlled environmental conditions and the caution required in the interpretation of data generated in constrained environments.

- The boundary layer developments within the wind tunnel environment have been found to be an insignificant influence on the behaviour of the saltation system (see Ch. 6.1.(a)). In both the field and wind tunnel

environments mass flux overshoots at 4m downwind, prior to the overshoot in shear velocity (see Figs. 4.15. and 5.12.). Temporally, in both environments the saltation system experiences the change from a transport-limited to a supply-limited saltation system (see Figs. 4.24. and 5.16.).

- The vertical extent of a wind tunnel is the main limitation on the experimental environment (see Ch. 6.1.(b)). In wind tunnels of limited height the downwind location of the mass flux and shear velocity overshoots are potentially controlled, not by the self-regulation of the saltation system, but by the saturation of the boundary layer by sediment in transport. Calibration of the wind tunnel environment by comparable field experiments is required before data from confined environmental conditions can be accepted.

(iii) Testing of numerical models.

The two-dimensional numerical model of Spies (1996; Spies & McEwan, in press b) simulates the simultaneous development of the saltation system in space and through time. The numerical model has highlighted how discrepancies in the interpretation of data collected in a single domain (either space or time) can differ from that collected in two dimensions simultaneously (space and time).

- The data of this study can potentially be used to calibrate the numerical model of Spies (1996).

(iv) Practical applicability.

The existence of a 'separation distance' between the overshoots of mass flux and shear velocity questions the appropriateness of traditional mass flux formulae.

- It is found that conventional mass flux relationships with shear velocity, generated from data collected simultaneously at the same site, have the lowest predictive capability (see Tables. 5.2., 5.3., and 5.4.).

- The greatest confidence in the ability of shear velocity to predict mass flux is shown to occur when the shear velocity data are collected downwind of the mass flux data. The critical distance between the data collection points is demonstrated to be defined by the 'separation distance'.

- In experiments where no clear point of initiation exists or where the environment can not be calibrated sufficiently to identify the 'separation distance', it has been shown that greater statistical confidence in the prediction of mass flux from shear velocity is achieved by use of a spatial average of mass flux (and point shear velocity data), rather than the misapplication of point mass flux data (see Tables. 5.2., 5.3. and 5.4.).

(6.5.) FUTURE WORK.

- In the Queen Mary and Westfield wind tunnel although the limited height of the wind tunnel does not influence the location of the mass flux overshoot (see Figs. 4.15. and 5.12.), it does effect the location of the overshoot in shear velocity (see Ch. 6.1.(b)). Future experiments should investigate the exact influence of wind tunnel height on the velocity dependence/independence of the location of the mass flux and shear

velocity overshoots, and the suspicion that shear velocity is more sensitive to the vertical extent of the experimental environment than mass flux.

- In this study the 'separation distance' for the best predictive relationship of mass flux from shear velocity was identified as 4m (see Figs. 4.15. and 5.12.). Future studies should investigate the suspected velocity dependence of the 'separation distance'. Similarly, in circumstances where the 'separation distance' can not be defined, it would be beneficial for future experiments to attempt to quantify the volume of data required to maximise the spatially averaged mass flux:shear velocity relationship (see Tables 5.2., 5.3. and 5.4.).

- No attempt has been made to quantitatively improve the exiting mass transport formulae, however, existing relationships between shear velocity and mass flux should be applied within the context of the findings of this work. For the future prediction of the rate of mass flux under supply-limited transport conditions a new generation of mass flux formulae must be developed. The interaction between the changing state of the sand bed and the rate of mass flux under various wind regimes must be understood.

- The main conclusion to arise from the comparison of the physically collected laboratory and field results, and the results of the numerical models is the importance of the sand bed. For a more correct understanding of the development of the saltation system the numerical models must incorporate the full bed response, both spatial and temporal, of a mixed grain-sized sand bed. To date this must be one of the most pressing requirements for future investigations.

(6.6.) CONCLUSION.

Despite differences in the environmental parameters of the wind tunnel and field experiments, data from the two environments can cautiously be compared. Spatially the saltation system has been shown to develop with an overshoot in both mass flux and shear velocity in both the wind tunnel and field environments. Temporally, the saltation system has been shown to develop from a transport-limited to a supply-limited state as the sand bed develops (see Figs. 4.24. and 5.16.).

The development of the sand bed has further highlighted the inadequacy of current sediment transport equations. More importantly, the transient nature of the sand bed, and hence mass flux, renders the concept of a time and space independent state of equilibrium inappropriate for the universal applicability of sediment transport formulae.

REFERENCES

Al-Awadhi J.M. and Willetts, B.B. (1998) Transient sand transport rates after wind tunnel start-up. *Earth Surface Processes and Landforms*, 22:21-30.

Abdullah, J.M.A. (1996) Sand transport and deposition over non erodible elements. Thesis for Doctor of Philosophy, Department of Engineering, Aberdeen University 133pp.

Al-Sudairawi, M. (1992) The effect of non erodible elements on sand transport rate. Thesis for Doctor of Philosophy, Department of Engineering, Aberdeen University 253pp.

Anderson, R.S. and Haff, P.K. (1988) Simulation of aeolian saltation. *Science*, 241:820-823.

Anderson, R.S. and Haff, P.K. (1991) Wind modification and bed response during saltation of sand in air. In Barndorff-Neilsen, O.E. and Willetts, B.B. (eds.) Aeolian Grain Transport 1, *Acta Mechanica*, **Suppl.**1:21-51. (Springer-Verlag, Wein New York).

Antonia, R.A. and Luxton, R.E. (1971) The response of a turbulent boundary layer to a step change in surface roughness. Part 1, Smooth to rough. *Journal of Fluid Mechanics*, **48**(4):721-761.

Arens, S.M., Van Kaam-Peters, H.M.E. and Van Boxel, J.H. (1995) Air flow over foredunes and implications for sand transport. *Earth Surface Processes and Landforms*, 20:315-332.

Bagnold, R.A. (1935) The movement of desert sand. *Geographical Journal*, 85: 342-369.

Bagnold, R.A. (1936) The movement of desert sand. *Proceedings of the Royal Society (A)*, **157**:594-620.

Bagnold, R.A. (1937) The transport of sand by wind. *Geographical Journal,* 89:409-438.

Bagnold, R.A. (1941) *The Physics of Wind Blown Sand and Desert Dunes.* (Methuen & Co. Ltd, London) 265pp.

Bagnold, R.A. (1954) The surface movement of blown sand in relation to meteorology. *Desert Research, Proceedings of the International symposium of Jerusalem, Research Council of Israel.* p.89-93.

Bagnold, R.A. (1956) Flow of cohesionless grains. *Royal Society London Philosophical Transaction (A),* 249:235-297.

Bagnold, R.A. (1973) The nature of saltation and the bed load transport in water movement of desert sand. *Proceedings of the Royal Society (A),* 332:473-504.

Barker, G. and Grimson, M. (1990) The physics of muesli. *New Scientist,* May 26:37-40.

Bauer, B.O., Sherman, D.J., Nordstrom, K.F. and Gares, P.A. (1990) Aeolian transport measurement and prediction across a beach and dune at Castroville, California. In *Coastal Dunes Form and Process.* Ed. Nordstrom, K.F., Psuty, N.P. and Carter, R.W.G. (John Wiley & Sons Ltd) p39-55.

Bauer, B.O., Sherman, D.J. and Wolcott, J.F. (1992) Sources of uncertainty in shear stress and roughness length estimates derived from velocity profiles. *Professional Geographer,* 44(4):453-464.

Bauer, B.O. & Namikas, S.L. (in press) Design and field test of a continuously-weighing, tipping-bucket assembly for aeolian sand traps. *Earth Surface Processes and Landforms, Technical and Software Bulletin,* 23.

Begin, C., Michaud, Y. and Filion, L. (1995) Dynamics of a Holocene cliff-top dune along Mountain River, Northwest Territories, Canada. *Quaternary Research,* 44:392-404.

Bennett, S.J. and Best, J.L. (1995) Mean flow and turbulence structure over fixed, two dimensional dunes: implications for sediment transport and bedform stability. *Sedimentology*, 42:491-513.

Bennett, S.J. and Bridge, J.S. (1995) An experimental study of flow, bedload transport and bed topography under conditions of erosion and deposition and comparison with theoretical models. *Sedimentology,* 42:117-146.

Bisal, F. and Hsieh, J. (1966) Influence of soil moisture on the erodibility of soil by wind. *Soil Science,* 102:143-146.

Blom, J. and Wartena, L. (1969) The influence of changes in surface roughness on the development of the turbulent boundary layer in the lower layers of the atmosphere. *Journal of Atmospheric Sciences,* 26:255-265.

Bradley, E.F. (1968) A micrometeorological study of velocity profiles and surface drag in the region modified by a step change in roughness. *Quarterly Journal of the Royal Meteorological Society,* 94:361-379.

Butterfield, G.R. (1991) Grain transport rates in steady and unsteady turbulent airflows. In Barndorff-Neilsen, O.E. and Willetts, B.B. (eds.) Aeolian Grain Transport 1, *Acta Mechanica,* **Suppl.** 1:97-122. (Springer-Verlag, Wein New York).

Butterfield, G.R. (1993) Sand transport response to fluctuating wind velocity. In Clifford, N.J., French, J.R. and Hardisty, J. (eds.), *Turbulence: Perspectives on flow and sediment transport,* (John Wiley & Sons Ltd) p.305-335.

Buttefield, G.R. (in press) Transitional behaviour of saltation: wind tunnel observations of unsteady winds. *Journal of Arid Environments.*

Cahill, T.A., Gill, T.E., Reid, J.S., Gearhart, E.A. and Gillette, D.A. (1996) Saltating particles, playa crusts and dust aerosols at Owens (dry) lake, California. *Earth Surface Processes and Landforms,* 21:621-639.

Chamberlain, A.C. (1983) Roughness length of sea, sand and snow. *Boundary Layer Meteorology,* 25:405-409.

Charnock, H. (1955) Wind stress on water surfaces. *Quarterly Journal of the Royal Meteorological Society,* 81:631-640.

Chepil, W.S. (1946) Dynamics of wind erosion V: Cumulative intensity of soil drifting across eroding fields. *Soil Science,* 60:257-263.

Chepil, W.S. (1957) Width of field strips to control wind erosion. *Kansas State Agricultural Experiments Station Technical Bulletin* 92.

Chepil, W.S. (1965) Transport of soil and snow by wind. *Meteorological Monographs,* 6(28):123-132.

Clark, A.N. (1985) Dictionary of Geography. Longman.

Coleman, N.L. (1981) Velocity profile with suspended sediment. *Journal of Hydraulic Research,* 19(3):211-229.

Coles, D. (1956) The law of the wake in the turbulent boundary layer. *Journal of Fluid Mechanics,* 1:191-226.

Damnati, B., Petit-Marie, N., Fontugne, M., Meco, J. and Williamson, D. (1996) Quaternary palaeoclimates in the Eastern Canary Islands. *Quaternary International,* 31:37-46.

Dery, S.J. and Taylor, P.A. (1996) Some aspects of the interaction of blowing snow with the atmospheric boundary layer. *Hydrological Processes,* 10:1345-1358.

Dungan Smith, J. and McLean, S.R. (1977) Spatially averaged flow over a wavy surface. *Journal of Geophysical Research,* 82(12):1735-1746.

Frank, A. and Kocurek, G. (1994) Effects of atmospheric conditions on wind profile and aeolian sand transport with an example from White Sands National Monument. *Earth Surface Processes and Landforms,* 19:735-745.

Fryrear, D.W., Stout, J.E., Hagen, L.J. and Vories, E.D. (1991) Wind erosion: Field measurement and analysis. *Transactions of the ASAE.* 34(1):155-160.

Gares, P.A., Davidson-Arnott, R.G.D., Bauer, B.O., Sherman, D.J., Carter, R.W.G., Jackson, D.W.T. and Nordstrom, K.F. (1996) Alongshore variations in aeolian sediment transport: Carrick Finn Strand, Ireland. *Journal of Coastal Research,* 12(3):673-682.

Garratt, J.R. (1990) The internal boundary layer - a review. *Boundary Layer Meteorology,* 50:171-203.

Garratt, J.R. (1992) *The Atmospheric Boundary Layer.* (Cambridge University Press), Houghton, J.T., Rycroft, M.J. and Dessier, A.J. (eds.) pp316.

Gerety, K.M. (1985) Problems with determination of U* from wind-velocity profiles measured in experiments with saltation. In *Proceedings of the International Workshop on the Physics of Blown Sand, Aarhus,* memoirs No.8(2):271-300.

Gillette, D.A., Herbert, G., Stockton, P.H. and Owen, P.R. (1996) Causes of the fetch effect in wind erosion. *Earth Surface Processes and Landforms,* 21:641-659.

Grass, A.J. (1970) Initial instability of fine bed sand, *Journal of the Hydraulic Division. Proceedings of the American Society of Civil Engineers,* 96(HY3):619-32.

Greeley, R. (1986) Aeolian landforms: laboratory simulations and field studies. In Nickling, W.G. (eds.) *Aeolian Geomorphology.* The Binghampton Symposia in Geomorphology: International Series, no.17, p195-211, (Allen and Unwin).

Glennie, K.W. (1998) *Lower Permian Rotliegend.* In: *Petroleum Geology of the North Sea. Basic Concepts and Recent Advances,* 4th editions (Ed. K.W. Glennie), Blackwell, p137-173.

Greeley, R. and Blumberg, D.G. (1995) Preliminary analysis of Shuttle Radar Laboratory (SRL-1) data to study aeolian features and processes. *IEEE Transactions on Geoscience and Remote Sensing,* 33(4):927-933.

Greeley, R., Blumberg, D.G. and Williams, S.H. (1996) Field measurements of the flux and speed of wind blown sand. *Sedimentology,* 43:41-52.

Greeley, R. and Iversen, J.D. (1985) *Wind as a Geological Process.* (Cambridge University Press, Cambridge) 333pp.

Greeley, R., Leach, R., White, B., Iversen, J. and Pollack. J. (1980) Threshold wind speeds for sand on Mars: Wind tunnel simulations. *Geophysical Research Letters,* 7(2):121-124.

Greeley, R., Skypeck, A. and Pollack, J.B. (1993) Martian aeolian features and deposits - comparisons with general circulation model results. *Journal of Geophysical Research - Planets,* 98(E2):3183-3196.

Greeley, R., Williams, S.H. and Marshall, J.R. (1983) Velocities of wind blown particles in saltation preliminary laboratory and field experiments. In Brookfield, M.E., and Ahlbrandt, T.S. (eds.) Aeolian Sediments and Processes, Developments in Sedimentology, 38:133-148. (Amsterdam, Elsiever).

Haff, P.K. and Anderson, R.S. (1993) Grain scale simulations of loose sedimentary beds: Example of grain bed impacts in aeolian saltation. *Sedimentology,* 40:175-198.

Hayashi, Y. (1984) Direct measurement of friction velocity using a drag plate in a wind tunnel. Annual Report of the Institute of Geological Sciences, University of Tsukaba, 10:44-48.

Hicks, B.B. (1972) Some evaluations of drag and bulk transfer coefficients over water bodies of different sizes. *Boundary layer Meteorology,* 3:201-213.

Horikawa, K. and Shen, H.W. (1960) Sand movement by wind action (on the characteristics of sand traps). U.S. Army Corps of Engineers, Beach Erosion Board Technical Memo 119:1-51.

Hsu, S.A. (1971a) Measurement of shear stress and roughness length on a beach. *Journal of Geophysical Research,* 76(12):2880-2885.

Hsu, S.A. (1971b) Wind stress criteria in Eolian sand transport. *Journal of Geophysical Research,* 76(12):8684-8686.

Jackson, D.W.T. (1996a) Potential inertial effects in aeolian sand transport:preliminary results. *Sedimentary Geology,* 106:193-201.

Jackson, D.W.T. (1996b) A new, instantaneous aeolian sand trap design for field use. *Sedimentology,* 43:791-796.

Jackson, D.W.T. and McCloskey, J. (1997) Preliminary results from a field investigation of aeolian sand transport using high resolution wind and transport measurements. *Geophysical Research Letters,* 24(2):163-166.

Jackson, N.A. (1976) The propagation of modified flow downstream of a change in roughness. *Quarterly Journal of the Royal Meteorological Society,* 102:924-933.

Jackson, P.S. (1981) On the displacement height in the logarithmic profile. *Journal of Fluid Mechanics,* 111:15-25.

Janin, F. and Cermak, J.E. (1988) Sediment laden wind profiles developed in a long boundary layer wind tunnel. *Journal of Wind Engineering and Industrial Aerodynamics,* 28:159-68.

Jensen, N.O. (1978) Change in surface roughness and the planetary boundary layer. *Quarterly Journal of the Royal Meteorological Society,* 104:51-356.

Jensen, N.O. and Zeman, O. (1985) Perturbations to mean wind and turbulence in flow over topographic forms. *Proceedings of the International Workshop of the Physics of Blown Sand, Aarhus.* memoirs No.8(2):328-351.

Jones, J.R. and Willetts, B.B. (1979) Errors in measuring uniform aeolian sand flow by means of an adjustable trap. *Sedimentology,* 26:463-468.

Kawamura, R. (1951) Study of sand movement by wind. *Report of the Institute of Science and Technology, University of Tokyo* vol5, no.3/4, 215pp.

Kline, S.R., Reynolds, W.C., Schraub, F.A. and Runstadler, P.W. (1967) The structure of turbulent boundary layers. *Journal of Fluid Mechanics,* 30:741-773.

Lancaster, N. and Nickling, W.G. (1994) *Aeolian Sediment Transport.* In Abrahams, A.D., & Parsons, A.J. (eds.), *Geomorphology of Desert Environments.* (Chapman & Hall, London), p.445-473.

Leys, J.F. and McTainsh, G.H. (1996) Sediment fluxes and particle grain size characteristics of wind eroded sediments in South Eastern Australia. *Earth Surface Processes and Landforms,* 21:661-671.

Li, L. and Martz. L.W. (1995) Aerodynamic dislodgement of multiple-size sand grains over time. *Sedimentology,* 42:683-694.

Lyles, L. and Krauss, R. K. (1971) Threshold velocity and initial particle motion as influenced by air turbulence. *Transactions of the American Society of Agricultural Engineers,* 14:563-566.

Madole, R.F. (1995) Spatial and temporal patterns of late quaternary aeolian deposition, Eastern Colorado, U.S.A. *Quaternary Science Reviews,* 14:155-177.

Martz, L.W. and Li, L. (1997) Grain size analysis of surface material under wind erosion using the effective surface concept. *Earth Surface Processes and Landforms,* 22:19-29.

McEwan, I. K. (1991) The Physics of Sand Transport by Wind. Thesis for Doctor of Philosophy, Department of Engineering, Aberdeen University, 121pp.

McEwan, I.K. (1993) Bagnold's Kink: A Physical feature of a wind velocity profile modified by blown sand? *Earth Surface Processes and Landforms,* 18:145-156.

McEwan, I.K. and Willetts, B.B. (1991) Numerical model of the saltation cloud. In Barndorff-Neilsen, O.E., & Willetts, B.B. (eds.), Aeolian Grain Transport 1, *Acta Mechanica,* **Suppl.1**:53-66. (Springer-Verlag, Wein New York).

McEwan, I.K. and Willetts, B.B. (1993a) Adaptation of the near-surface wind to the development of sand transport. *Journal Fluid Mechanics,* 252:99-115.

McEwan, I.K. and Willetts, B.B. (1993b) Sand transport by wind: a review of the current conceptual model. In Pye (ed.) Geological Society Special Publication. *The Dynamics and Environmental Context of Aeolian Sedimentary Systems,* p.7-16.

McEwan, I.K. and Willetts, B.B. (1994) On the prediction of bed-load sand transport rate in air. *Sedimentology*, 41:1241-1251.

McKenna Neuman, C. & Maljaars, M. (1997) Wind tunnel measurement of boundary-layer response to sediment transport. *Boundary Layer Meteorology,* 84:67-83.

McLean, S.R. and Dungan Smith, J. (1986) A model for flow over two-dimensional bed forms. *Journal of Hydrological Engineering,* 112:300-317.

Meco, J. and Petit-Marie, N. (1995) Climates of the past. *Proceedings of the CLIP meeting, June 2-7, Lanzarote and Fuerteventura (Canary Islands, Spain), International Union of Geological Sciences - UNESCO.*

Miller, M.C., McCave, I.N. and Komar, P.D. (1977) Threshold of sediment motion in unidirectional currents. *Sedimentology*, 24:504-27.

Mitha, S., Tran, M.Q., Werner, B.T. and Haff, P.K. (1986) The grain-bed impact process in aeolian saltation. *Acta Mechanica,* 63:267-278.

Mulligan, K.R. (1988) Velocity profiles measured on the windward slope of a transverse dune. *Earth Surface Processes and Landforms,* 13:573-582.

Munn, R.E., (1966) *Descriptive Micrometeorology,* (Academic Press, New York and London), 245pp.

Nalpanis, P., Hunt, J.C.R. and Barratt, C.F. (1993) Saltating particles over flat beds. *Journal of Fluid Mechanics,* 251:661-685.

Namikas, S.L. & Sherman, D.J. (1995) A review of the effects of surface moisture content on aeolian sand transport. In Tchakerian, V.P. (eds.) *Desert Aeolian Processes,* p269-293, (Chapman and Hall).

Nickling, W.G. (1984) The stabilising role of bonding agents on the entrainment of sediment by wind. *Sedimentology,* 31:111-117.

Nickling, W.G. (1988) The initiation of particle movement by wind. *Sedimentology,* 35:499-511.

Nickling, W.G. and McKenna Neuman, C. (1995) Development of deflation lag surfaces. *Sedimentology,* 42:403-414.

Nickling, W.G. and McKenna Neuman, C. (1997) Wind tunnel evaluation of a wedge shaped aeolian sediment trap. *Geomorphology,* 18:333-345.

O'Brien, M.P. and Rindlaub, B.D. (1936) The transport of sand by wind. *Civil Engineering,* 6:325-327.

Oke, T.R. (1978) *Boundary Layer Climates,* (Methuen & Co. Ltd), 416pp.

Owen, P.R. (1964) Saltation of uniform grains in air. *Journal of Fluid Mechanics,* 20(2):225-242.

Owen, P. and Gillette, D. (1985) Wind tunnel constraint on Saltation. *Proceedings of the International Workshop on the Physics of Blown Sand, Aarhus,* memoirs No.8(2):253-270.

Panofsky, H.A. and Townsend, A.A. (1964) Change of terrain roughness and the wind profile. *Quarterly Journal of the Royal Meteorological Society,* 90:147-155.

Pearce, F. (1992) Mirage of the shifting sands. *New Scientist,* 136(12 Dec):38-42.

Pomeroy, J.W., Gray, D.M. and Landine, P.G. (1993) The Prairie blowing snow model:characteristics, validation, operation. *Journal of Hydrology,* 144:165-192.

Pye, K. (1987) *Aeolian Dust and Dust Deposits* (Academic Press, Harcourt Bruce Jovanovich) 334pp.

Pye, K. (1994) *Sediment Transport and Depositional Processes.* (Blackwell Scientific), 397pp.

Rasmussen, K.R. (1989) Some aspects of flow over coastal dunes. *Proceedings of the Royal Society of Edinburgh,* 96B:129-149.

Rasmussen, K.R. and Mikkelsen, H.E. (1991) Wind tunnel observations of aeolian transport rates. In Barndorff-Neilsen, O.E. and Willetts, B.B. (eds.), Aeolian Grain Transport 1, Mechanics, *Acta Mechanica,* **Suppl.1**:135-144. (Springer-Verlag, Wein New York).

Rasmussen, K.R. and Mikkelsen, H.E. (in press) Efficiency of sand Traps. *Sedimentology.*

Rasmussen, K.R., Sørensen, M. and Willetts, B.B. (1985) Measurement of saltation and wind strength on beaches. *Proceedings of the International Workshop on the Physics of Blown Sand, Aarhus,* memoirs No.8(2):301-326.

Raupach, M.R. (1991) Saltation layers, vegetation canopies and roughness lengths. In Barndorff-Neilsen, O.E. and Willetts, B.B. (eds.), Aeolian Grain Transport 1, *Acta Mechanica,* **Suppl.1**:83-96. (Springer-Verlag, Wein New York).

Rice, M.A. (1991) Grain shape effects on aeolian sediment transport. In Barndorff-Neilsen, O.E. and Willetts, B.B. (eds.), Aeolian Grain Transport 1, *Acta Mechanica,* **Suppl.1**:159-166. (Springer-Verlag, Wein New York).

Rice, M.A., Willetts, B.B. and McEwan, I.K. (1995) An experimental study of multiple grain size ejecta produced by collisions of saltating grains with a flat bed. *Sedimentology,* 42:695-706.

Rice, M.A., Willetts, B.B. and McEwan, I.K. (1996) Observations of collision of saltating grains with a granular bed form high-speed cine-film. *Sedimentology,* 43:21-31.

Rodriguez Rodriguez, A., Gonzalez Soto, M.C., Hernandez Hernandez, L.A., Jimenez Mendoza, C.C., Ortega Gonzalez, M.J., Padron Padron, P.A., Torres Cabrera, J.M. and Vargas Chavez, G.E. (1993) Assessment of soil degradation in the Canary Islands (Spain). *Land Degradation and Rehabilitation,* 4:11-20.

Rumpel, D.A. (1985) Successive aeolian saltation: studies of idealised collisions. *Sedimentology,* 32:267-280.

Sarre, R.D. (1987) Aeolian sand transport. *Progress in Physical Geography;* 11:157-182.

Sarre, R.D. (1988) Evaluation of aeolian sand transport equations using intertidal zone measurements, Saunton Sands, England. *Sedimentology,* 35:671-679.

Schlichting, H. (1968) *Boundary Layer Theory.* (McGraw-Hill), 748pp.

Shao, Y. and Raupach, M.R. (1992) The overshoot and equilibrium of saltation. *Journal of Geophysical Research,* 97(D18):20559-20564.

Shao, Y., McTainsh, G.H., Leys, J.F. and Raupach, M.R. (1993) Efficiencies of sediment samplers for wind erosion measurements. *Soil and Water Management and Conservation, Australian Journal of Soil Research,* 37:519-531.

Sharp, R.P. (1963) Wind ripples. *Journal of Geology,* 71:617-36.

Shaw, E.R, (1988) *Hydrology in Practice.* (Chapman and Hall), 539pp.

Sherman, D.J. (1992) An equilibrium relationship for shear velocity and apparent roughness length in aeolian saltation. *Geomorphology,* 5:419-431.

Sørensen, M. (1991) An analytic model of wind-blown sand transport. In Barndorff-Neilsen, O.E. and Willetts, B.B. (eds.), Aeolian Grain Transport 1, *Acta Mechanica,* **Suppl.1**:67-81. (Springer-Verlag, Wein New York).

Sørensen, M. and McEwan, I. (1996) On the effect of mid-air collisions on aeolian saltation. *Sedimentology,* 43:65-76.

Spies, P.J. (1996) The Transport of sand in unsteady Winds. Thesis for Doctor of Philosophy, Department of Engineering, Aberdeen University, 93pp.

Spies, P.J., McEwan, I.K. and Butterfield, G.R. (1995) On wind velocity profile measurements taken in wind tunnels with saltating grains. *Sedimentology,* 42:515-521.

Spies, P.J. & McEwan, I.K. (in press a) One-dimensional transitional behaviour in saltation. *Sedimentology.*

Spies, P.J. & McEwan, I.K. (in press b) Equilibration of saltation. *Sedimentology.*

Steers, J.A. (1937) The Culbin Sands and Burhead Bay. *Geographical Journal,* 90:498-523.

Steers, J.A. (1959) Archaeology and physiography in coastal studies. *Second Coastal Geography Conference, Louisiana,* p.317-340.

Sterk, G. and Stein, A. (1997) Mapping wind blown mass transport by modelling variability in space and time. *Soil Science Society of America Journal,* 61:232-239.

Stetler, L.D. and Saxton, K.E. (1996) Erosion and PM_{10} emissions from agricultural fields on the Columbia plateau. *Earth Surface Processes and Landforms,* 21:673-685.

Stout, J.E. (1990) Wind erosion in a simple field. *Transactions of the ASAE.* 33(5):1597-1600.

Stout, J.E. and Zobeck, T.M. (1996) The Wolfforth field experiment: A wind erosion study. *Soil Science,* 161(9):616-632.

Takeuchi, M. (1980) Vertical profile and horizontal increase of drift-snow transport. *Journal of Glaciology,* 26(94):481-492.

Tennekes, H. & Lumley, J.L. (1972) *A First Course in Turbulence.* (MIT Press), 300pp.

Tritton, D.J. (1988) *Physical Fluid Dynamics.* (Clarendon Press Oxford) (2nd Edition), 430pp.

Ungar, J.E. and Haff, P.K. (1987) Steady state saltation in air. *Sedimentology,* 34:289-299.

Watson, A. (1985) The control of wind blown sand and moving dunes: a review of the methods of sand control in deserts, with observations from Saudi Arabia. *Quarterly Journal of Engineering Geology of London,* 18:237-252.

Werner, B.T. and Haff, P.K. (1988) The impact process in aeolian saltation: two-dimensional simulations. *Sedimentology,* 35:189-196.

Werner, B.T. (1990) A steady state model of wind blown sand transport. *Journal of Geology,* 98(1):1-17.

White, B.R. and Mounla, H. (1991) An experimental study of Froude number effect on wind-tunnel saltation. In Barndorff-Neilsen, O.E. and Willetts, B.B. (eds.), Aeolian Grain Transport 1, *Acta Mechanica,* **Suppl.1**:145-157. (Springer-Verlag, Wein New York).

Wiggs, G.F.S., Livingstone, I. , Thomas, D.S.G. and Bullard, J.E. (1996a) Airflow and roughness characteristics over partially vegetated linear dunes in the Southwest Kalahari desert. *Earth Surface Processes and Landforms,* 21:19-34.

Wiggs, G.F.S., Livingstone, I. and Warren, A. (1996b) The role of streamline curvature in sand dune dynamics: evidence from field and wind tunnel measurements. *Geomorphology,* 17:29-46.

Willetts, B.B., McEwan, I.K. and Rice, M.A. (1991) Initiation of motion of quartz sand grains. In Barndorff-Neilsen, O.E. and Willetts, B.B. (eds.), Aeolian Grain Transport 1, *Acta Mechanica,* **Suppl.1**:123-134. (Springer-Verlag, Wein New York).

Willetts, B.B. and Rice, M.A., (1985a) Inter-saltation collisions. *Proceedings of the International Workshop on the Physics of Blown Sand, Aarhus,* memoirs No.8(1):83-100.

Willetts, B.B. and Rice, M.A. (1985b) Wind tunnel tracer experiments using dyed sand. *Proceedings of the International Workshop on the Physics of Blown Sand, Aarhus, memoirs* No.8(2):225-242.

Willetts, B.B. and Rice, M.A. (1989) Collisions of quartz grains with a sand bed, the influence of incident angle. *Earth Surface Processes and Landforms,* 14:719-730.

Williams, G. (1964) Some aspects of the aeolian saltation load. *Sedimentology,* 3:257-287.

Williams, J.J. (1986) Aeolian entrainment threshold in a developing boundary layer, Thesis for Doctor of Philosophy, Department of Geography and Earth Science, Queen Mary College, University of London, 524pp.

Williams, J.J., Butterfield, G.R. and Clark, D.G. (1990a) Aerodynamic entrainment thresholds and dislodgement rates on impervious and permeable beds. *Earth Surface Processes and Landforms,* 15:255-264.

Williams, J.J., Butterfield, G.R. and Clark, D.G. (1990b) Rates of aerodynamic entrainment in a developing boundary layer. *Sedimentology,* 37:1039-1048.

Williams, J.J., Butterfield, G.R. and Clark, D.G. (1994) Aerodynamic entrainment threshold: effects of boundary layer flow conditions. *Sedimentology,* 41:309-328.

Young, A.D. (1989) *Boundary Layers*, (BSP Professional Books, a division of Blackwell Scientific Publications Ltd), 296pp.

Zingg, A.W. (1953) Wind tunnel studies on the movement of sedimentary material. IOWA state University, 5th Hydraulics Conference Proceedings Bulletin, 34:111-135.